Universiteit Utrecht

On the protolith assemblage, the tectonostratigraphic position and metamorphic history of some orogenic peridotites in the lower Köli nappe, Southern Västerbotten, Central Swedish Caledonides.

Essers, S

Master thesis, Department of earth sciences, Utrecht University,
Utrecht, the Netherlands, April 2017

First supervisor: dr. Herman van Roermund

Second supervisor: prof. dr. Martyn Drury

Abstract

Orogenic peridotites are present in most of the higher nappes of the Scandinavian Caledonides. However, the origin of these orogenic peridotites is still under discussion. The Köli Nappe, subdivided in lower (eastern Iapetus) and upper Köli (western Iapetus), consists of the Iapetus related terrains and contains peridotite bodies of various sizes. During fieldwork in southern Västerbotten samples of some lower Köli peridotites were collected for further analysis using EMP, XRF and Raman spectroscopy. This work proposes an oceanic origin for the lower Köli peridotites based on the composition of protolith spinel and the magnesium number of protolith olivine grains. After protolith formation serpentinisation is inferred to have taken place at the ocean floor or after obduction onto a (micro) continent during the Finnmarkian Orogeny. The peak metamorphic conditions during the prograde metamorphism of the Scandian Orogeny are 400-500 ˚C and 5kb based on the stability of antigorite and olivine in the absence of talc. These PT conditions are subsequently used to improve earlier made tectonic models of the formation of the Scandinavian Caledonides.

.

Contents

.

1 Introduction

Ultramafic rocks are present throughout various mountain belts formed during plate collision processes. The Scandinavian Caledonides is perfect to study ultramafic bodies due to intense erosion uncovering the deeper parts of the orogen and the presence of ultramafic rocks throughout the upper nappes. The Scandinavian Caledonides is a 1500 kilometer long mountain belt that consist of several westward dipping major nappes (fig. 1.1). This major nappes may consist of several smaller local nappes. The Scandinavian Caledonides formed during the major mountain building event, the Caledonian orogeny (500-360 Ma).

The Scandinavian Caledonides has a complex history with multiple stages of collision. These events can be described in five main phases; the Finnmarkian event (500 Ma) (Andréasson & Albrecht, 1995), the Trondheim event (480 Ma) (Gee, 1987), the Taconian event (460Ma) (Roberts, 1980), the Jämtlandian event (450 Ma) (Brueckner & van Roermund, 2004) and the Scandian event (430-390 Ma) (Gee, 1975). The Taconian and Trondheim event occurred along the Laurentian margin (Gee, 1987 & Roberts 1980) whereas the Finnmarkian and Jamtlandian event occurred along the Baltic margin (Andréasson & Albrecht, 1995 & Brueckner & van Roermund, 2004) .

The foreland regions of Baltica and Laurentia are dominated by crystalline crust. Neoproterozoic basins were formed as a result of rifting and extension between Baltica and Laurentia between 800-500 Ma (Gee, 2008). Rifting was initially slow but truly initiated in the Vendian now observable as mafic dike swarms. It is likely that at this time the Laurentian and Baltic margins were adjacent.

The pre-Caledonian sedimentary covers of both continental margins are significantly different in nature reflecting the different latitudes of the continents at this time (Gee 2008). The Baltic side is dominated by siliciclastics, most notable the black shales (Andersen et al., 1986), whereas the Laurentian cover is characterized by thick carbonate sequences underlain by siliciclastics during the Cambrian (Swett, 1981). The Ordovician deposits are dominated by carbonates on both sides. Silurian turbedites are the result of initiation of the Scandian collision at the Baltoscandian margin.

The terranes of the Scandinavian Caledonides characterize the different depositional ‘environments’ which refer to their pre-collision position. From bottom to the top these are the Autochthon, Lower Allochthon, Middle Allochthon, Upper Allochthon and Uppermost Allochthon. The Autochthon consists of the pre-Caledonian basement of Baltica and related sediments, the Lower and Middle Allochthon consists of the continental to oceanic transitional sediments (Gee et al., 2008). The Upper Allochthon represents the Iapetus Ocean examplified by an ophiolite sequence (Gee, 1975). The Uppermost Allochthon is related to the continentally derived sediments of Laurentia (Stephens & Gee, 1985).

.

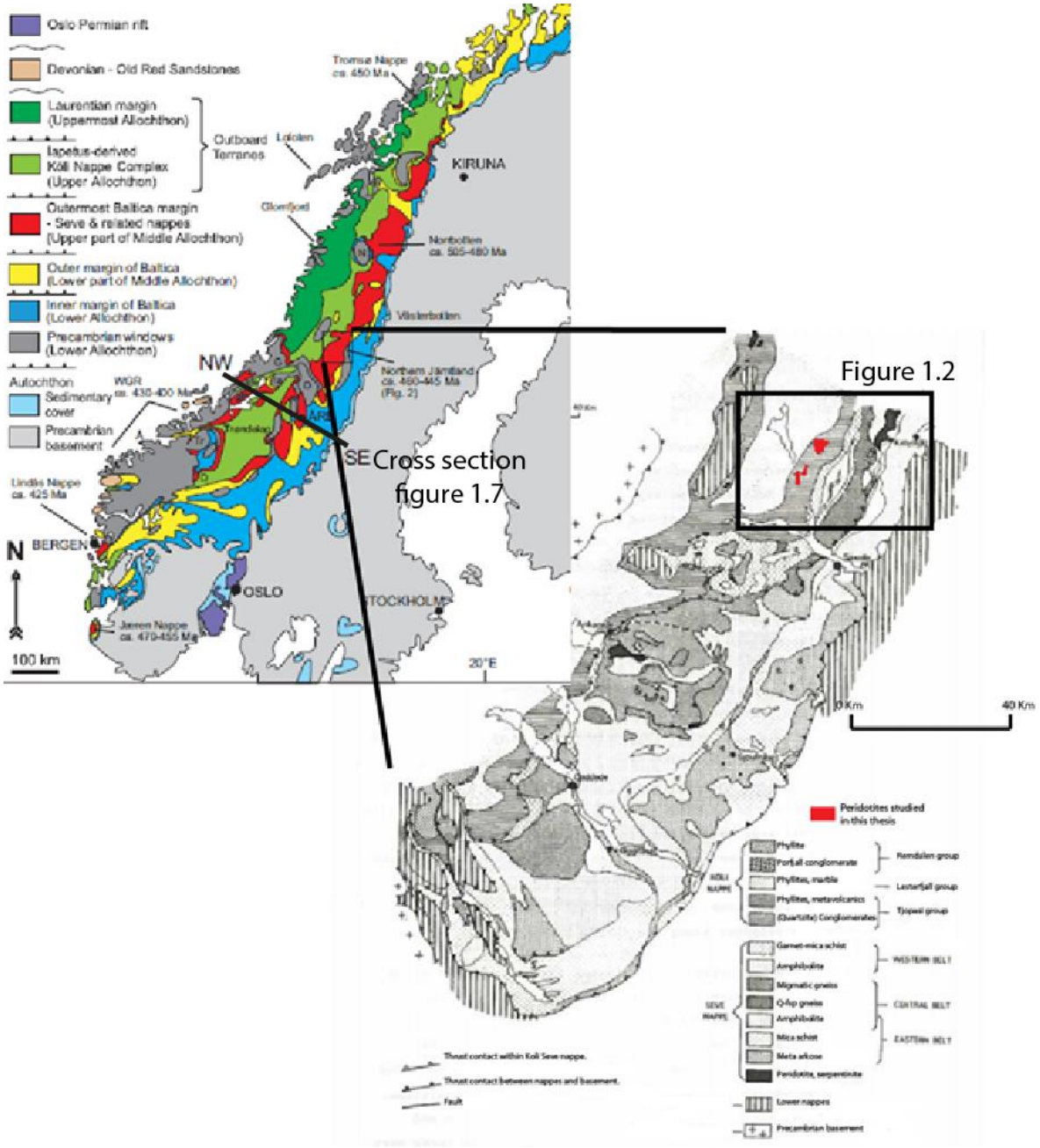

Figure 1.1. Terrane map of the Scandinavian Caledonides (after Gee,2010) and map of the research area after Reymer (1979).

Figure 1.2. Map showing the three investigated peridotite bodies (Aunere, Grundfors and Rödberget) in the lower Köli nappe. After Grimmer (2012).

This work will focus on the lower part of the Köli Nappe Complex (KNC) which is part of the Upper Allochthon and therefore thought to be related to Iapetus volcanic sequences and sediments (fig 1.2). Orogenic peridotite bodies are present in the lower part of the Köli nappe. This thesis will structurally and chemically characterize these orogenic peridotite bodies and determine their origin. The origin of the peridotites will be determined using the chemical composition of the primary minerals as well as the bulk rock chemistry (BRC) of the orogenic peridotites. In addition geobarothermometry will be applied to the primary assemblage to determine the PT condition at which it last equilibrated. The PT path after protolith PT conditions in the mantle will be determined using the microstructural relations between the various metamorphic minerals. Finally results of the tectonometamorphic conditions will be applied to tectonic models proposed by Roberts, 2003 and Bruckner and van Roermund, 2004.

.

1.1 Continental configurations involved in forming Caledonides.

During pre-Scandian times the continents were arranged in a super continent, Rodinia. Rodinia consisted of Laurentia as the center of the continent, Baltica to the east and Siberia to the north (fig 1.3) (Torsvik et al., 1996). The first signs of breakup appear around 600-550 Ma reflected in tholeiitic magma activity (Kumpulainen and Nystuen, 1985). In addition a variety of dike swarms with concurrent chemistry typical for rifting (T-MORB and N-MORB) have been dated in the Särv nappe, northern and southwest Norway, Greenland and northeast Russia at 665 Ma (Särv nappe, Claesson and Roddick, 1983), 580-600 Ma (Greenland, Soper, 1994a) and similar timings. These age results indicate that rifting initiated in the north and proceeded southward over time.

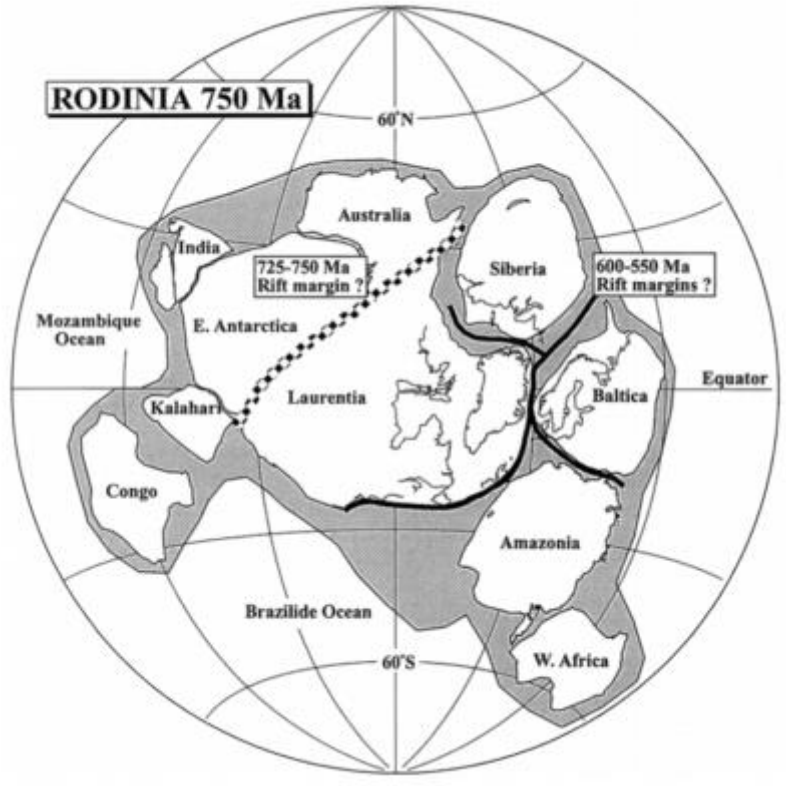

Figure 1.3. Model for the configuration of Rodinia by Torsvik et al. (1996),

partly based on Dalziel (1992).

.

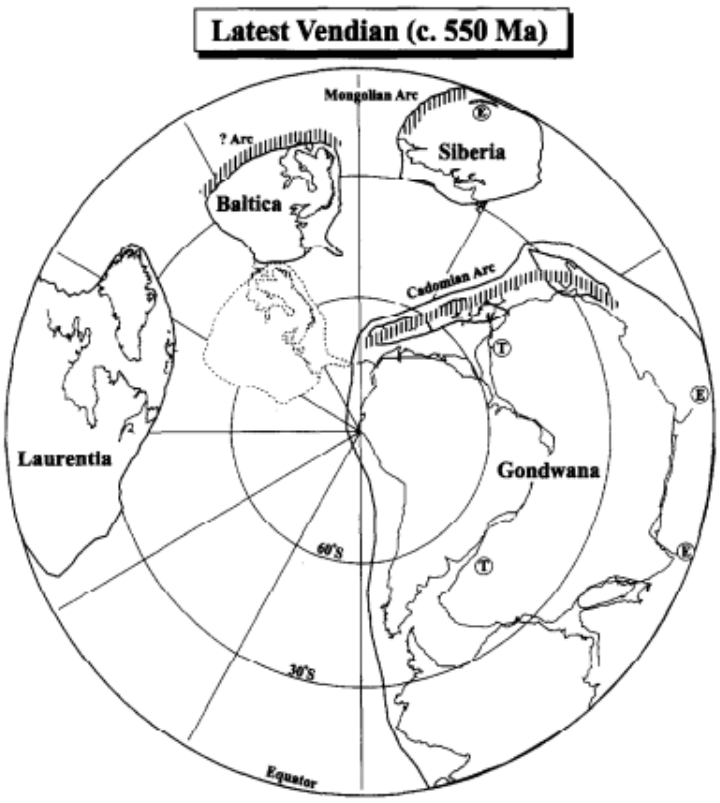

Figure 1.4. Continental configuration during latest Vendian times where Laurentia and Baltica have rifted apart. After Torsvik et al,. (1996) partly based on Meert et al., (1995).

The eventual opening of the Iapetus Ocean involved the clockwise rotation of Baltica and anticlockwise rotation of Laurentia. However, some authors argue that these rotations would lead to a lack of space (e.g. Torsvik et al., 1995a). This could be a result of inaccurate paleo-magnetic data, earlier rifting of Amazonia or a different arrangement between Laurentia and Amazonia. Finally during late Vendian times Baltica and Laurentia rifted apart (fig 1.4).

.

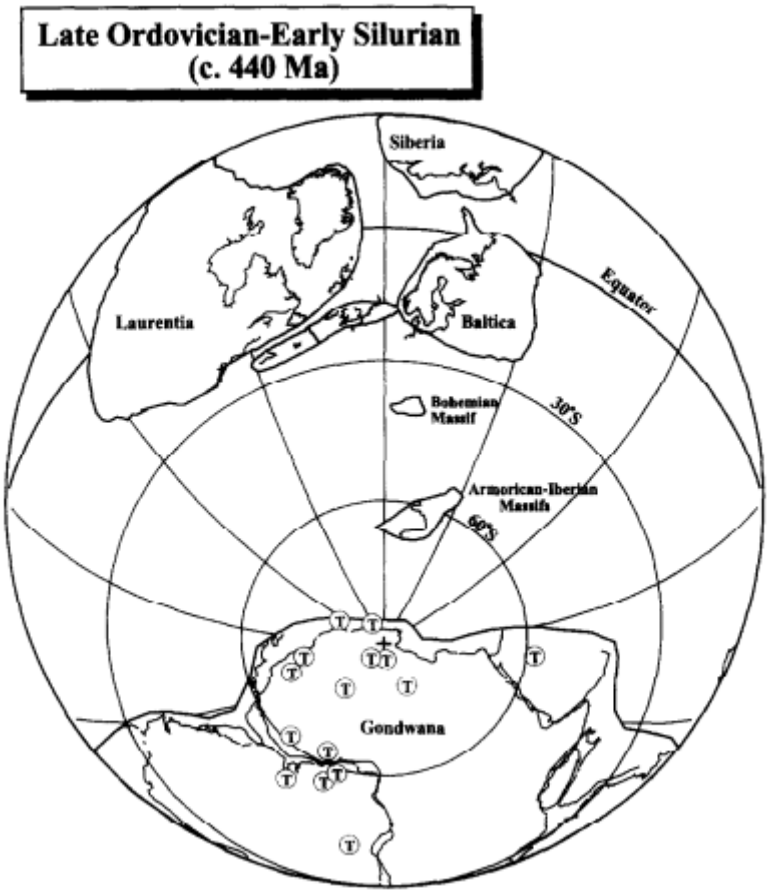

Figure 1.55. Continental configuration during the Late Ordovician – Early Silurian. Baltica and Avalonia are now considered one whole after Torsvik et al. (1996).

At the end of the pre-Cambrian Laurentia had drifted to lower latitudes remaining there until the Ordovician. During mid-Ordovician times Gondwana started to rift apart resulting in the disconnection of Avalonia, which moved towards the Laurentia Baltica margin following the Tornquist sea closure (fig 1.5) (Noble et al., 1993). The breakup of Gondwana also initiated the convergent movement between Laurentia and Baltica which eventually led into the collision between Laurentia, Baltica and Avalonia (fig 1.6).

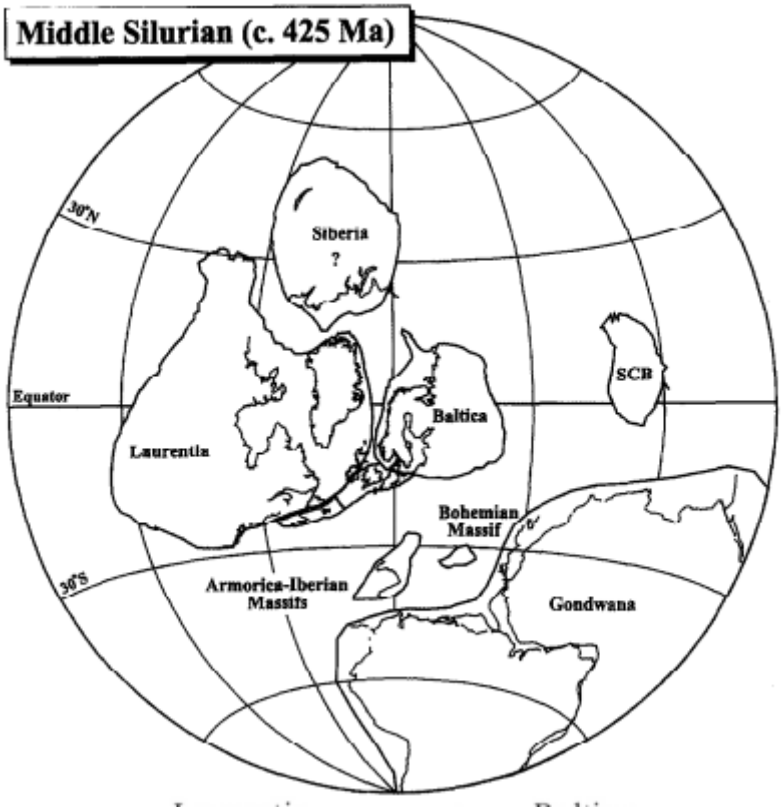

Figure 1.6. Middle Silurian collision between Laurentia, Baltica and Avalonia. Torsvik et Al. (1996).

1.2 Köli Nappe Complex (KNC)

The Koli nappe complex is presently situated on top of the Seve Nappe Complex (SNC) (fig 1.7). Together the KNC and SNC form the transition from the Iapetus Ocean to the Baltic continent. The KNC is generally devided in two major units, the lower Koli nappe thought to represent the Eastern Iapetus Ocean and the upper Koli nappe thought to represent the Wester Iapetus Ocean (with Laurentian imput of sediment). In Swedish and Norwegian scientific publications these major units consist of locally present nappes; i.e. Leipvik, Gelvenåkko, Remdalen, Stikke and Björkvattnet nappe.

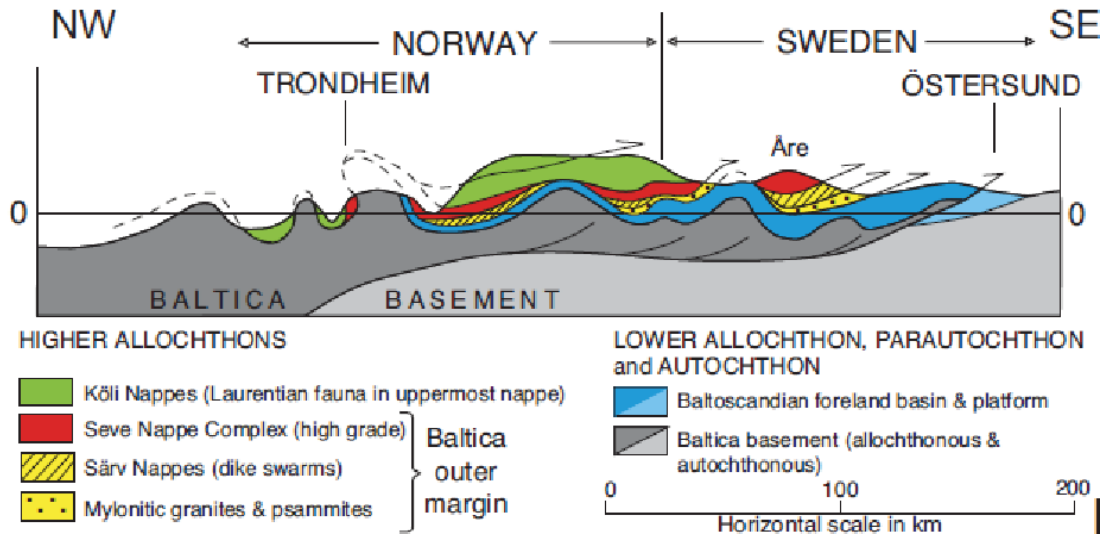

Figure 1.7. Tectonostratigraphic section through of the Scandinavian Caledonides through Are, 100km south of the S Vasterbotten area marked in figure 1.2. After Gee et al. (2013).

The Köli nappe is generally considered as a composition of oceanic and island-arc terranes (Stephans & Roberts 2002; Stephens 1988; Stephens & Gee 1989). However, the lower Köli nappe derived from the Virisen terrane and is most likely derived close to Baltica (Pickering & Smith 1995; Harper 1998, 2001; Sundblad et al. 2006).

In the investigated area (fig 1.2) the Köli nappe is exposed in two large scale north south running synforms, while the antiform in between exposes the middle allochthon. These folds strike sub parallel to the strike of the Caledonides, NNE-SSW (Zachrisson 1969; Gee et al. 1985) (fig 1.7).

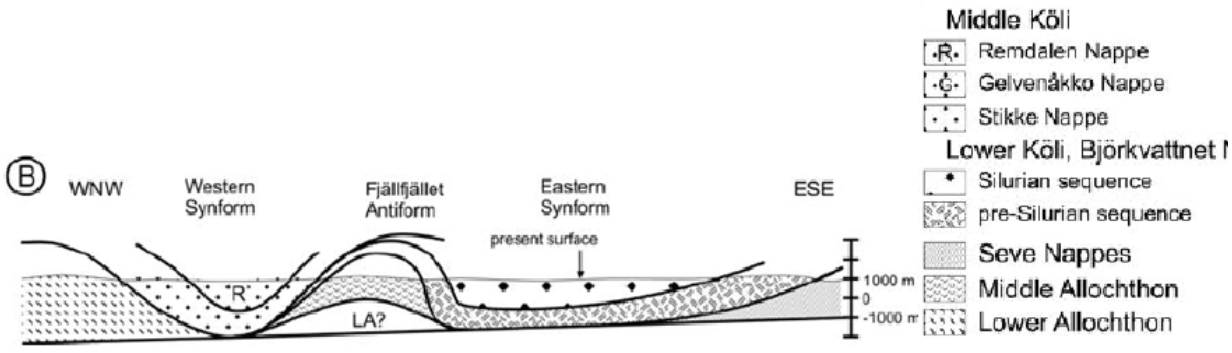

Figure 1.8. Structural cross section showing major thrust units and regional folds. Structural data from Zachrisson (1991, 1993) and Greiling & Grimmer (2007).

.

Kulling (1933, 1955, 1972) and Stephens (1982) determined a normal stratigraphic succession for the lower Köli nappe, Björkvattnet nappe, with a younging up direction whereas the middle Köli nappe has an inversed stratigraphy. The lower Köli nappe is composed of several formations. The lower part consists of Kvarnbäcken Conglomerate, Kvemoen Mica Schist, and Klumplidklumpen Formations (Sjöstrand 1978). The middle part of the lower Köli consists of the Ankarede formation and the upper part of the lower Köli nappe is either the Björnhögen or Gilliks Formation (Kulling 1933; Sjöstrand 1978; Stephens 1982). The middle Köli nappe consists of The Vojtja, Slätdal and Silurian formations.

The tectonostratigraphy of the lower and middle Köli nappe is shown in figure 1.9. However it may vary laterally along the Köli nappe but this stratigraphy is accurate for Northern Jämtland. Serpentinites and peridotites are often present at the lower boundary of the lower Köli nappe. Serpentinites higher up in tectonostratigraphy may be related to intrusions or volcanism but were not investigated in this work.

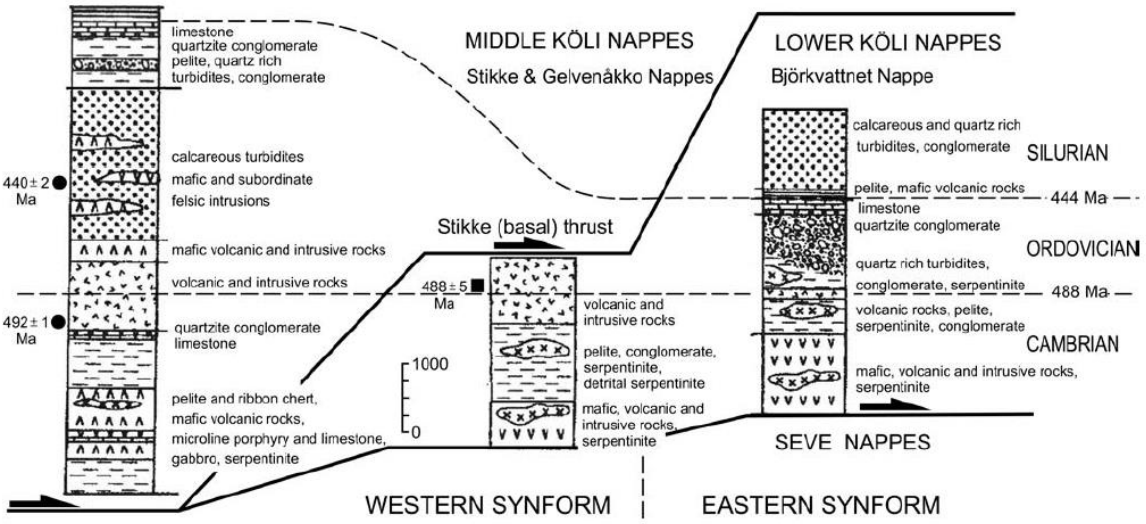

Figure 1.9. Reinterpretation of the Lower and Middle Köli stratigraphy and the relationships between the Björkvattnet and Stikke Nappes. Columns modified from Claesson et al. (1988) by Greiling & Grimmer (2007)

The tectonostratigraphy has been further analyzed to determine the different sedimentary components. The lower Köli nappe consist of mica schists and conglomerates, overlain by a volcanic sequence (Kvarnbäcken Conglomerate & Ankarede volcanic sequence). The middle Koli nappe consists of various quartzites, conglomerates, limestones and shales (Gilliks formation, Vojtja and Slätdal formations and Silurian black shales).

The Kvarnbäcken Conglomerate is exposed as lenses within the Kvemoen Mica Schist and is composed of quartzitic and felsic pebble. The Kvemoen Mica Schist also contains lenses of serpentinites and serpentine conglomerates. It is overlain by a sequence of quartzites, quartz phyllites, and occasionally graphitic phyllites and finally thin carbonate horizons (Sjöstrand 1978).

The Ankarede volcanic sequence is dominated by intermediate to mafic volcanic rocks interlain with phyllites and tuffites. The felsic metavolcanics are characterized by garnet, biotite-chlorite and hornblende in a quartz-feldspar-mica matrix whereas the metabasic rocks are

characterized by amphibole, biotite, chlorite, ±epidote, and albitic feldspar. Grimmer (2008) reports that these rocks sequence are considered primitive low-K island arc tholeiites with intermediate to acidic differentiation products. This is typical for ensimatic, convergent plate margin with subduction and marginal-basin development (Stephens & Gee 1985). A subvolcanic intrusion has been dated to 488±5 Ma, the Cambrian-Ordovician transition (Claesson et al. 1983).

The Gilliks formation, overlaying the Ankarede formation, consists of quartzites and quartzite conglomerates. It is intercalated with thin carbonate rocks that occasionally contain fossil corals, crinoid stems, and brachiopodes. These carbonate layers are replaced by impure quartzites and phyllites higher in the stratigraphy. This formation also contains meter to kilometer scale lenses of serpentinites. Zachrisson (1993) determined the origin of intercalated sand and siltstones as graywackes representing the more coarse grained part of a turbidite.

The Vojtja and Slätdal Formations overlay the Gilliks formation and consist of conglomerates overlain by grey, centimetre-scale banded limestones with grey phyllite intercalations (Kulling 1933, 1955). They contain fossils that limit the age to latest Ordovician age (Kulling 1933, 1955).

Highest in the stratigraphy lie the Silurian rocks, black shales and graphitic phyllite, that contain early Silurian graptolites (Kulling 1955), and latest 436 Ma (Gradstein et al., 2004). They are finally overlain by greywackes and quartzites which make up the highest stratigraphy.

Metamorphism within the Köli nappe has been studied by several authors. McClellan (2004) has determined the peak metamorphic temperature of garnet-biotite and amphibole assemblages near the Trondheim region. These thermometers yield maximum temperatures of approximately 550 ˚C. This temperature is in agreement with the presence of staurolite bearing schists in the nearby Hummelfjell nappe (Ramsay & Sturt, 1998) and the presence of kyanite (McClellan, 2004).

1.2 Seve Nappe Complex (SNC)

The SNC, in earlier work also referred to as the upper allochthon (now middle allochthon, Gee et al., 2008) is generally regarded as the outer western margin of Baltica. It shows evidence of a complex metamorphic history with higher metamorphic grades then overlying and underlying nappes. In addition it has been transported more than 200 km eastwards (Gee, 1975).

Recently the Seve nappe has been categorized as the top of the middle allochthon (Gee et al. 2008) instead of the base of the upper allochthon due to its chemical affinity (Asklund, 1961 and Hollocher et al., 2007).

	Major rock type	Metamorphic indicator minerals	Metamorphic grade
Western Belt	Kya-Sill Gneiss	Garnet, staurolite-kyanite	Medium T
Central Belt	Amphibolite	Staurolite-kyanite	Medium T/Medium P
	Ertsekey (U)HP lens	Kyanite- potassium feldspar	High T/ High P
Eastern Belt	Amphibolite	Kyanite-Staurolite	Medium T/Medium P
	Tjeliken (U)HP lens	Garnet	Medium T/ High P
	Garnet Biotite Rocks		
	Amphibolite	Garnet	Medium T/Medium P
	Garnet mica schist		
	Quartz-feldspar Gneiss		
Lower nappes	Undifferentiated	Undifferentiated	

Table 1.1. Tectonostratigraphy of the Seve nappe describing the different major rock types, associated metamorphic indicator minerals (Zwart, 1974) and metamorphic grade (Clos et al., 2014) present in the three main belts of the Seve Nappe in the Tången—Inviken area (van Roermund & Bakker, 1983) and the Southern Västerbotten area (van Bruchem, 2017) . Western belt after Van Bruchem (2017). Central and eastern belt after Van Roermund & Bakker (1983).

The SNC is usually described in respect to three belts, from top to bottom the upper/middle/lower or western/central/eastern belts (Zwart, 1974) (table 1.1). The upper belt is overlain by the Köli nappe

.

but the contact is not well defined. In some places the contact is tectonic while in others the contact is more gradual. The rocks of the upper/western belt are mostly kya-sill gneisses, garnet mica-schists, quartzitic garnet mica-schists, amfibolites and some ultramafic bodies (van Roermund & Bakker, 1983 and van Bruchem, 2017). However due to the unclear nature and location of the Seve-Köli boundary orogenic peridotites may belong to the Köli nappe.

The contact between the upper/western and middle/central belt is not well exposed and therefor its nature is unclear. The central/middle belt has a higher metamorphic grade then the upper/western belt. It primarily consists of migmatic gneisses and metabasic rocks (granulites and/or eclogites) (Zwart, 1974). The metamorphic grade of these units varies significantly throughout the central/middle belt from Marsfjället gneisses with granulite facies metamorphism (Zwart, 1974; Williams & Zwart, 1977) to Avardo gneisses (Ertsekey UHP lens) with ecologite facies metamorphism (Gilio et al., 2014). The highest metamorphic grade has been found within the Friningen garnet peridotite with UHP metamorphism (Janak et al., 2013). Ultramafic bodies are present in the gneisses of the middle/central belt.

The lower/eastern belt has a tectonic contact with the middle/central belt (Zwart, 1974). This belt consists of marble, meta-arkose, quartzite, garnet-micaschist , amphibolite and minor ultramafic bodies (Zwart, 1974; van Roermund & Bakker, 1983) and is underlain by the lower allochthon. The lower/eastern belt also contains one HP lens, the Tjeliken HP lens. A major tectonic boundary seperates the lower belt from the lower allochthon (Gee et al., 2008 & Zwart, 1974)

.

1.3 Orogenic peridotite terminology and modal metamorphic reactions of an ophiolitic peridotite.

Orogenic peridotites are subdivided in several categories according to their mineral content. The most commonly used diagram is based on the relative (modal) content of olivine, clino pyroxene and ortho pyroxene. In this case the upper part of figure 1.10 is applicable, where lherzolites, harzburgites and dunites make up the vast majority of ultramafic rocks. If the rock contains >10% CPX and >40% olivine it is considered a lherzolite. If it contains <10% CPX but ≤60% OPX and >40% olivine it is a harzburgite. If the rock is >90% olivine it is a dunite.

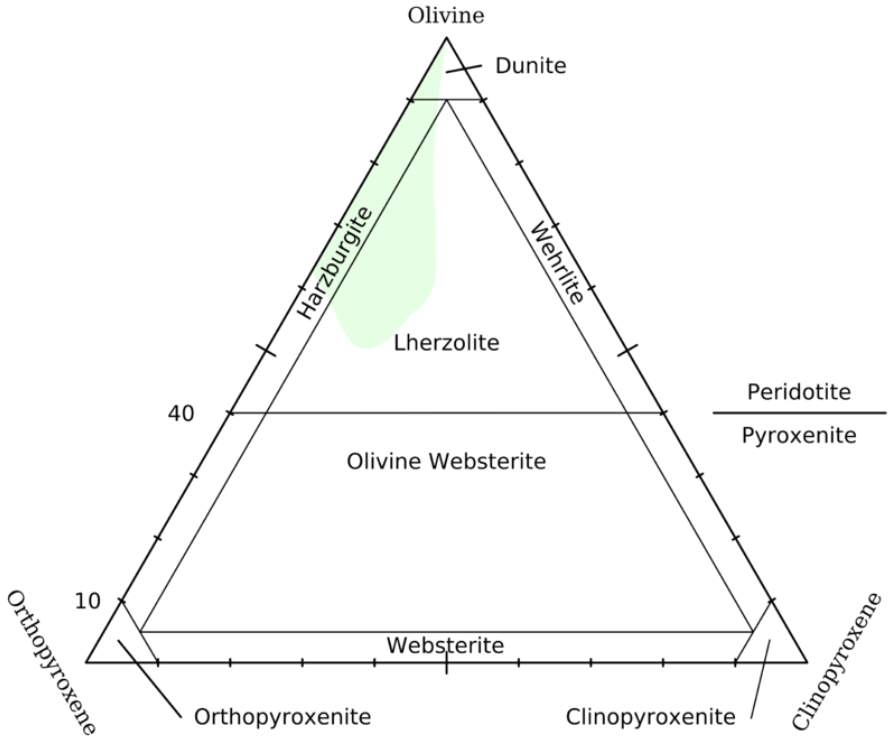

Figure 1.10. Ultramafic classification diagram. Bodinier and Godard (2004).

Peridotites can be equilibrated at a vast range of different pressure and temperature conditions depending on the geological environment. Common minerals that form are serpentine, spinel, olivine, OPX, brucite, talc and calcium phases such as CPX, tremolite and aluminum phases such as chlorite, garnet and plagioclase. Different serpentine minerals form at different PT conditions; chrysotile and lizardite at low temperature conditions (T<250 ˚C) and antigorite at higher temperature conditions (T>250-300 ˚C). Figure 1.11 shows the stability of the afore mentioned minerals along a standard geothermal gradient, 20 ˚C/Km (Bucher,2005 chapter 5).

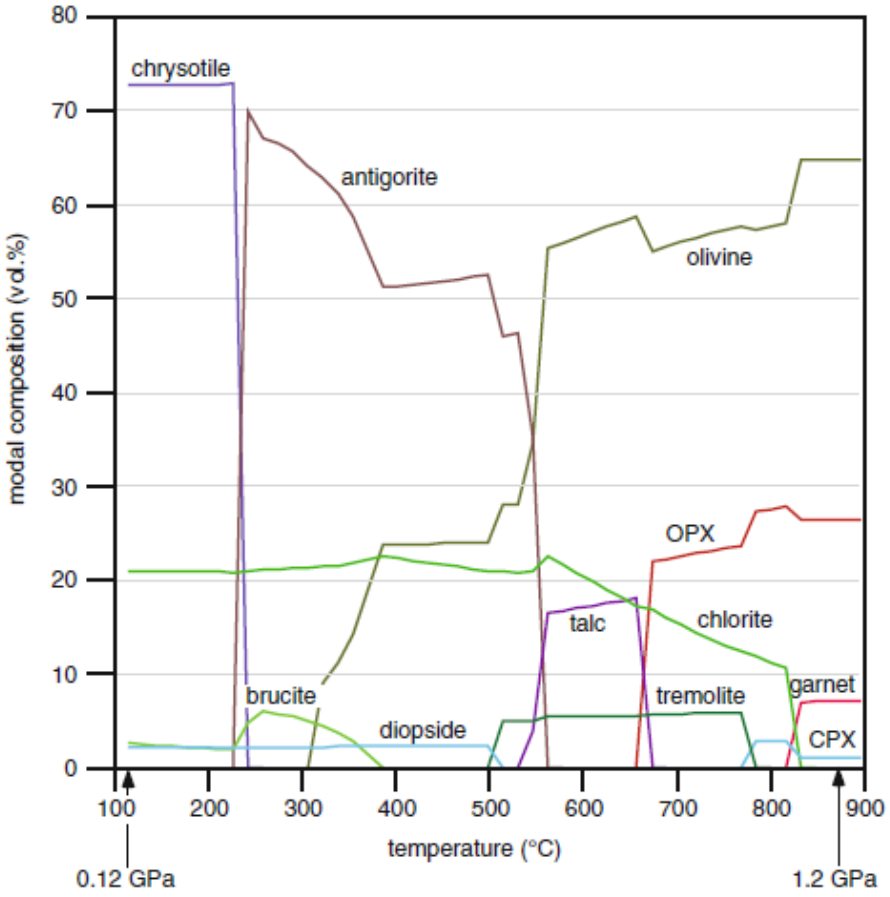

Figure 1.11. Model metamorphism along a geothermal (gradient of 20 ˚C /km) with an average bulk composition of the Zermatt-Saas meta-ophiolite/peridotite. Bucher (2011).

1.4 Retrograde metamorphism

In an ophiolitic ocean floor setting metamorphic processes are retrograde and controlled by hydration and hydrothermal processes. The first reaction, using a harzburgite with a minor presence of diopside, at 620 ˚C, is the formation antigorite from enstatite + olivine.

$$14Fo + 10\,En + 21\,H_2O \;=> Atg$$

This results, given sufficient time, in either Atg+ Fo or Atg+ En depending on which constituent is used up earliest. If enstatite is still present it reacts to antigorite and talc.

$$45En + 55H_2O \;=> Atg + 14\,Tlc$$

If olivine is still present it reacts to antigorite and brucite.

$$34Fo + 51H_2O \;=> Atg + 20\,Br$$

However it is fairly common for pieces of the mantle to remain dehydrated till it has cooled down to near surface temperatures (0-50 ˚C). In this case all reactions above are skipped and from 400 ˚C downward it directly forms chrysotile from olivine and enstatite.

$$2Fo + En + 4H_2O \;=>\; 2\,Ctl$$

.

The remaining olivine or enstatite is either reacted to a combination of chrysotile and talc or it is removed through circulating fluids.

In the above reactions the iron free end members of olivine and OPX are used because iron complicates these reactions as the products are iron free minerals (serpentine and chrysotile). In the case of olivine chemistry of $Fo_{90}Fa_{10}$ the following additional reactions take place.

$$3FeSiO_4 + 2H_2O \Rightarrow 2Fe_3O_4 + 3\,SiO_{2_{aq}} + 2H_2$$

This reaction involves the formation of magnetite as an iron phase. The resulting SiO_2 is used to form chrysotile from the forsterite component according to;

$$3MgSiO_4 + SiO_2\ aq + 2H_2O \Rightarrow 2Mg_3Si_2O_5(OH)_4$$

All SiO_2 produced is used in the formation of chrysotile up to olivine compositions of $Fo_{75}Fa_{25}$, but since most mantle olivine compositions are much more forsterite rich it is typical to have slightly too much magnesium to form chrysotile. This remaining magnesium may be incorporated in minor amounts of brucite, however brucite is very soluble and is readily transported out of an open system.

1.4.1 Spinel chemistry

The spinel mineral group is made up of several different minerals with the general composition $A^{2+}B^{3+}{}_2O_4$ where A can be Mg^{2+} or Fe^{2+} and B can be Fe^{3+} Al^{3+} and Cr^{3+}. Minor amounts of Ti and trace amount of Zn, Mn, V and Ni may be present.

A study by Barnes and Roeder (2001) has collected a large amount of spinels from various tectonic settings. Barnes and Roeder (2011) compare these samples using ternary iondiagrams with Fe^{3+} Al^{3+} and Cr^{3+}, Cr# vs Fe^{2+}#, Fe^{3+}# vs Fe^{2+}# and TiO vs Fe^{3+}# (fig 1.12).

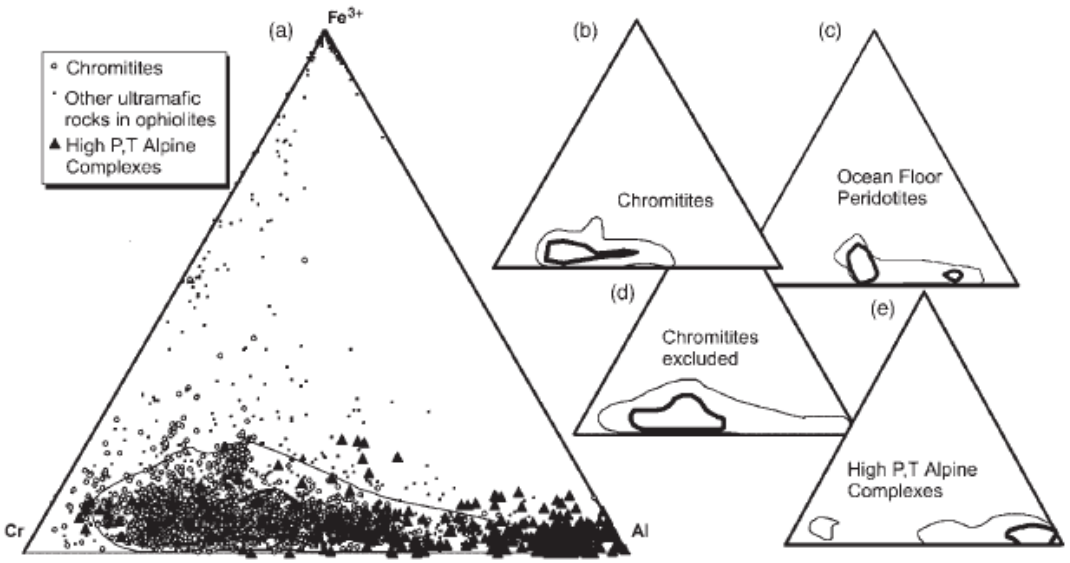

Figure 1.12. Trivalent ion plots for ophiolites, alpine type peridotites and abyssal peridotites. (a) all points (b) chromitites seams (c) ocean floor (d) all points except chromitites (e) high P,T alpine complexes. Barnes and Roeder (2001).

.

From figure 1.12 it can be shown that most spinels from peridotites from an oceanic setting have a low Fe^{3+} content and a variable Cr^{3+} to Al^{3+} content. Barnes and Roeder argue that the Al^{3+} content in spinel is controlled by pressure (and in a less persistent way T) where a high P will result in a larger fraction Al^{3+}.

Ophiolitic and alpine type peridotites show a relatively low Fe^{2+}# as compared to Cr#, where oceanic peridotites tend to have a slightly higher Cr# (fig 1.13). Both ophiolitic and alpine type peridotites show Fe^{3+}# of approximately 0.3 to 0.5 without much scatter (fig 1.13).

In addition the Ti component of spinels from ophiolitic as well as alpine type peridotites is negligible and can thus not be used as a discriminating factor.

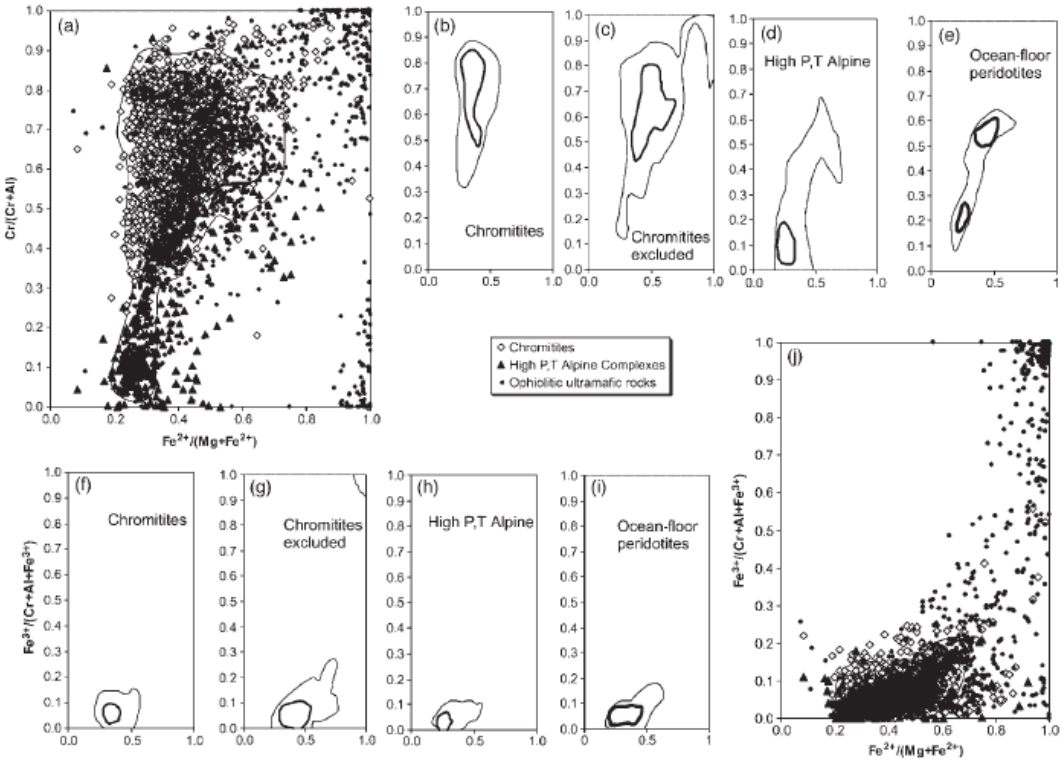

Figure 1.13. Cr# vs Fe^{2+}# data points and contours (upper diagrams) and Fe^{3+}# vs Fe^{2+}# data points and contours (lower diagrams). Barnes and Roeder (2001)

The chemical composition of metamorphic spinel is greatly dependent on the available consitituents. If spinel is formed during serpentinisation the iron released by olivine (see section 1.4.2) can be used in spinel. Metamorphic spinels can be distinguished from primary magmatic magnetites due to the low Cr/(Cr+Al) since when the liquidus of magnetite is reached the melt generally has <100 ppm Cr but a significant amount of Al. However during metamorphism spinels lose their Al content due to reactions with silicates to form chlorite or amphibole. The resulting spinels with a high Fe3+ and Cr3+ content are often referred to as ferritchromites.

Dick and Bullen (1984) distinguished 3 types of alpine peridotites according to their spinel compositions. A spinel from their type I peridotite has a Cr#<60 and overlaps with the spinel compositions found in abyssal or ocean floor peridotites. Type I peridotites with high Al spinel

compositions are typical of lherzolites whereas those along the Cr Al side of the triangular diagram (fig 1.12) can be lherzolites as well as harzburgites/dunites. Spinels from type III peridotites have a Cr#<60 and do not overlap with the abyssal spinel composition of type I. Spinels from type III are usually refractory and usually have harzburgitic or dunitic bulk rock compositions. Type II peridotites are a transitional group making up the range between type I & II peridotites and often within one peridotite exposure both types can be separately identified.

1.4.2 Olivine chemistry

The range in chemical composition of olivine is small, involving the partitioning between iron and magnesium, but can still be of great value for determining conditions during metamorphism. The solid solution between forsterite and fayelite is dependent on several factors; pressure, temperature and partial melting.

In serpentinized rocks the Mg# can be used to differentiate between olivine with a mantle composition and metamorphic olivine. Mantle compositions generally vary between Mg# 88-92. The lowest Mg# (88-89 Mg#) constitute the primitive mantle. Melt extraction from the primitive mantle will lead to an increase of Mg# (Arai 1994). This process is paired with a change in Cr# in spinel and both are often used to determine the amount of melt extraction (Arai 1994).

Since serpentine is dominantly an iron free phase (or low Fe content for antigorite) magnetite will crystallize separately. When the metamorphic conditions favor the growth for olivine the serpentine will be devoid of iron and the metamorphic olivine will be enriched in magnesium resulting in Mg# between 95 and 98.

.

2.0 Tectonic models

Several tectonic models have been proposed describing tectonic process and the structures they produced. Many of these tectonic models are applicable to one specific small region, however several authors have proposed a large scale tectonic model for the entire Scandinavian Caledonides. Two of these models, Roberts (2003) and Bruckner and van Roermund (2004), will be discussed in this section. The results of this work will later be discussed in regards to these models (see model discussion section, chapter 7).

2.1 Roberts (2003)

Roberts (2003) describes the first phase of deformation, called the Finnmarkian event, using ages acquired by K –Ar and Rb –Sr age dating techniques. This phase involves the outermost Baltoscandian margin also known as the Seve-Kalak or upper parts of the middle allochthon, also called the ocean to continent transition zone (Andréasson et al., 1998). This resulted in the collision of the Baltoscandian margin with an inferred magmatic arc via a seaward dipping subduction zone (figure 2.1). Torsvik & Rehnström (2001) and Hartz & Torsvik (2002) suggested that this arc mainly consisted of oceanic crust and was located between Siberia and Baltica or was a micro continent partly rifted away from Baltica.

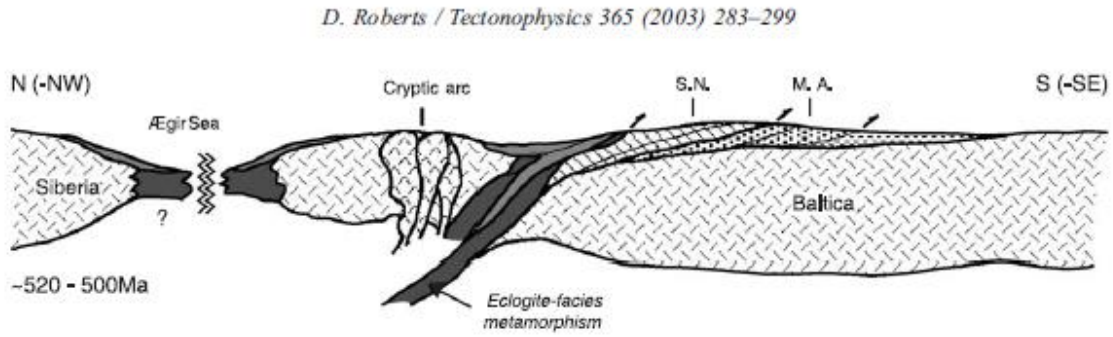

Figure 2.1. Schematic, composite profile illustrating the Finnmarkian accretionary event, in Late Cambrian time, ca. 520–500 Ma. The profile covers the northern most parts of Norway and Sweden, roughly northeast of Lyngen. Oceanward subduction of the continental margin/ocean transition zone down to at least eclogite-facies depths was followed by rapid exhumation and emplacement of the Finnmarkian nappes onto the Baltoscandian margin. Baltica is considered to have faced Siberia (or Laurentia) at this time, across the Ægir Sea (or Iapetus Ocean) (Torsvik and Rehnström, 2001). A microcontinental block (rifted off Baltica) has been inferred to have been involved—the 'Barents microcontinent' of Gayer et al. (1987). S.N.—Seve Nappes; M.A.—Middle Allochthon. Roberts (2003).

Subsequently the Trondheim event has been identified in parts of the lower and upper Köli nappe, first by Holtedahl (1920) and later by Gee (1986). Even though it has been related to the Finnmarkian event it is a distinct and separate tectonothermal event which includes obduction of ophiolite and blueschist facies metamorphism (Eide and Lardeaux, 2002). U-Pb dating of zircons in plagiogranitic dykes yielded 493–482 Ma ages for this event (Dunning, 1987).

.

The obduction of these Köli ophiolites during the Trondheim event is thought to be the result of oceanward subduction between oceanic lithosphere and the Gula complex (upper Köli nappe), a micro continent rifted from Baltica (fig 2.2). The overlying sediments contain fossils with a mid to Late Arenig age limiting the timing of the obduction and indicating a Baltican origin of the microcontinent (Bruton and Bockelie, 1980). However Laurentian fauna related fossils have been found in Støren Nappe, overlying the Gula complex, possibly indicating a Laurentian derived microcontinent (Stephens and Gee, 1985).

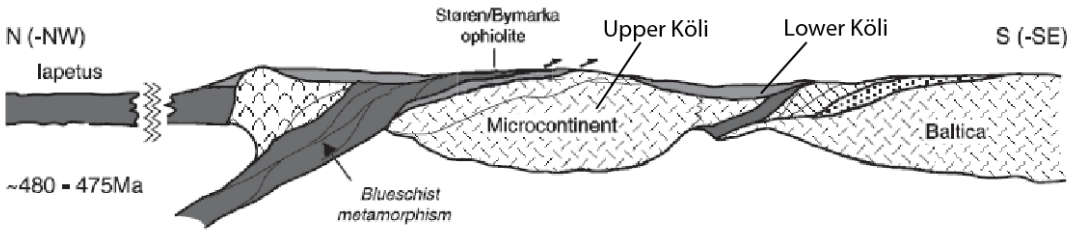

Figure 2.2. Schematic, composite profile illustrating the Trondheim event in SW Norway, in latest Tremadoc to Early Arenig time, c. 480– 475 Ma. The profile covers the Trondheim region of Mid Norway. Again, oceanward subduction is inferred, down to at least blueschist-forming depths (Eide and Lardeaux, 2002), prior to or partly coeval with Early to Mid Arenig, ophiolite obduction onto the mainly epicontinental Köli Nappe rocks (Gula complex) covering the 'Gula microcontinent'. The earlier, Finnmarkian-accreted, magmato-sedimentary complexes (Seve/Kalak Nappes, etc.) are shown farther S-SE, draping the margin of Baltica. By this time, Baltica had started to rotate anticlockwise, eventually to face Laurentia, across the Iapetus Ocean. Roberts (2003).

The Taconian tectonothermal event which took place in the mid to late Ordovician is characterized in several of the outboard Köli (upper Köli) terranes and the uppermost allochton (Roberts, 1980) (fig 2.3). In southwest Norway this event is characterized by accretion of fragmented ophiolites onto a continental margin around 470–465 Ma (Dunning and Pedersen, 1988; Pedersen et al., 1988, 1992; Pedersen and Furnes, 1991). Pedersen et al. (1988) also reported obduction and associated deformation at Laurentia's margin during the Taconian.

Fault, fold and cleavage data from the Fauske nappe, in northern Norway, shows that the shelf, related successions and magmatic arc complexes have been included in the Taconian accretionary wedge on the margin of Laurentia due to oceanward subduction, and later detached from Laurentia and emplaced high in the Scandinavian Caledonide tectonostratigraphy during the Scandian, i.e. the first collision between Baltica and Laurentia (Roberts et al., 2001; St. Julien and Hubert, 1975; Stanley and Ratcliffe, 1985; Roberts et al.,2002a) (fig 2.4).

Metamorphism during the Taconian event, along the Laurentian margin, has been studied in several regions. The upper most allochthon underwent metamorphism locally up to eclogite grade and ophiolite obduction took place during the mid to early Ordovician (Dallmeyer and Andresen, 1992; Nordgulen et al., 1993; Selbekk et al., 2000; Yoshinobu et al., 2002). Similar conclusions were drawn

by Stephens et al. (1993) studying upper allochthonous rocks in northern Sweden, however further south the Ekne disturbance is thought to be related to the Taconian orogeny (Vogt, 1936).

The upper boundary of the Taconian event is defined by a former sedimentary basin, near Troms in northern Norway, with the Lyngen ophiolite as a primary source with an Ordovician–Early Silurian age (Bjørlykke and Olaussen, 1981). These rocks only show deformation related to the Scandian orogenic event.

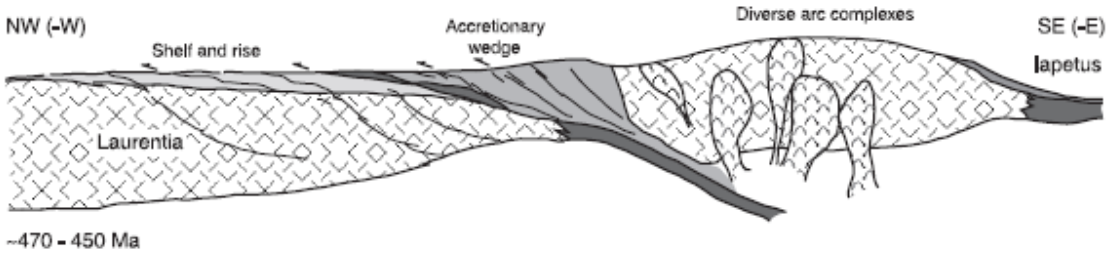

Figure 2.3. Schematic, composite profile showing the palaeotectonic situation during the Taconian event, in Mid to Late Ordovician (Llanvirn to Caradoc) time, c. 470– 450 Ma. In this case, subduction and accretion, including eclogite generation and ophiolite obduction, occurred along the continental margin of Laurentia, quite remote from Baltica. Parts of these Laurentian shelf-and-rise and peri-Laurentian arc-complex terranes were later detached and retransported onto the nappes carpeting the Baltoscandian margin of Baltica during the Scandian collisional event. Roberts (2003).

The main tectonometamorphic event in the Scandinavian Caladonides is called the Scandian (Gee, 1975) and is responsible for the transport of the Iapetus and Laurentian related nappes on top of Baltica (fig 2.4). It is the result of the first oblique collision between Laurentia and Baltica during Late Silurian to Early Devonian time further progressing southward into the subduction of the outermost margin of Baltica below Laurentia. The timing of this event varies laterally as well as transversely. The presence of monazites in the western gneiss region in Norway shows that subduction (to depths of 120km) and exhumation were very fast processes wich took place (there) around 407 Ma (Terry et al., 2000).

All major nappes were influenced by the Scandian tectonic event. The upper allochthon has been detached from Laurentia and transported on top of Iaptus related terranes. Recent findings in Greenland suggest that it is possible that crustal thrust-imbrication and thickening may have been a more important process then continental subduction (Elvevold and Gilotti, 2000; Ryan, 2001; Gilotti and Ravna, 2002) while evidence of the thin skinned tectonics in southern Norway implies the classical subduction of Baltica under Laurentia.

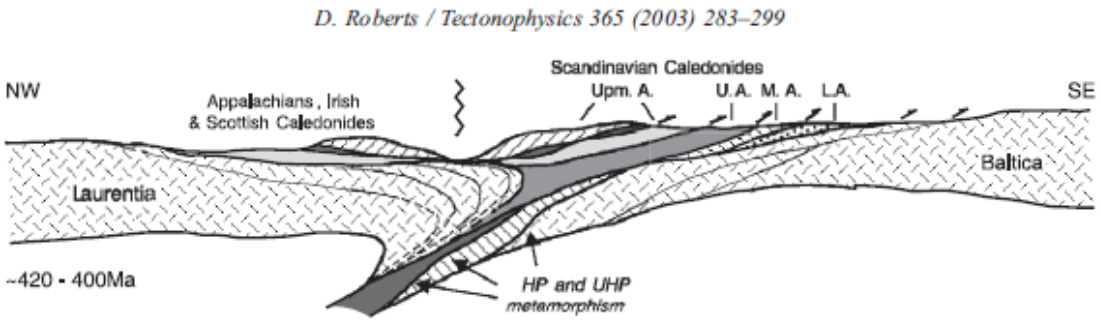

Figure 2.4. Schematic, composite profile illustrating the major Scandian, Baltica– Laurentia collisional event, in Mid Silurian to Early Devonian time, c. 420–390 Ma. Subduction of the Baltican margin and overlying volcanosedimentary assemblages and earlier nappes beneath the Laurentian plate is generally inferred. During rapid exhumation, numerous thrust sheets were emplaced onto Baltica and partly above earlier nappes. Some Taconian-deformed terranes were supposedly unrooted from Laurentia and emplaced into the higher levels of the Scandian orogenic wedge, where they now form parts of the Uppermost Allochthon. L.A., M.A., U.A. and Upm.A.—Lower, Middle, Upper and Uppermost Allochthons, respectively. Roberts (2003).

The late Scandian events are characterized by extensional deformation related to the gravitational collapse of the orogen (Roberts, 1983; Andersen, 1998). This was accommodated by low angle, ductile detachments relating to top-W to –SW shear and Early to Mid Devonian basinal sedimentation (Hossack, 1984; Norton, 1987; Séranne, 1992; Fossen and Dunlap, 1998; Osmundsen et al., 1998, 2003; Braathen et al., 2000) and ductile, sinistral shear along vertical faults (Grønlie and Roberts, 1989; Grønlie et al., 1991; Robinson, 1995). This phase was followed by a post-Scandian, low grade, brittle reactivation and NE-SW to E-W trending open folding of possible Late Devonian to Carboniferous age (Sturt, 1983).

So the Scandian is a 3 phase discrete, arc– continent collisional or accretionary events approximately 50 million years of Late Cambrian to Mid/Late Ordovician time. This followed by the oblique collision of Baltica and Laurentia and associated processes and finally late stage extension.

2.2 Brueckner and van Roermund (2004)

Brueckner and van Roermund (2004) propose a ‘dunk’ tectonics model for the Scandinavian Caladonides. They propose that buoyant crustal material will only subduct due to a slab pull effect of the attached oceanic lithosphere. However, at some point the amount of (buoyant) continental crustal material outweighs the slab pull effect and the oceanic lithosphere will break off (von Blanckenburg and Davies, 1995). If the continental crustal portion can separate from the underlying lithosphere (delamination) it becomes buoyant and will rise towards the surface. However, in the crust the material is no longer more buoyant in respect to its surroundings and other mechanisms are needed to transport this subducted material to the surface (i.e. regional thrusting eastwards).

Peridotitic rocks from the mantle are thought to be emplaced during the subduction phase of this process. The overlying upper mantle (wedge) can ‘intrude’/sink into the crustal portion of the subduction slab since peridotite material is heavier in comparison to the crustal material. These peridotites will have a chemical signature and/or age that deviates from those that were part of an ophiolite section.

.

Such peridotite bodies are present at several locations within the Scandinavian Caladonides associated with the Finnmarkian as well as the Scandian implying that dunk tectonics have played a major role in both orogenic events.

Brueckner and van Roermund have proposed three distinct phases of subduction and subsequent obduction at 500, 450 and 400 Ma. These tectonometamorphic events occurred at the Baltoscandian margin.

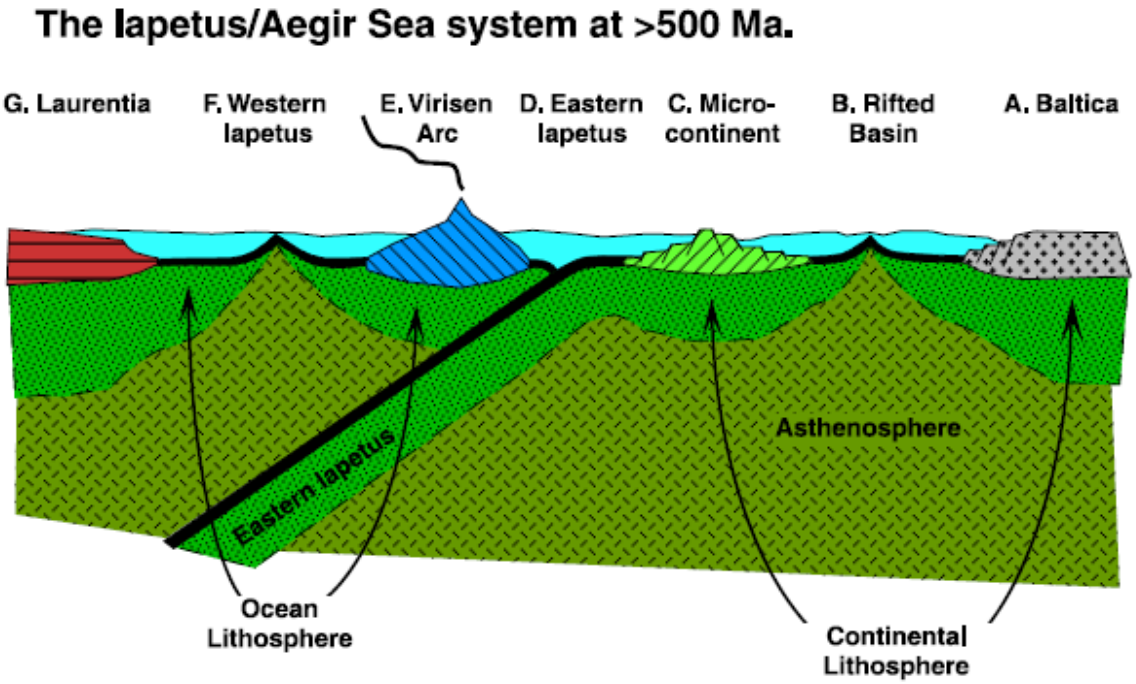

Figure 2.5. Pre-collision setup of the Laurentia-Baltica collision before 500Ma. Brueckner and van Roermund (2004).

The first orogenic phase, the Finnmarkian (500 Ma), represents the collision of an arc, called the Virisen arc and the western part of the Baltica (fig 2.6). This microcontinental block forms the continental lithosphere that has rifted off the main continent. This collision phase is associated with the prograde insertion of peridotites with suboceanic affinity and resulted in the Virisen-Norrbotten-composite-terrain (VNCT) (fig 2.6). The subsequent exhumation of this terrane has been dated to 480-470 Ma (Essex et al., 1997) and formed the Virisen/Norrbotten composite terrain (VNCT).

.

The second phase of collision, the Jämtlandian, has been dated to ~450 Ma and involves the units under the Köli nappe and above the lower allochthon overlying Baltica (fig 2.7). They represent the collision between the VNCT and the Baltic continent. The subduction is subsequent to the subduction of a basin between the VNCT and the SNC. During this phase (sub continental) peridotites were introduced to the subducting slab which was exhumed by 440 Ma. These (sub continental) peridotites were derived from underneath the aforementioned microcontinent.

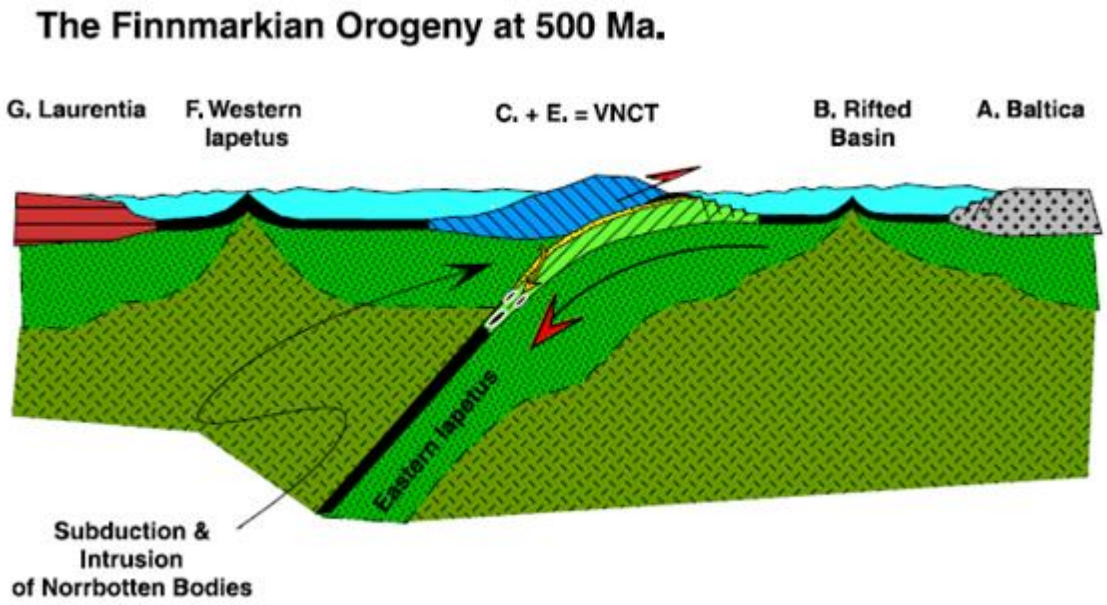

Figure 2.6. The Finnmarkian Orogeny, the subduction of a microcontinent under the Virisen Arc, parts of the Köli could be located between the Virisen Arc and the microcontinent as they were pushed on top of the micro continent. Brueckner and van Roermund (2004).

The Finnmarkian and Jämtlandian orogenic events show great similarity in units and subduction mechanism but are separated by the geochemical data of their associated peridotites (Brueckner et al., 2004). The Jämtlandian peridotites have an ancient subcontinental lithospheric source whereas the Finnmarkian peridotites have a youthful oceanic lithospheric source (fig 2.8).

The western Iapetus Ocean between Baltica (with the VNCT and Jämtlandian terrane) and Laurentia closed between 440 Ma and 425 Ma. Eventually the two continents collided resulting in the thrusting of Laurentia over the Köli nappe (Baltica). This subsequently induced complex renewed movement along the base sole thrust of the Scaninavian Caledonides, dated at 425-415 Ma.

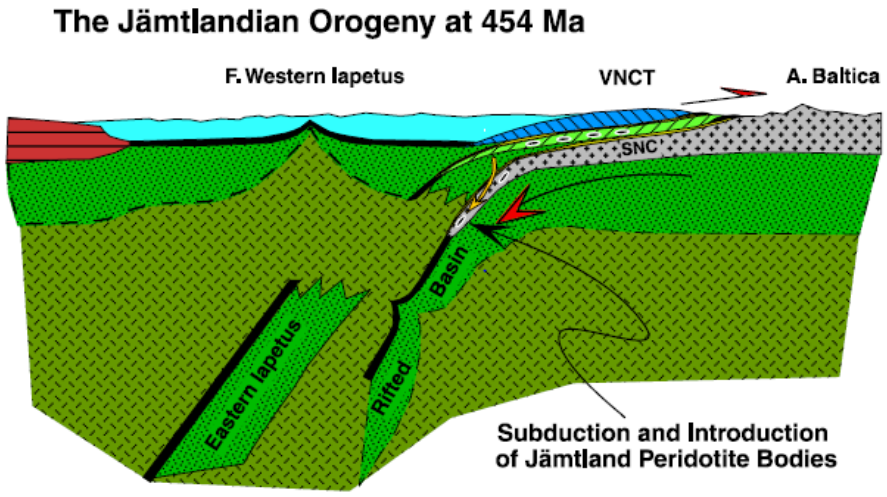

Figure 2.7. The Jämtlandian Orogeny, the subduction of Baltica under the Virisen/Norbotten composite terrain. At this point SCLM peridotites may have been inserted into the SNC. Brueckner and van Roermund (2004).

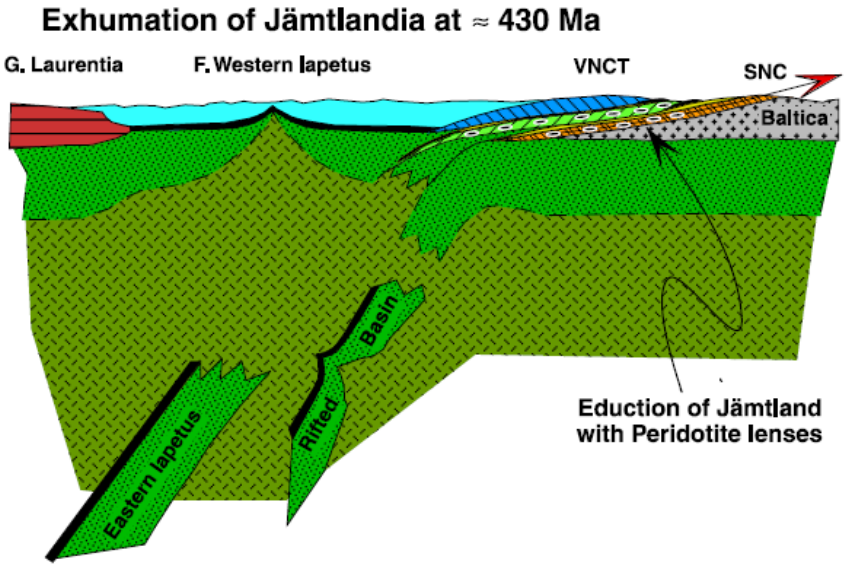

Figure 2.8. The exhumation of the SNC and further eastwards movement over the Baltic shield. Brueckner and van Roermund (2004).

.

3.0 Methods

Samples were collected throughout the lower Köli nappe in S. Västerbotten. Sample locations were choosen using geological maps issued by the Swedish Geological Survey (SGU) and/or Trouw (1973). The locations investigated and sampled were chosen to be representative for both the large peridotite bodies as well as the smaller peridotite bodies along the boundary between the SNC and the KNC (locations further described in sample location section). In addition several country rock samples have been taken near the peridotite bodies. Strike and dip of bedding and/or foliation, if present, were denoted as strike + dip direction for example 067/42N has a strike of 067 degrees and dips 42 degrees north.

Samples are numbered according XX.YY.ZZ where XX displays the day on which it was collected, YY the location (or stop) during this day and ZZ the samples at that specific location (if ZZ contains a letter different lithologies were present if not several samples of the same lithology were taken). The day of collection is concurrent with one specific peridotite body; day 1 & 2 were collected at Aunere, day 3 was collected at Gründfors and day 4 was collected at Rödberget.

Samples were prepared for optical microscopy at Utrecht University. The samples have been cut, perpendicular to the foliation (if present), and polished into 30 µm thick slices. Overview and detailed photos (see appendix 11.1) were made using a Leica camera. Afterwards the uncovered thin sections were carbon coated in a carbon coater to prepare them for the scanning electron microscope (SEM) and electron micro probe (EMP).

The mineralogy and structural relations within the thin sections were determined using optical microscopy (all photographs of thin sections can be found in appendix 11.1). In addition the identity of all optically identified minerals were later confirmed using table top SEM and/or EMP chemical data (appendix 11.3 through 11.8).

Analytical SEM measurements were acquired using a table-top JEOL JCM-6000 SEM (with attached EDX facilities) present at Utrecht University. These measurements were used to confirm optically obtained mineralogical data and to acquire an estimate of the chemical constituents present in minerals. Operation conditions were 15 Kv acceleration voltage under high vacuum conditions with a 3 µm spotsize.

EMP measurements constitute the bulk of the chemical data presented in this thesis, unless stated differently chemical data has been obtained by EMP mineral analysis as the precision is better than that of the SEM (±1.5% S.Ω for the EMP). Measurements were taken with a FEG-JEOL at Utrecht University. Operation conditions; 15 kV acceleration voltage and 20 nA beam current. A 1 µm spot size was used for all anhydrous minerals whereas a beam radius 3-5 µm has been used for all hydrous minerals. The measurement locations in appendix 11.3 through 11.8 refer to the locations indicated on the back scatter images attached in appendix 11.1 for all investigated samples.

In addition all analysis locations within thinsections have been photographed using backscatter imaging (see appendix 11.1). These locations are marked on the photographs on the overview photos presented in appendix 11.1 and are refered to according to the earlier mentioned system XX.YY.ZZ location #1-6.

.

The bulk rock chemistry of samples 3.2A and 1.1 (See section 5.5) were acquired using x-ray fluorescence at the Utrecht University. The BRC was used to model metamorphic reactions using Perplex in combination with the thermodynamic data proposed by Holland & Powell (1998), adjusted in 2002. Solution models from Holland & Powell (2002) were used for olivine, spinel, chlorite and OPX and a solution model for serpentine by Padrón-Navarta et al. (2013).

Different types of serpentine minerals in different microstructural posititions were identified using micro-Raman spectroscopy (in sample 1.1 and 3.4.2). Micro-Raman spectra were acquired using a WIRec Alpha 300R with a 532 nm Nd: YAG laser (green) at Utrecht University. The calibration of the instrument was verified by measuring the position of the Si band at ±520.7 cm^{-1}. The spectral resolution, calculated using the calibration lamp, was 1 cm^{-1}. Continuous scan maps, 120x80 µm, were made with step size of 2 µm. The counting time was 0.5s per spot with a laser penetration of 1-2 µm. The spectral region from 100-3750 cm-1 was considered to include the interaction of H-O vibrations. The spectra were further processed using project four software to remove (linear) background noise.

4.0 Sample locations

The peridotites present in the S. Västerbotten area are all located along the boundary between the SNC and the KNC. While the peridotites are dominantly present in the lower part of the KNC several peridotite bodies are also present in the higher parts of the SNC. In the S Västerbotten area the peridotite bodies (in the lower KNC) are enveloped in gray phillites and quartzite whereas the the peridotites at the top of the SNC are enveloped in silliminite gneisses and amphibolites.

4.1 Aunere samples

Aunere is a large peridotite body located 20 km west of the Swedish town Kittelfjäl (fig 4.1, sample locations 1.1 through 2.4). It covers approximately 7 square kilometers and has a brown reddish appearance (due to Fe oxidation during the ice ages). It is clearly visible due to the strong resistance of peridotite against erosion. Several smaller peridotite bodies are located along a NE-SW trending orientation (fig 4.1).

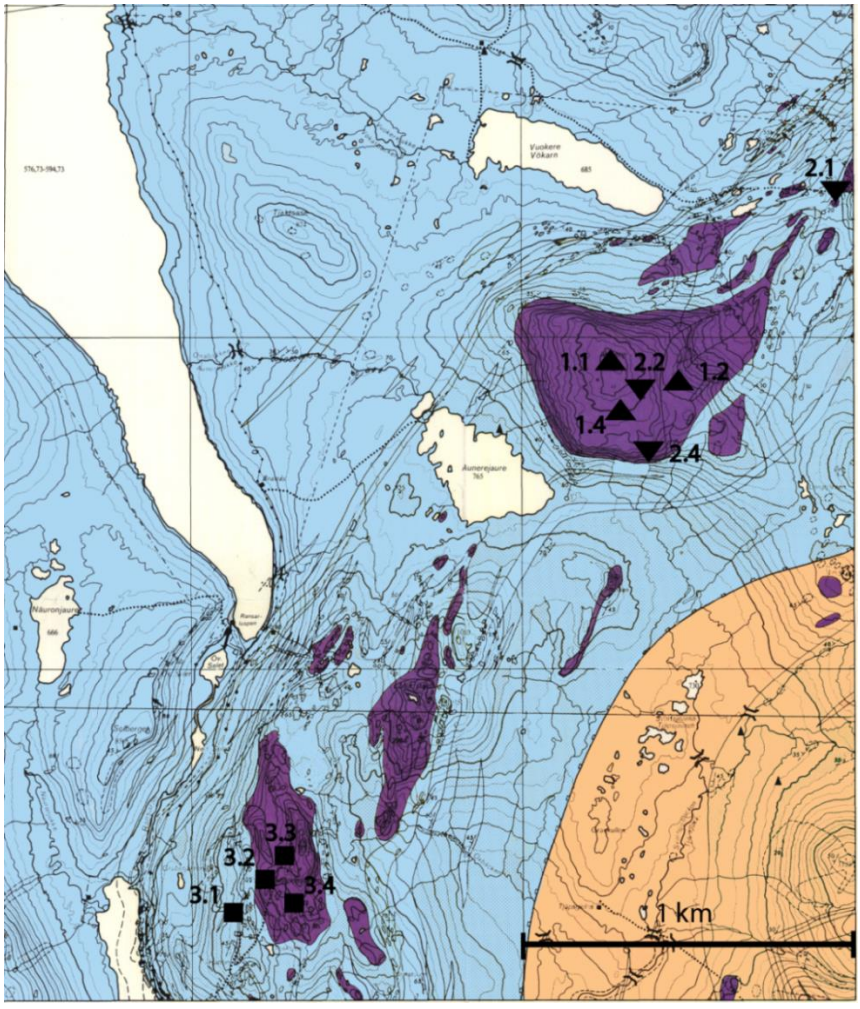

Figure 4.1. Aunere (top) and Grundfors (bottom) peridotites. Blue colours indicate Köli nappe, beige colours indicate Seve nappe. Enlargement of Fatmomakke 23F-NV from SGU and Trouw (1973). For larger scale map see figure 1.1.

.

The Aunere body is so large that a single description of the deformation structure is insufficient as deformation apparently did not always penetrate into the center of the body. However a foliation is present, denoted S_2, at the outer margin of the Aunere body and also present within the smaller bodies nearby. This foliation, 067/42N is roughly parallel to the strike of the body itself. The foliation within the enveloping country rock bends around the larger peridotite bodies (i.e. Aunere). The Aunere body itself is not completely structurally and chemically homogeneous. Mineralogical and chemical variations occur throughout the body indicating either primary layering (harzburgite and dunite), denoted S_0, or the variable extent of serpentinisation (varying from 30% to 100% serpentinisation).

Additionally some parts of the outer margin of the Aunere body show a distinct 'different' structure. Characterized by several larger pebbles separated by a different matrix (see fig 5.5).

The mineralogy of the Aunere peridotites vary greatly throughout the body and appear to be related to distance from the margin (% serpentinized) and/or variations in the primary composition (presence of OPX/CPX).

4.2 Grundfors and Röberget samples

The Grundfors body is half the size of the Aunere body surfacing for approximately 3 km^2 (fig 4.1, sample locations 3.1 through 3.4). Similarly to Aunere it forms a mountain due to its relative hardness in comparison with the surrounding meta-sediments and meta-volcanics. The foliation in the Grundfors body is more penetrative in nature due to the smaller size of the body. It is clearly visible in many of the outcrops. The foliation is orientated east-west, dipping north and south. In addition primary layering (S0) is also present in this body due to variation in harzburgitic and dunitic compositions but also in regions with a higher concentration of chromite. The serpentinisation in the Grundfors body is much more intense, resulting in a much darker colour of the rocks (fresh surface).

Rödberget is the smallest investigated peridotite body (fig 4.2, location 4.1), approximately 0.5 km^2 (figure 4.2 sample location 4.1). It shows intense deformation and has been completely serpentinized. In addition Rödberget is partly carbonatized, showing areas containing carbonate minerals.

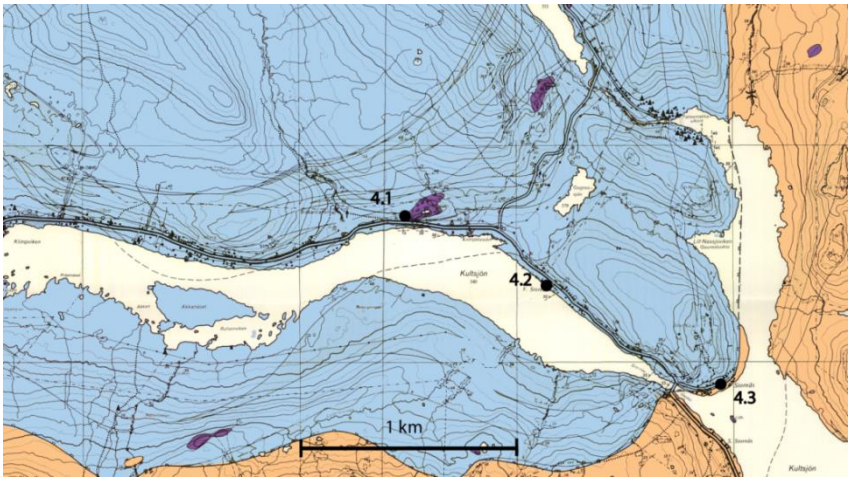

Figure 4.2. Rodberget sample locations. Blue colours indicate Köli nappe, beige colours indicate Seve nappe. Enlargement of Fatmomakke 23F-NV from SGU and Trouw (1973)

4.3 Other peridotite bodies in the (lower) Köli nappe

4.3.1 Raudfjellet

The Raudfjellet peridotite (fig 4.3 & 4.5) was initially identified as a greenstone and serpentine sequence (Törneböhme, 1896) outcropping along the boundary between the SNC and KNC. Foslie (1959) further defined the rocks present at Raudfjellet as a variation, or compositional layering, of peridotite, pyroxenite and gabbro. The Raudflellet exposure was first identified as an (fragmented) ophiolite sequence by Roberts (1997). They determined the internal structure of the sequence as ultramafics overlain by massive, layered metagabbros topped by doleritic dykes. At the top the (ultra)mafic sequence is unconformably overlain by an (ultra)mafic conglomerate. Roberts (1997) does not report the findings of pillow basalts, which are expected to be present on top of the doleritic dykes. The (ultra)mafic conglomerate contains a specific type of fossil which was present, latest, during the mid Arenig (478.6±1.7 Ma – 471.8±1.6 Ma) (Vogt, 1945 & Ryan et al. 1980). However Nillson et al. (2005) argues for a Cambrian to early Ordovician age with regard to the first deformation events present in the overlying metavolcanic sediments.

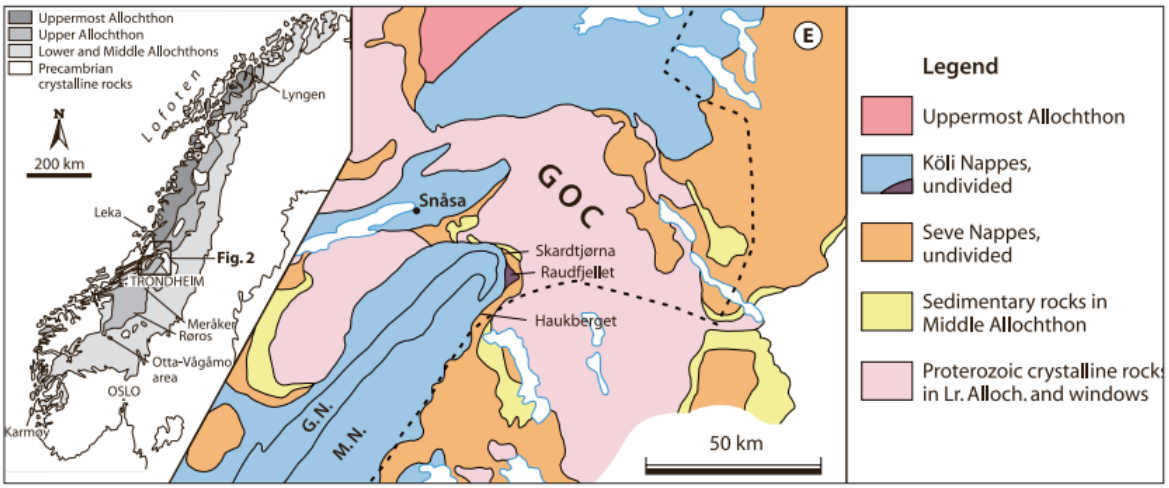

Fig. 4.3 Simplified tectonostratigraphic map of the region in the vicinity of Raudfjellet. E – eclogite locality ('middle nappe') in the Seve Nappes; GOC –
Grong-Olden Culmination; G.N. – Gula Nappe; M.N. – Meråker Nappe. After Nilsson et al. 2005.

4.3.2 The Händol and Otto-Vågåmo area.

The (ultra)mafic complexes at Händol and Otto-Vågåmo are situated at the same boundary between the SNC and KNC (fig 4.4). Most of the bodies present consist of only one (ultra)mafic component but some consists of several mafic components together (e.g. dunites (cumulates), gabbros, mafic (doleritic) dykes and plagiogranites) (Bergman 1993).

The internal structure of the bodies that contain several (ultra)mafic components are dunitic material overlain by fully reworked antigorite schist. These schists are overlain by cumulates of meta pyroxenites and meta gabbros. A mélange, consisting of the aforementioned (ultra)mafic components and an antigorite matrix, is present at the top of the sequence. The mélange is overlain by meta-(volcanic)sediments.

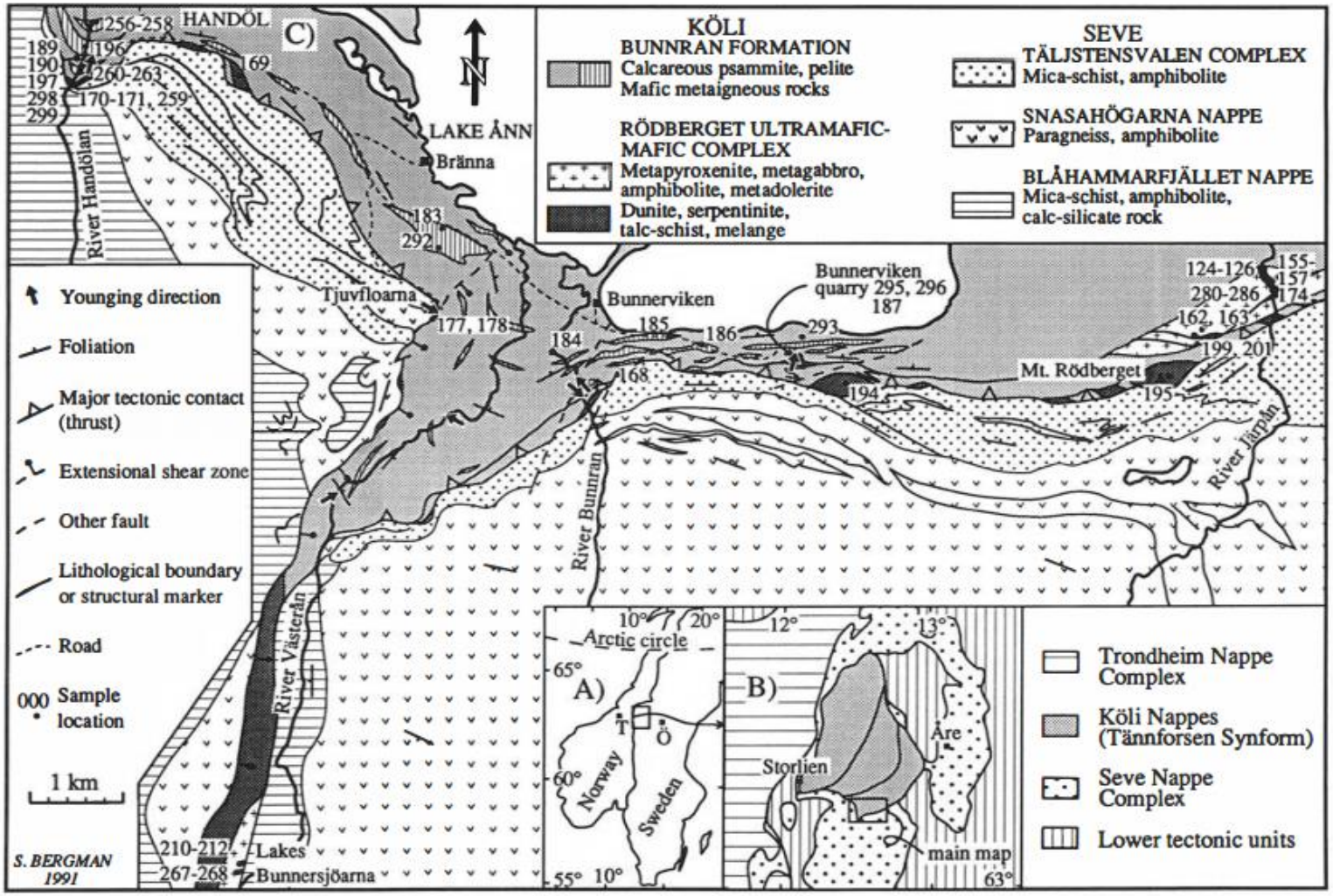

Fig 4.4. T =Trondheim, (j =Ostersund. A) Location of Tiinnforsen area indicated in B in scandinavia. B) Map of the Tiinnforsen area and surroundings, simplified after Gee & Sturt (1985) and Beckholmen (1984) (square indicates the the location of the geological map indicated at C). C) Geological map of the study area with sample locations. Most of the boundaries from the western part of the area are from Sjostrom (1983). Adapted from Bergman (1993).

Additionally Berman (1993) describes the olivine microstructure present within the dunitic part of the sequence. Large undulose olivine grains have recrystallized to smaller, strain free olivine grains with straight grain boundaries meeting in triple point junctions. This olivine microstructure is overgrown by several generations of serpentine and talc veins. The reddish brown chrome spinel which is present is partly altered to magnetite and associated with secondary Al-rich chlorite.

Bergman (1993) argues that the formation of the Rödberget ultramafic-mafic complex (part of the Händol and Otto-Vågåmo area) (fig 4.4) occurred within a oceanic basin coinciding with the formation of the overlying Bunnran Formation. Bergman (1993) proposes that during the formation of the oceanic crust fracture zones may lead to serpentinisation of underlying ultramafics forming serpentine diapirs and mélanges based on the work of Stigh (1979).

Sturt et al. (1991) determined the BRC (major and trace elements, see fig 5.11, 5.12 & table 5.3) of the Vågåmo Ophiolite (fig 4.4) (consisting of ultramafics at the base overlain by layered and isotropic gabbros overlain by gabbros with dykes, a sheeted dyke complex and finally poorly preserved pillow lavas). The BRC composition suggests a (almost) perfect N-MORB composition indicting either an ancient part of the Iapetus Ocean or a hardly contaminated oceanic crust at a marginal basin (Sturt et al., 1991).

4.3.3 Other smaller bodies along the Seve/Koli boundary.

A large amount of smaller (ultra)mafic bodies are present at the boundary between the SNC and KNC (fig 4.5) in central Jämtland, Sweden. Most of these bodies were first described by Foslie in his early notebooks (1930's). Nilsson & Roberts (2015) reused these notes and summarized Foslies findings in a modern setting.

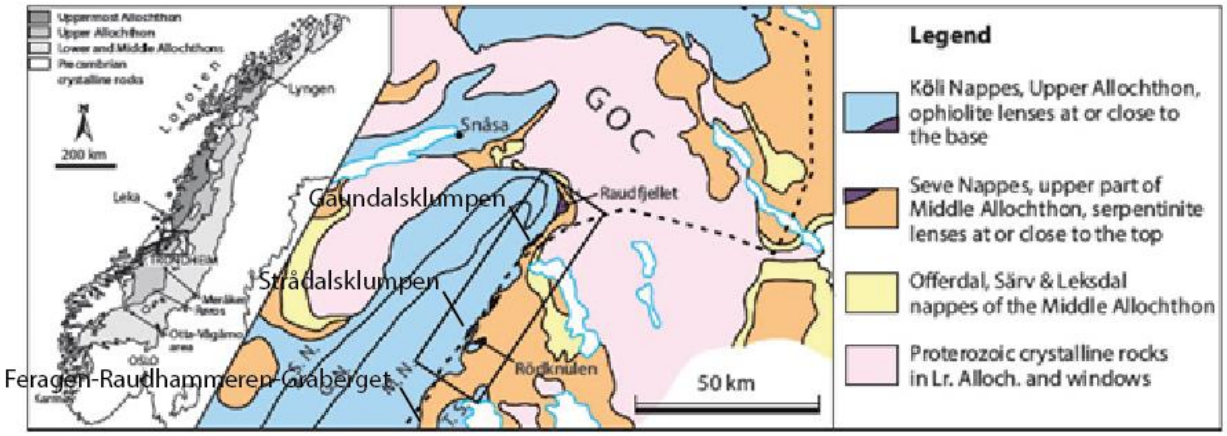

Figure 4.5. Simplified tectonostratigraphic map of the Raudfjellet region showing the locations of some of the ultramafic-mafic (ophiolitic) lenses discussed in the text. GOC –
Grong-Olden Culmination; G.N. – Gula Nappe; M.N. – Meråker Nappe; S.N. – Støren Nappe; T.S. – Tännfors synform. The grey-tone map to the left shows the location of
the main map, northeast of Trondheim, and the approximate position of the Otta-Vågåmo area southwest of Røros. After Nilsson & Roberts (2014).

The Gaundalsklumpen –Haukberger body consists of 50% harzburgite and 50% dunite. Metamorphism lead to large amphibole prisms in a green (serpentine) matrix derived from olivine and pyroxene (fig 4.5, located between Rödknullen and Raudfjellet). The body is overlain by a small gabbroic body at the northwestern part and an ultramafic conglomerate along the boundary with the overlying sediments.

The Stradalsklumpen body (fig 4.5, small body, located between Rödknullen and Raudfjellet) shows stronger serpentinisation near the margins. Tremolite has formed at the boundary witht the surrounding garnet-mica schist.

The peridotitic body at Feragen-Raudhammeren-Graberget (fig 4.5, small bodies, located south of Rödknullen) shows duplication as a result of internal thrusting. It consists of 25% harzburgite, 25% lherzolite and 50% dunite. The dunite shows regular layering.

Leka ophiolite

The Leka ophiolite is an almost complete ophiolite section within the higher parts of the KNC. It comprises all of the standard ophiolite sequence; ultramafic mantle rocks, layered ultramafics and metagabbros, minor acid intrusions, metabasalt dykes and volcanic and volcanoclastic rocks (including pillow basalts). U-Pb dating of zircons resulted in an age of 497±2 Ma (Dunning & Pedersen, 1988).

The relation between the ultramafic part of the Leka Ophiolite and surrounding rocks is different in comparison with the earlier mentioned ultramafic bodies as the underlying contact is not exposed (as Leka is an island) which makes its position within the KNC difficult. In addition all parts of the ophiolite are present which makes it rare within the bodies exposed at the KNC/SNC boundary. The mantle part of the ophiolite (disregarding the tectonite) shows compositional layering between wehrlites and dunites on three scales; large scale layering of 100's meter thickness, macro scale between 10 and 50 meter and on a 10-30cm scale. Metamorphism in the Leka Ophiolite is limited to (retrograde) greenschist facies resulting in serpentinisation within the ultramafics (20-100% serpentinisation).

The bulk rock compositions of several peridotites of the Leka ophiolite are included in the section dealing with the bulk rock compositions (section 5.5) and plotted in figure 5.11 and 5.12. The Leka samples turn out to be fairly depleted and similar to the samples collected during this work.

5.0 Results

5.1 Macro structure

The Aunere peridotite body, the largest of all bodies present in the S. västerbotten area, shows a primary layering (S0) defined by alternating layers of dunite and harzburgite (with variable thicknesses). Areas of (serpentinized) CPX are present in the harzburgitic layers (brownish areas in fig 5.1). The difference in composition is often hard to distinguish due to intense serpentinisation. In addition the Aunere peridotite body shows a distinct tectonic foliation (S2) oriented roughly 067/42N at the margins defined by serpentine minerals (D2 in fig 5.10). This S2 foliation becomes less pronounced towards the center of the body where eventually it becomes hard to observe. An earlier foliation (S1) can be recognized in the protolith assemblage (fig 5.1 white lines) defined by the elongation of (now reworked) protolith olivine grains. These orientations are determined using the optical extinction patterns of individual olivine grains. However this foliation was not observed in the field, therefore the exact orientation of this foliation is unkown. This S1 folation may be sub-parallel to the compositional layering.

The edges of the Aunere body show a brecciated/tectonized appearance in the field. This appearance is also present within the smaller bodies located northeast of the Aunere body (fig 5.5). These structural characteristics have not been found within the other investigated peridotite bodies.

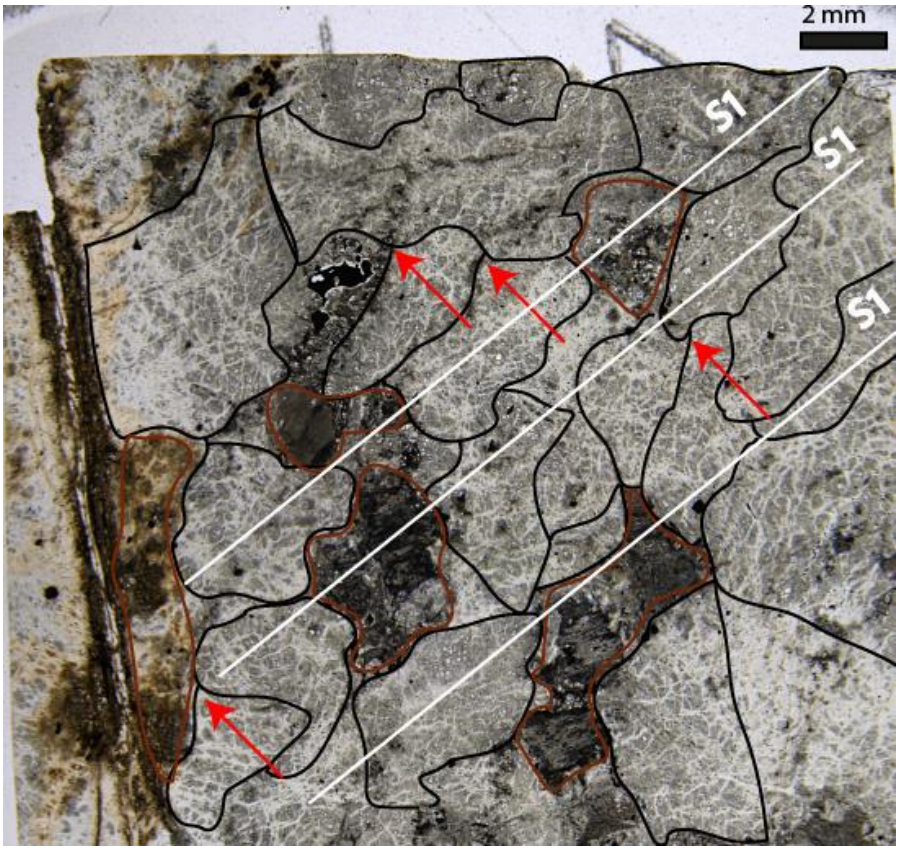

Figure 5.1. The protolith olivine microstructure of sample 1.4. The grain boundary configuration (black lines in optical image) are determined using the optical extinction of individual olivine grains. Red arrows indicate former triple junctions. Brown bordered zones indicate former OPX grains.

5.2 Microstructures

5.2.1 Protolith microstructure

The protolith microstructure of olivine was determined using the extinction pattern of olivine and optical microscopy techniques in relatively unaltered samples of the Aunere peridotite (fig 5.1). These olivine crystals, if recrystallized, show a pseudomorphic texture. This pseudomorphic texture results in a similar extinction pattern of separated olivine grains (altered during later serpentinization) that were once part of the same (protolith) olivine grain. This pseudomorphic texture is typical for lowgrade, retrograde serpentinisation in serpentinites (Wicks & Whittaker, 1997). The microstructure consists dominantly of olivine, up to a cm in size. The olivine grains are slightly elongated (fig 5.1) but show no relation to the S2 foliation (no foliation present in this sample). The grainboundaries of the protolith olivine tend to be straight or are gently curved. In some cases relics of triple points are present (fig 5.1, red arrows). This olivine microstructure is indicative for protolitic conditions in the mantle (lithosphere). These relict olivine grains form a foliation (S1) illustrated in figure 5.1 by white lines.

5.2.2 Secondary olivine microstructure and veining

Veins are present throughout all samples in different forms and are likely to be the result of different deformation phases. These veins may reflect different metamorphic mineral assemblages. If a vein starts growing under low T serpentine conditions it may, during prograde metamorphism, grow and (possibly) recrystallize (from the center outwards) different mineral assemblages associated with higher grade metamorphism. Therefore the internal structure of these veins may be very complicated. There are 3 types of veins present. The 3 types of veins can be distinguished by their mineral content. The most easily distinguished veins, for example in sample 1.4, show a complex internal structure. The center of the vein (fig 5.2 & 5.3) consists of serpentine (in elongated needles, A in fig 5.2 & 5.3) with a mixed layer of serpentine and olivine next to it (B in fig 5.2 & 5.3) . Further toward the margin thin layers of pure magnetite alternate with a layer of olivine (C in fig 5.2 & 5.3).

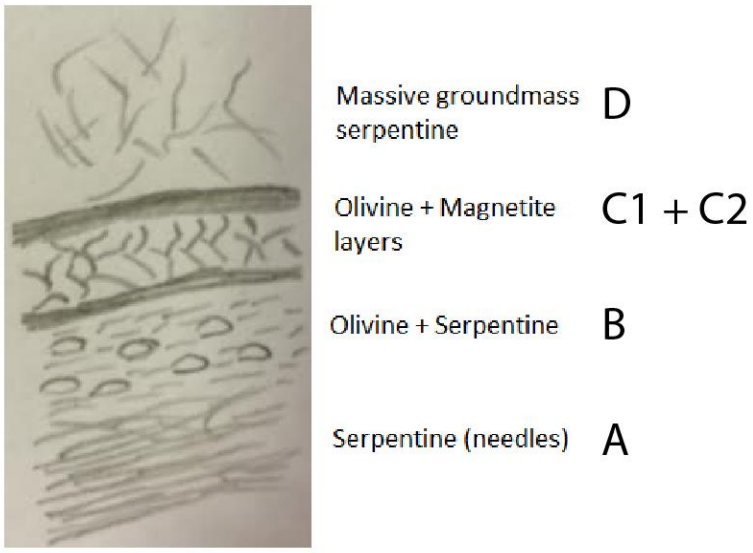

Figure 5.2. Sketch of the vein structure in sample 1.4 consisting of a serpentine core (A), serpentine + olivine layer (B), an olivine layer (C2) and pure magnetite layers (C1) surrounded by the massive groundmass serpentine (D).

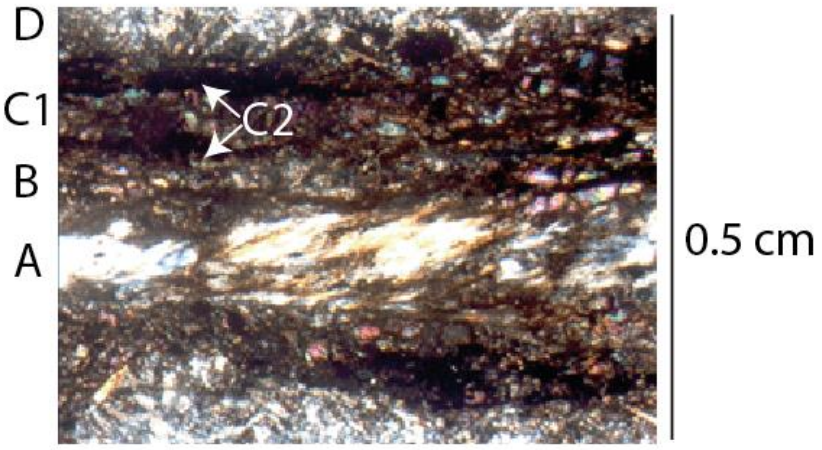

Figure 5.3. XPL view of the vein in sample 1.4 which shows (less clearly) the different zones of the vein. Vein is 2 mm thick. (A, B, C, D represent the same constituents as fig 5.2)

In the less altered samples of the Aunere peridotite body veins show a different structure (fig 5.4). These olivine veins are characterized by less variation. The olivine in the center of the veins has the same chemical composition as the olivine matrix. This chemical similarity is likely due to the low amount of serpentinisation in contrast to the samples from other bodies and the margin of the Aunere body. The margins of the olivine veins are often dominated by magnetite grains (fig 5.4). These olivine grains probably underwent brittle grain size reduction at low temperature conditions.

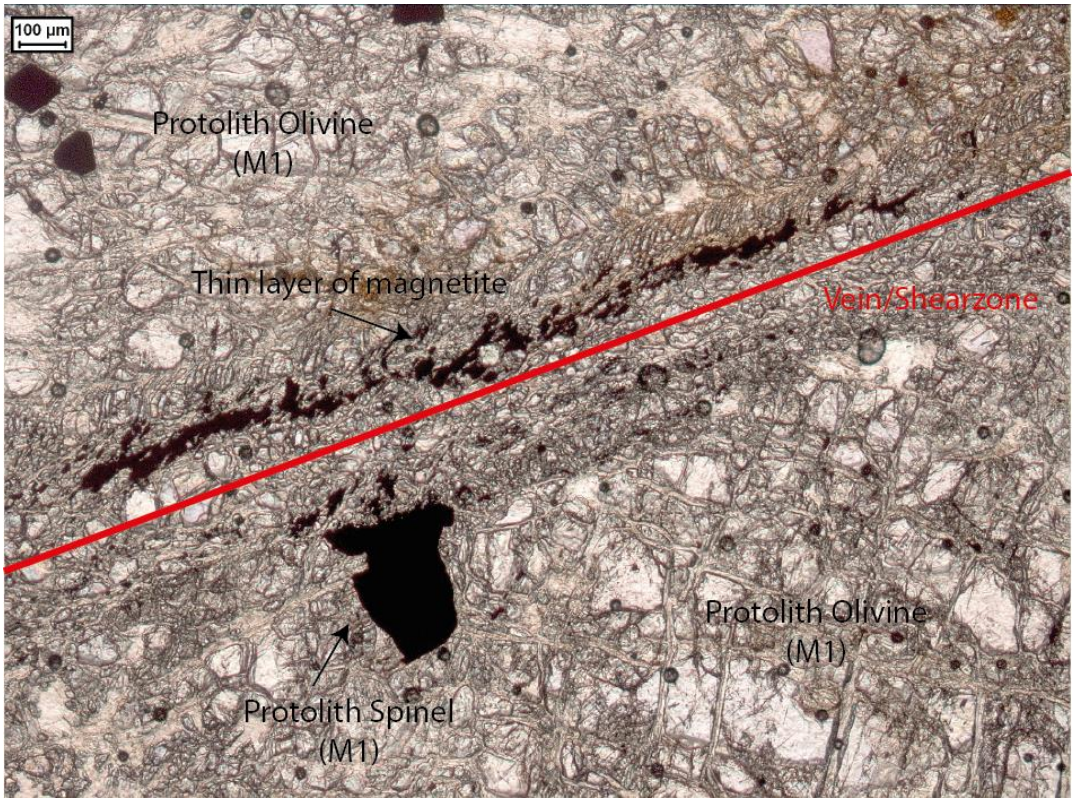

Figure 5.4. PPL view of a Shear zone/vein in a relatively unaltered sample (1.1). The NE-SW running vein/shearzone includes a thin magnetite layer at its margin in.

Finally there are veins in many of the samples that consist of underformed olivine grains (M3 olivine, see section 5.3) (significantly larger then those in sample 1.1) (Appendix 11.1, sample 2.1b1). These veins contain no serpentine, although serpentine may have overgrown the vein in a later metamorphic stage or serpentine may be present as inclusions in large olivine grains (fig 5.6C).

Some of the samples (sample 2.2 A through D) near the margin of the Aunere peridotite show a distinct 'different' microstructure, which is also clearly present on the macro scale (figure 5.5).These samples are made up of clasts with a different mineral essemblage between the clasts. The clasts size ranges up to 2 cm, individual clasts are fairly unrounded and elongated. The clasts themselves consists of serpentine however they are welded together by seams that consist of olivine (M3) (see section 5.3.3 M3 metamorphism).

Both of the vein types filled by (almost exclusively) olivine may have formed during hydraulic fracturing of the rocks (in a brittle environment). The water present during hydraulic fracturing may have assisted with the transportation of chemical constituents needed for the formation of olivine. This could also explain the lack of these types of (veining) structures in the centre of the Aunere body as deformation may not have penetrated to the center of the body.

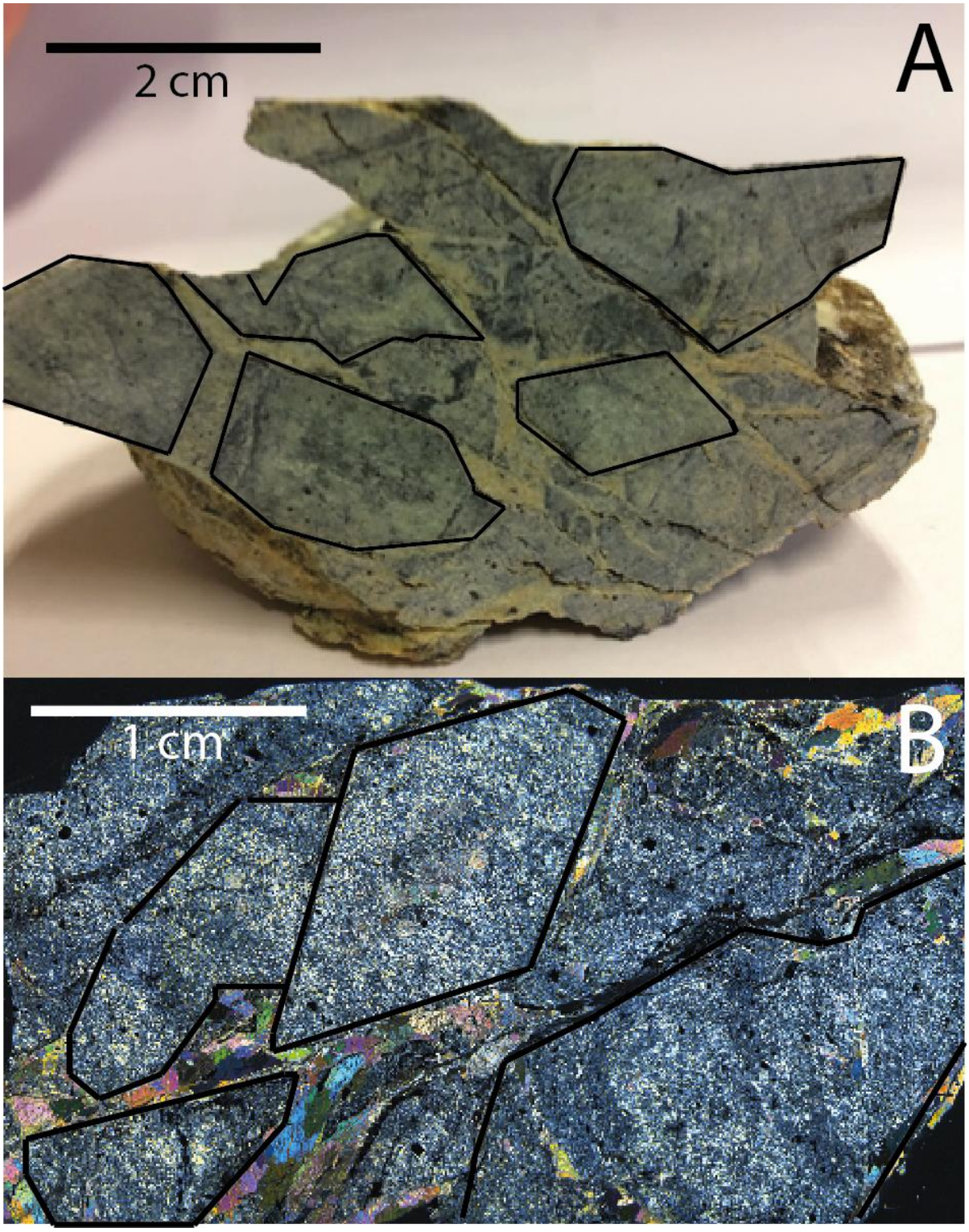

Figure 5.5. A) Sample 2.2b2 showing a 'cataclatic' structure with clasts of serpentine (black lined) (+- M3 olivine) surrounded by well-developed olivine bearing veins (greenish veins). B) A XPL view of sample 2.2b2 with clasts of serpentine (black lined) (+- M3 olivine) surrounded by well-developed olivine bearing veins (second order interference colours in the veins).

In summary there are several deformation phases expressed as different structures. The oldest structures, primary layering between harzburgite and dunite, are observable in areas that have not undergone intense deformation (S0, center of Aunere). A primary foliation (S1) is present as an elongation of protolith olivine grains but was not observed at a macroscale. A foliation defined by serpentine in present (067/42N) and defines the macro foliation seen in the field (S2). Several veining structures are present. Veins filled with serpentine which are thought to be related to the same deformational event that formed the S2 foliation, which may have grown during later metamorphic events. A different type of vein, filled with (mostly) M3 olivine, is thought to be the result of hydraulic fracturing of the rocks.

S0	Layering between harzburgite and dunite.	
S1	Elongation of protolith olivine (M1).	D1
S2	Foliation defined by serpentine minerals (M2).	D2
Vein (concurrent with S2)	Veins formed by serpentine (M2) which may have grown during later metamorphic /deformation events.	D2
Hydraulic fractured veins	Veins formed during hydraulic fracturing in a brittle environment (M3).	D3

Table 5.1 Deformation structures and phases.

5.3 Metamorphism

The orogenic peridotites of the lower Köli nappe appear to have a complex metamorphic history. The protolith esemblage (M1) which refers to a stable mantle mineralogy, a mantle peridotite, is replaced during the emplacement period by the first serpentinization phase (M2). The M2 serpentinization phase is overgrown by a (spinifex) olivine dominated esemblage (M3) associated with prograde metamorphism. Finally the M3 mineral assemblage is overgrown by a second (and final) serpentinization event with minor amounts of magnesite (M4).

M1	Protolith
M2	First serpentinisation phase (lizardite + brucite + chlorite + magnetite and later antigorite)
M3	Peak metamorphism (olivine stability, spinel and minor antigorite)
M4	Second serpentinisation phase (antigorite + magnetite + magnesite)

Table 5.2 Metamorphic phases.

5.3.1 M1

In the Aunere samples the M1 mineral assemblage consists of M1 olivines ranging in size from mm to cm sized grains. The M1 olivine crystals are deformed, fractured and heavily replaced by later stage mineral assemblages (M2 and M3) (fig 5.6A). However the size of individual olivine grains may still be recognized by their similar extinction pattern (fig 5.6A) outlining the microstructure of the primary protolith assemblage (figure 5.1). In addition the M1 assemblage contains spinel grains which may be up to a ½ a cm (fig 5.6C). These M1 spinels often show a distinct reaction rim formed during later metamorphic events (M2-M4) (fig 5.6B and 5.6C). Primary M1 spinels can still be recognized by their dark red core color opposed to the black color indicative for the later modified metamorphic spinel. Some of the samples contain a significant amount of CPX, their size ranges from mm to cm (fig 32D). The presence of CPX is dependent on the primary bulk rock composition of the peridotite sample. As noted by Zwart (1974), the Aunere peridotite contains a primary compositional layering (S0) defined by alternating dunitic and harzburgite/lherzolite compositions. Exsolution lamellae, present in CPX, indicate a high temperature subsolidus environment, and are therefor interpreted subsolidus mantle modifications related to M1.

The primary M1 olivine (and possibly CPX/OPX) in the Gründfors and Röberget samples is no longer present and has been completely replaced by a later serpentinisation event (M2 & M4). In contrast, M1 spinel is still present and can easily be recognized by the deep red colour of their cores using optical microscopy (and their chemistry, see section 5.6.2).

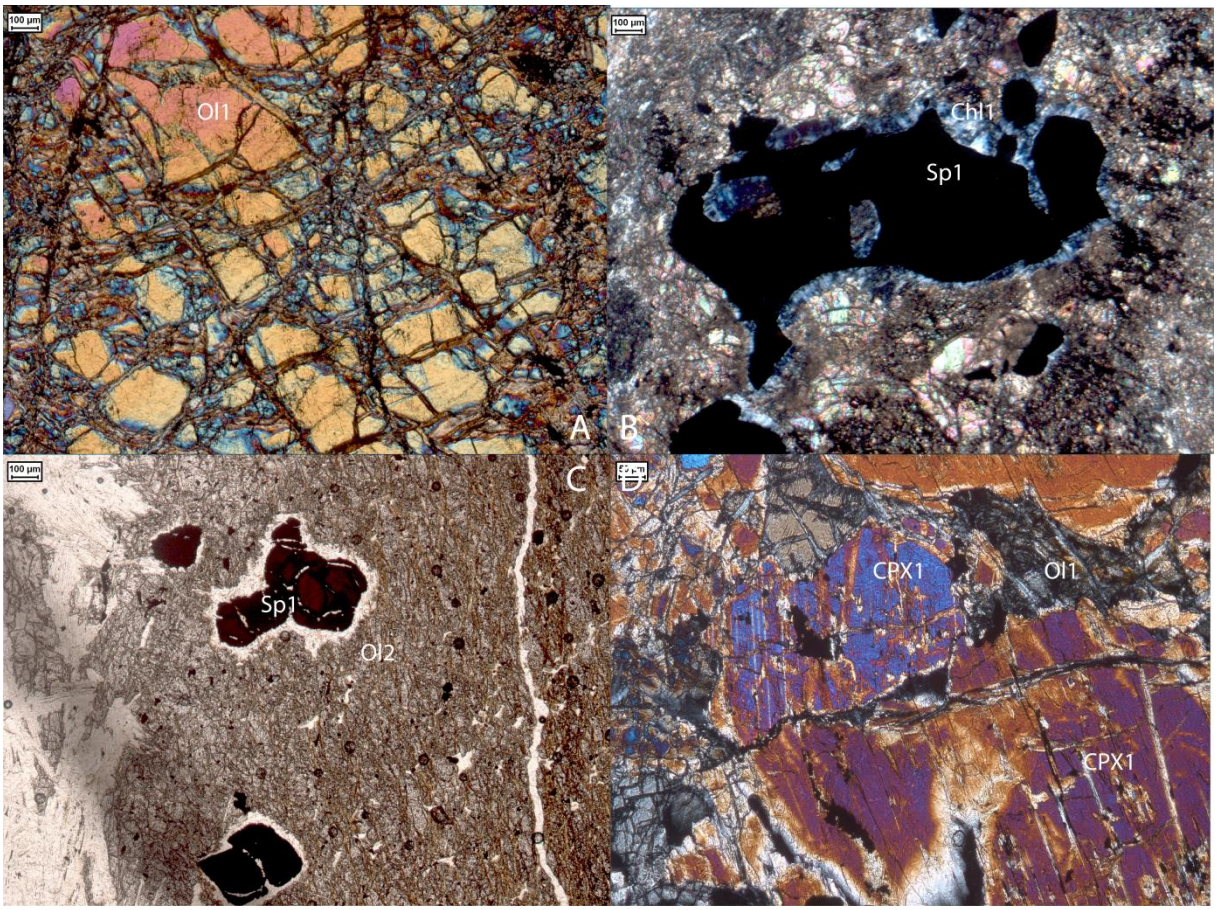

Figure 5.6. (A) XPL view of M1 olivine with minor replacement by M2 serpentine, sample 1.1. (B) XPL view of M1 spinel with a blueish chlorite reaction rim, sample 1.4. (C) PPL view of M1 spinel with clear deep red cores, black rims surrounded by transparent chlorite at the margin with the matrix, sample 3.4.2. (D) XPL view of M1 CPX surrounded by M1 olivine and minor serpentine, sample 2ext2.

5.3.2 M2

In the Aunere samples the M2 mineral assemblage consists of serpentine, present as channels and thin layers within and between M1 olivine crystals (fig 5.6A). The observed serpentine texture shows a pseudomorphic mesh structure (fig 5.6A). The mesh rims are formed by lizardite whereas the mesh cores are occupied by M1 olivine (fig 5.7A & fig 5.6A). Brucite is present between the lizardite grains. The brucite grains are fine grained, between a few µm to mm's (fig 5.7C). In addition M2 spinel is present as nearly pure magnetite minerals. The M2 magnetite grains are small grained, never larger than a few mm. They are spread out throughout the serpentinized matrix and are present in 'channels' where olivine has been replaced by serpentine. In addition the reaction rims around M1 spinel are related to the M2 serpentinisation phase where the spinel compositions have been altered by chlorite minerals (fig 5.6 B+C).

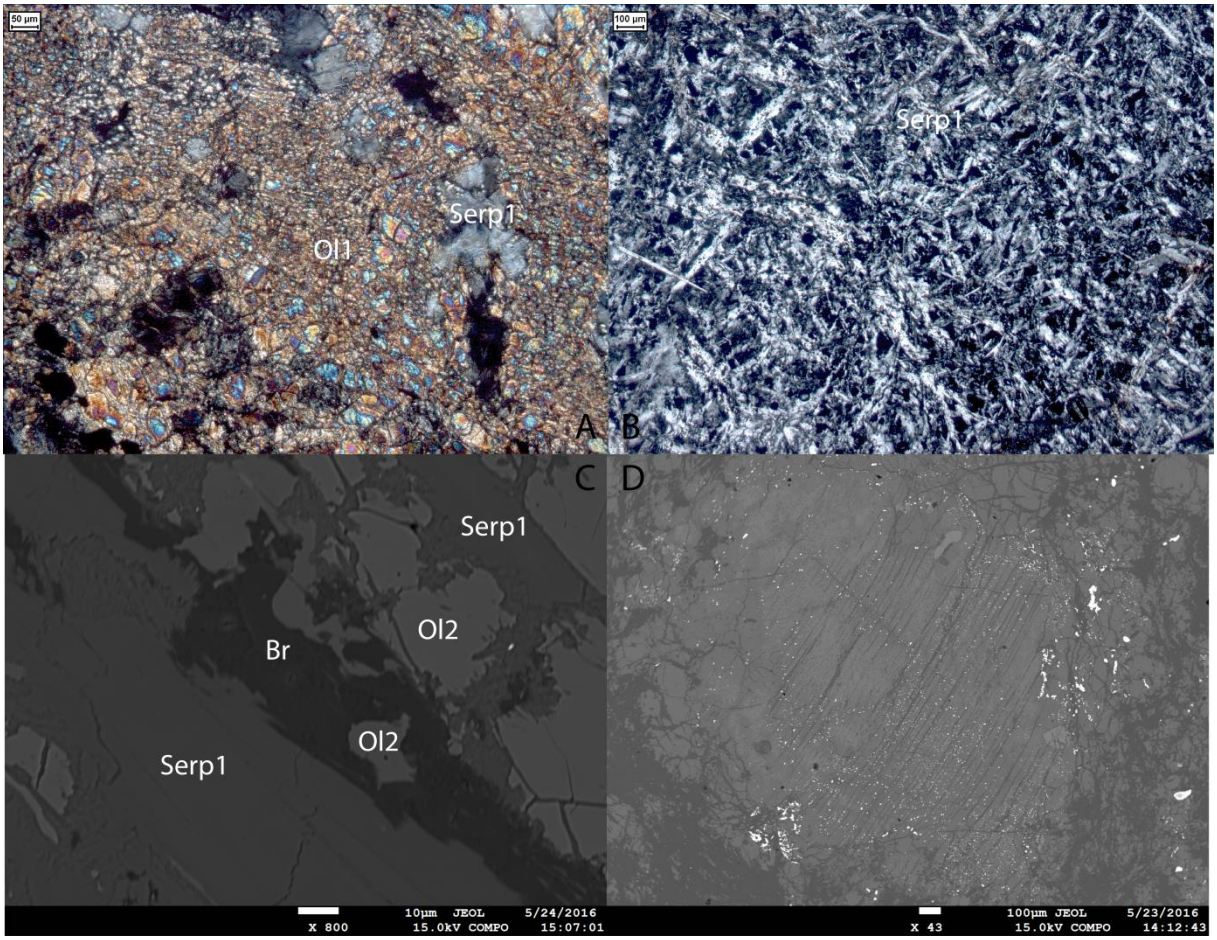

Figure 5.7. (A) XPL view of serpentine overgrowing M1 olivine, sample 1.1. (B) XPL view of the interpenetrating M2 serpentine matrix, sample 3.4.2. (C) Backscatter electron image of brucite overgrown by M3 metamorphic olivine, sample 3.4.1. (D) Backscatter electron image of bastite (replacement of pyroxene by M2 serpentine retaining exsolution lamella).

In the Gründfors and Röberget samples (samples 3.## and 4.##) the first serpentinisation phase has been so effective that the samples have been reworked entirely resulting in a mineral assemblage that is consistent with the M2 conditions. In this case the growth of the serpentine is less limited by the channels through the M1 olivine. The M2 serpentine grains are on µm scale but are hard to distinguish separately. Small µm scale brucite grains are located between the serpentine grains. Several samples show an intergrowth of M2 serpentine and M2 tremolite in finely layered zones. These intergrowths are known as bastites, the serpentinisation product of orthopyroxene where the distinct layering of serpentine (replaced OPX) and tremolite (replaced CPX) is a result of the primary exsolution pattern in M1 CPX (fig 5.7D). In addition these samples also show small grained opaque mineral grains, which consist completely of magnetite (fig 5.7 B).

In all samples rare Fe-Ni alloys have been found which are characteristic for serpentinites as both elements are present in olivine in contrast to serpentine which can not contain much of either Fe or Ni. The FeNi alloys are often small grained (up to a mm). They share all their characteristics with magnetite and therefore cannot be identified by optical microscopy but only by chemically means.

5.3.3 M3

In the samples from the center of the Aunere body the M3 metamorhpic event is present as metamorphic olivine which turns out to be chemically similar to the M1 olivine (see section 5.6.1) as a result of the lack of serpentinization. However here the M3 olivine crystals are much smaller in size (µm to mm scale) and show much less internal deformation. These metamorphic M3 olivine grains are localized in patches and/or along shear zones (fig 5.8C & 5.8D).

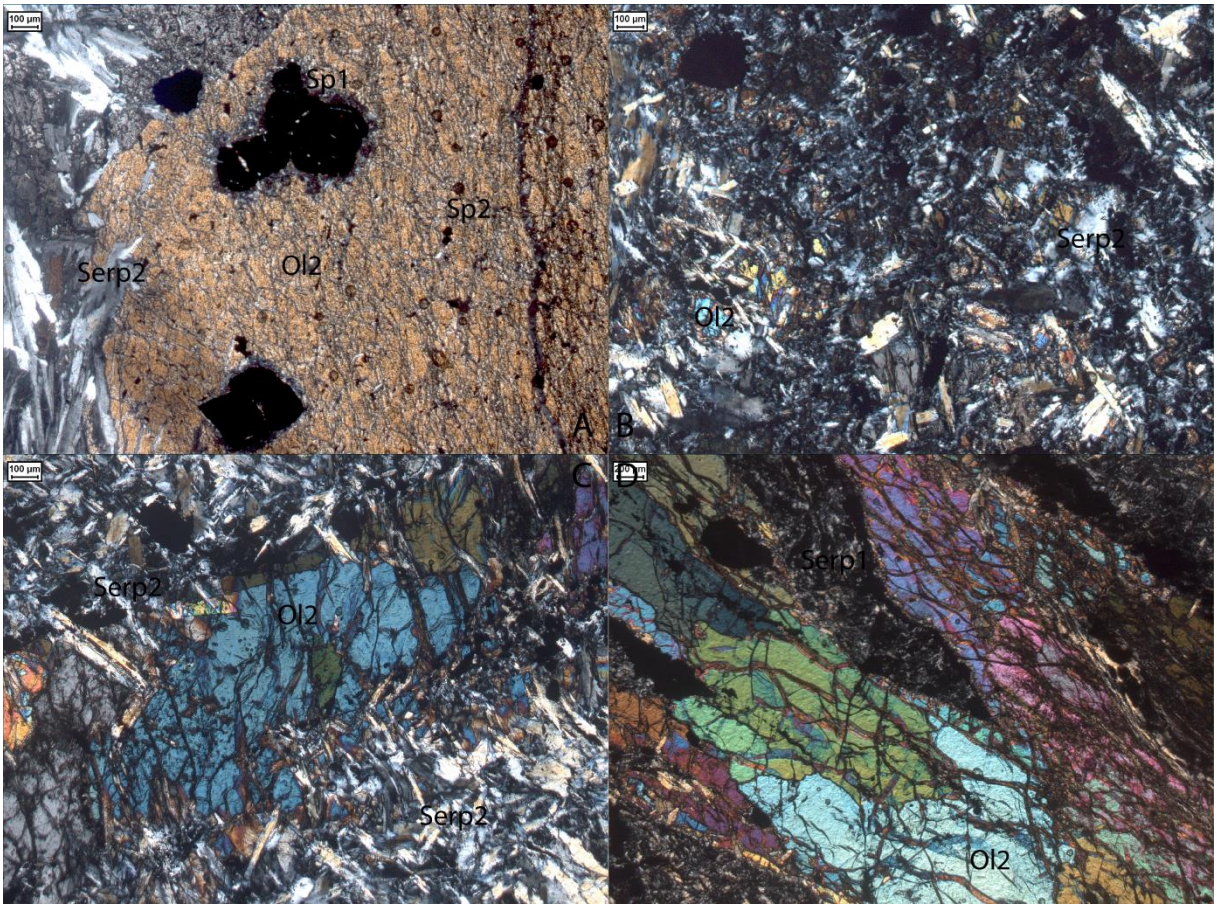

Figure 5.8. (A) XPL view of M3 olivine with M1 spinel, sample 3.4.2. (B) XPL view of M3 Ol in matrix overgrown by M4 serpentine, sample 2.1b1. (C) XPL view of elongated M3 olivine in between clasts of serpentinized (M2) tectonite, sample 2.1b1. (D) XPL view of elongated M3 olivines growing within veins that are partly modified by serpentine (M4), sample 2.1b2.

The samples (2.1B1, 2.1B2) taken at the margin of the Aunere body show a distinctly different microstructure of M3 olivine grains. Here, M3 olivine grains are much larger ranging in size up to a cm (fig 5.8D). These M3 olivine grains are located between the serpentinized clasts (consisting of M2 and M4 serpentine) as well developed, relatively unaltered grains. In addition they may occur inside the clasts in which case they are more altered by the M4 serpentinization event.

In the Gründfors and Röberget M3 is reflected in metamorphic olivine grains. These grains are coarse, on a mm to cm scale (fig 5.8A). M3 olivine grain boundaries are often straight ending in triple junctions. Inclusions of M1 spinel cores are occasionally present in these olivine grains (fig 5.8A).

5.3.4 M4

In the Aunere samples the M4 serpentinisation phase has modified the microstructure of samples from various locations differently. Samples near the core of the body show little of this second serpentinization event and are only moderately afflicted by flakey serpentine grains in patched areas. However the samples near the margin of the Aunere body, including the tectonite (sample 2.2.2b), show distinctively more serpentinization. Firstly M3 olivine and M4 serpentine show a mesh structure which is not as well developed as the M2 mesh structure. In addition relatively large (mm scale) antigorite grains overgrow all previous structures characteristic for the M4 metamorphic event (fig 5.9B).

The Gründfors samples show a distinct serpentinisation phase as M4, where the new serpentine grains overgrow the M2 serpentine groundmass and the M3 olivine porphyroblasts. The new serpentine grains can grow up to a few mm long and are all elongated. In addition M3 olivine shows a mesh structure with serpentine but is not as well developed as during the M2 serpentinisation phase.

Several samples (3.3A, 3.2C, 2.1) show considerable amount carbonized minerals, it is, in general, magnesite but small amounts of calcite are also present (fig 5.9C).

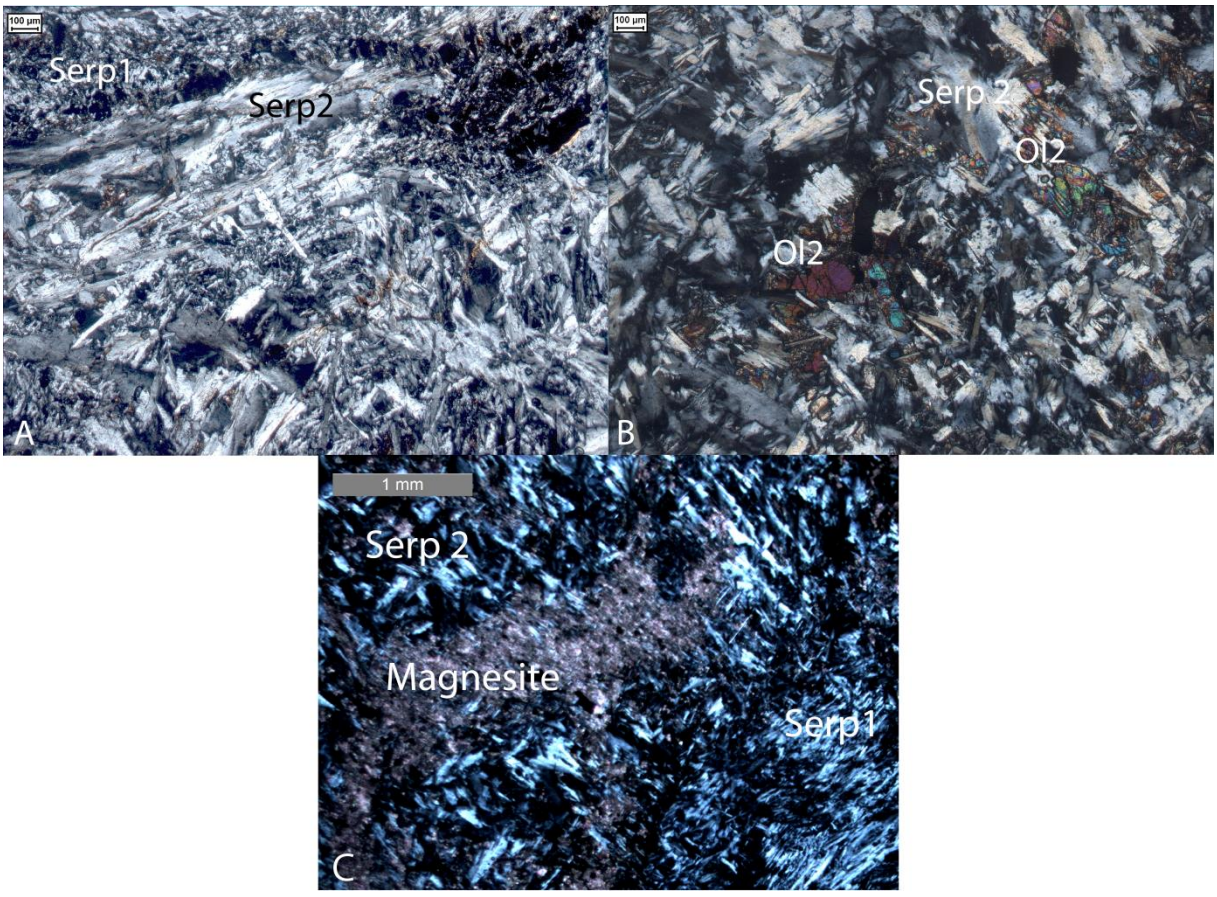

Figure 5.9. (A) XPL view of the growth of M4 serp over M2 serp, sample 3.4.2. (B) XPL view the growth of M4 serp over M3 olivine, sample 2ext2. (C) XPL view of M4 Magnesite over M2 Serpentine in combination with M4 serpentine, sample 3.2C.

5.4 Paragenetic diagram

In conclusion the metamorphic phases (M1, M2, M3 and M4) are shown in figure 5.10 with a primary mineral assemblage of olivine + chromite +- OPX +- CPX. M2 consists of early lizardite, later antigorite + chlorite (near chromite) + brucite + magnetite. The M3 phase is characterized by Olivine +- antigorite and the M4 phase consists of antigorite + magnetite +- magnesite. Additionally the deformation phases presented in table 1 are interpreted as being coinciding with the first three metamorphic phases where M1 concides with D1, M2 coincides with D2 and M3 coincides with D3 (corresponding structures are defined in table 1).

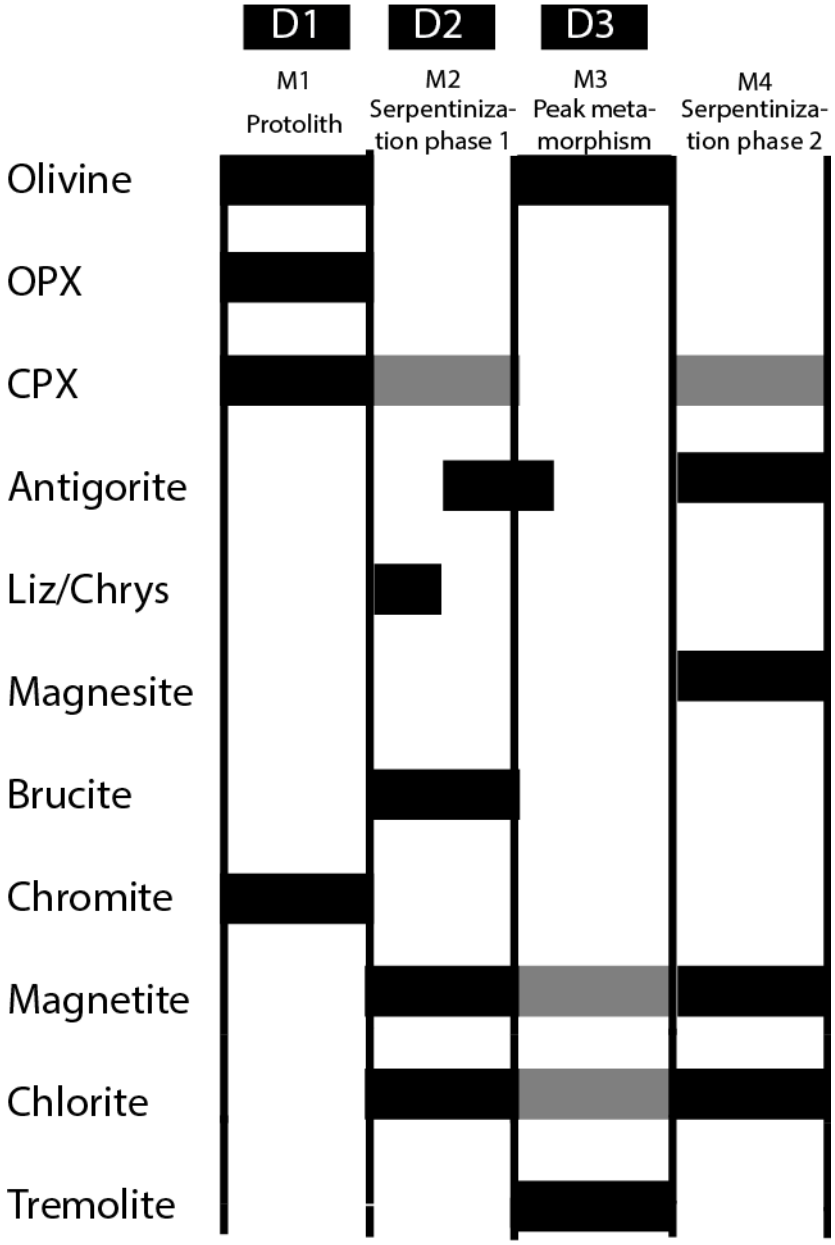

Figure 5.10. Paragenetic diagram of some lower Koli peridotites.

5.5 Bulk rock chemistry

The bulk rock composition (BRC) of sample 3.2A and 1.1 are shown in table 5.3. The analyses were done by XRF at Utrecht University (see section 3). In addition the BRC of 2 samples collected and analyzed by Du Rietz (1935), 3 samples by Bergman (1993), 6 samples by Furnes (1991), 4 samples by Stigh (1979) are shown and 4 characteristic peridotite samples from different tectonic settings by Deschamps (2012) are shown. Sample 3.2A was chosen for its intense serpentinisation whereas sample 1.1 was taken because it shows the least alteration by metamorphism, metasomatism and erosion. An approximate increase of 0,5 wt% Al_2O_3 is present between unserpentinized and serpentinized samples but this difference may be related to the protolith composition. Overall the lower Koli peridotites have a very depleted BRC character with very low Al_2O_3 and CaO contents (fig 5.11). In addition the TiO content is relatively low.

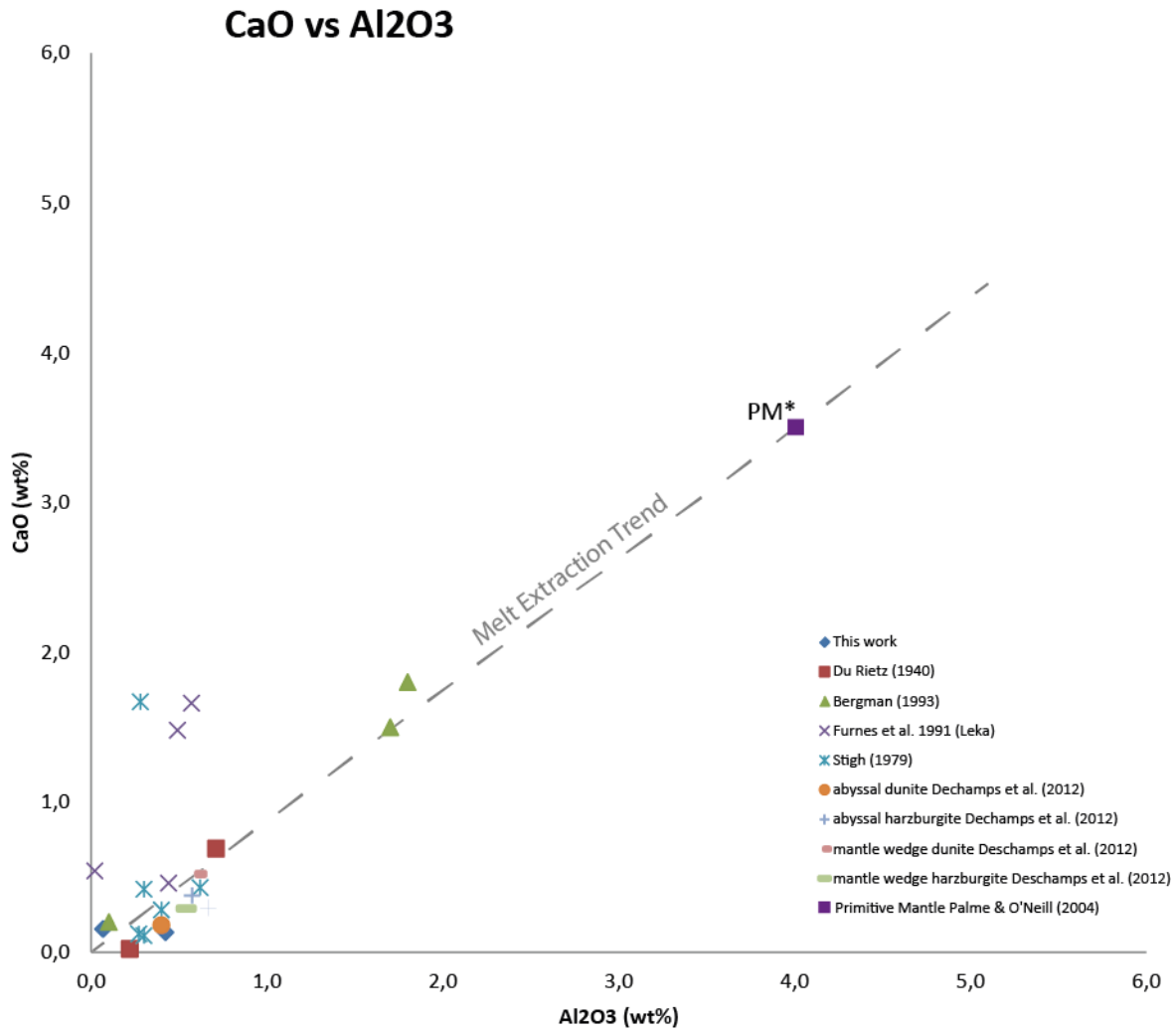

Figure 5.11. CaO vs Al_2O_3 trend in orogenic peridotites (dunite and harzburgite) of the lower Köli nappe. The origin of the dataset is given in the index, additionally the value of Dechamps represents an average for selected peridotite types.

Additionally all lower Köli peridotites show this depleted melt characteristic in their MgO, CaO and SiO_2 content (fig 5.12).

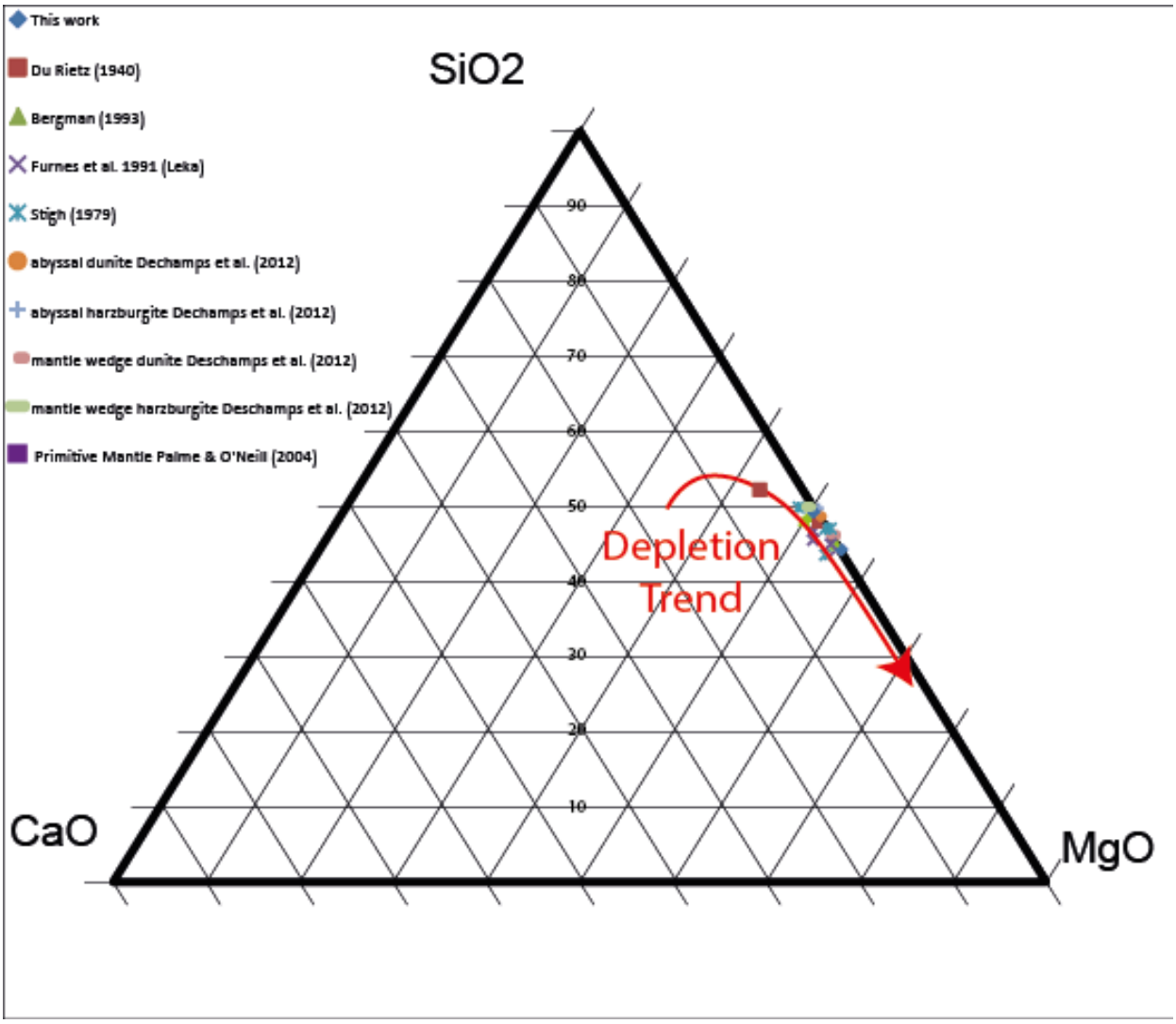

Fig 5.12 Ternary diagram showing SiO_2, MgO and CaO content in the bulkrock samples shown in figure 5.11. Red arrow shows depletion by intial melt extraction of CPX followed by the melt extraction of OPX.

Table 5.4 shows the concentrations of trace elements obtained for sample 3.2A and 1.1. Other elements were measured but were either below the measurement threshold or not present. The trace elements measured in this work are insufficient to produce meaningfull discrimination diagrams. A more accurate trace element analysis method is needed to properly characterize the bulk rock trace element chemistry of the presented samples. Additionally the trace element chemistry of specific minerals (serpentine & CPX) could be of further use in order to characterize these orogenic peridotites.

Article	Du Rietz 1935		Bergman 1993			Furnes 1991						Stigh 1979				This work	
Sample location	Junster-Klumpen	Vuoka Ruopsok	Handol 1	Handol 2	Handol 3	T1.20	P39	T2.11	P21	V29	V14	V40	R103	R106	RR36	3.2A	1.1
SiO2 (wt%)	40,5	43,1	40,4	43,2	43,0	41,6	42,5	40,1	40,7	38,7	36,5	36,9	40,3	39,6	39,8	41,2	39,6
TiO2 (wt%)	0,0	0,0	0,0	0,0	0,0	0,0	0,0	0,0	0,0	0,3	0,2	0,1	0,3	0,3	0,3	0,0	0,0
Al2O3 (wt%)	0,2	0,7	0,1	1,8	1,7	0,5	0,6	0,4	0,0	0,3	0,4	0,3	0,6	0,3	0,3	0,4	0,1
Cr2O3 (wt%)	0,4	0,7	0,6	0,4	0,3	0,4	0,5	0,4	0,5	0,4	0,7	0,2	0,4	0,3	0,3	0,3	0,4
Fe2O3 (wt%)	2,0	1,4	8,4	8,7	8,8	10,9	10,9	12,7	12,5	7,0	6,9	8,6	6,1	7,7	7,2	5,1	7,5
FeO (wt%)	4,9	6,7															
MnO (wt%)	0,1	0,0	0,1	0,1	0,1	0,2	0,2	0,2	0,2	0,1	0,1	0,1	0,1	0,1	0,1	0,1	0,1
MgO (wt%)	49,3	45,7	50,7	44,4	43,5	45,1	45,8	46,4	47,6	41,5	41,9	42,2	40,0	43,7	44,5	41,1	45,9
CaO (wt%)	0,0	0,7	0,2	1,8	1,5	1,5	1,7	0,5	0,5	0,4	0,3	1,7	0,4	0,1	0,1	0,1	0,2
NiO (wt%)	-	-	0,3	0,3	0,2	0,3	0,3	0,4	0,5	0,3	0,2	0,3	0,3	0,3	0,4	0,3	0,3
Na2O+K2O (wt%)	2,1	0,4	0,3	0,1	0,1	-	-	-	-	0,1	0,5	0,6	0,8	0,9	0,9	0,0	0,0
P2O5 (wt%)	-	-	0,0	0,1	0,1	-	-	-	-	-	-	-	-	-	-	-	-
total	99,7	99,4	101,2	100,9	99,3	100,4	102,3	100,9	102,4	89,1	87,5	91,1	89,4	93,3	93,9	93,3	99,7
LOI	-	-	1,3	6,1	18,4	9,3	10,0	12,7	12,7	-	-	-	-	-	-	6,7	0,3
CO2	-	-	-	-	-	-	-	-	-	6,9	7,4	6,8	6,7	2,1	2,0	-	-

Table 5.3. XRF derived bulk rock chemical composition of investigated peridotites (in wt%) by Du Rietz, 1935 (Junsterklumpen and Vuoka Ruopsok), Bergman, 1993 (Handol area), Furnes et al., 1991 (Leka), Stigh, 1979 (Vasterbotten area) and this work (3.2A and 1.1).

	I	Au	Ag2O	Am2O3	BaO	CeO2	Co2O3	Cs2O	CuO	Er2O3	HgO	La2O3	Nd2O3	OsO4	P2O5
3.2A	0,0203	0,0163	0,0028	0,002	0,0409	0,0045	0,0124	0,0282	0,0025	-	-	0,0051	0,0027	0,0037	-
1.1	0,0195	0,0174	0,0056	0,0011	0,0342	-	0,013	0,0289	-	0,0017	0,0013	0,001	-	-	0,0018

	P2O5	PtO2	PuO2	RbO2	Sm2O3	SO3	SrO	Tb4O7	TeO2	V2O5	WO3	Yb2O3	ZnO	ZrO2
3.2A	-	0,0111	0,0035	0,0009	0,0047	0,2023	0,002	0,0042	0,0046	0,0059	0,0115	0,0048	0,0059	-
1.1	0,0018	-	0,0034	-	-	-	0,0022	0,0061	0,0059	-	0,005	0,0015	0,0069	0,0017

Table 5.4. XRF derived trace elements (in wt%) of samples 3.2A and 1.1 (same as previous BRC compositions).

5.6 Mineral chemistry

5.6.1 Olivine (appendix 11.3)

The chemical composition of olivine varies between the metamorphic phases (M1 vs M3 fig 5.13). M1 olivine has a higher Fe content and a Mg# ranging between 90 to 93. M3 olivine diverges from M1 olivine values as M3 olivine has significantly lower (1-2 wt%) Fe concentrations and a Mg# of 95-97. In addition the Ni content is varies between the two olivine groups where M1 olivine has, on average a slightly higher NiO content (0.4 wt%) and M3 olivine a slightly lower wt% NiO (0.3 wt%).

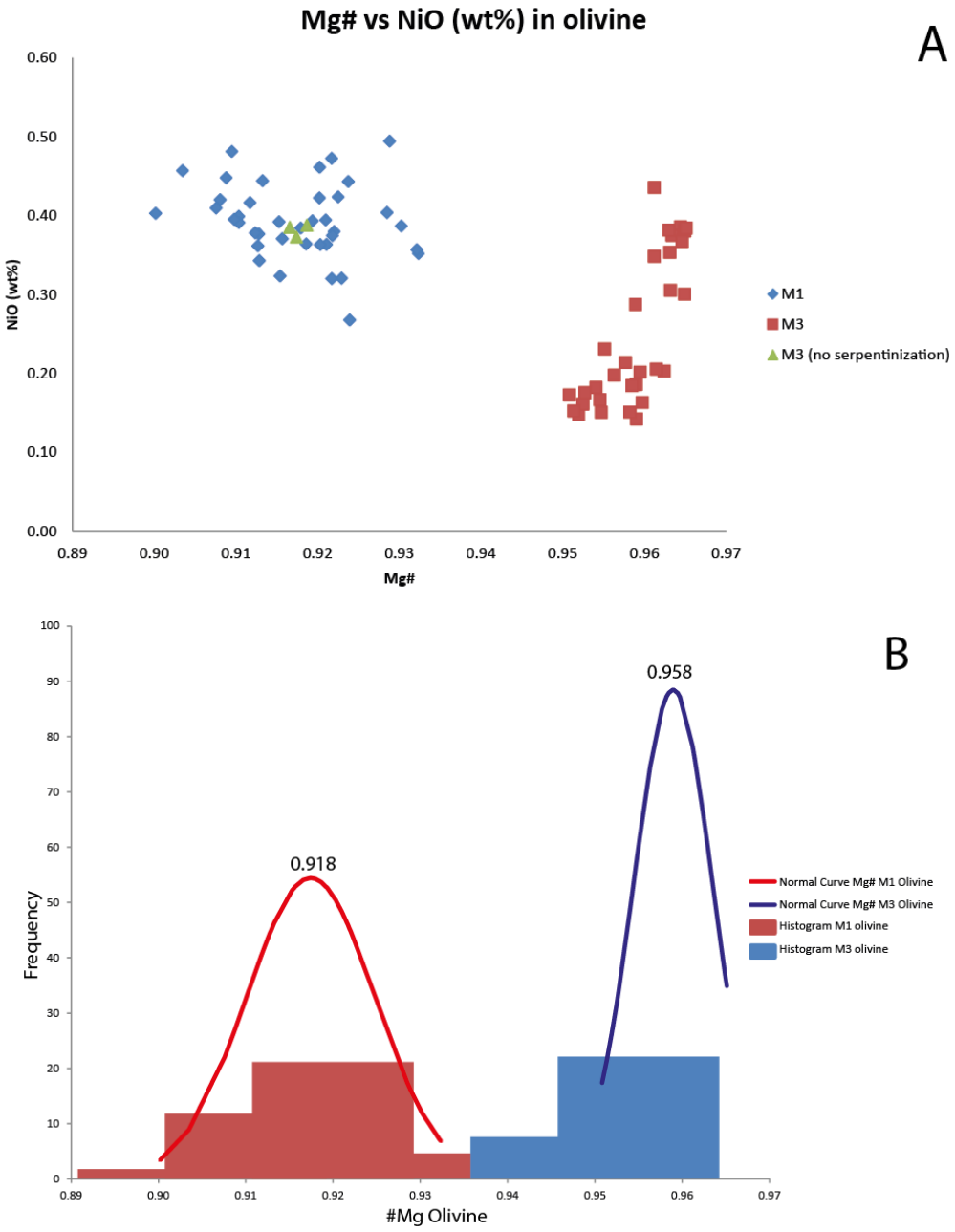

Figure 5.13. A) Diagram with Mg# vs NiO contents (wt%) in olivine. B) Histrogram of the Mg# of M1 and M3 olivine with associated normal distributions. Values at the top of the curves represent the centre of the normal curve and the 'mean' Mg# per olivine phase.

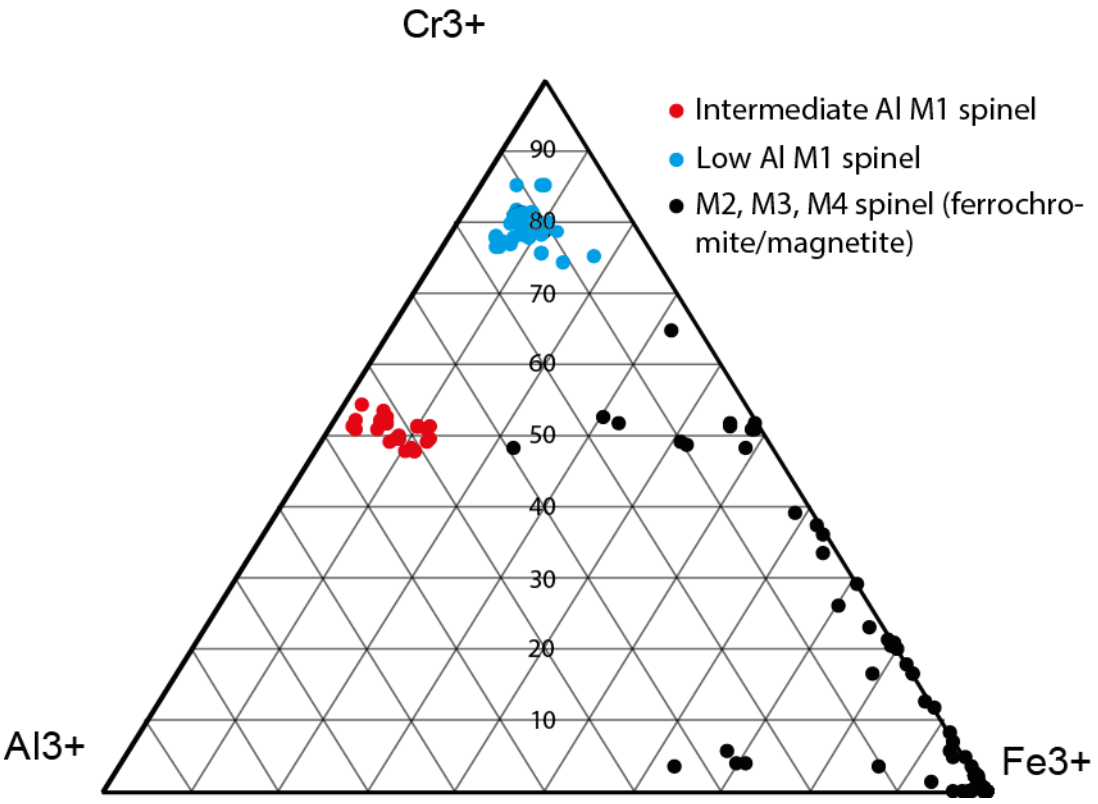

Figure 5.14. Ternary diagram of trivalent ions (Fe^{3+}, Al^{3+} & Cr^{3+}) in spinel of EMP measurements of spinel compositions. Representative spinel/magnetite EMP analysis are given in appendix 11.4.

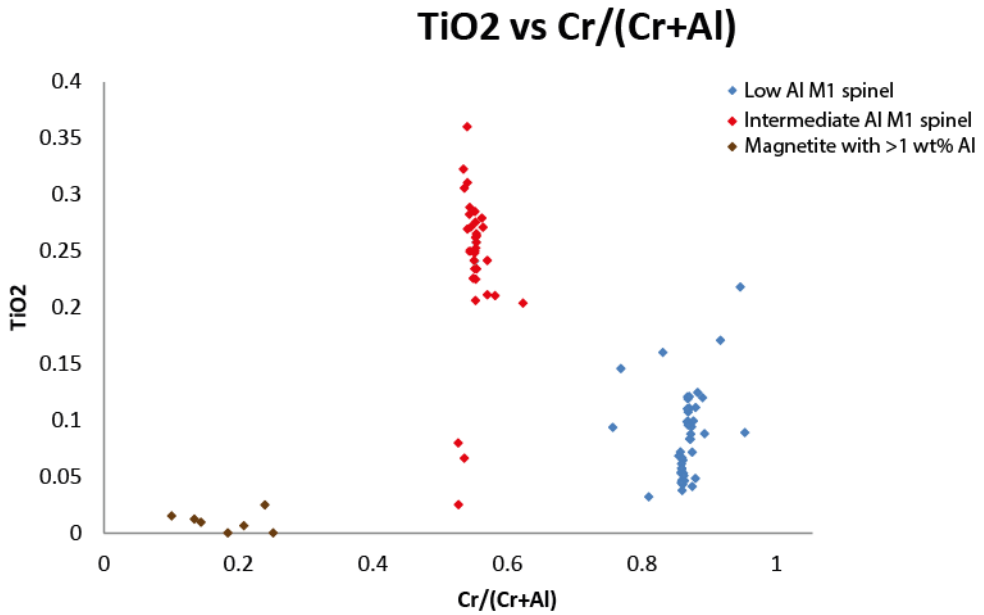

Figure 5.15. TiO2 vs Cr/(Cr+Al). Two distinct phases can be recognized, a high #Cr which are metamorphic chromite spinels and a lower #Cr which represent primary spinel compositions.

5.6.2 Spinel (appendix 11.4)

The spinel phases have distinct chemical characteristics in four distinct phases (fig 5.14). The first phase has an Al_2O_3 component varying between 5 to 45 wt% Al_2O_3 and TiO_2 content of >0.1 (fig 5.14). This phase (5-25 wt% Al) can be further distinguished into two types of spinel, a spinel with >20 wt% Al (red points fig 5.14) and <20% wt% Al (blue points fig 5.14). These spinels (as described in section 5.3) show red cores and are interpreted as M1 spinels.

A third spinel phase is present at the margins of the spinels and present as grains in the matrix. These spinels are low in Al but have a varying chromite composition,20-70 wt% Cr_2O_3. In addition they contain 0,25-0,5 mass% TiO_2 (appendix 11.4) (black points along the Fe3+/Cr3+ line fig 5.14).

A more finely dispersed magnetite phase is present throughout all samples. These magnetite grains are (almost) always Al free and contain very little amounts of Cr_2O_3 (<2 mass% Cr_2O_3) and contain negligible amounts of TiO_2 (appendix 11.4) (black point in the Fe3+ corner fig 5.14). In addition there are several magnetite grains that contain a significant amount of Al. These grains occur around or within the chlorite rim of M1 spinels. Al is thought to be incorporated due to the release of Al from M1 spinel and possibly chlorite (brown points fig 5.15)

Figure 5.16 shows the relation between the ratio of Mg^{2+}/Fe^{2+} and Cr# in primary (protolith) M1 spinels. There is a clear distinction between high Mg^{2+}/Fe^{2+} ratios, high Cr# and low Mg^{2+}/Fe^{2+} ratios, low Cr#.

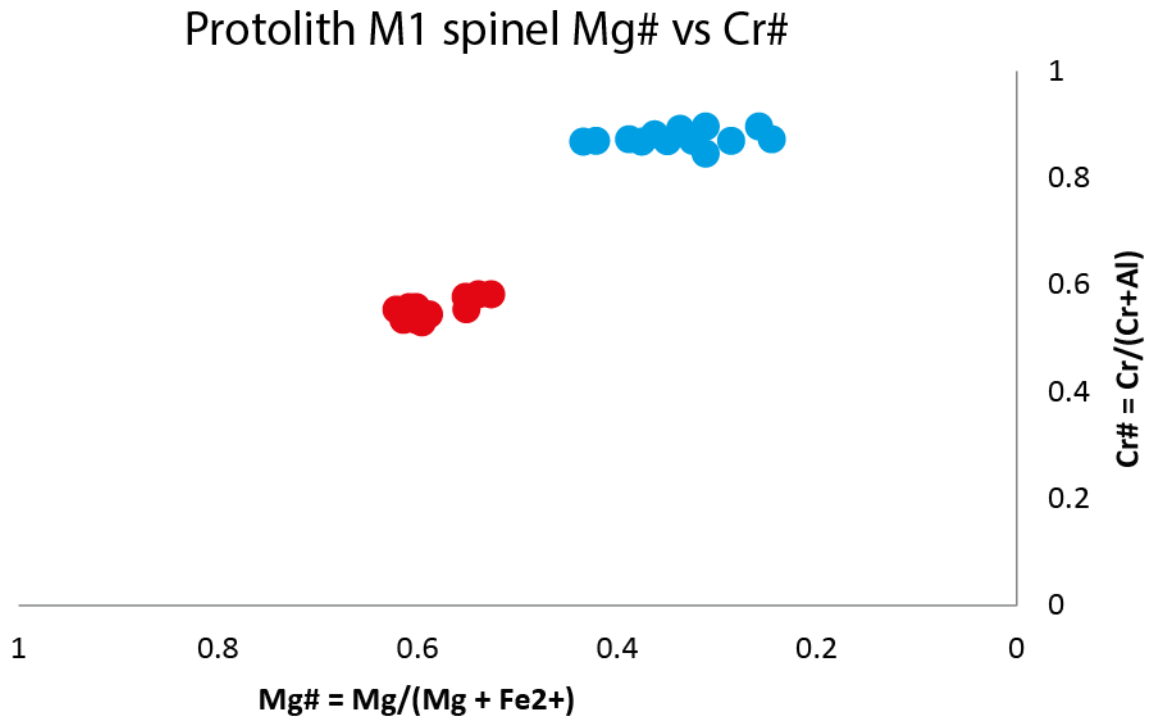

Figure 5.16 Mg/Fe vs Cr# in protolith spinel (that contain Al).

5.6.3 Serpentine (appendix 11.5)

The Si/Mg value of serpentine minerals present in the samples is not constant. Different ratios indicate a different type of serpentine mineral (Moody, 1976). In addition the Al_2O_3 content is dependent on the type of serpentine. The data presented in figure 5.17A, i.e. the wt% water (calculated using 100-total wt% probe data, assuming all weight not measured is water) vs Si/Mg in

serpentine, is undecisive for drawing conclusions about the type of serpentine as the water content varies a lot within and between serpentine types.

Figure 5.17B clearly shows the two groups of serpentine minerals present, antigorite with a high Si/Mg ratio and a high Al_2O_3 content and lizardite with a lower, but variable, Si/Mg ratio and a low Al_2O_3 content (Moody, 1976). In theory lizardite and chrysotile are chemically almost identical, but their growth habit varies significantly, it is therefore very likely that the low Si/Mg and low Al2O3 values in figure 44 (and appendix 11.5) can be interpreted as lizardite and unless the growth habit is very well defined all low Al_2O_3, low Si/Mg is taken as lizardite. The serpentine grains within well-developed veins are likely to be chrysotile, as the grains show a distinctive fibrous growth habit.

Serpentine measurement are organized according to the location of their occurrence (in fig 5.17A&B). Antigorite is mainly present in the groundmass and lizardite is mainly present between M1 olivine grains. However some lizardite is still present in te groundmass, this lizardite is a result of the first serpentinisation phase but was later overgrown by antigorite.

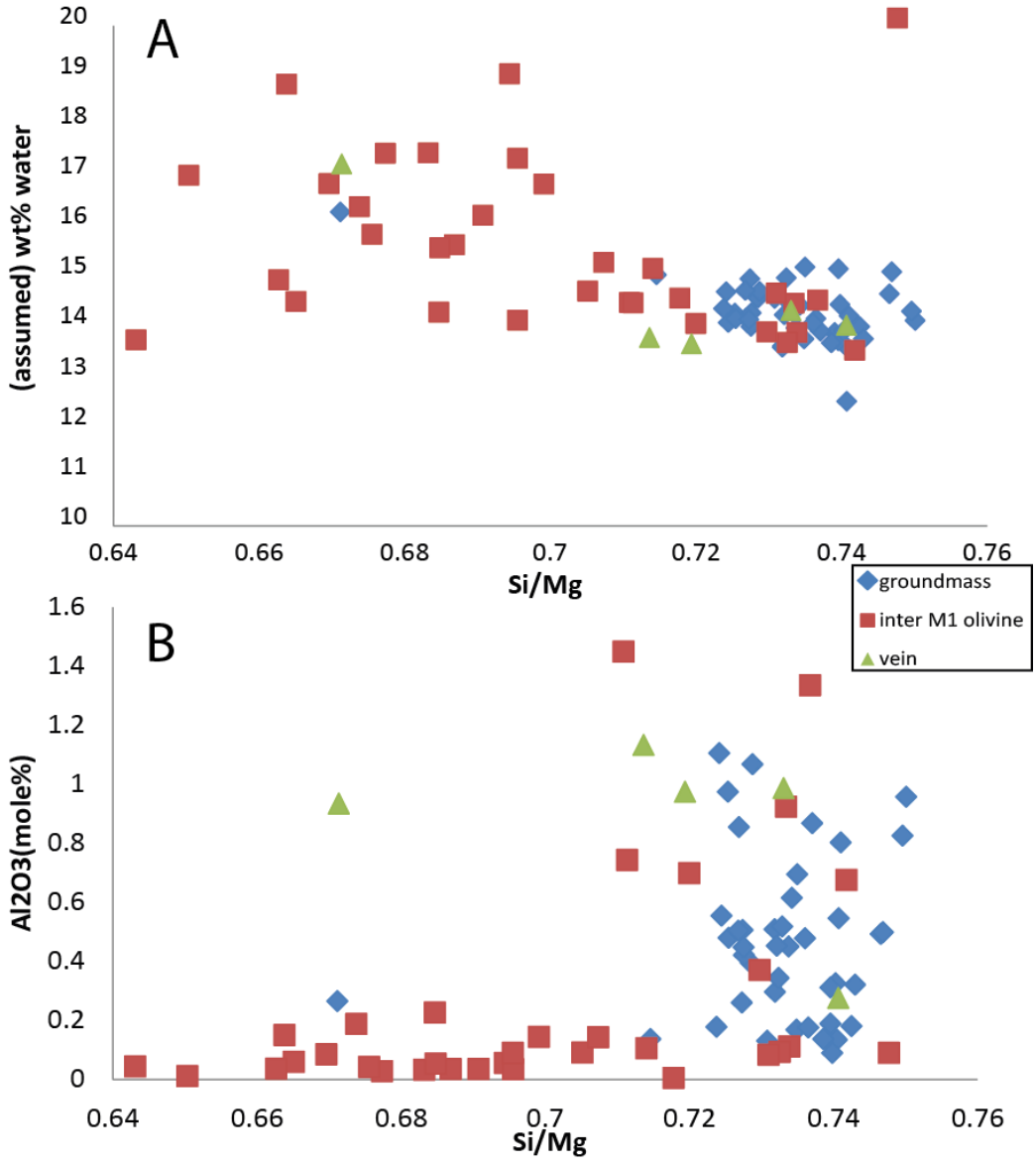

Figure 5.17. A) (assumed) wt% water vs Si/Mg in serpentine. Two types of serpentine can be recognized, antigorite with high Si/Mg (>0.72) and lizardite with low Si/Mg (<0.72) and variable water content. B) Al_2O_3 vs Si/Mg in serpentine. Two types of serpentine can be recognized, antigorite with high Si/Mg (>0.72) and high Al_2O_3 abd lizardite with low Si/Mg (<0.72) and low Al_2O_3 content.

5.6.4 Chlorite (appendix 11.7)

Since there is no data available on the Fe^{2+}/Fe^{3+} ratio using the EMPA it is assumed that all measured Fe is Fe2+. This assumption has been shown sufficient for chlorite by Foster, 1992 and Zane & Weiss, 1998 using 174 samples. This allows the usage of a triplot with Fe^{2+}, Mg^{2+}, Al^{3+} as occupants of the octahedral sites (fig 5.18).

Using the chlorite classification proposed by Zane & Weiss, 1998 all chlorites present at all localities are classified as Mg-chlorites (see appendix 11.7).

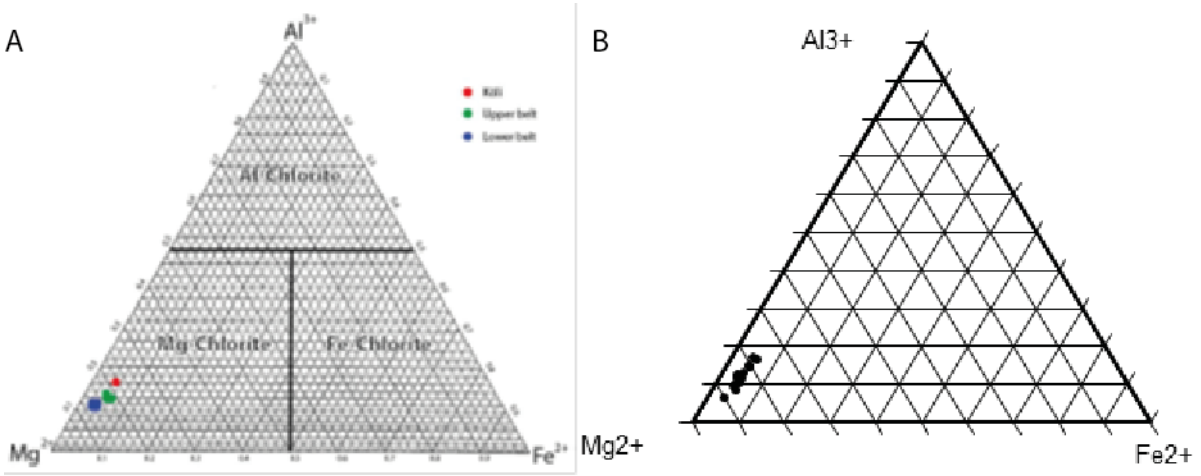

Figure 5.18. A) Ternary diagram (Mg2+, Al3+ and Fe2+) of chlorite mineral chemistry in the Köli, upper and lower Seve belt Benders (2015). B) Ternary diagram (Mg2+, Al3+ and Fe2+) of chlorite mineral chemistry in the lower Köli nappe, this work.

5.6.5 Clinopyroxene (appendix 11.8)

Clinopyroxene was found in only one sample (2ext1) and in that case constitutes more than 40 percent of the total mineral assemblage (i.e. 40% modal clinopyroxene). Its chromium content is variable between 0.2 and 0.7 wt%. The Al_2O_3 content is fairly constant with an average of 2.33 wt% (fig 5.19A). Additionally FeO content is also constant with an average of 2 mass percent. The TiO varies between 0 and 0.2 wt% (see appendix 11.8). In addition Fe/Fe+Mg of olivine CPX pairs are shown in figure 5.19B in combination with olivine CPX pairs examined by White (1966).

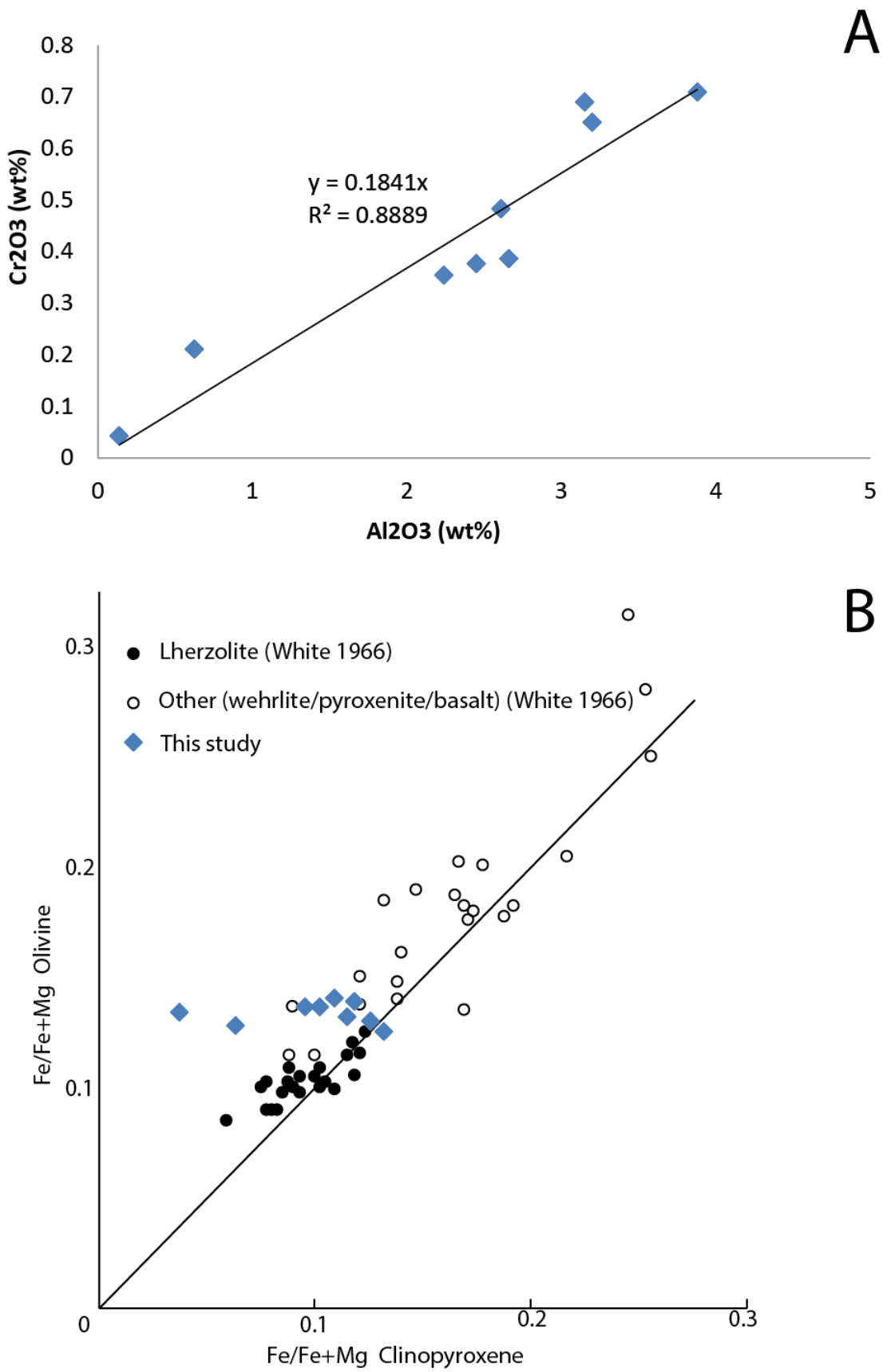

Figure 5.19. A) Cr_2O_3 vs Al_2O_3 in CPX (sample 2ext1) with a trendline depicting the depletion of Cr_2O_3 and Al_2O_3. B) Fe/Fe+Mg in olivine and CPX pairs (sample 2ext1). Lherzolite and 'Other' points used from White 1966 from mantle xenoliths (various BRC compositions).

5.7 Raman Spectroscopy

Raman spectroscopy can be used to determine chemically identical minerals. The various serpentine minerals, as well as brucite, show a very similar chemistry and can therefore more easily (in comparison to EMP) be identified using Raman spectroscopy. Samples 1.1 and 3.4.2 were analyzed using Raman spectroscopy to determine the presence and relation between the hydrous mineral phases. The Raman spectra for specific samples and minerals are presented in appendix 11.2)

Sample 1.1 shows two growth habits of serpentine; a non-pseudomorphic flacky phase that occurs in patches (M4 antigorite) and a pseudomorphic phase that occurs between protolith olivine grains (M2 lizardite). Figure 5.20 shows the edge of a patch of flackey serpentine, with three relict olivine grains on the left side.

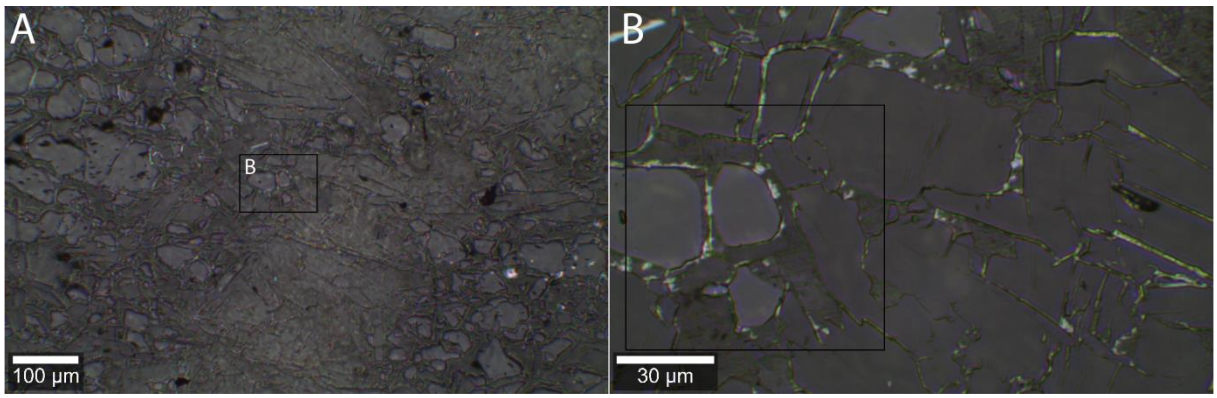

Figure 5.20 Location is indicated in appendix 11.1 on the large overview of sample 1.1 A) overview sample 1.1 location 1, black square indicates B. B) Zoomed view of the Raman Intensity maps made, black square indicates the maps presented in figure 5.21.

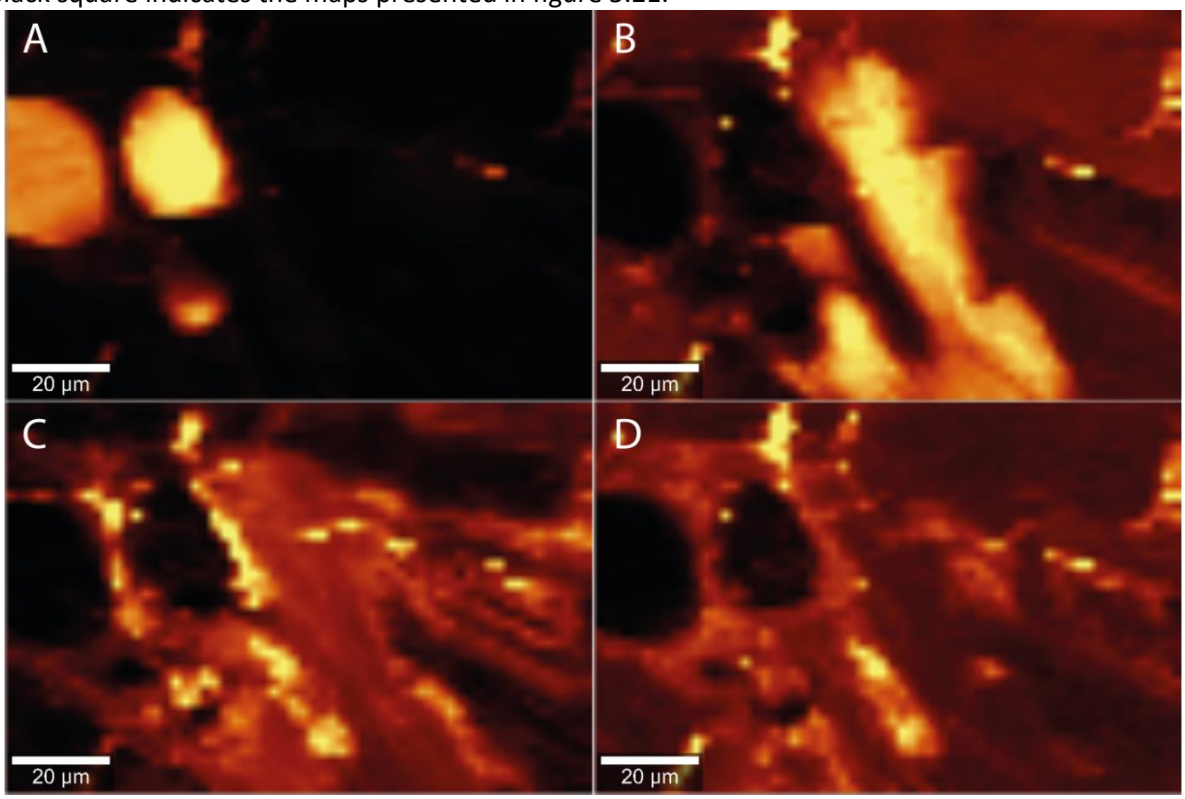

Figure 5.21 Respective Raman (wavelength) spectra are presented in appendix 11.1 .A) Raman intensity map of olivine. B) Raman intensity map of antigorite. C) Raman intensity map lizardite. D) Raman intensity map of brucite.

Raman intensity maps are shown in figure 5.21, these illustrate selected wavelength bands characteristic for specific minerals. Figure 5.21A shows the occurrence of three small olivine grains. (Low temperature) Lizardite and Brucite are present at the boundaries of olivine (fig 5.21 C&D) whereas the larger (flackey) antigorite grains are present in patches with no lizardite or brucite in between (the small patches that do light up are holes).

Figure 5.22 shows relict protolith olivine grains altered by pseudomorphic serpentine (fig 5.22D). The only serpentine present between the protolith olivine relicts is lizardite (as there is no signal at the 1040 cm-1 wavelength band at all at this sample location). There is a small increase in intensity at 440 cm-1 related to the presence of brucite.

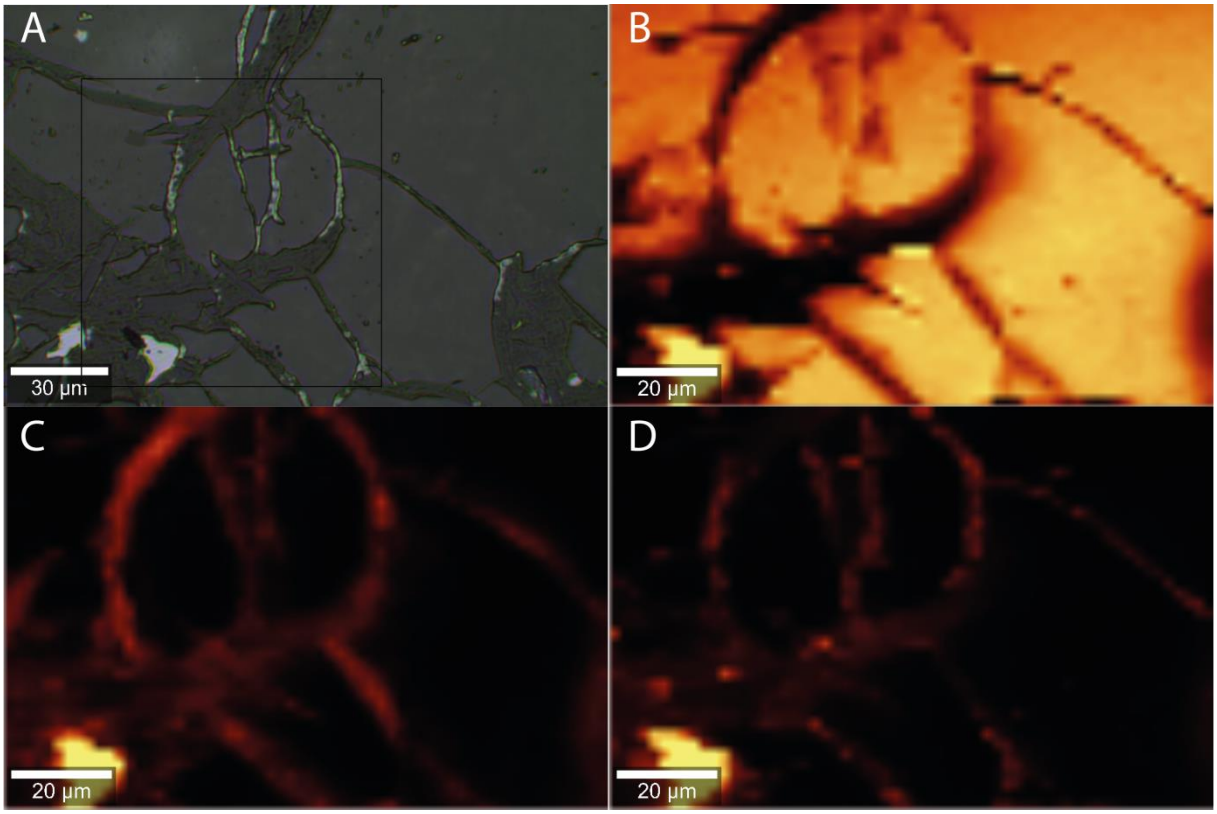

Figure 5.22 Respective Raman (wavelength) spectra are presented in appendix 11.1 . A) Relict protolith olivine grains in a mesh structure with serpentine (lizardite) and brucite in the alterated areas. Sample 1.1. B) Raman intensity map of olivine. C) Raman intensity map of lizardite. D) Raman intensity map of brucite.

In addition the matrix of sample 3.4.2 was analysed using Raman spectroscopy to confirm the presence of antigorite and the apparent lack of other serpentine minerals. Figure 5.23 shows an overview of the investigated area, consisting of interlocking serpentine grains. All grains show a signal characteristic for antigorite. Other areas, those between the antigorite grains, are filled with epoxy hars or carbon coating resulting in a wide band between 1100-2000 cm-1. The matrix in this case is formed entirely by antigorite which may be related to M2 but it is likely that most antigorite is M4 antigorite replacing M2 antigorite.

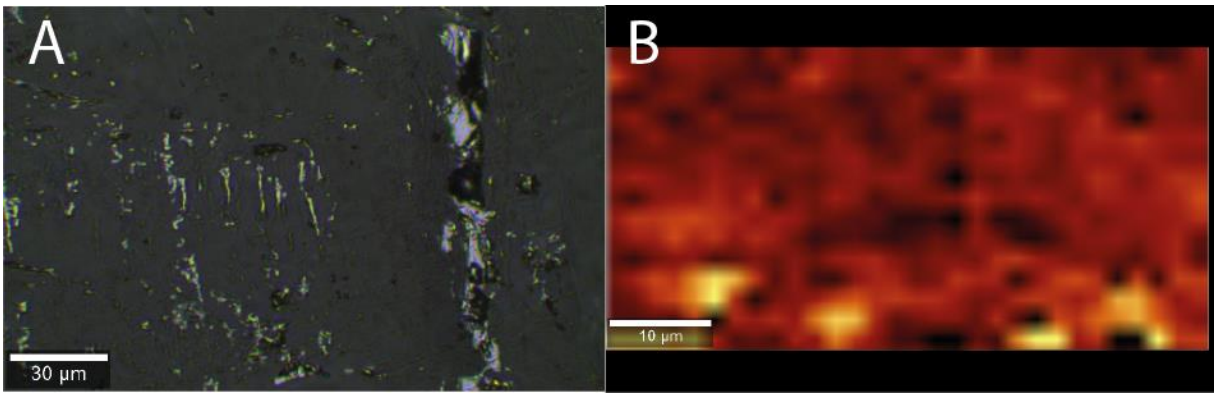

Figure 5.23 A) Overview of the investigated serpentine matrix. B) Antigorite shown by the 1040cm-1 band intensity, holes (black) are filled with epoxy glue or carbon coating.

6 Interpretation

The geological evolution of the lower Köli peridotites in terms of PT conditions have changed significantly during the Caledonian orogeny. In this section the mineral chemistry, bulk rock chemistry and structural relations will be interpreted in order to distinguish the geological processes that occurred. The tectonic setting of the protolith (M1) assemblage will be determined and an estimate for the PT conditions at which this protolith last reequilibrated with the lithospheric mantle will be calculated using geobarothermometry. Afterwards the M2, M3 and M4 metamorphic phases will be characterized and interpreted in order to determine the processes responsible.

6.1 Composition and origin of the M1 protolith assemblage

The M1 protolith assemblage, consisting of Olivine, Chromite +- CPX +- OPX has a mantle origin that can be formed in different tectonic settings (Arai, 1996). Different peridotite bulk rock compositions are present at the sampled peridotite locations, most commonly harzburgite and dunite. These bulk rock compositions, dunite vs harzburgite/lherzolite are determined through bulk chemistry. But the bulk rock chemistry can drastically change due to meta-somatic overprints (i.e. a metasomatic input of Ca will result in a false modal amount of CPX).

However harzburgitic/dunitic bulk rock compositions could also influence spinel chemistry. As seen in figure 5.14 two M1 spinel phases are present in the analysed samples. A low aluminum phase (blue dots in fig 5.14) represents the dunites and the phase with up to 40% aluminum (red dots in fig 5.14) represents the harzburgite. This relation is also present in the TiO vs Cr/(Cr+Al) (figure 5.15) where measurements with a low TiO number and a Cr#<0.6 represent harzburgite samples whereas TiO>0.1 and Cr#<0.6 represent dunites. However these chemical variations in spinel compositions may also result from later modification induced by volcanism (see below, 三浦, 真 2015).

The relation between the Mg# of olivine and the Cr# of spinel can be used to differentiate between the different tectonic settings that incorporate peridotites (Arai, 1994). Orogenic peridotites with an ophiolitic source (or a SOLM source) have a ‘low’ Mg# in olivine and a high Cr# in spinel whereas root-zone peridotites (or SCLM peridotites) have ‘high’ Mg# in olivine and low Cr# in spinel.

The mineral chemical data presented in this work (see section 5.6 and appendix 11.3 through 11.8) is represented by the red (high Al) and blue (low Al) circles in figure 6.1. In the $Mg\#_{olivine}$-$Cr\#_{spinel}$ plots of the lower Köli orogenic peridotites are plotted as the high Al spinel clusters at the boundary (defined by Clos et al., 2014) between cratonic and abyssal peridotites. Alternatively the low Al spinels do not fall into the known compositional range of cratonic and abyssal peridotites.

However spinel compositions by themselves are more likely to indicate an abyssal affiliation of the investigated lower Koli peridotites. Barnes and Roedel, 2000 presented a data set for protolith spinel compositions derived from different tectonic settings (fig 6.3). The red box in this figure indicates the spread of the M1 spinel compositions of lower Köli orogenic peridotites (in this work). According to this discrimination method the latter shows the greatest overlap with spinel compositions derived from ocean-floor/abyssal peridotites.

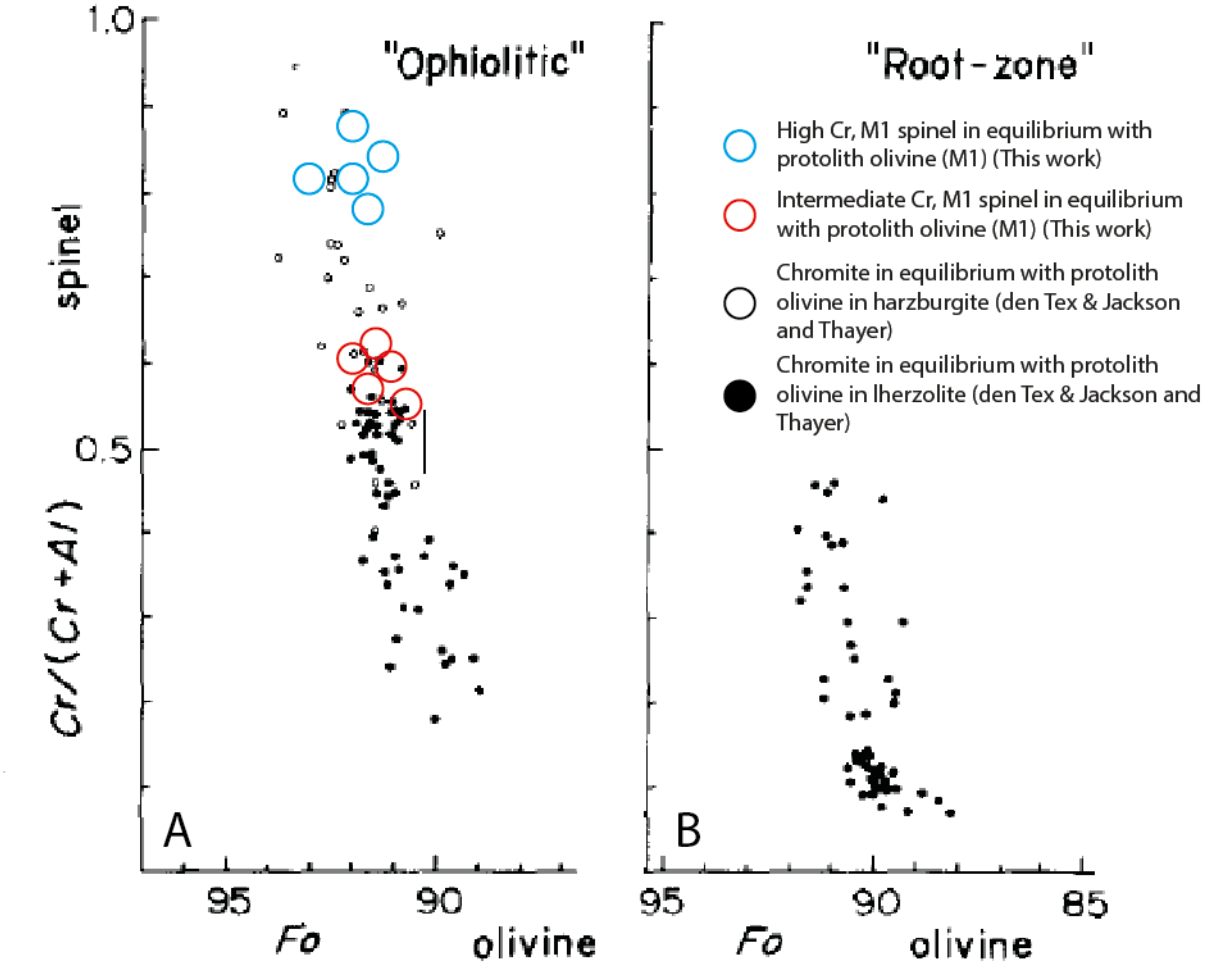

Figure 6.1. $Mg\#_{ol}$-$Cr\#_{sp}$ relationships in alpine-type peridotites from (A) "ophiolitic" (or harzburgite subtype, SOLM) masses and from (B) "root-zone" (or lherzolite subtype, SCLM) masses. The distinction of the two types of alpine masses is after den Tex (1969) and Jackson and Thayer (1972). Open circles= harzburgite; closed circles=lherzolite. Arai, 1992.

There is also a relation between modal olivine and Mg# of olivine in abyssal peridotites (Boyd, 1989). Increasing amounts of modal olivine correlate with higher Mg# in olivine (fig 6.2). The sampled lower Köli peridotites contain high amounts of modal olivine (up to 90% in sample 1.1, estimated 80% in most samples, see appendix 11.1). Plotting modal olivine vs Mg# of M1 olivine (in fig 6.2) shows that the Mg# of olivine is higher then traditionally expected for abyssal peridotites (Mg# olivine 89-90) (in comparison the the values proposed by Arai 1992). This trend has been related to the low pressure and relatively dry lithosphere forming processes in oceanic domains in contrast with that of cratonic affiliation (Boyd, 1989).

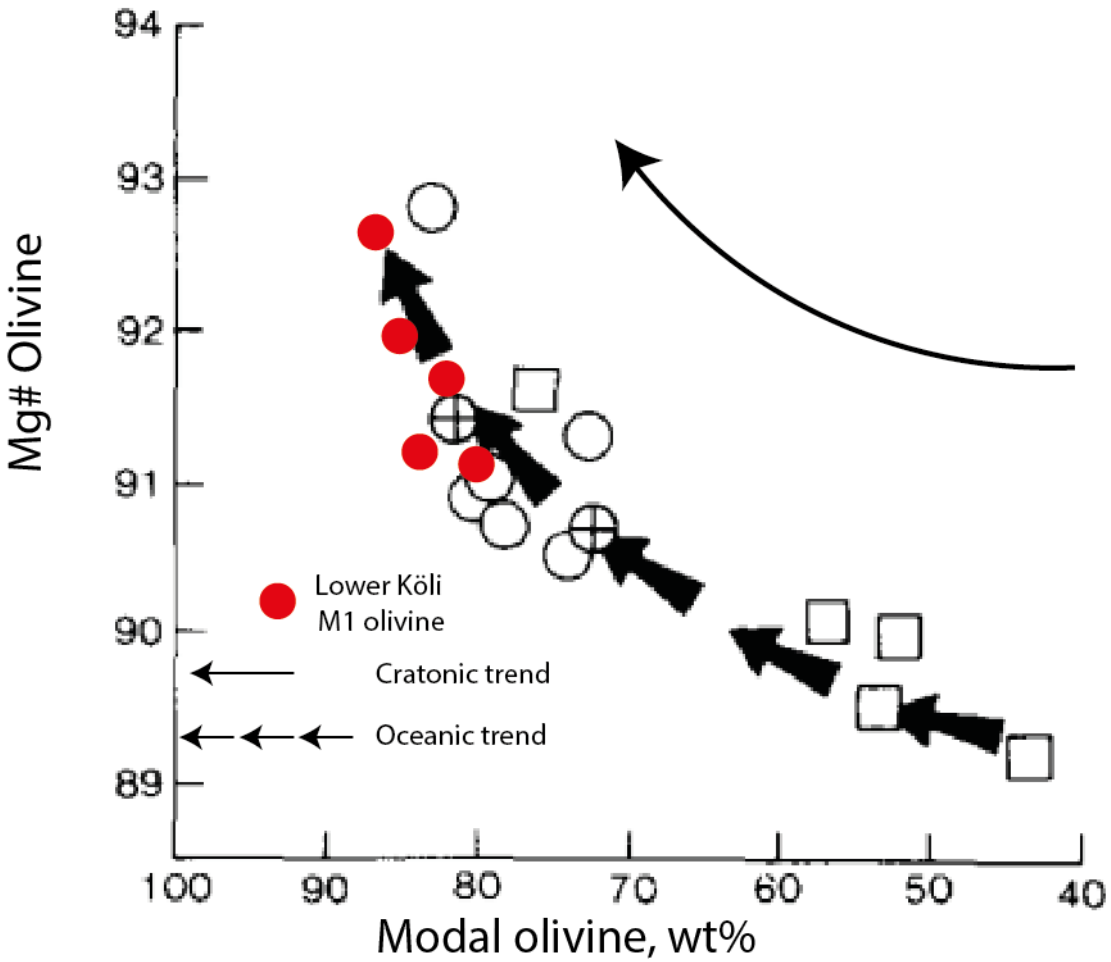

Figure 6.2 Diagram illustrating the trend defined by modal olivine vs Mg# olivine from an oceanic setting. Lower Köli peridotites fall within this trend. Boyd 1989.

More recently, the dominant occurrence of two contrasting chromespinel types within abyssal peridotites has been attributed to the differentiation by a completely different geodynamic process (三浦, 真 2015). In podiform chromitites derived from abyssal peridotites two different spinel compositions reflect two origins for chromite. A low Cr# low Mg# reflects an midocean ridge affiliation whereas a high Cr# in combination with high Mg# reflect later volcanic interaction. These two spinel compositions are present in the samples presented in this thesis (fig 5.16). 三浦, 真 (2015) argues that the formation of the high Cr#, high Mg# spinel group is related to the interaction between a melt passing through the peridotite (also Arai and Yurimoto 1994). This melt, which is often a boninitic melt (Fisk 1986), will assimilate OPX and CPX. As a result the harzburgitic mantle will be more depleted and transition into dunite in addition to the formation of chromitite pods. This process is reflected in the podiform chromitite composition, as Al2O3 is leeched and Al2O3 poor spinel is formed. This assimilation process is also reflected in the enrichment of LREE and Na content of spinel (Arai et al., 1997).

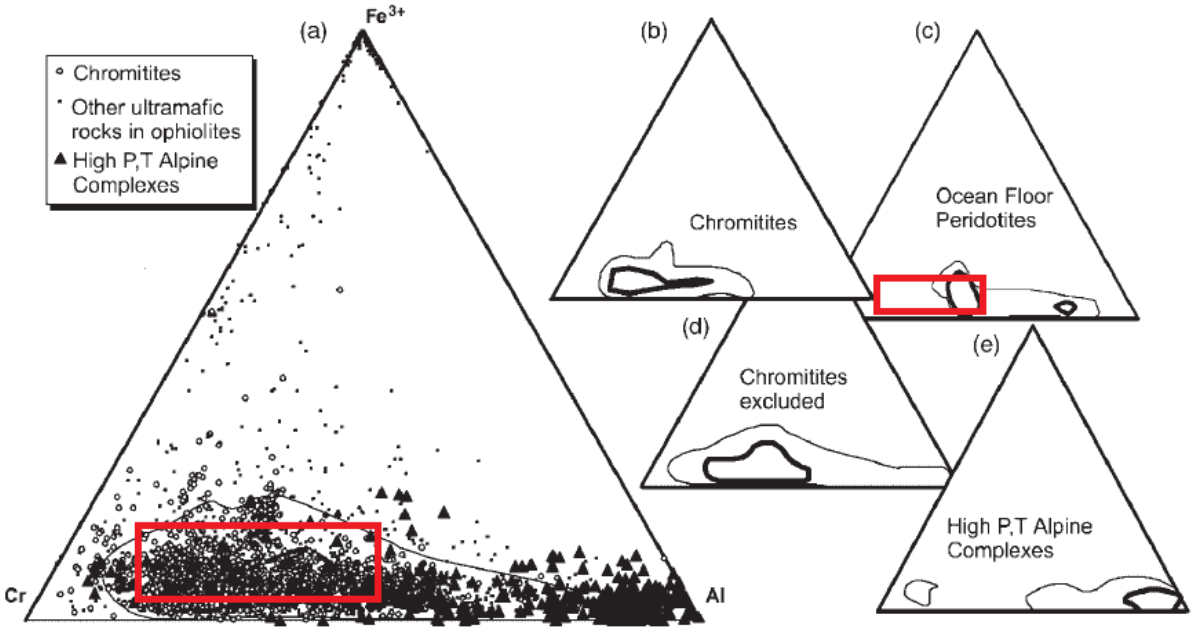

Figure 6.3. Trivalent ion plots for ophiolites, 'Alpine ultramafics' and abyssal (ocean-floor). (a) all data points and contour on complete dataset (b) data from chromite seams only (c) ocean floor peridotites (d) chromitites excluded (e) High P, T Alpine complexes. Indicated in red primary compositions in this work. Adjusted after Barnes and Roedel, 2000.

The position of the chromitites, concordant or discordant, can also be used to attribute a chromitite to a ophiolitic or 'volcanic interaction' type. The concordant pods, parallel with the foliation, are older and therefor experienced the same (plastic) deformation as the surrounding peridotites and the foliation would be parallel. However the chromitites that result from volcanic interaction are younger, did not expierence the same stresses as their oceanic counterparts, and can be discordant (i.e. not parallel to the foliation).

The reaction trends as a result of melt-mantle interactions is illustrated in figure 6.4. The horizontal trend in the low Cr# spinels illustrates the interaction between a MORB-like melt and a relatively depleted mantle (15-20% partial melt). The high Cr# spinels correspond to the interaction between a boninite melt and the mantle. In the latter case the spinels have reached (partial) equilibrium with the interacting melt. This boninite-melt mantle interaction often occurs in a fore-arc setting which could correspond with the Virisen arc.

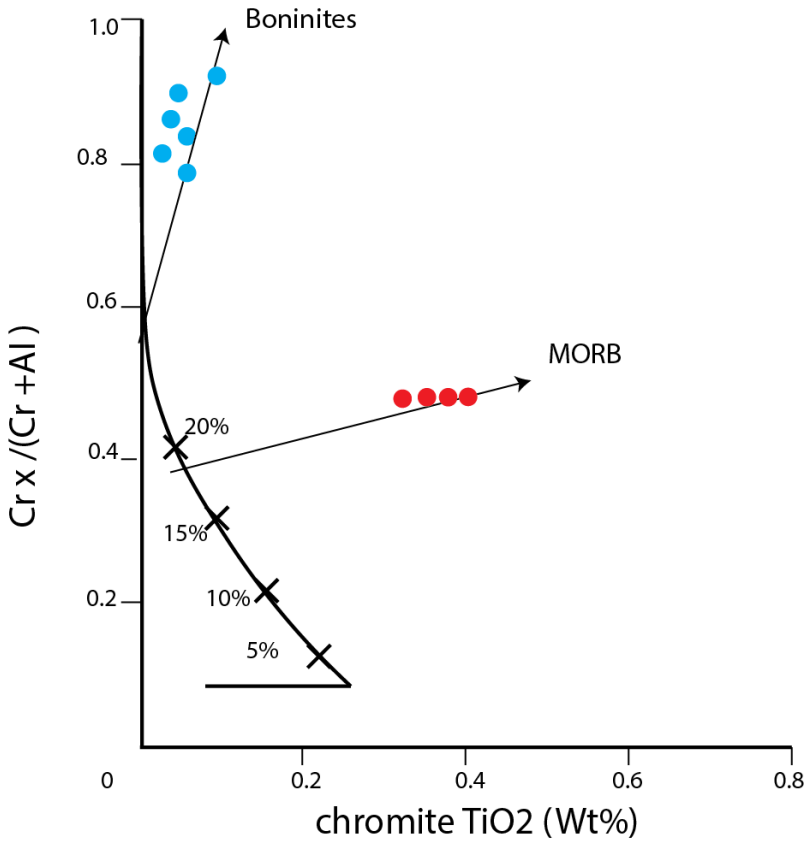

Figure 6.4. Pearce et al., 2000. Cr# vs TiO2 in spinel. Melt-mantle interactions in different tectonic setting are shown with increasing TiO2 related to MORB interaction and increasing Cr# related to arc interaction.

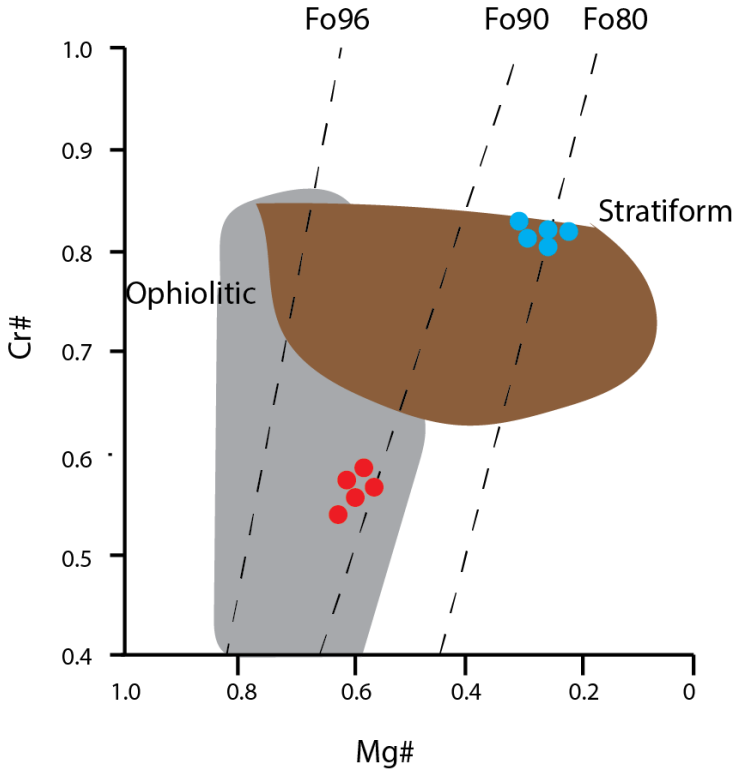

Figure 6.5. Mg# vs Cr# in spinel. Ophiolitic and stratiform fields after Leblanc and Nicolas (1992).

In addition, the tectonic setting can be distinguished from Cr# vs Mg# in spinel (fig 6.5). Fig 6.5 shows that the low Cr# spinel can be associated with ophiolites whereas the high Cr# spinel is associated with stratiform deposits related to later alteration (partial melt/melt interaction).

The division between oceanic and arc related spinels may be reflected by the spinel chemical composition presented in this work (see fig 5.14). The latter results in combination with the M1 $Mg\#_{olivine}$ were plotted in the discrimination diagram of Arai (1991) (fig 6.6). The high Al variant plots within the abyssal peridotite field and the low Al variant plots outside the field of known compositions for abbysal peridotites.

The low Al spinels may thus be the result of the interaction of a melt with the oceanic mantle in an arc environment. The lack of true chromitites may be a result the later obduction and other deformation phases. It is therefor possible that the spinel compositions presented in this work were formed in a mid oceanic setting and were later altered due to volcanic processes in an island arc setting. Similar chemical trends within spinel chemistry are present in the Leka ophiolite which is thought to be altered in a supra subduction zone environement (Furnes et al., 2012).

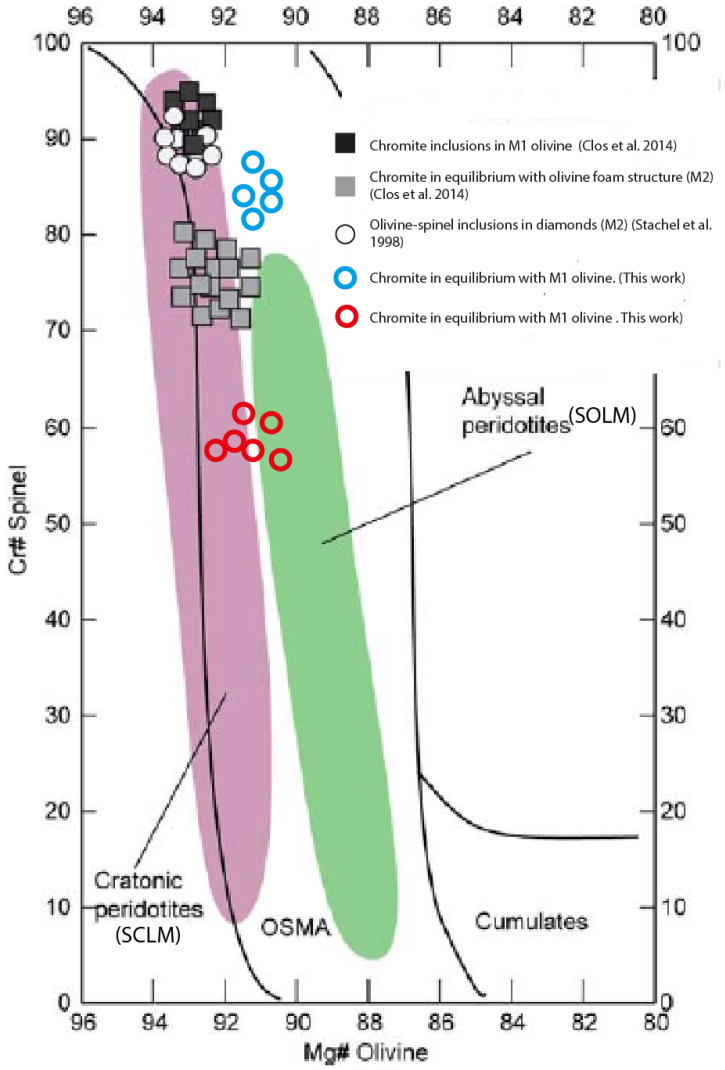

Figure 6.6. Discrimination diagram that allows the usage of the $Cr\#_{spinel}$ and Mg#olivine from orogenic peridotites to subdivide between cratonic (SCLM) and abyssal (SOLM) peridotites. After

Clos et al. (2014) and Arai (1991).
Additionally CPX can be used as an indicator for the tectonic environment in which it reached equilibrium. Several CPX grains present in sample 2ext1 were analysed (fig 5.19). These CPX grains our thought to be part of the protolith assemblage as they do not plot in the low pressure field (fig 6.7).

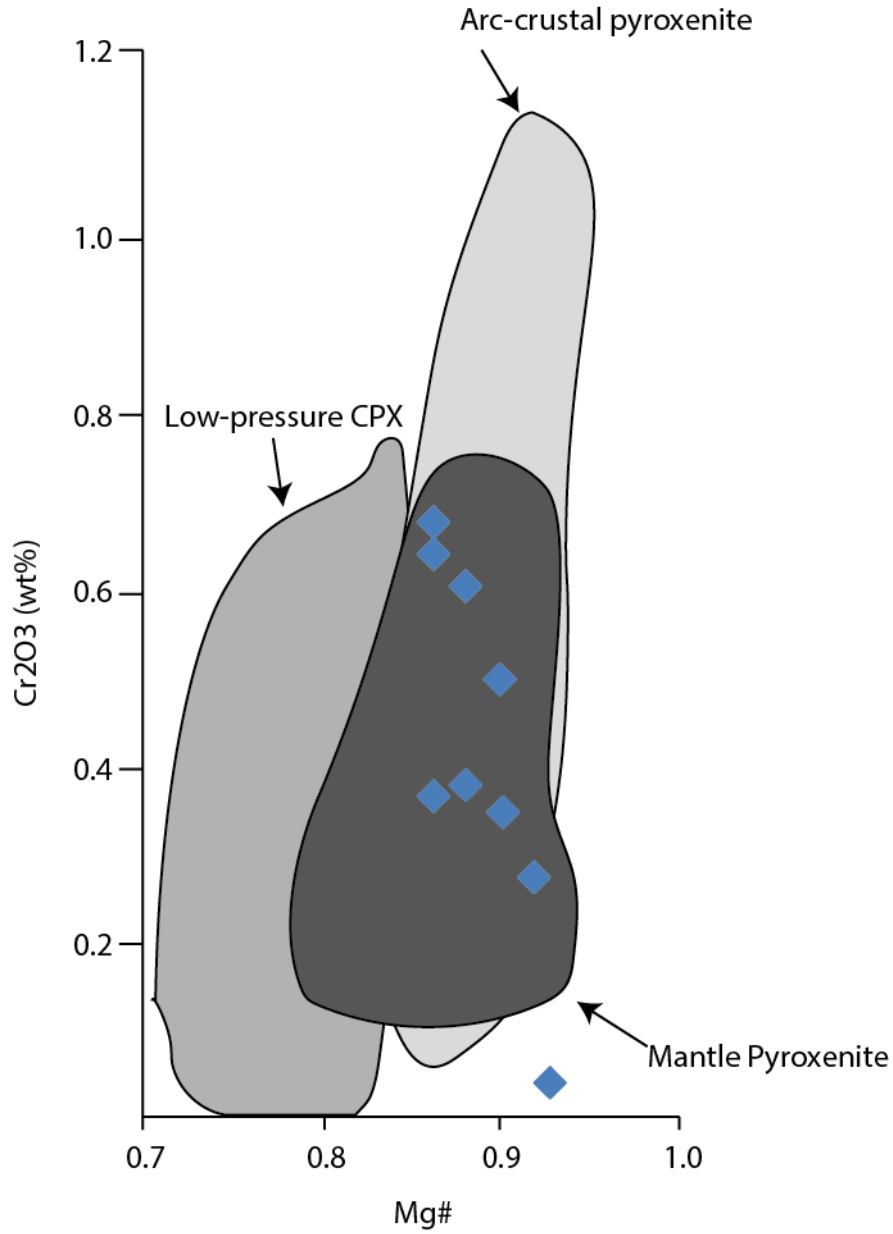

Figure 6.7. Cr_2O_3 (wt%) vs Mg# in CPX of sample 2ext1. Most CPX grains fall within the mantle pyroxenite field. None fall into the Low-pressure CPX field excluding a later (low P/T metamorphic origin). Fields after Murray (2006).

To further determine the geological setting Murray (2006) and Dick (1989) analysed CPX grains from various settings. Figure 6.7 through 6.8 show the fields thought to be related to the tectonic setting of peridotites. Although the CPX data in relation to the Al2O3 content of CPX is not very decisive the TiO2 content indicates an abyssal setting.

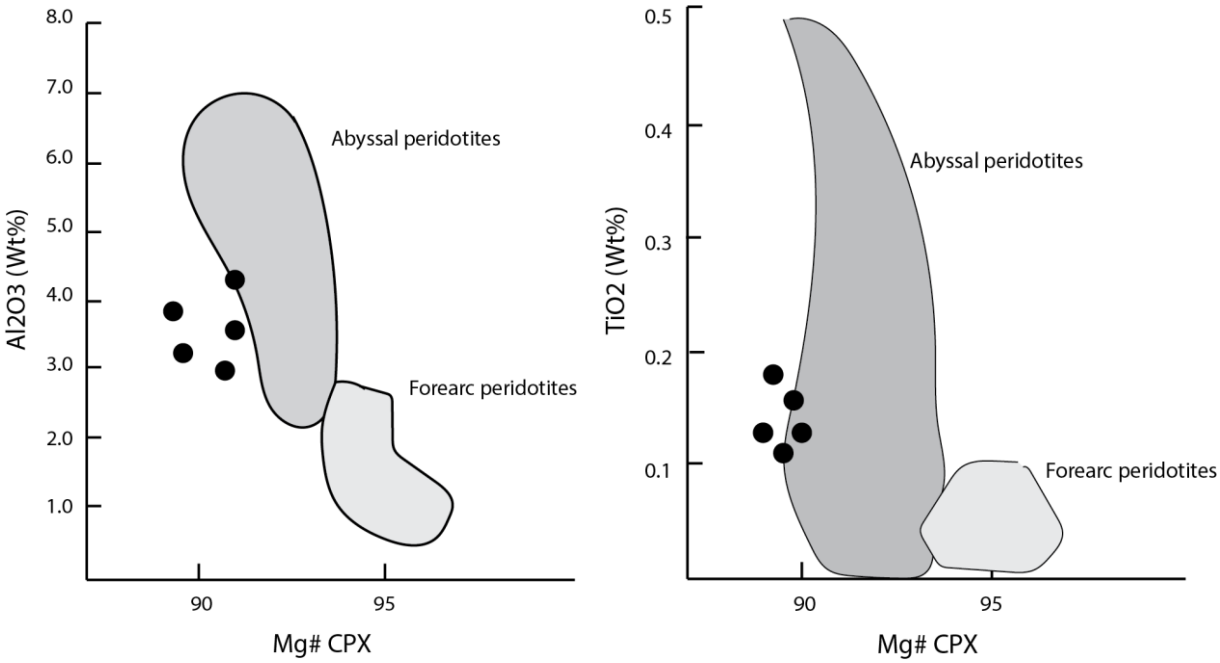

Figure 6.8. Al2O3 (wt%) vs Mg# and TiO2(wt%) vs Mg# in CPX. Dominant field for abyssal peridotites from Dick (1989) Johnson et al. (1990) Juteau et al. (1990) Johnson & Dick (1992) Dick & Natland (1996). Dominant field for forearc peridotites from Ishii et al. (1992) Parkinson & Pearce (1998) Pearce et al. (2000)

6.2 Geobarothermometry

Several geothermometers have been proposed for ultramafic rocks. The most commonly used thermometer involves the partitioning of calcium between OPX and CPX, however there are no (clear) pristine primary OPX grains present in the investigated samples. Therefore, other geothermometers have to be considered which are generally less accurate.

The geothermometer first presented by Frost and Evans (1975, T_{F+E75}) and later calibrated by Fabriés (T_{F79}) (1979) is based on Mg2+ and Fe2+ partitioning between spinel and olivine.

$$T°(K) = \frac{4250Y_{Cr}^{Sp} + 1343}{LnK_D^o + 1{,}825Y_{Cr}^{Sp} + 0{,}571}$$

$$Y_{Cr}^{Sp} = \frac{Cr}{Cr + Al + Fe^{3+}}$$

$$K_D^o = \frac{X_{Mg}^{Ol} * X_{Fe}^{Sp}}{X_{Fe}^{Ol} * X_{Mg}^{Sp}}$$

X_j^i is the mole fraction where i indicates a mineral and j a specific element. Using the spinel, olivine mineral pair from sample 1.4 (appendix sample 1.4), with the most pristine red spinel cores and M1 olivine grains (with low Mg#) results in T=700 ˚C.

The former geothermometer, T_{F+E75}, has been improved by Li Jianping (1995) (T_{J95}) using new experimental data. In addition he has shown that these results more accurately fit natural data.

$$T°(K) = \frac{4299Y_{Cr}^{Sp} + 1283}{LnK_D^o + 1{,}469Y_{Cr}^{Sp} + 0{,}363}$$

Application of T_{J95} resulted in a slightly higher temperature, T=800 ˚C.

Geobarometers are often dependent on temperature; the best calibrated geobarometer is based on the aluminum exchange between spinel and OPX. However pristine primary OPX is not present in the samples. In addition the temperature was calculated using spinel and olivine pairs; it is preferable to also use at least one of these minerals for geobarometery.

Therefore, in this case, the best suitable geobarometer involves the partitioning of calcium between CPX and spinel (Köhler and Brey, 1990, $P_{K\&B90}$). The used mineral pairs are from a different sample but samples 2.1b1 & 1.4 both originate from the Aunere body and will likely have experienced the same PT conditions.

The geobarometer by Köhler and Brey (1990) is applicable to natural peridotites between 2 and 60 kb.

$$P[kb] = \frac{(-T * Ln(D_{Ca}) - 11982 + 3{,}61 * T)}{56{,}2} \; for\; T \geq 1275{,}25 + 2{,}827 * P$$

$$P[kb] = \frac{(-T * Ln(D_{Ca}) - 5792 - 1{,}25 * T)}{42{,}5} \; for\; T \leq 1275{,}25 + 2{,}827 * P$$

Where

$$D_{ca} = \frac{Ca^{Ol}}{Ca^{CPX}}$$

Using sample 2.1b1, with clearly unaltered CPX (appendix sample 2.1b) and olivine (Mg# 92, altered only at the margin), and the temperature obtained through the spinel and olivine thermometer (T_{J95}, 1070 ˚K) the calculated lithospheric pressure is approximately 9 kb indicative of subsolidus lithospheric conditions. These temperature and pressure results fit fairly well together, assuming a geothermal gradient of 25 ˚C/km. 9 kb is roughly equivalent to 30 km depth and 800/25=32 km.

This depth is thought to be where the peridotites were located, and reached an equilibrium state, before crustal emplacement took place. However these geothermobarometers are far from perfect, especially the high temperature dependence of the geobarometer, and are therefore only an indication of subsolidus equilibrium processes in the lithospheric mantle.

6.3 M2 serpentinisation

The first serpentinisation phase (M2) is clearly present in samples from the smaller bodies but also in the samples taken at the margins of the larger bodies. The amount of fluid present is the limiting factor of serpentinisation if conditions favor the growth of serpentine over M1 olivine (and pyroxene). The intense serpentinisation of the smaller bodies implies that enough fluid was present

during serpentinisation. The lack of thourough serpentinisation in the centre of the Aunere body implies that water was not able to penetrate deep into the peridotite body.

Wicks and Whittaker (1977) argue that the pseudomorphic textures and growth habit of the M2 lizardite is a result of retrograde metamorphism. This is naturally supported by the presence of brucite which is stable at temperatures lower than 300 degrees. The growth of serpentine veins may be concurrent with the formation of lizardite even when the veins consist of chrysotile.

The PT conditions of the M2 serpentinisation process, in combination with the abyssal peridotite origin, imply that serpentinisation occurred at, or near the sea floor. However, M2 serpentinisation could also have occured after obduction of the ophiolite section. In that case M2 serpentinisation is limited by erosional processes and fluid penetration into the body. A study of the fractionation rates of sulfur and oxygen isotopes as well as more accurate trace element measurements could provide a more conclusive vision of the serpentinisation process as it allows for discrimination between an oceanic or meteoric fluid origin.

6.4 Syn/post-M2 deformation

The presence of a tectonized texture (fig 5.5), greatly resembling a 'conglomerate', implies that either brittle deformation, hydraulic fracturing or surface erosion has occurred. The peridotite has an abyssal origin and would normally be incorporated in the lower part of an ophiolite sequence. However a large part of this ophiolite sequence is absent. It is therefor likely that the ophiolite was thrusted onto an island arc, micro continent or continent and during this deformation event a large part of the overlying ophiolite sequence was lost. The latter may be the result of erosion at the surface.

In addition the lower Köli nappe contains several 'serpentine conglomerate' deposits formed at surface conditions (Otta conglomerate, Sturt at al., 1991, see section 4.3). Therefore it is likely that peridotites or other ultramafic related rocks were thrusted above sea level to allow erosional processes to become operative.

6.5 Serpentinite diapirism

A different origin for the peridotite bodies and the accompanied (M2) serpentinisation has been proposed by Stigh (1979) and later Grimmer and Greiling (2012). The lack of other parts of the ophiolite sequence, the presence of monomictic serpentine conglomerates, the irregular distribution and geometry of the bodies and presence of serpentinites in the higher parts of the Köli nappe are seen as arguments in favor of a diapiric origin for the serpentinites in the lower Köli nappe.

However, as earlier described (see section 4.3) other peridotite bodies in the lower Köli include other parts of an ophiolite section (Bergman 1993, Nilsson & Roberts 2015). In addition the serpentine conglomerates may have formed after obduction of the ophiolite.

However, the peridotite bodies that do not show any evidence of other parts of an ophiolite section may be the result of serpentine diapirism. For a more definitive answer the serpentinisation fluid has to be determined (fractionation rates of sulfur and oxygen isotopes as well as more accurate trace element measurements), where a subductionzone fluid will indicate serpentinites diapirism whereas an oceanic fluid will indicate obduction of an ophiolite section followed with erosion.

6.6 Hyperextended continental margin

Alternatively, as a result of deep sea drilling, another origin has been proposed for peridotites in an extensional setting; (hyper) extended margins (Boillot et al. 1987). Hyperextended margins occur at extensional continental margins where the upper and lower crust become de-coupled (Manatschal, 2004). This de-coupling allows major faults to penetrate into the mantle resulting in (partial) serpentinisation of the mantle (see figure 7.4 and model discussion).

At the continental margin extension may result in stretching up to a factor 4, resulting in thinned crustal thicknesses of approximately 8 km. In other extensional settings the exhumed mantle extends as 50-100 km thick belts between very thin oceanic crust (Penrose crust) and extended basins (Doré & Lundin, 2015).

The mineral chemistry of protolith spinel-olivine pairs can not be used to indicate a definitive peridotite affiliation (SOLM vs SCLM) as the chemical composition of the spinels and olivine presented in this work, overlap both fields (see fig 6.4). These orogenic peridotites thus may have a SCLM and/or SOLM origin. In a hyperextended margin SCLM can surface at the seafloor in close proximity to extended (continental) basins. In this case the serpentinisation fluid would be oceanic and can not be used to discriminate between the two types of peridotite. In addition the depleted bulk rock compositions (low Al2O3 and low CaO) indicate a highly depleted source, which is not common for a mid oceanic ridge environment.

The lack of deep sea sediments, but instead conglomerates of siliclastic sediments overlying the lower Köli peridotites (Sjöstrand, 1978, see section 1.2)) could indicate that the peridotites were emplaced near or at a continental shelf. However obduction to the surface, intiating erosion of the top of the ophiolite section, followed by (near continental) sedimentation could result in the same stratigraphic sequence.

However extended margins could have been present at the continent ocean transition zone along the margins of Baltica and possibly an unnamed microcontinent (see model discussion). The serpentinized peridotites resulting from the (hyper)extended margin of Baltica would therefor be present in the upper Seve nappe. In addition the (hyper)extended margin may, in a later stage, form the oceanic crust needed to initiate subduction of the middle Seve nappe.

6.7 M3 prograde metamorphism

The prograde M3 metamorphic event is accompanied by the growth of M3 olivine at peak metamorphic conditions. The replacement of the M2 serpentine mineral assemblage by M3 olivine has not been completed, this may be due to the timeframe at which the rocks where within the olivine stability field or growth may have been enhanced at some places due to the presence of a fluid (water).

Olivine in the samples at the center of the Aunere body does not show clear new grains related to this M3 phase. However, different grain sizes are present throughout these samples. The smaller grains, often situated in zones or bands, may be the result of this M3 phase. However due to the small amount of serpentinisation iron present in M1 olivine has not been incorporated in magnetite and the chemistry of M3 olivine is likely to be similar to M1 olivine. In addition the growth of olivine

in these samples may be limited due to a limited amount of water. The PT conditions during M3 could reflect a burial effect resulting in a geothermal gradient sufficient to enter the olivine stability field.

In the country rocks surrounding the peridotites biotites, phengites and muscovites were dated by the Rb-Sr and K-Ar technique by Reymer (1979). Results indicate that these biotites, phengites and muscovites were formed at 440-410 Ma. The pressure temperature range during prograde M3 metamorphism for these biotites is within the range for the M3 olivine growth. It is therefore likely that the biotite and olivine grew simultaneously during the Scandian Orogeny at approximately 430 Ma.

6.8 M4 serpentinisation phase

This serpentinisation phase is characterized by the growth of large antigorite grains, which mainly overgrow the already serpentinized matrix (fig 5.9). In addition the presence of carbonate minerals (appendix 11.1) implies the influx of a new serpentinisation fluid enriched in carbon. This fluid may be enriched in carbon due to percolation through the overlying or underlying (volcanic) sediments. However the degree of carbonization is not as intense as that in the ophiolites in surrounding areas (i.e. Leka ophiolite).

6.9 PT path

PT conditions have been modeled using the BRC obtained for sample 1.1 (see table 5.3), i.e. the sample with the least amount of serpentinisation. This sample is thought to accurately represent the bulk rock chemistry of the investigated lower Köli peridotites. The subsolidus PT conditions of the protolith assemblage (M1) has earlier been determined using geobarothermometry. Mantle rocks near spreading ridges generally undergo adiabatic decompression (which induced melting) due to the velocity of spreading during mantle upwelling. Afterwards rocks slowly cool down near the ocean floor, which represents the path from M1 to M2. At M2 the peridotites either fully or partly equilibrate with their surroundings depending on the presence of water. Obduction initiates uplift of the sequence and surface conditions are reached during the M2 phase. Alternatively diapirism due to serpentinisation by a subduction fluid may be responsible for the uplift and emplacement of the peridotite sequence. The peridotites were at surface conditions during the formation of the conglomerates present at the margins of several lower Köli peridotite bodies (this work, Sturt et al. 1991 and others). After the formation of the conglomerates, burial of the peridotites, as a result of thrusting and accretion, is thought to cause the increase of pressure and temperature related to M3. Prograde metamorphism (M3) is generally constrained to a geotherm. An average geotherm of 25˚C/km is projected in figure 6.7 as a red line. The absence of talc in all samples limits the maximum metamorphic temperature during M3 to approximately 500 ˚C. In addition the presence of >20% modal olivine further limits the temperature down to ≥400 ˚C (see fig 6.7). Along a standard geotherm this would coincide with 5Kb pressure or approximately 18km of burial. Afterwards erosion slowly decreased the pressure and temperature conditions resulting in favorable growth for M4 antigorite during retrogradation.

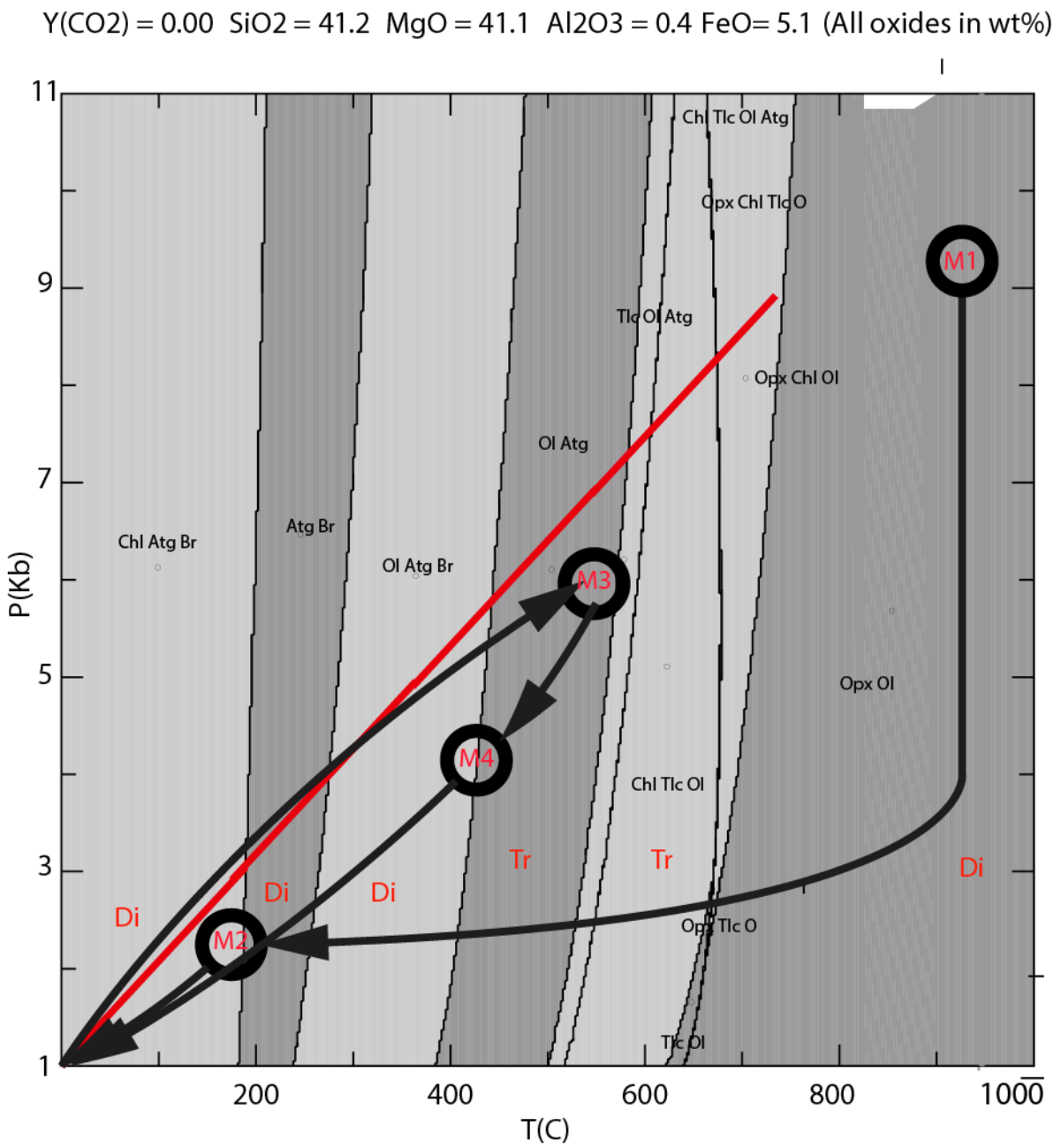

Figure 6.7. Reconstructed PT path, calculated using the BRC of sample 1.1, for all investigated lower Köli nappe peridotites. Mineral assemblages are plotted in the background, red line is the 25˚C/km geotherm. The stability of diopside and tremolite has been manually added (in red) since no CaO was present in the BRC.

7 Model discussion

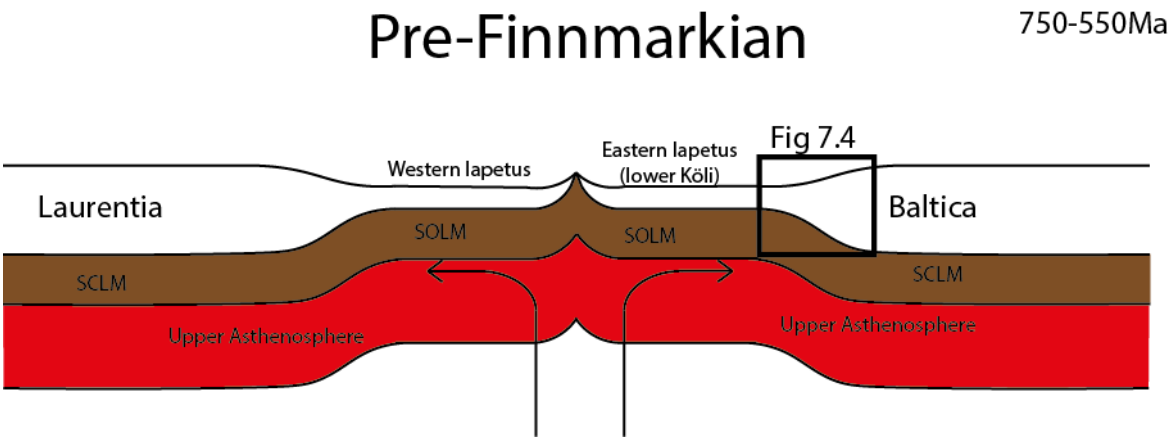

Figure 7.1. The opening of the Iapetus and/or Aegir Oceans. Asthenospheric mantle rocks are transported to and incorporated into the oceanic lithosphere (SOLM). Serpentinisation processes may have initiated as soon as oceanic water reached the abyssal peridotites.

The abyssal peridotites are likely to have an oceanic origin and have most likely formed in the time period between the opening of the Iapetus ocean and the first collision event (Finnmarkian, fig 7.2). The opening of the Iapetus/Aegir oceans occurred between 750 (start of rifting, dike swarms in Sarv nappe, Claesson and Roddick, 1983) and 550 Ma (start of the closure of the Iapetus Ocean). However a more precise date for the onset of collision is difficult to give since the age obtained by radiometric isotope analysis corresponds to the age at which the peridotite cooled down to the closure temperature which may not overlap with the age of uplift towards the surface.

The M2 metamorphic phase is characterized by low temperature (and pressure) lizardite, common for peridotites near the ocean floor. The formation of antigorite can be avoided if water is only allowed to penetrate the peridotite body near the ocean floor. Water may penetrate along faults created by sea floor spreading mechanisms. Faulting will be assisted by a volume increase from olivine to serpentine. This serpentinisation process will most likely continue for the time that the peridotites remain close to the sea floor. However, if water was not able to penetrate down to the lower parts of the ophiolite section serpentinisation may have been initiated at a later stage.

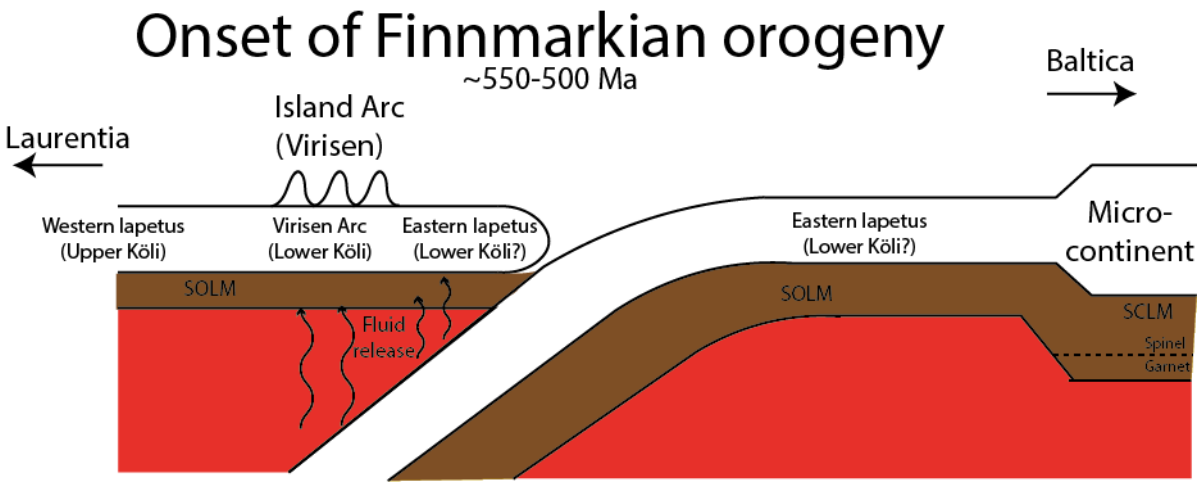

Figure 7.2. Formation of an island arc after initiation of convergent plate motions.

As closure of the Iaptus initiated intra-oceanic subduction processes started along the Iaptus ocean. One such subduction zone resulted in the formation of the Virisen Island Arc (fig 7.2). The interaction of Island Arc magmas and the overlying ophiolite may be the cause of the 'volcanic alteration' spinels present in the presented peridotites.

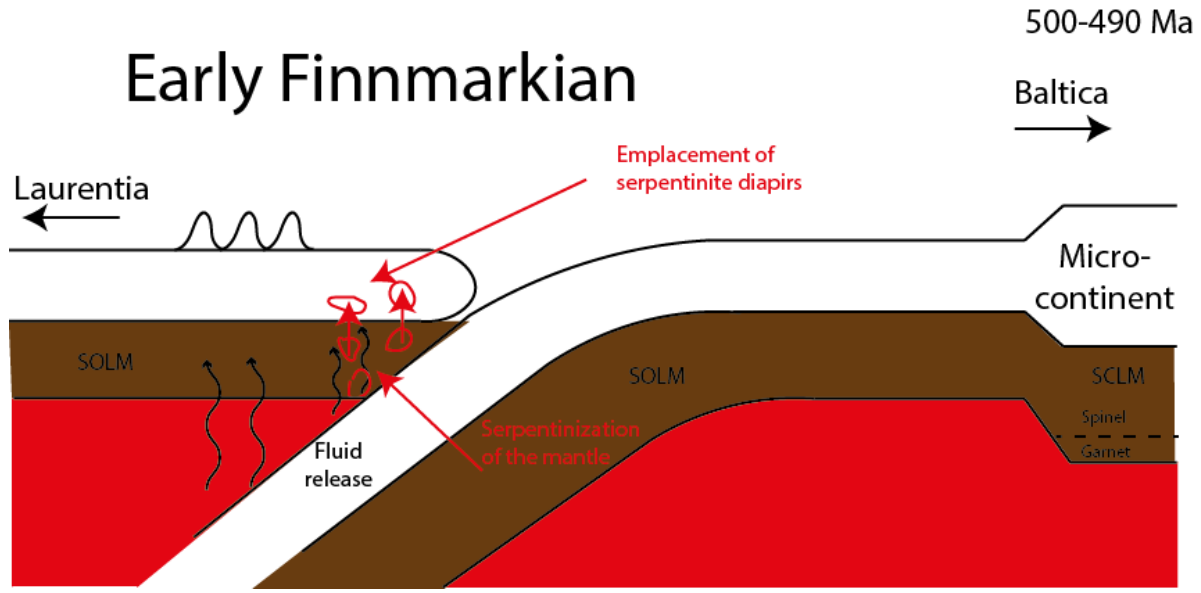

Figure 7.3. Serpentinization of sub-oceanic lithospheric mantle by subduction fluids resulting in serpentinites diapirsm and emplacement in the overlying crust.

In addition intra oceanic subduction can initiate the emplacement of peridotites into the overlying oceanic crust through serpentinite diapirism (Stigh 1979). In this case fluid released from the subducting slab serpentinizes the overlying (oceanic) lithospheric mantle. The related volume increase will enable the serpentinites to rise towards the surface (fig 7.3). However the presence of other parts of an ophiolite section at other peridotites in the lower Köli poses a problem for this scenario. A more detailed study of the nature of the serpentinisation fluids may provide additional information whether the lower Köli peridotites were emplaced by serpentinite diapirs or not.

The microcontinent, that has rifted away from Baltica, and the margin of Baltica itself, have experienced rifting. The western Seve nappe in northern Jämtland contains several orogenic peridotite lenses. Crustal emplacement of the latter may be the result of SCLM upwelling and accompanied serpentinisation (van Bruchem, 2016). The formation of oceanic crust is essential for initiation of subduction of the central Seve nappe during the Jämtlandian (Brueckner and van Roermund, 2004). Figure 58 illustrates rifting at a passive continental margin. In this case SCLM may rise to the surface after slow rifting. This will result in serpentinized SCLM between continental (or proximal) sediments.

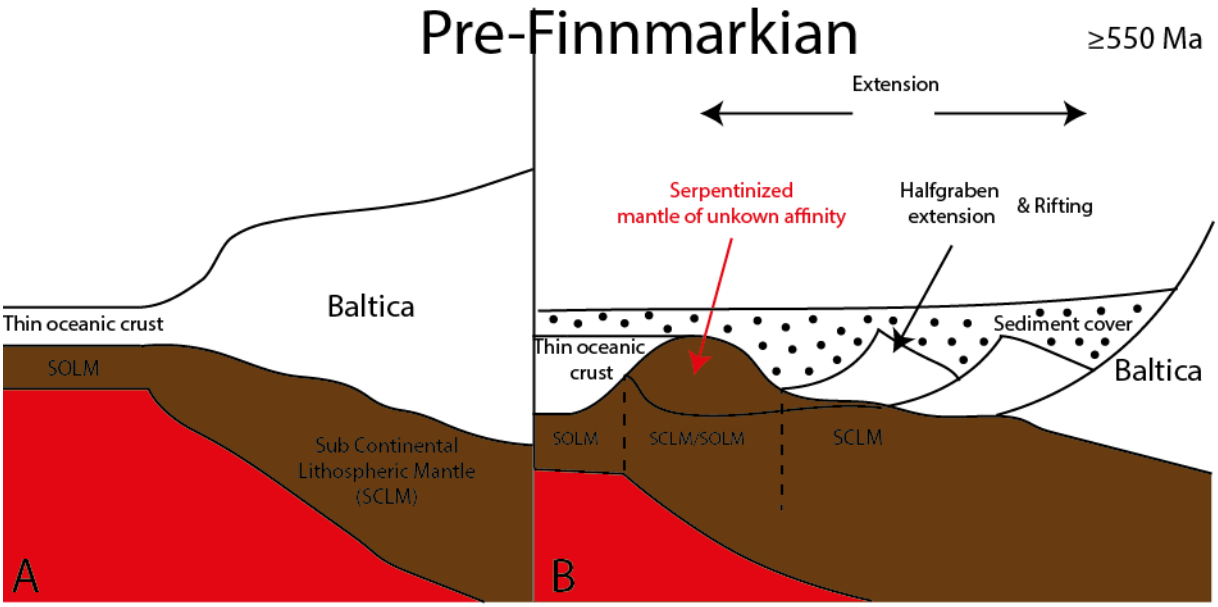

Figure 7.4 (Hyper)extended margin at the Baltic margin. Initiating of slow rifting with little magma production. Mantle upwelling, resulting in serpentinized SCLM. Later stages result in the formation of oceanic crust.

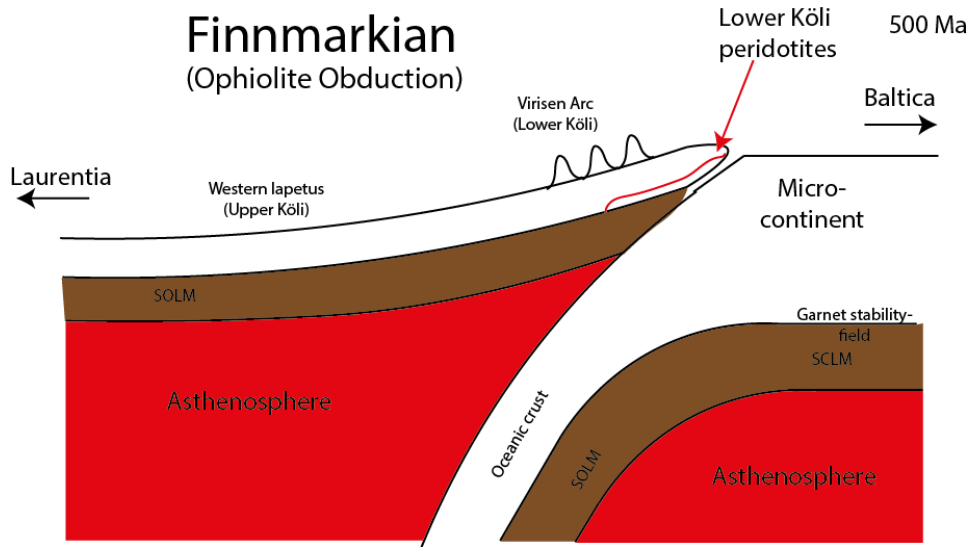

Figure 7.5. The collision between an island arc and a microcontinent and subsequent obduction of the lower Köli nappe onto a micro continent.

Eventually collision between the Virisen arc and a micro continent, that has rifted away from Baltica, occurred (Brueckner and van Roermund, 2004; figure 7.5). The details of the process under which ophiolites are thrusted onto island arcs or continents are not yet fully understood. But Dewey (1975) shows that ophiolite sequences may be obducted onto (micro) continents after partial delamination of the underlying lithosphere has taken place.

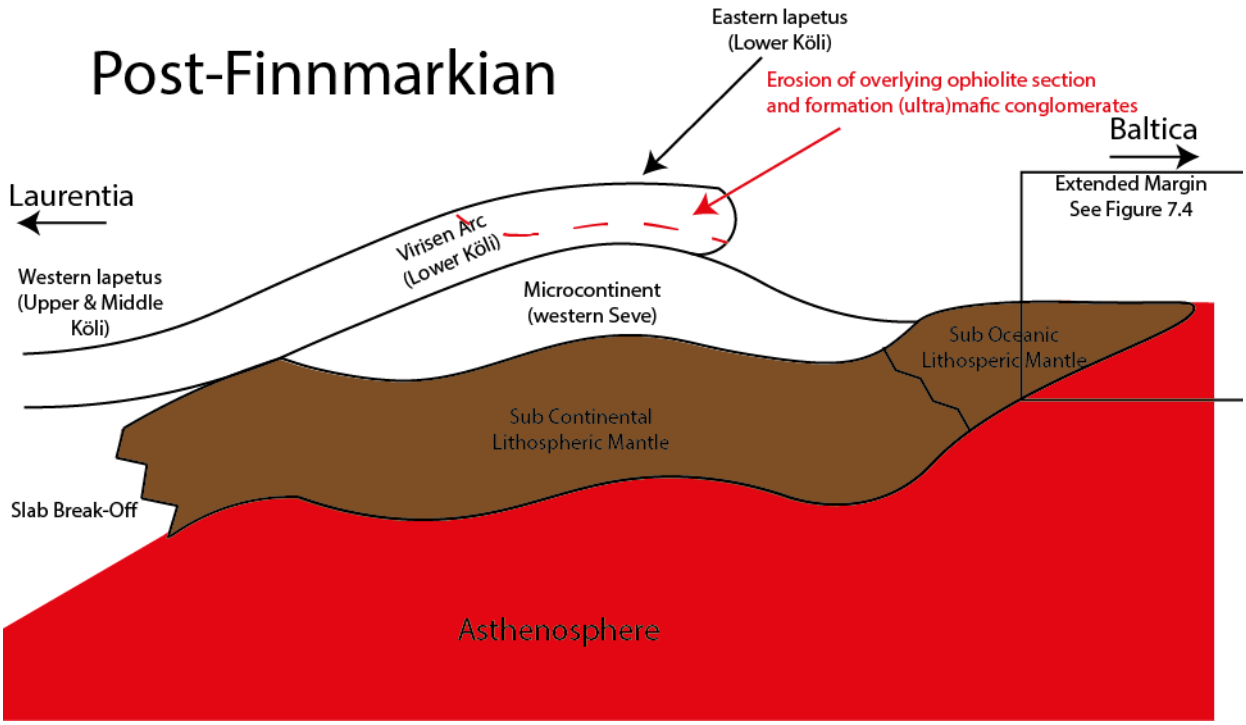

Figure 7.6. The accretion of the Eastern Köli (including the Virisen Arc) onto a microcontinent. Erosional processes can remove large parts of the ophiolite sequence as well as form (ultra)mafic conglomerates at this point.

After obduction the ophiolite sequence experienced erosional processes which removed large parts of the higher sequence resulting in the (dispersed) peridotite distribution currently present (figure 7.6). (Ultra)Mafic conglomerates, present at the margins of peridotite bodies in the lower Köli nappe, are likely to have formed during this peridiod while the peridotites were exposed at the surface. Serpentinisation process could have initiated during this phase as well. However, the amounts of water and reaction kinetics at surface temperature do not favor the quick growth of serpentine.

After the Finnmarkian orogeny Baltica collided with the microcontinent (+Köli) initiating the subduction of the Seve nappe (fig 7.7). During this phase 3 types of peridotites were incorporated into the Seve nappe; low pressure SCLM peridotites in the western Seve (may also be related to the passive margin as earlier described), medium pressure SCLM peridotites in the eastern Seve and high

pressure SCLM peridotites in the central Seve (fig 7.7) (western/eastern peridotites Van Bruchem, 2016) (central peridotites van Roermund, 1989). Van Roermund (2004) proposes that after slab breakoff the Seve nappe complex was exhumed and was emplaced under the Köli nappe (figure 7.8).

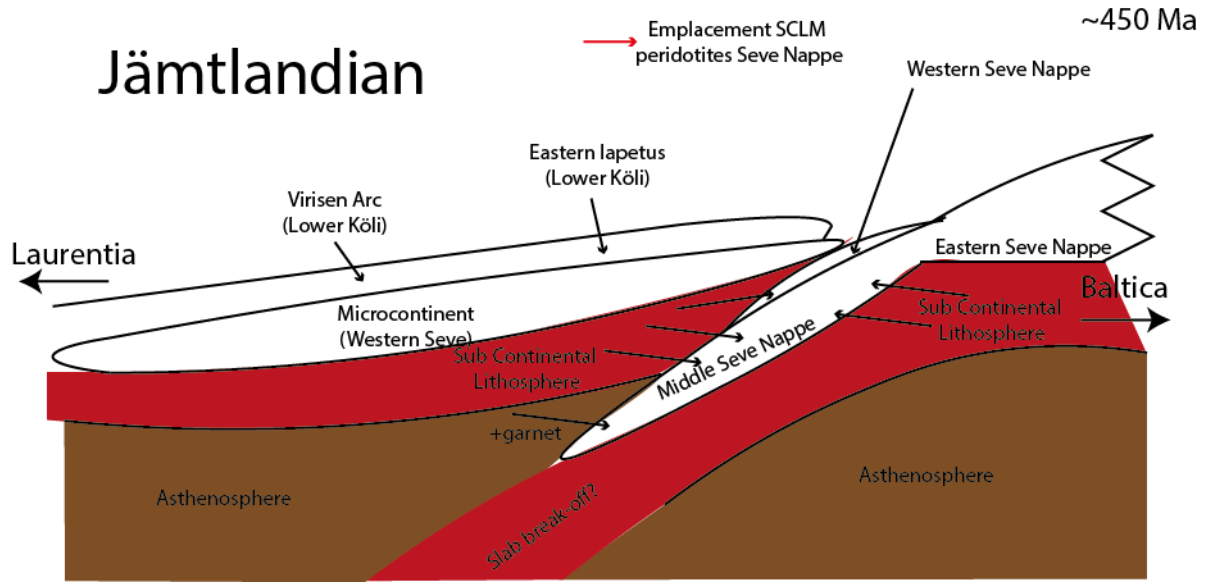

Figure 7.7. Initiation subduction of Baltica and incorporation of SCLM peridotites in the Seve nappe.

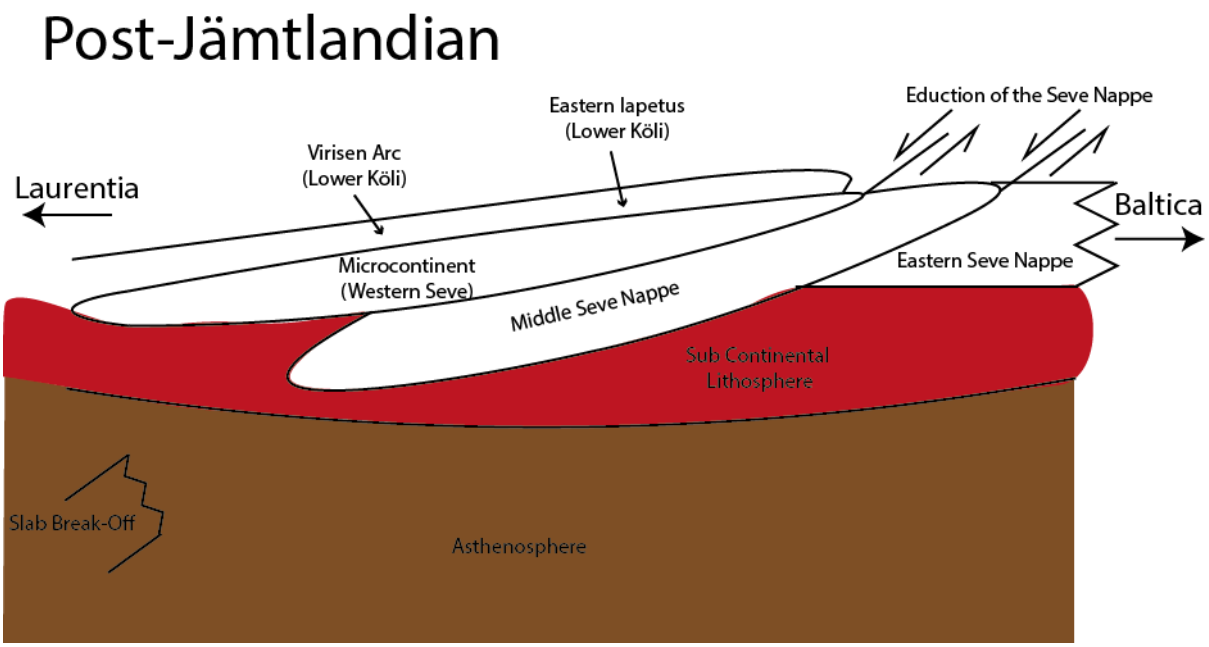

Figure 7.8. eduction of the Seve nappe, as a result of slab break-off, and emplacement under the Köli nappe.

Afterwards the PT conditions change significantly into the olivine stability field as a result of ongoing thrusting. The west ward thrusting of the Virisen Arc and Laurentia derived nappes (upper most nappe) cause great enough of a burial effect to enter the olivine stability field however growth is still limited by the presence (or lack of) water. This thrusting is attributed to the Scandian Orogeny that transpired around 425 to 415 Ma (fig 7.9). In addition Baltica started to underplate under Laurentia, which may have eventually led to shallow subduction. The Western Gneiss Region reached peak metamorphic conditions of 820 °C, 39 kbar (Terry et al., 2000) during this subduction phase which occurred relatively far west (in comparison to the Köli/Seve nappe complex). Finally all nappes were thrusted on top of the Baltic continent in an eastern direction while Baltica moved westwards. The nappes thin or are completely cut off towards the west.

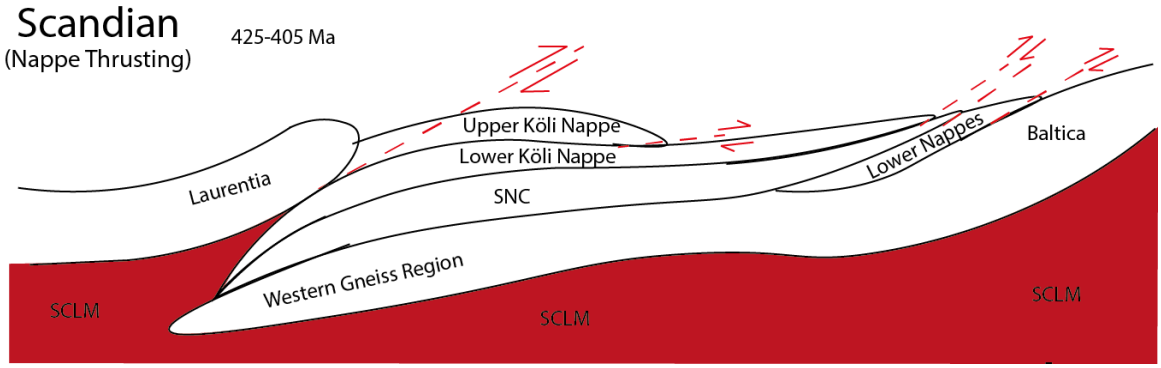

Figure 7.9. Scandian thrusting, Nappes are transported eastwards. Baltica underplates Laurentia in a westwards direction. The nappes thin or are completely cut off westwards.

8 Conclusions

1) This work confirms the oceanic origin of the Koli peridotites through EMP analysis of spinel compositions and Mg# of olivine.
2) The serpentinisation conditions for the first serpentinisation phase (M2) are low P/T reflected in the presence of brucite and lizardite.
3) The peak metamorphic temperature is determined between 400 and 500 ˚C through pseudo section analysis of peridotite BRC.
4) The peak metamorphic pressure is determined to be 5kb along a standard geotherm.

9 Future Work

1) The serpentinisation fluid for the first serpentinisation phase should be determined through sulfur and oxygen isotope fractionation analysis to determine the location of serpentinisation. In addition this may give more insight into serpentinite diapirism being responsible for the emplacement of peridotites.
2) An accurate analysis of trace elements is necessary to further confirm the origin of the Köli peridotites.
3) Further analysis of the serpentine conglomerates may reveal information on the timing of obduction and conditions after obduction.

Acknowledgements

I would like to thank Dr. H.L.M. van Roermund for his extensive willingness for discussion and opportunity to visit S. Västerbotten during a fieldtrip. I would also like to thank mrs. M.J.C. Bouten for assisting me at the EMP and SEM and dr. H. King for assistance during Raman spectroscopy. Finally I would like to thank S.D.A.van Bruchem and H. van Schrojenstein Lantman for their discussions during the project.

10 References

Andersen, A., Dahlman, B., Gee, D.G. and Snäll, S., 1986, The Scandinavian Alum Shales: Sveriges Geologiska Undersökning, Ser. Ca 56, 50 pp.

Andersen, T.B., 1998. Extensional tectonics in the Caledonides of southern Norway, an overview. Tectonophysics 285, 333–351.

Arnbom J.O. 1980 Metamorphism of the Seve Nappes at Åreskutan Swedish Caledonides Geologiska Föreningens i Stockholm Förhandlingar, 102 (1980), pp. 359–371

Asklund B. 1961 The extension of the Serv Nappe in the Scandinavian Mountain Chain Sveriges Geologiska Undersökning, C584 (1961), p. 28

Barnes, S. J., Roeder, P. L., 2001. The range of spinel compositions in terrestrial mafic and ultramafic rocks. Journal of Petrology, 42, 12 2279-2302.

Bergman S., Geology and geochemistry of mafic-ultramafic rocks (Koli) in the Handol area, central Scandinavian Caledonides. Norsk Geologisk Tidsskrift, Vol. 73, pp. 2 1-42. Oslo 1993.

Bjørlykke, A., Olaussen, S., 1981. Silurian sediments, volcanics and mineral deposits in the Sagelvvatn area, Troms, north Norway. Nor. Geol. Unders. 365, 1 –38.

Bodinier, J. L., Godard, M., 2004. Treatise on Geochemistry, Volume 2: The Mantle and Core.

Boillot G, Grimaud S, Mauffret A, Mougenot D, Kornprobst J, Mergoil-Daniel J, Torrent G (1980) Ocean-continent boundary off the Iberian margin: A serpentinite diapir west of the Galicia Bank. Earth Planet Sci Lett 48:23–34

Boyd F.R., 1989. Compositional distinction between oceanic and cratonic lithosphere. Earth and Planetary Science Letters, 96 (1989) 15-26

Braathen, A., Nordgulen, Ø., Osmundsen, P.T., Andersen, T.B., Solli, A., Roberts, D., 2000. Devonian, orogen-parallel, opposed extension in the Central Norwegian Caledonides. Geology 28, 615– 618.

Brueckner, H. K., and van Roermund H. L. M., 2001. ‘‘Dunk’’ tectonics as a model for the evolution of the Scandinavian Caledonides, Geol. Soc. Am. Abstr. Programs, 137 – 0.

Brueckner H. K., Roermund L. H. M., 2004. Dunk tectonics: A multiple subduction//eduction model for the evolution of the Scandinavian Caledonides. tectonics, vol. 23, tc2004

(Brueckner and Medaris, 2000)

Van Bruchem, S. D. A. 2017. Master thesis: Petrogenesis of orogenic peridotites and emplacement in the lower- and upper belt of the Seve Nappe Complex, Northern Sweden, Central Scandinavian Caledonides.

Bruton, D.L., Bockelie, J.F., 1980. Geology and paleontology of the Hølonda area, western Norway, a fragment of North America? In: Wones, D.R. (Ed.), The Caledonides in the USA. Virginia Poly. Inst. Dept. Geol. Sci. Memoir, vol. 2, pp. 41–47.

Bucher, K., 1990. Mantle fragments in the Scandinavian Caledonides. Tectonophysics, 190 (1991) 173-192.

Bucher, K., Grapes, R., 2011. Petrogenesis of metamorphic rocks.

Claesson S., Roddick K.C., 1983. 40Ar/39Ar data on the age and metamorphism of the Ottfjället dolerites, Särv Nappe, Swedish Caledonines Geol. Fören. Stockholm Förh., 98 (1983), pp. 370–374

Claesson, S., Stephens, M.B. & Klingspor, I., 1988: U-Pb zircon dating of felsic intrusions, Middle Köli Nappes, central Scandinavian Caledonides. Norsk Geologisk Tidsskrift 68, 89–97.

Clos F., Gilio M., van Roermund H. L. M., 2014. Fragments of deeper parts of the hanging wall mantle preserved as orogenic peridotites in the central belt of the Seve Nappe Complex, Sweden. Lithos 192–195 (2014) 8–20.

Dallmeyer, R.D., Andresen, A., 1992. Polyphase tectonothermal evolution of Caledonian nappes in Tromsø, Norway: evidence from 40Ar/39Ar mineral ages. Lithos 29, 19– 42.

Dalziel, I. W. D., 1992. On the organization of American plates in the Neoproterozoic and the breakout of Laurentia GSA Today, 2 (11) (1992), pp. 237–241

den Tex, E., 1969. Origin of ultramafic rocks, their tectonic setting and history. Tectonophysics, 7: 457-488.

Denschamps F., Godard M., Guillot S., Hattori K., 2012. Geochemistry of subduction zone serpentinites: A review. Lithos 178 96-127.

Dick, H. J. B., Bullen, T., 1984. Chromian spinel as a petrogenetic indicator in abyssal and alpine-type peridotites and spatially associated lavas. Contrib Mineral Petrol (1984) 86:54-76

Dick, H. J. B., 1989. Abyssal peridotites, very slow spreading ridges and ocean ridge magmatism. Geological Society, London, Special Publications 1989, v. 42, p. 71-105

Dick H.J.B. & Natland J.H. 1996. Late-stage melt evolution and transport in the shallow mantle beneath the East Pacific Rise. In: M6vel C., Gillis K.M., Allan J.F. & Meyer P.S. eds. Proceedings of the Ocean Drilling Program, Scientific Results 147, pp. 103-134. Ocean Drilling Program, College Station, Texas.

Doré, T. and Lundin, E., 2015. Hyperextended continental margins—Knowns and unknowns GEOLOGY, January 2015; v. 43; no. 1; p. 95–96.

Dunning, G.R., 1987. U–Pb zircon ages of Caledonian ophiolites and arc sequences: implications for tectonic setting (abstract). Terra Abstr., EUG IV, Strasbourg, 179.

Dunning, G.R., Pedersen, R.B., 1988. U/Pb ages of ophiolites and arc-related plutons of the Norwegian Caledonides: implications for the development of Iapetus. Contrib. Mineral. Petrol. 98, 13– 23.

Du Rietz, T., 1935. Peridotites, serpentines and soapstones of northern Sweden. GFF 57, 133–260.

Eide, E.A., Lardeaux, J.M., 2002. A relict blueschist in meta-ophiolite from the central Norwegian Caledonides—discovery and consequences. Lithos 60, 1 – 19.

Elvevold, S., Gilotti, J.A., 2000. Pressure– temperature evolution of retrogressed kyanite eclogites, Weinschenk Island, north-east Greenland Caledonides. Lithos 53, 127– 147.

Evans, B.W., Frost, B.R.: Chrome-spinel in progressive metamorphism - a preliminary analysis. Geochim. Cosmochim. Acta 39, 959-972 (1975).

(Essex et al., 1997).

Fabries, J. 1979. Spinel-olivine geothermometry in peridotites from ultramafic complexes. Contributions to Mineralogy and Petrology, 69: 329–336.

Fisk, M.R. (1986) Basalt magma interaction with harzburgites and the formation of high-magnesium andesites. Geophysical Research Letters 13, 5, 467-470. Foslie,S.1959:Geologisk kart JÆVSJØEN (Rektangel 51C).Norges geologiskeundersøkelse.

Fossen, H., Dunlap, W.J., 1998. Timing and kinematics of Caledonian thrusting and extensional collapse, southern Norway: evidence form 40Ar/39Ar thermochronology. J. Struct. Geol. 20, 765–781.

Furnes H., Pedersen R.B., Hertogen J., Albrektsen B.A., 1991. Magma development of the Leka Ophiolite Complex, central Norwegian Caledonides. Lithos 27(4):259-277

Gayer, R.A., Rice, A.H.N., Roberts, D., Townsend, C., Welbon, A., 1987. Restoration of the Caledonian Baltoscandian margin from balanced cross-sections: the problem of excess continental crust. Trans. R. Soc. Edinb. 78, 197– 217.

Gee, D.G., 1975. A tectonic model for the central part of the Scandinavian Caledonides. Am. J. Sci. 275A, 468– 515.

Gee, D.G., Kumpulainen, R., Roberts, D., Stephens, M.B., Thon, A. & Zachrisson, E., 1985: Scandinavian Caledonides – Tectonostratigraphic Map. Sveriges geologiska undersökning Ba 35.

Gee D.G., Guezou J.-C.A., Roberts D., Wolff F.C.A. The central–southern part of the Scandinavian Caledonides D.G. Gee, B.A. Sturt (Eds.), The Caledonide Orogen–Scandinavia and Related Areas, Wiley, Chichester (1985), pp. 109–133

Gee, D.G., 1986. Early Caledonian tectonothermal activity in the Scandes—the Finnmarkian and Trondheimian episodes (extended abstract). Geol. Fören. Stockh. Förh. 109, 343–345.

Gilotti, J.A., Ravna, E.J.K., 2002. First evidence for ultrahigh-pressure metamorphism in the northeast Greenland Caledonides. Geology 30, 551–554.

Greiling, R. O., Grimmer, J. C., 2007 Köli nappes in the northcentral Swedish Caledonides – new views on stratigraphy and structural evolution, GFF, 129:2, 141-153.

Grimmer, J. C.; Greiling, R. O., 2008. Geochemistry and tectonic significance of silicic island-arc volcanic rocks from the Lower Koli Nappe, north-central Swedish Caledonides (Kultsjon area). Geotectonic Research Volume 95 Number 0 (2008), p. 56 – 58.

Grønlie, A., Roberts, D., 1989. Resurgent strike-slip duplex development along the Hitra– Sna°sa and Verran faults, Møre– Trøndelag Fault Zone, central Norway. J. Struct. Geol. 11, 295– 305.

Grønlie, A., Nilsen, B., Roberts, D., 1991. Brittle deformation history of fault rocks on the Fosen Peninsula, Trøndelag, central Norway. Nor. Geol. Unders. Bull. 421, 357– 393.

Harper, D., 1998: Interpreting Orogenic Belts: Principles and Examples: Unlocking the Stratigraphical Record. In P. Doyle & M.R. Bennet (eds.): Advances in Modern Stratigraphy, 491–524. John Wiley & Sons.

Hartz, E., Torsvik, T.H., 2002. Baltica upside down: a new plate tectonic model for Rodinia and the Iapetus Ocean. Geology 30, 255– 258.

Hollocher K., Robinson P., Walsh E., Terry M.P. 2007 The Neoproterozoic Ottfjället dike swarm of the Middle Allochthon, traced geochemically into the Scandian Hinterland Western Gneiss Region, Norway American Journal of Science, 307 (2007), pp. 901–953.

Holtedahl, O., 1920. Palaeogeography and diastrophism in the Atlantic –Arctic region during Palaeozoic time. Am. J. Sci. 49, 1 – 25.

Hossack, J.R., 1984. The geometry of listric growth faults in the Devonian basins of Sunnfjord, west Norway. J. Geol. Soc. Lond. 135, 705– 711.

Ishii T., Robinson P.T., Maekawa H. & Fiske R. 1992. Petrological studies of peridotites kom diapiric serpentinite seamounts in the Izu-Ogasawara-Mariana forearc, Leg 125. In: Flyer P., Pearce J.A., Stokking L.B. ef al. Proceedings of the Ocean Drilling Program, Scientific Results 125, pp. 445485. Ocean Drilling Program, College Station, Texas.

Jackson, E.D. and Thayer, T.P., 1972. Some criteria for distinguishing between stratiform, concentric and alpine peridotite-gabbro complexes. 24th Int. Geol. Congr., Sect. 2, 289-296.

Janák, M., Van Roermund, H., Majka, J., and Gee, D.G., 2013a, UHP metamorphism recorded by kyanite-bearing eclogite in the Seve Nappe Complex of northern Jämtland, Swedish Caledonides: Gondwana Research, v. 23, p. 865– 879.

Jianping L., Kornprobst J., Vielzeuf D., Fabriès, J. 1995. An improved experimental calibration of the olivine-spinel geothermometer. Chinese Journal of Geochemistry 14(1):68-77

Johnson K.T.M., Dick H.J.B. and Shimizu N. 1990. Melting in the oceanic upper mantle: an ion microprobe study of diopsides in abyssal peridotites. Journal of Geophysical Research 95,2661-2678.

Johnson K.T.M. & Dick H.J.B. 1992. Open system melting and temporal and spatial variation of peridotite and basalt at the Atlantis I1 fracture zone. Journal of Geophysical Research 97,9219-9241.

Juteau T., Berger E & Cannat M. 1990. Serpentinized, residual mantle peridotites from the M.A.R. median valley, ODP Hole 670A (21°10'N, 4S002W, Leg 109): primary mineralogy and

geothermometry. In: Detrick R., Honnorez J., Bryan W.B., Juteau T. et al. Proceedings of the Ocean Drilling Program, Scientific Results 1061109, pp. 27- 45. Ocean Drilling Program, College Station, Texas.

Köhler T. P., Brey G. P., 1990. Calcium exchange between olivine and clinopyroxene calibrated as a geotbermobarometer for natural peridotites from 2 to 60 kb with applications. Geochimica et Cosmochimica Acta Vol. 54, pp. 2375-2388.

Kumpulainen R., Nystuen J.P. Late Proterozoic basin evolution and sedimentation in the westernmost part of Baltoscandia D.G. Gee, B.A. Sturt (Eds.), The Caledonide Orogen – Scandinavia and Related Areas, John Wiley and Sons, Chichester (1985), pp. 213–232

Kulling, O., 1933: Bergbyggnaden inom Björkvattnet-Virisen-området i Västerbottensfjällens centrala del – en studie i den kaledoniska bergskedjans geologi. Geologiska Föreningens i Stockholm Förhandlingar 55, 167–422.

Kulling, O., 1955: Den Kaledoniska fjällkedjans berggrund inom Västerbottens län. In S. Gavelin & O. Kulling: Beskrivning till berggrundskarta över Västerbottens län. Sveriges geologiska undersökning Ca 37, 101–296.

Kulling, O., 1972: The Swedish Caledonides. In L.U. de Sitter (ed.): Scandinavian Caledonides, 149–285. Wiley Interscience.

Leblanc M., Nicolas A. Les chromitites ophiolitiques. Chronique de la Recherche Minière 507, pp. 3-25. 1992

McClellan E. A., 2004. Metamorphic conditions across the Seve-Köli Nappe boundary, southeastern Trondheim region, Norwegian Caledonides: Comparison of garnet-biotite thermometry and amphibole chemistry. Norwegian Journal of Geology, Vol. 84, pp. 257-282. Trondheim 2004.

Moody, J., B., 1976. Serpentinization: a review. Lithos 9, 125-138.

Murray, C. G. 2006. A Devonian origin for the Princhester ophiolite, northern New England Orogen. Extended Abstracts, Australian Earth Sciences Convention 2006, Melbourne.

Nilsson L. P., Roberts D., Ramsay D. M. The Raudfjellet ophiolite fragment, Central Norwegian Caledonides: principal lithological and structural features. ngu-bull 445, 2005 - page 102

Nilsson, L.-P. & Roberts, D. (2014) A trail of ophiolitic debris and its detritus along the Trøndelag-Jämtland border: correlations and palaeogeographical implications. Norges geologiske undersøkelse Bulletin, 453, 29–41.

Nordgulen, Ø., Bickford, M.E., Nissen, A.L., Wortman, G.L., 1993. U–Pb zircon ages from the Bindal Batholith, and the tectonic history of the Helgeland Nappe Complex, Scandinavian Caledonides. J. Geol. Soc. Lond. 150, 771– 783.

Noble S.R., Tucker R.D., Pharaoh T.C., 1993. Lower Palaeozoic and Precambrian igneous rocks from eastern England, and their bearing on late Ordovician closure of the Tornquist Sea: constraints from Usingle bondPb and Nd isotopes Geol. Mag., 130 (1993), pp. 835–846

Norton, M.G., 1987. The Nordfjord–Sogn detachment, W. Norway. Nor. Geol. Tidsskr. 67, 93– 96.

Osmundsen, P.T., Andersen, T.B., Markussen, S., Svendby, A.K., 1998. Tectonics and sedimentation in the hanging wall of a major extensional detachment: the Devonian Kvamshesten basin, western Norway. Basin Res. 10, 213– 234.

Osmundsen, P.T., Braathen, A., Nordgulen, Ø., Roberts, D., Meyer, G., Eide, E., 2003. The Devonian Nesna Shear Zone, north– central Norwegian Caledonides, and its regional implications. J. Geol. Soc. Lond. 160, 137– 150.

Palme, H. and O'Neill, H. St. C. (2004). Cosmochemical estimates of Mantle Composition. In: Treatise on Geochemistry. Holland, H.D. and Turrekian, K.K. (Editors), Elsevier, Amsterdam, The Netherlands. 2: 1-38.

Parkinson I.J. & Pearce J.A. 1998. Peridotites from the h-Bonin-Mariana forearc (ODP Leg 125): evidence for mantle melting and melt-mantle interaction in a suprasubduction zone setting. Journal of Petrology 39, 1577-1618.

Pearce J.A., Barker P.F., Edwards S.J., Parkinson I.J. & Leat P.T. 2000. Geochemistry and tectonic significance of peridotites from the South Sandwich arc-basin system, South Atlantic. Contributions to Mineralogy and Petrology 139, 36-53.

Pedersen, R.B., Furnes, H., Dunning, G.R., 1988. Some Norwegian ophiolite complexes reconsidered. Nor. Geol. Unders. Spec. Publ. 3, 80– 85.

Pedersen, R.B., Furnes, H., Dunning, G., 1991. A U/Pb age for the Sulitjelma Gabbro, north Norway: further evidence for the development of a Caledonian marginal basin in Ashgill– Llandovery time. Geol. Mag. 128, 141–153.

Pickering, K.T. & Smith, A.G., 1995: Arcs and backarc basins in the Early Paleozoic Iapetus Ocean. The Island Arc 4, 1–67.

Plink-Björklund P., Björklund L., Loorents K.-J. Sedimentary documentation of the break-up of Rodinia, Offerdal Nappe Swedish Caledonides Precambrian Research, 136 (2005), pp. 1–26.

Ramsay, D.M. & Sturt, B.A. 1998: Excursion Guide: The Otta Nappe and its integration into the Trondheim Nappe in the South-Central Scandinavian Caledonides. Norges Geologiske Undersøkelse Report 98.103, 42 pp.

Reymer, A. P. S., 1979. Investigations into the metamorphic nappes of the central Scandinavian Caledonides on the basis of Rb-Sr and K-Ar age determinations. Promotion at Leiden University.

Roberts, D., 1980. Petrochemistry and palaeogeographic setting of the Ordovician volcanic rocks of Smøla, central Norway. Nor. Geol. Unders. 359, 43–60.

Roberts, D., 1983. Devonian tectonic deformation in the Norwegian Caledonides and its regional perspectives. Nor. Geol. Unders. 380, 85– 96.

Roberts, D. 1997: Geologisk kart over Norge. Berggrunnsgeologisk kart GRONG, M 1:250 000. Norges geologiske undersøkelse.

Roberts, D., 2001. The Scandinavian Caledonides: a multiply deformed collage of Baltican, Laurentian, Iapetan and possible Siberia lithostructural elements. (Poster and extended abstract) IGCP Project 453 Symposium, Sion, Switzerland, September 2001, Abstract Volume.

van Roermund, H. L. M. and Bakker, E. 1983. 'Structure and metamorphism of the Tången—Inviken area, Seve Nappes, Central Scandinavian Caledonides', GFF, 105: 4, 301 — 319

van Roermund, H. L. M. (1989), High-pressure ultramafic rocks from the allochthonous nappes of the Swedish Caledonides, in The Caledonide Geology of Scandinavia, edited by R. A. Grayer, pp. 205 – 219, Graham and Trotman, Norwell, Mass.

Robinson, P., 1995. Extension of Trollheimen tectonostratigraphic sequence in deep synclines near Molde and Brattvåg, Western Gneiss Region, southern Norway. Nor. Geol. Tidsskr. 75, 181– 198.

Ryan, P.D., Williams, D.M. & Skevington, D. 1980: A revised interpretation of the Ordovician stratigraphy of Sør-Trøndelag, and its implications for the evolution of the Scandinavian Caledonides. In Wones, D.R. (ed.). The Caledonides in the USA. Virginia Polytechnic, Geological Sciences,Memoir 2, 99–105.

Ryan, P.D., 2001. The role of deep basement during continent– continent collision: a review. In: Miller, J.A., et al. (Ed.), Continental Reactivation and ReworkingGeol. Soc. London Special Publ., vol. 184, pp. 39– 55.

Selbekk, R.S., Skjerlie, K.P., Pedersen, R.B., 2000. Generation of anorthositic magmas by H2O-fluxed anatexis of silica-undersaturated gabbro: an example from the north Norwegian Caledonides. Geol. Mag. 137, 609– 621.

Séranne, M., 1992. Late Palaeozoic kinematics of the Møre–Trøndelag Fault Zone and adjacent areas, central Norway. Nor. Geol. Tidsskr. 72, 141– 158.

Sjöstrand, T., 1978: Caledonian geology of the Kvarnbergsvattnet area, northern Jämtland, central Sweden. Sveriges geologiska undersökning C 735, 1–107.

Soper N.J., 1994. Neoproterozoic sedimentation on the northeast margin of Laurentia and the opening of Iapetus. Geol. Mag., 131 (3) (1994), pp. 291–299

Stanley, R.S., Ratcliffe, N.M., 1985. Tectonic synthesis of the Taconian orogeny in western New England. Bull. Geol. Soc. Am. 96, 1227– 1250.

Stephens, M.B., Gee, D.G., 1985. A tectonic model for the evolution of the eugeoclinal terranes in the central Scandinavian Caledonides. In: Gee, D.G., Sturt, B.A. (Eds.), The Caledonide Orogen— Scandinavia and Related Areas. Wiley, Chichester, pp. 953– 970.

Stephens, M.B., 1982: Field relationships, petrochemistry, and petrogenesis of the Stekenjokk volcanites, central Scandinavian Caledonides. Sveriges geologiska undersökning C 786, 1–111.

Stephens, M.B., 1988: The Scandinavian Caledonides: a complexity of collisions. Geology Today 4, 20–26.

Stephens, M.B. & Gee, D.G., 1989: Terranes and polyphase accretionary history in the Scandinavian Caledonides. Geological Society of America, Special Paper 230, 17–30.

Stephens, M.B., Stejskal, V., Antal, I., 1993. Geologiska och geofysiska undersökningar i Landögssjöområdet, Jämtlands län. Sveriges Geologiska Undersökning. BRAP Rapport 93017, p. 35.

Stigh J. 1979 Origin and emplacement of two compositionally layered ultramafic bodies in the Caledonides of Vasterbotten, Sweden. Geologiska foreningens I Stockholm forhandlingar, vol 100, pt. 4, pp. 317-334.

St. Julien, P., Hubert, C., 1975. Evolution of the Taconic orogen in the Quebec Appalachians. Am. J. Sci. 275A, 337– 362.

Sturt, B.A., 1983. Late Caledonian and possible Variscan stages in the orogenic evolution of the Scandinavian Caledonides (abstract). IGCP Project 27 Symposium, Rabat, Morocco.

Sturt, B . A., Ramsay, D. M . & Neuman, R . B.: The Otta Conglomerate, the Vågåmo Ophiolite - further indications of early Ordovician Orogenesis in the Scandinavian Caledonides. Norsk Geologisk Tidsskrift, Vol. 71, pp. 107-115. Oslo 1991.

Sundblad, K. & Gee, D.G., 1984: Occurrence of a uraniferous-vanadiniferous graphitic phyllite in the Köli Nappes of the Stekenjokk area, central Swedish Caledonides. Geologiska Föreningens i Stockholm Förhandlingar 106, 269–274.

Swett, K., 1981, Cambro-Ordovician strata in Ny Friesland, Spitsbergen and their palaeotectonic significance: Geological Magazine, v. 118, pp. 225–250

Terry, M.P., Robinson, P., Hamilton, M.A., Jercinovic, M.J., 2000. Monazite geochronology of UHP and HP metamorphism, deformation and exhumation, Nordøyane, Western Gneiss Region, Norway. Am. Mineral. 85, 1651– 1664.

Törnebohm, A. E. 1896: Grunddragen af det centrala Skandinaviens bergbyggnad.Kung/iga Svenska Vetenskapsakademiens Hand/ingar 18, 210 pp.

Torsvik T.H., Lohmann K.C., Sturt B.A., 1995. Vendian glaciations and their relation to the dispersal of Rodinia: Paleomagnetic constraints Geology, 23 (1995), pp. 727–730

Torsvik, T.H., Smethurst, M., Meert, J., Van der Voo, R., McKerrow, W.S., Brazier, M., Sturt, B.A., Walderhaug, H., 1996. Continental break-up and collision in the Neo-proterozoic and Palaeozoic—a tale of Baltica and Laurentia. Earth-Sci. Rev. 40, 229– 258.

Torsvik, T.H., Rehnström, E.F., 2001. Cambrian palaeomagnetic data from Baltica: implications for true polar wander and Cambrian paleogeography. J. Geol. Soc. Lond. 158, 321–329.

Vogt, Th., 1936. Orogenesis in the region of Paleozoic folding of Scandinavia and Spitsbergen. 16th Intern. Geol. Congress, Washington, 1933.

Vogt, Th. 1945: The geology of part of the Hølonda-Horg district, a type area in the Trondheim region. Norsk Geologisk Tidsskrift 25, 449–528.

Von Blanckenburg, F., and Davies J. H., 1995. Slabbreakoff: A model for syncollisional magmatism and tectonics in the Alps, Tectonics, 14, 120 – 131.

White, R. W., 1966. Ultramafic Inclusions in Basaltic Rocks from Hawaii. Contr. MinerM. and Petrol. 12, 245--314

Wicks, F. J., Whittaker E. J. W., 1997. Serpentinte textures and serpentinisation. Canadian Mineralogist Vol. 15, W. 459-488.

Yoshinobu, A.S., Barnes, C.G., Nordgulen, Ø, Prestvik, T., Fanning, M., Pedersen, R.B., 2002. Ordovician magmatism, deformation, and exhumation in the Caledonides of central Norway: an orphan of the Taconic orogeny? Geology 30, 883– 886.

Zachrisson, E., 1969: Caledonian geology of northern Jämtland - southern Västerbotten. Sveriges geologiska undersökning C 644, 1–33.

三浦, 真 2015. Integrated petrogenesis of podiform chromitites. Kanazawa University Repository for Academic Resources, 2015.

11 Appendix

The following table shows an overview of the collected samples and the locations they were collected.

Sample number	Location
1.1	Aunere (main body)
1.2	Aunere (main body)
1.4	Aunere (main body)
2.1a	Aunere (margin)
2.1b1	Aunere (margin)
2.1b2	Aunere (margin)
2.4	Aunere (main body)
2ext1	Aunere (main body)
2ext2	Aunere (main body)
3.2a1	Gründfors
3.2a2	Gründfors
3.2c	Gründfors
3.3a	Gründfors
3.3b	Gründfors
3.4.1	Gründfors
3.4.2	Gründfors
4.1.2	Rödberget
4.2.5	Rödberget

11.1 Sample photographs and description

Sample 1.1

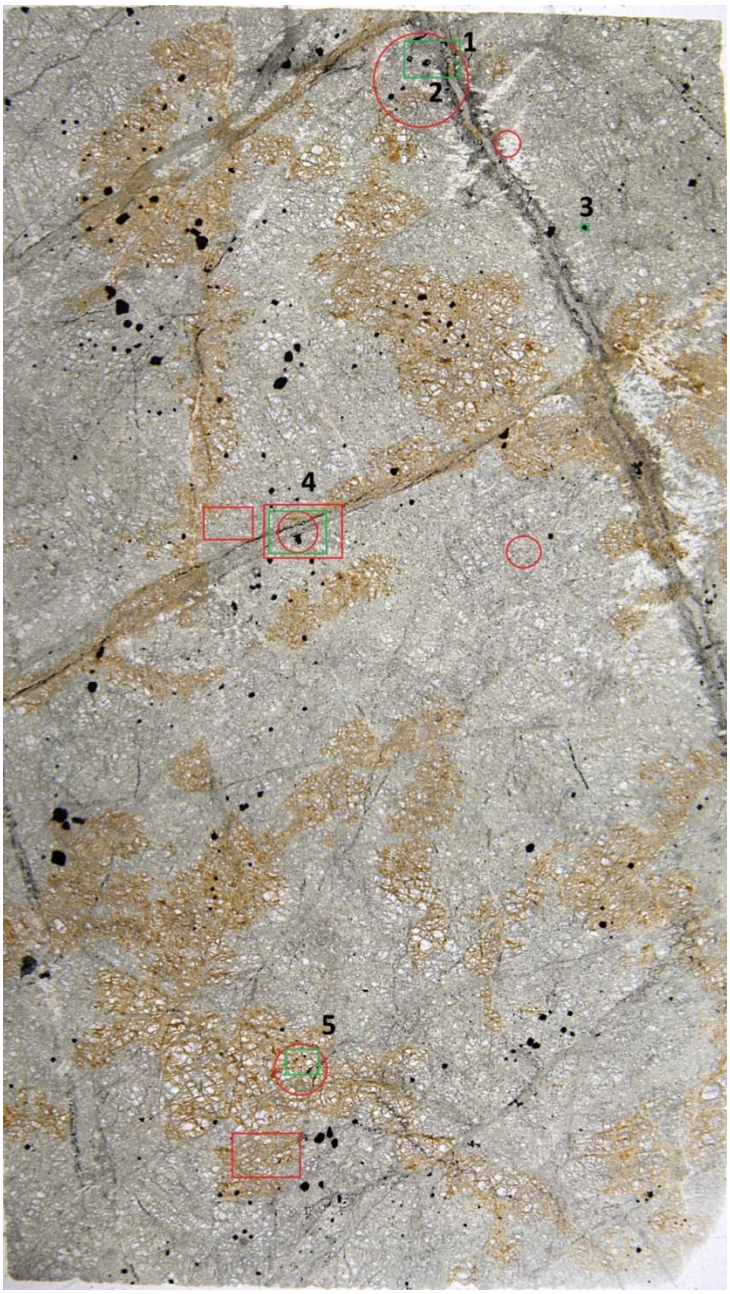

Sample 1.1 has experienced relatively little serpentinisation. Most of the mineralessemblage consists of broken up olivine grains (location 1 & 5) in a mesh structure. These olivine grains have been partly altered to serpentine. Lizardite is located between the grains themselves in a pseudomorphic growth structure (see also Raman spectroscopy). Antigorite is present as patches overgrowing all previous structures (location 2). Several veins or shearzones are present filled with finer grained olivine (location 4).

Sample 1.1 Location 1 olivine mesh structure.

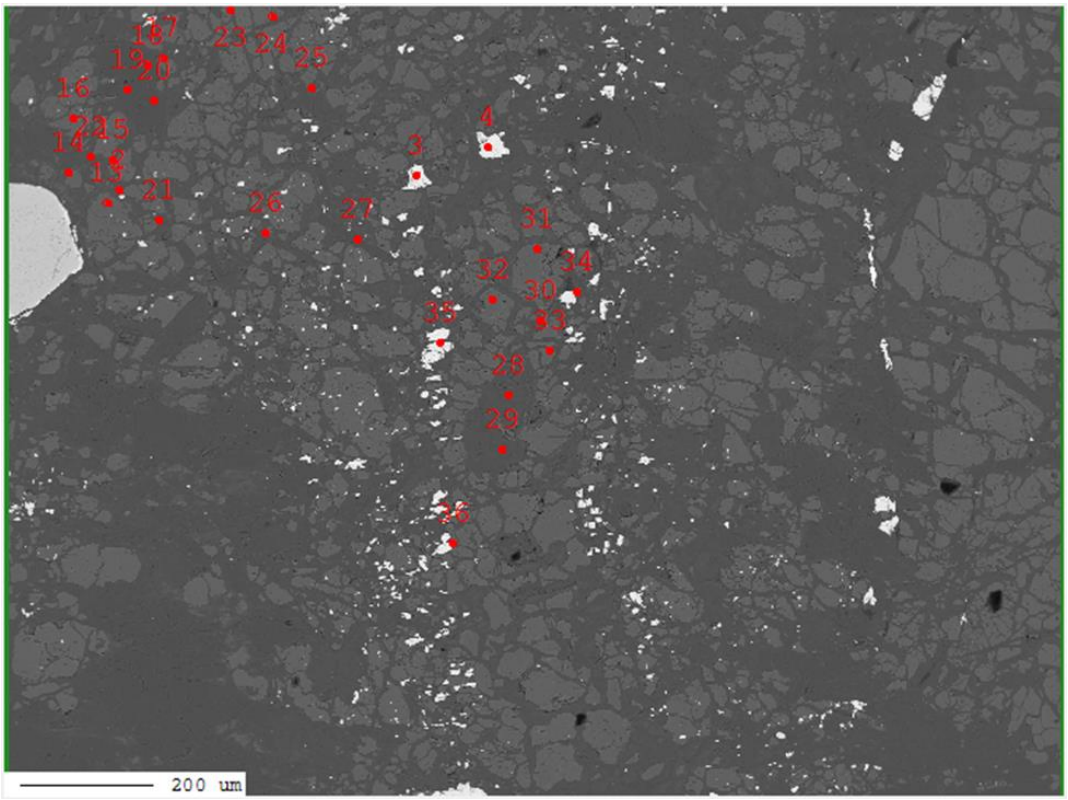

Sample 1.1 Locations 2 patchy antigorite.

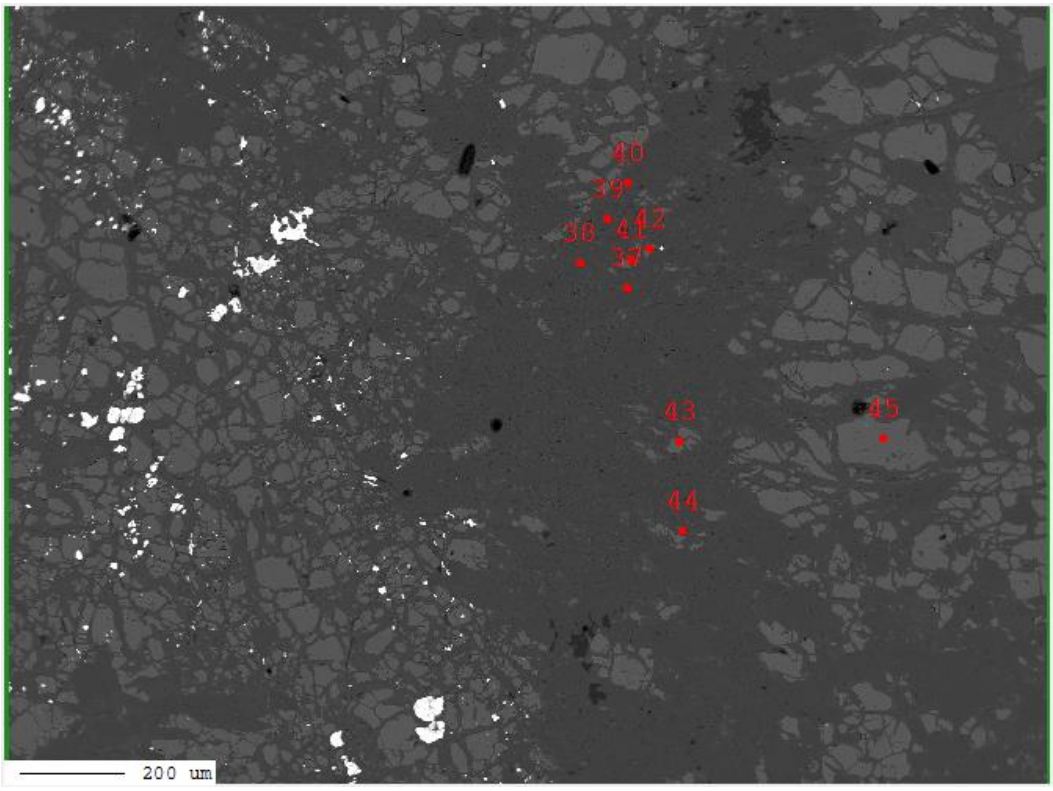

Sample 1.1 Location 3 large spinel grain.

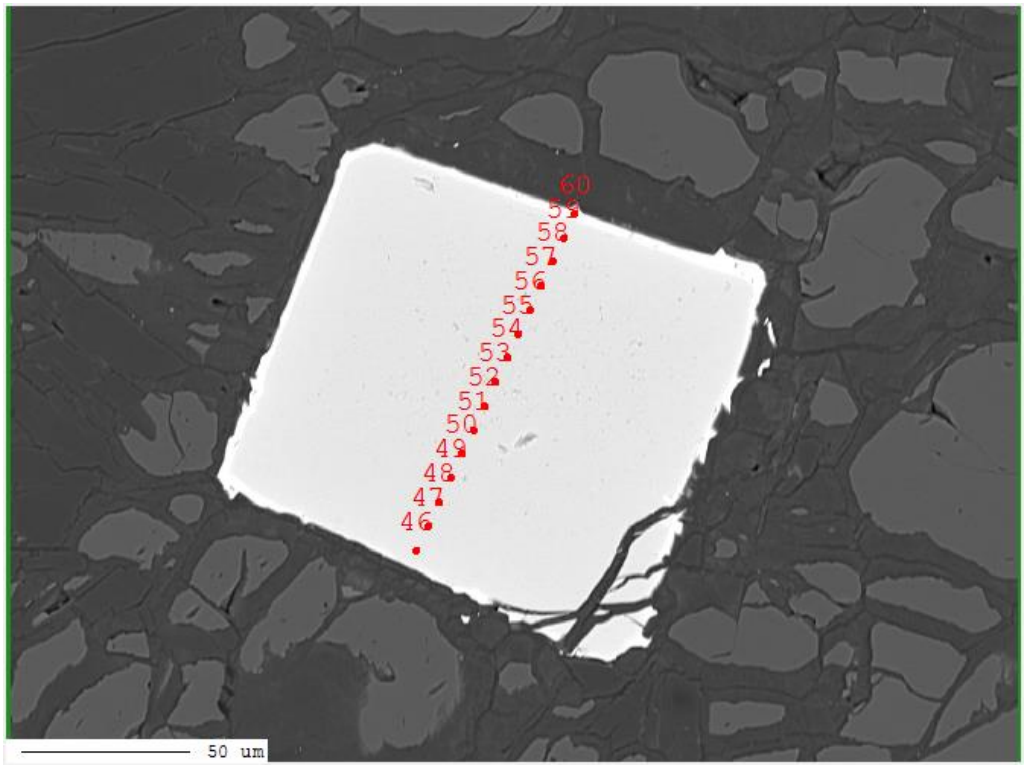

Sample 1.1 Location 4 veining/shearzone.

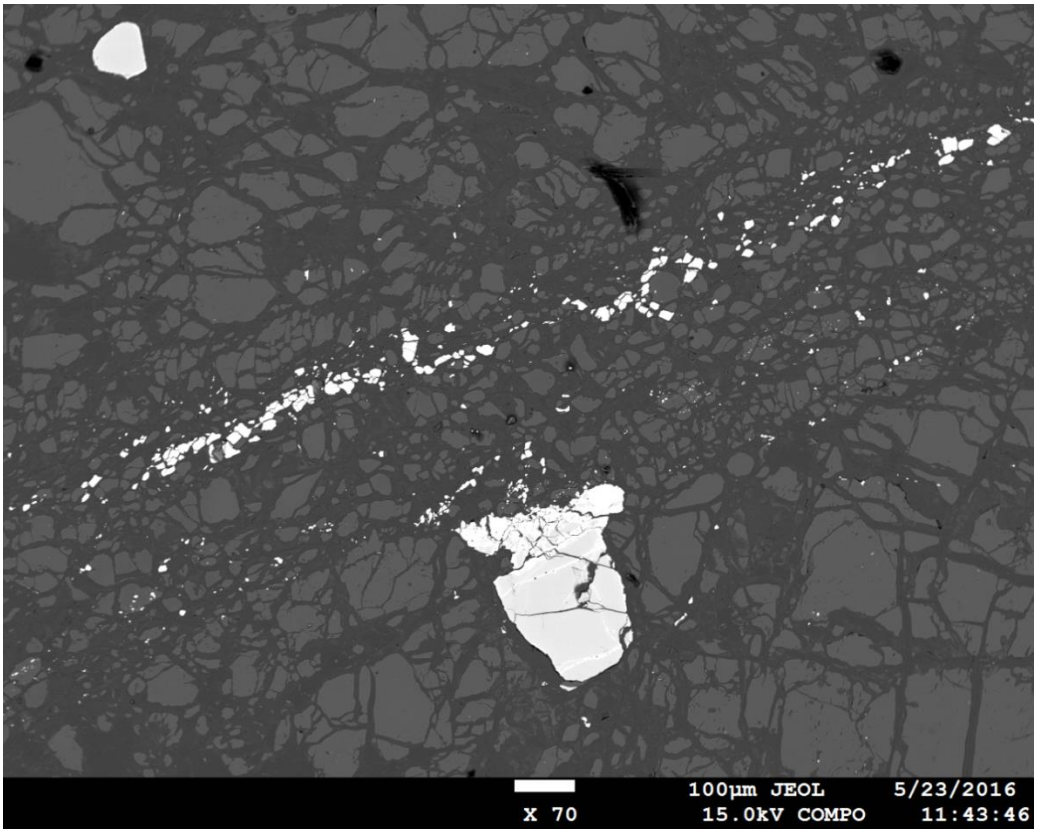

Sample 1.1 Location 5 olivine mesh structure.

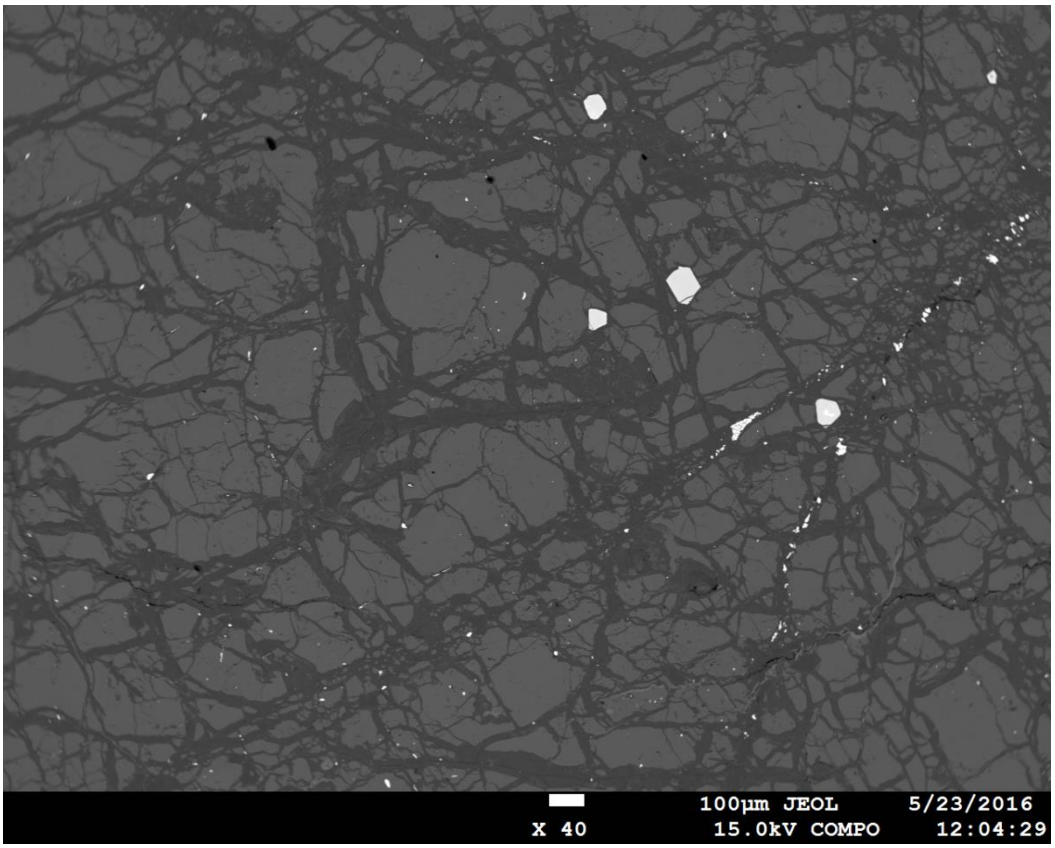

Sample 1.2

Sample 1.2 is veery similar to sample 1.1, showing the same protolith olivine grains that are altered to lizardite. Patches of antigorite are present overgrowing all previous structures. Several veinsa are present filled with finer grained olivine.

Sample 1.4

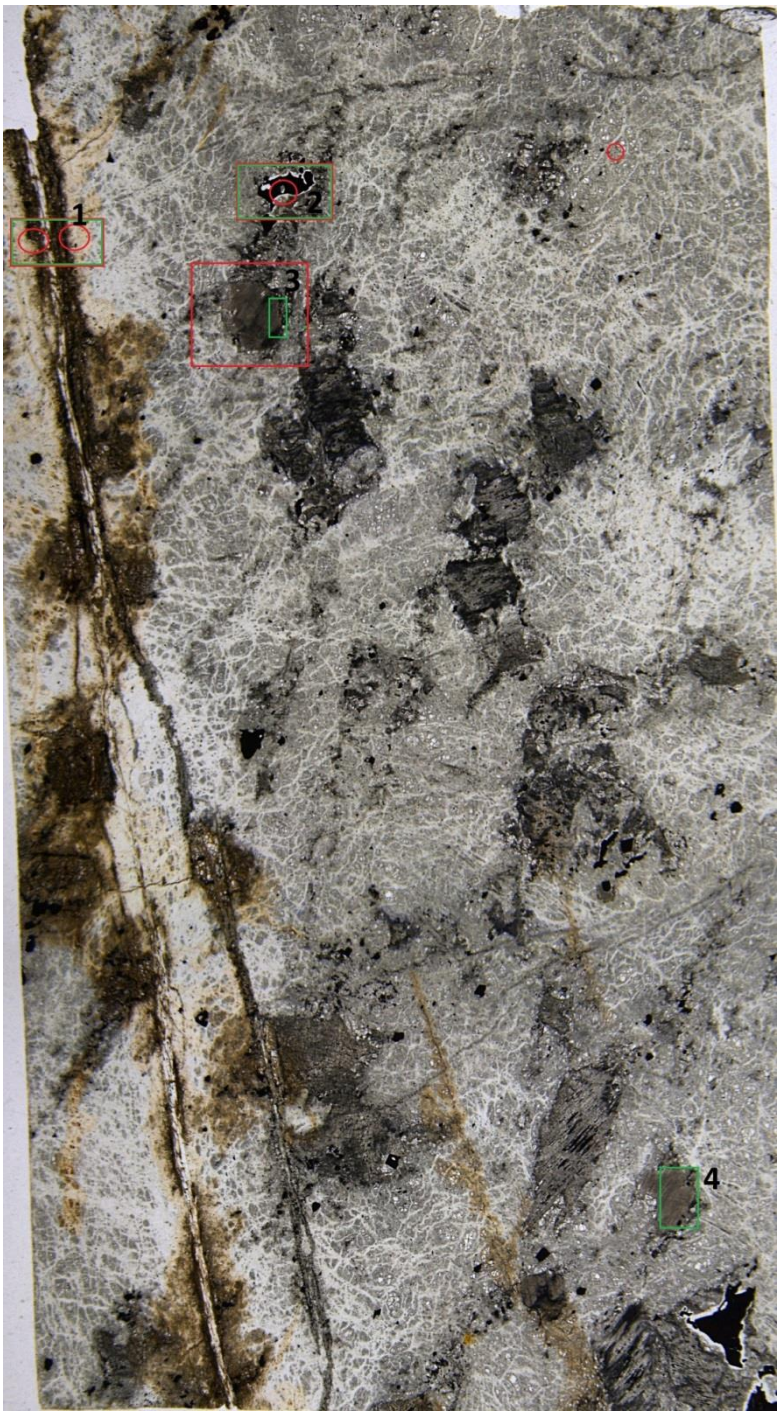

Sample 1.4 has a similar protolith olivine structure as sample 1.1 and 1.2 but has a more varied mineral content. In addition to olivine gray, striped areas reflect a former OPX grains which has been altered to serpentine, brucite and tremolite (bastite) (location 3 & 4). Large spinel grains are surrounded by a chlorite reaction rim and show a chemical zoning (location 2). A large vein is present on the left hand side of the sample, the vein is filled with a complicated zoning of serpentine, olivine and magnetite (see section microstructures) (location 1).

Sample 1.4 Location 1 Veining

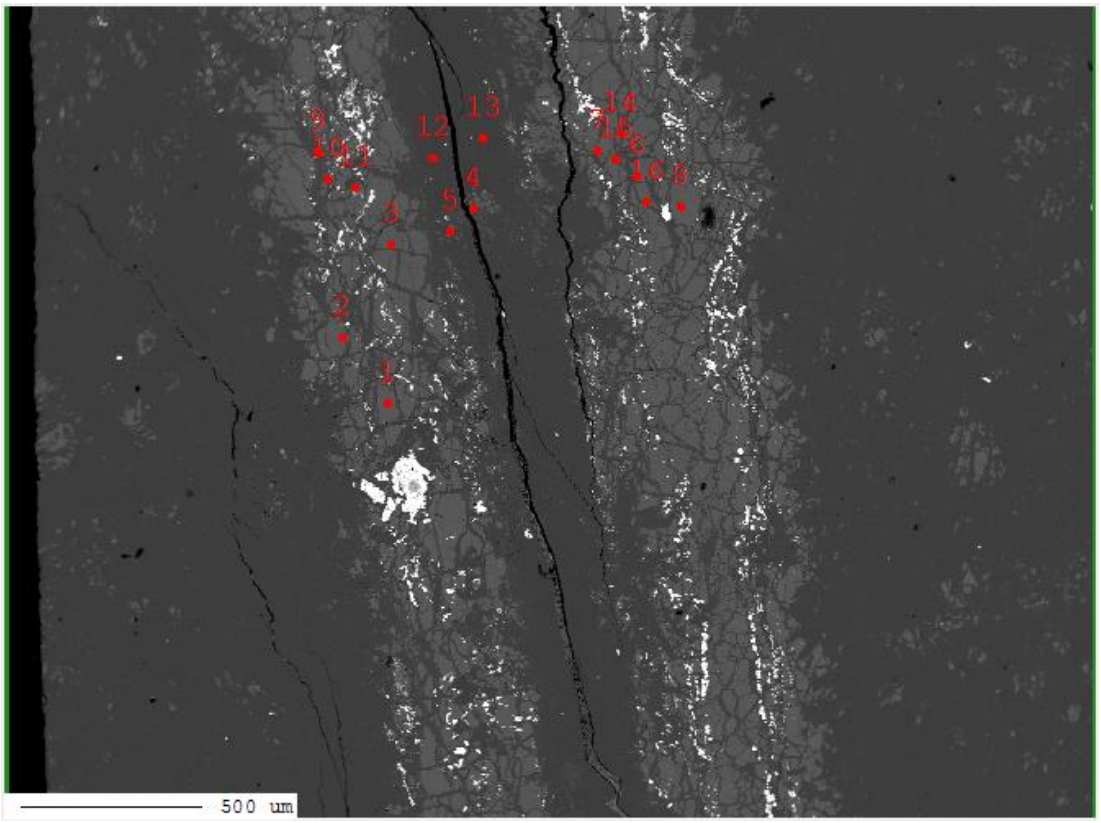

Sample 1.4 Location 2 Large spinel

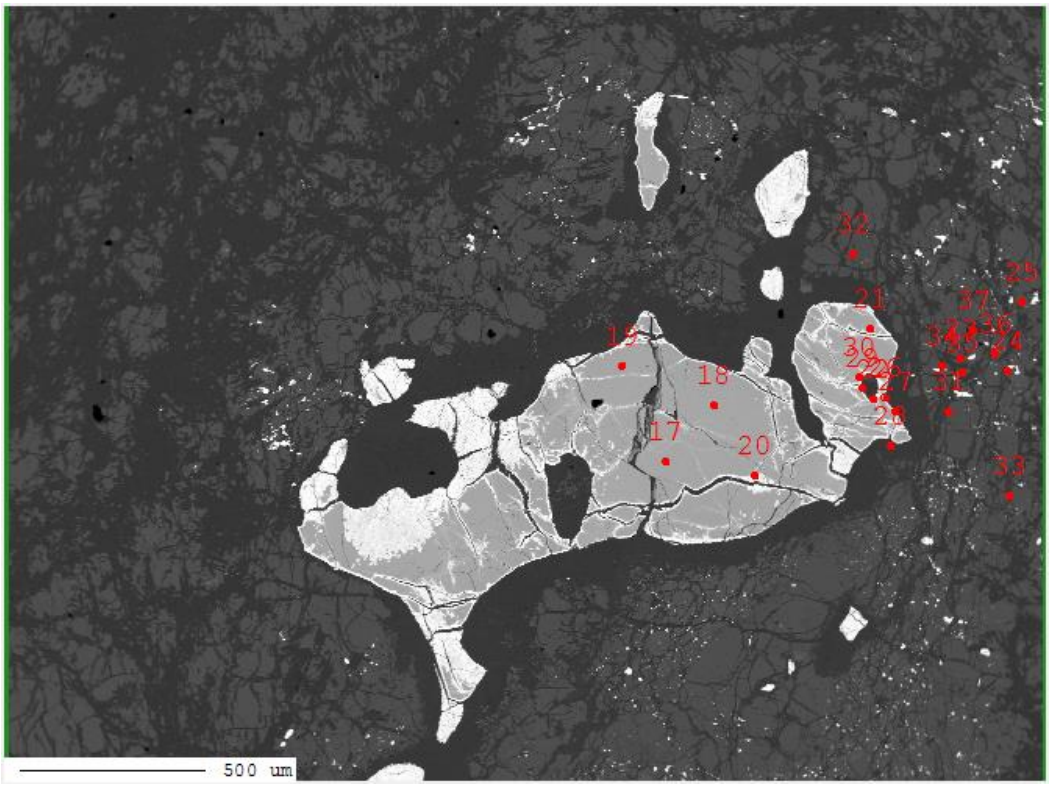

Sample 1.4 Location 3 Bastite

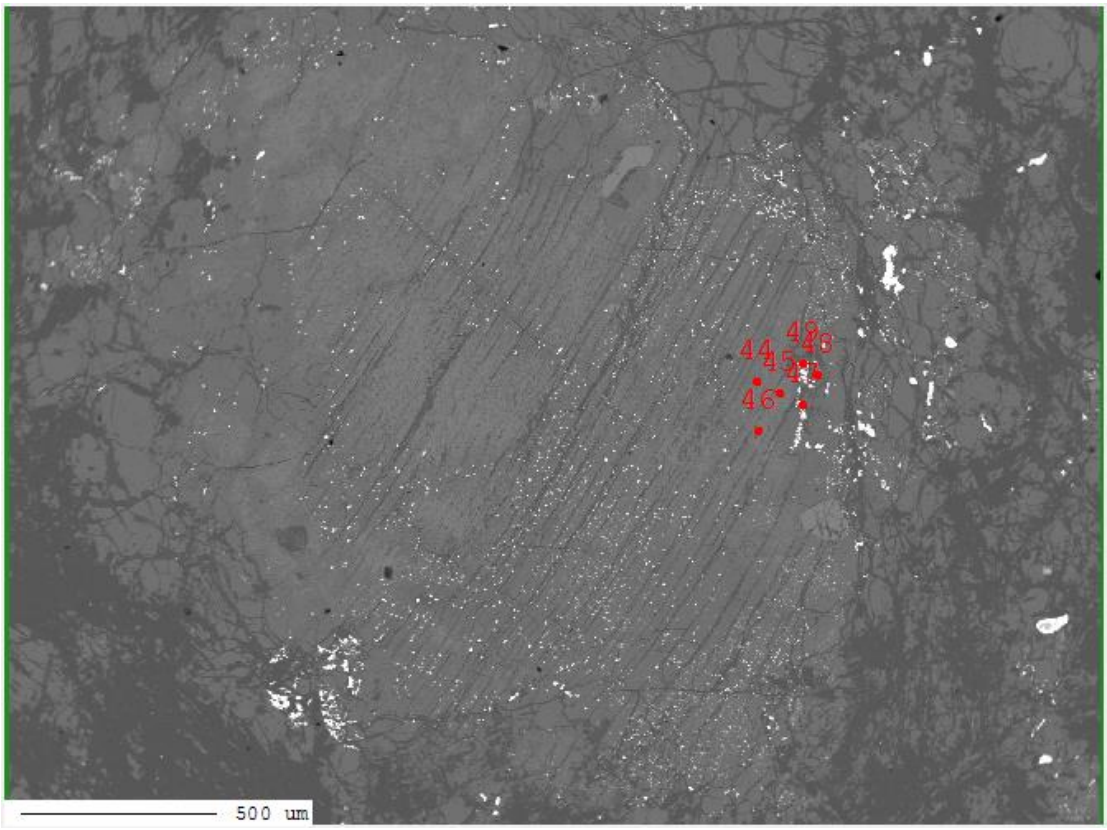

Sample 1.4 Location 4 Bastite

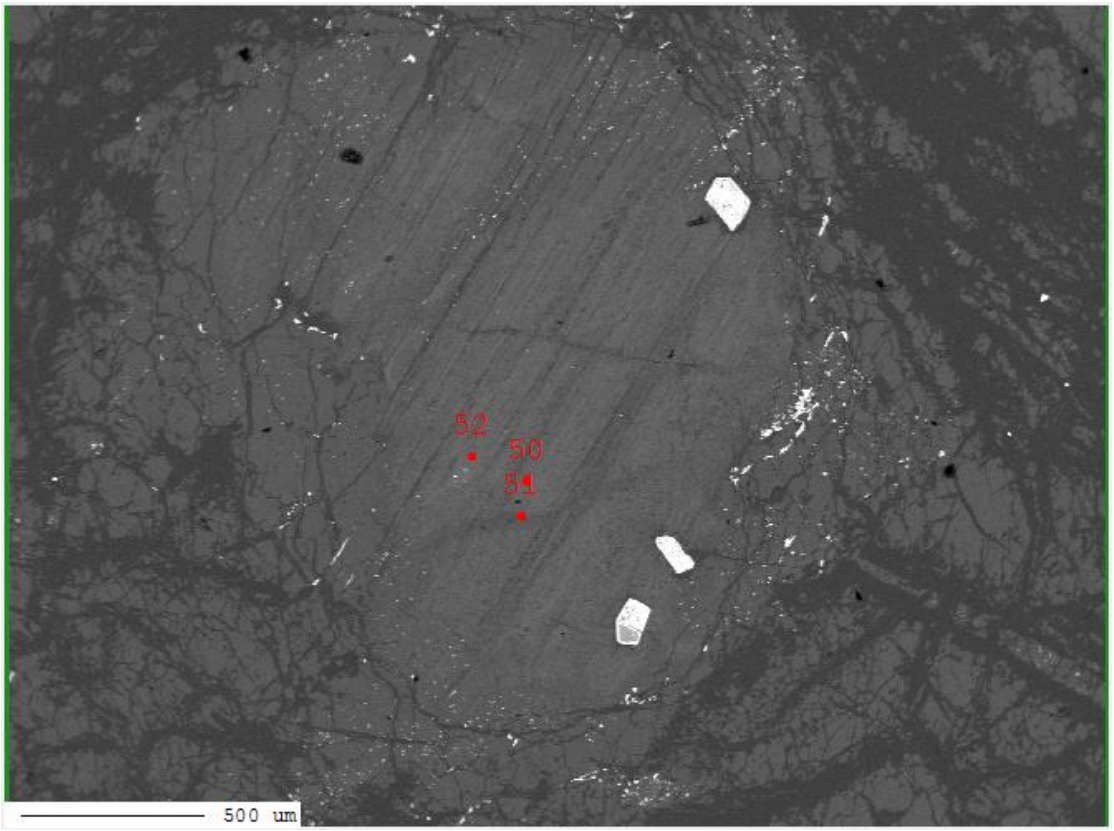

Sample 2.1a

Sample 2.1a has been heavily altered by the first serpentinisation phase. It contains large antigorite clasts but has metamorphic olivine between the clasts. This olivine has a higher Mg# number in respect to the olivine present in sample 1.1 through 1.4. A second serpentinisation phase is present overgrowing the metamorphic olivine as small needles. Large spinel grains show reaction rims made of chlorite.

Sample 2.1b1

Sample 2.1b is very similar to sample 2.1a. Heavy serpentinisation replaced all protolith olivine. Metamorphic olivine grew in a vein like structure between the antigorite. Finally, a later serpentinisation phase overgrew the metamporphic olivine. Large spinel grains may show a chlorite reaction rim. A finer grained magnetite phase is present through the entire sample.

Sample 2.1b2

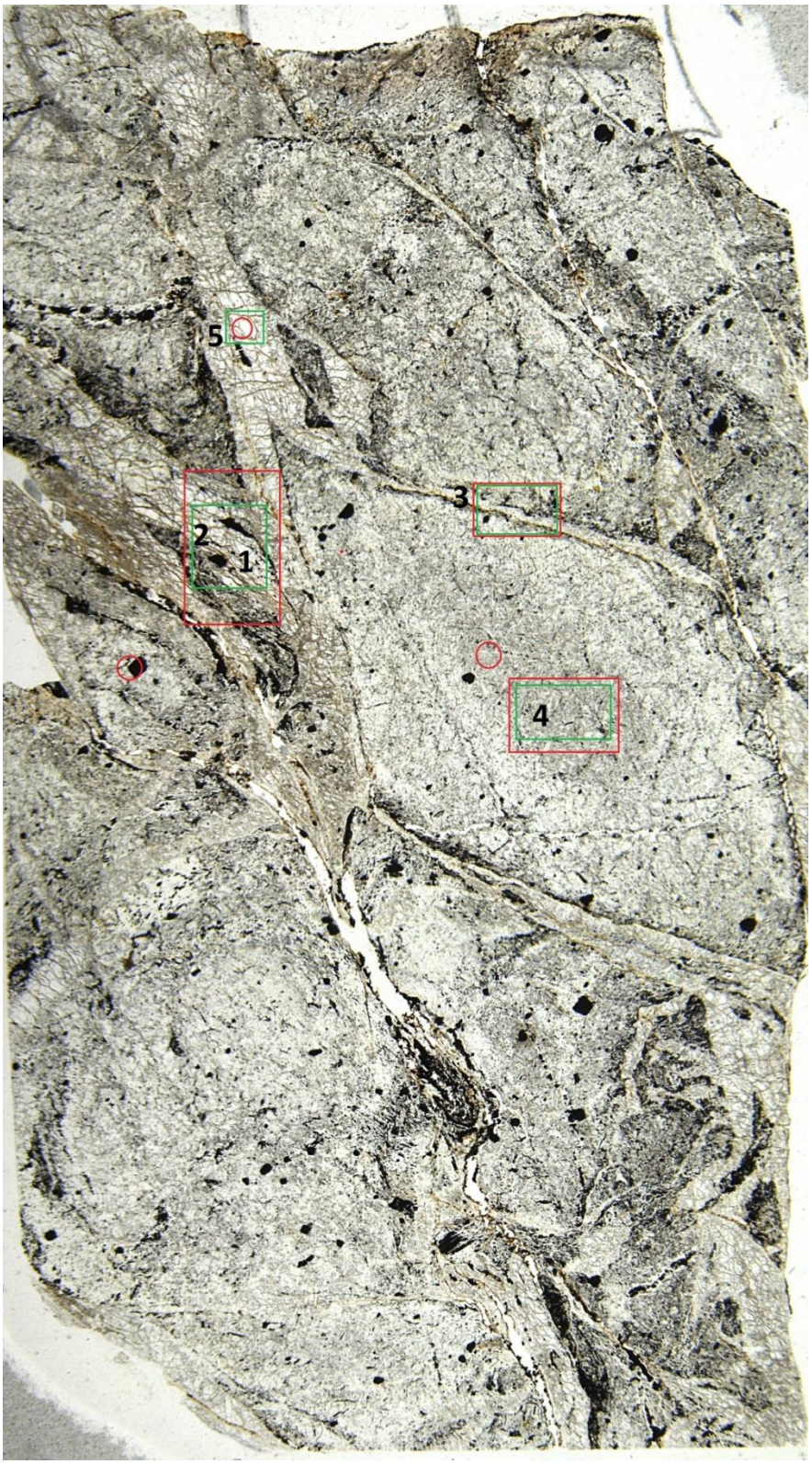

Sample 2.1b2 contains several large antigorite ‘clasts’ up to a few cm big. Metamorphic (M3) olivine is present between these antigorite clasts (location 1 ,2 & 3). Metamorphic olivine is also present in the antigorite matrix of the ‘clasts’ (location 4). The olivine is overgrown by a later serpentinisation phase (M4 antigorite) (location 1,2 & 4).

Sample 2.1b2 Location 1 metamorphic olivine and related spinel.

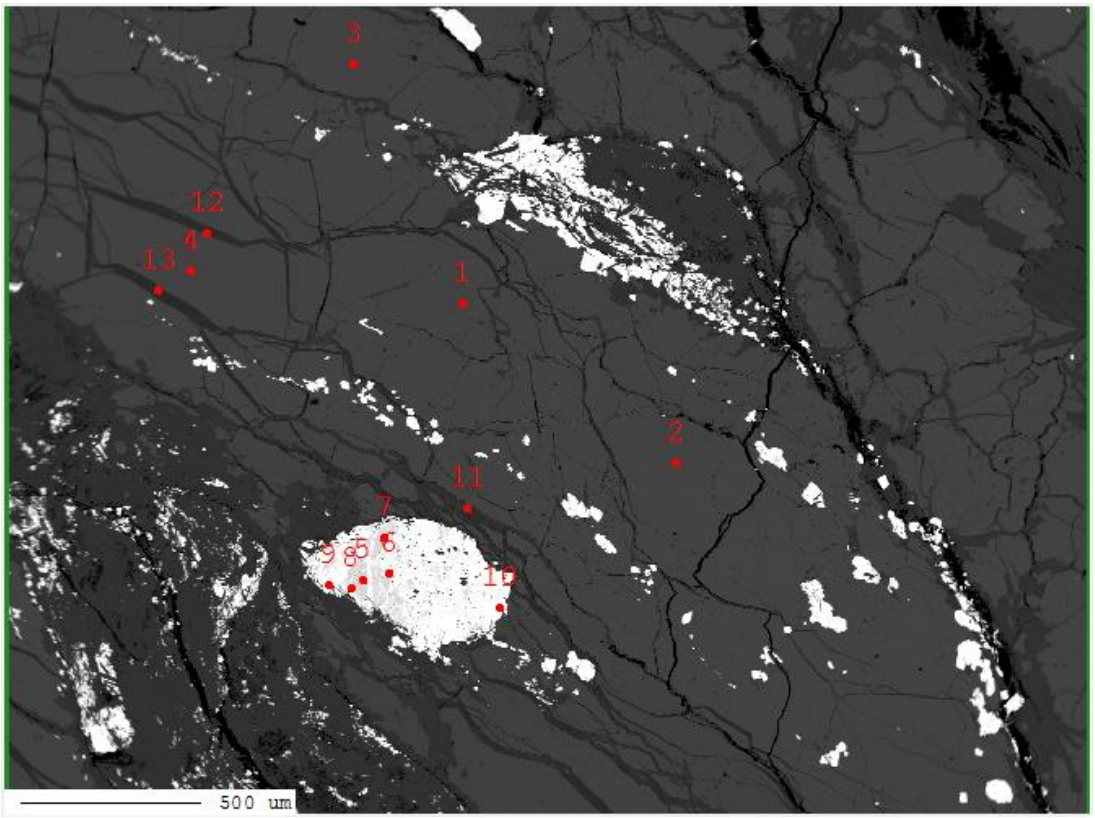

Sample 2.1b2 Location 1 large spinel grain.

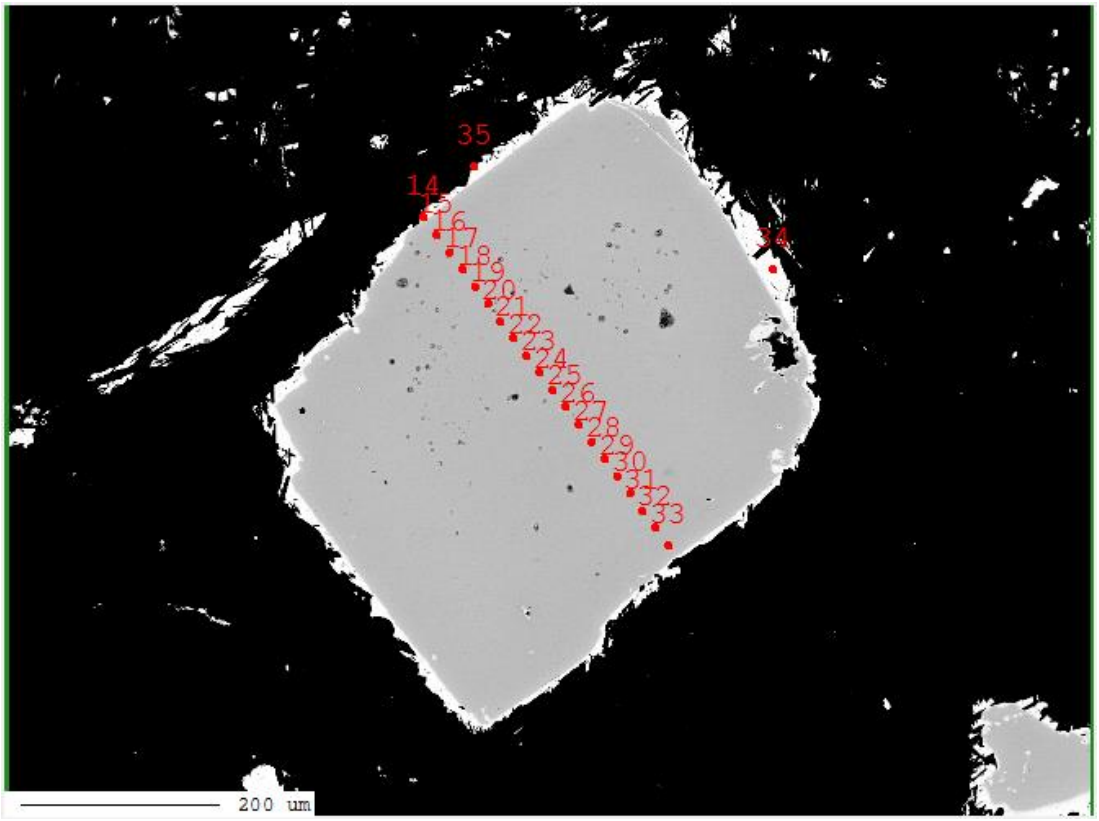

Sample 2.1b2 Location 3 olivine (M3) between the antigorite clasts.

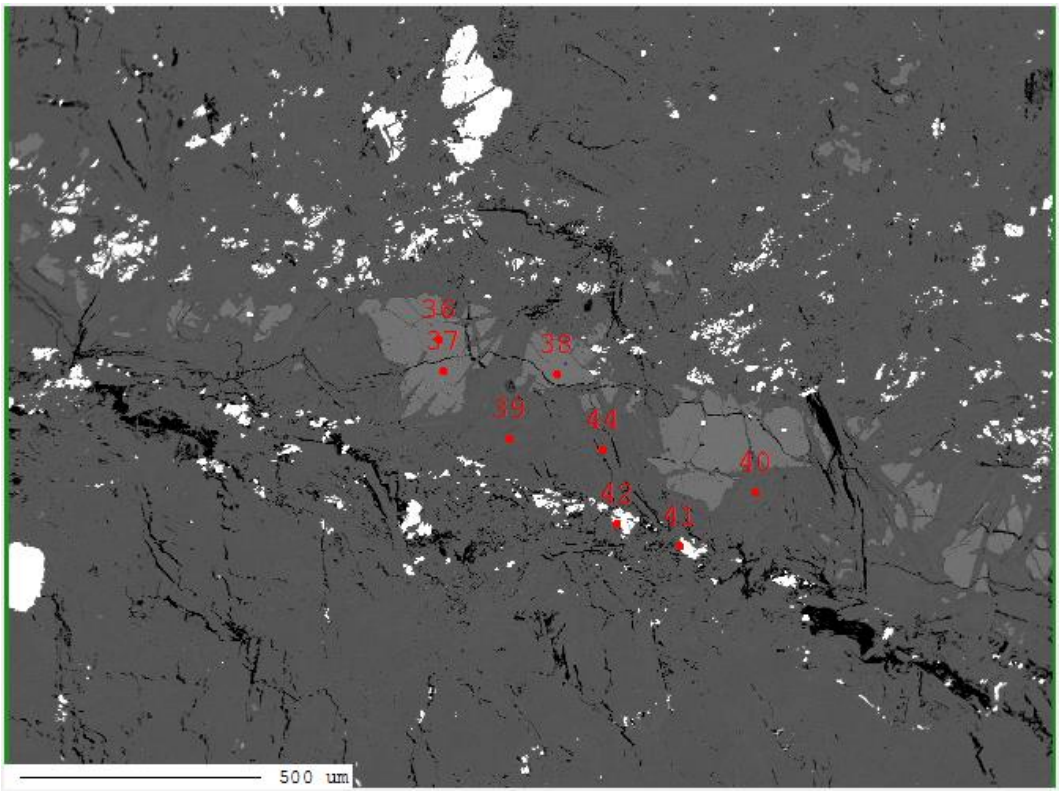

Sample 2.1b2 Location 4 antigorite matrix (M2 & M4) with metamorphic olvine (M3).

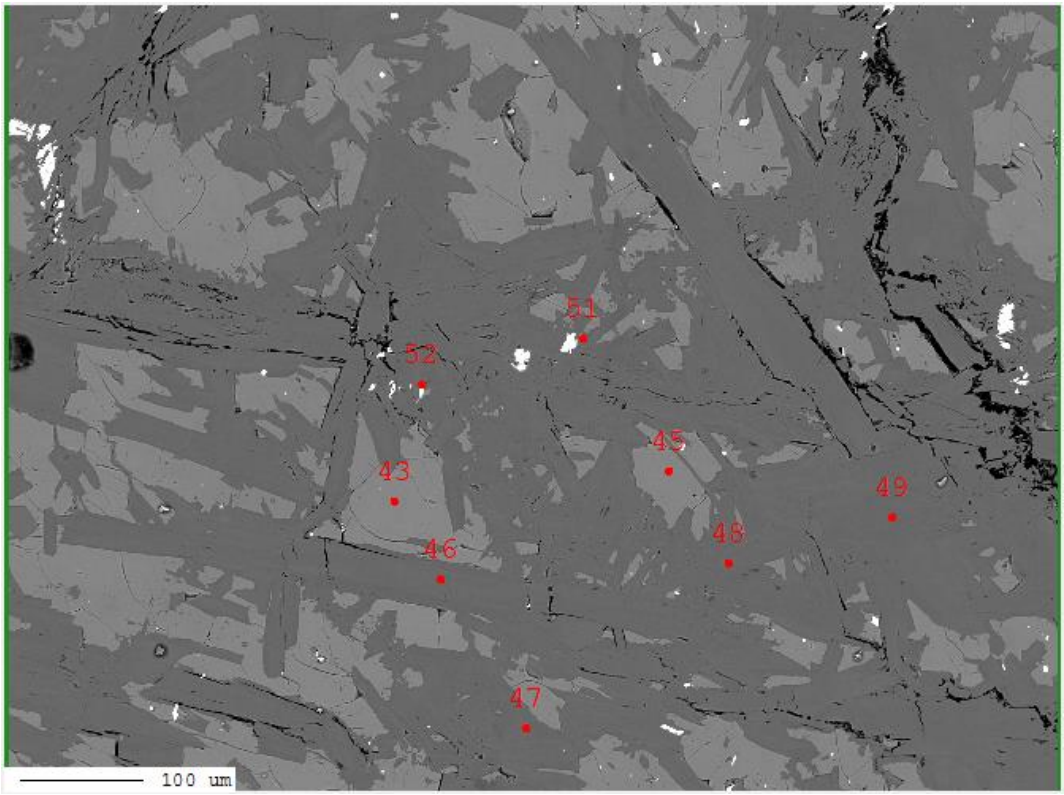

Sample 2.1b2 Location 5 M3 metamorphic olivine.

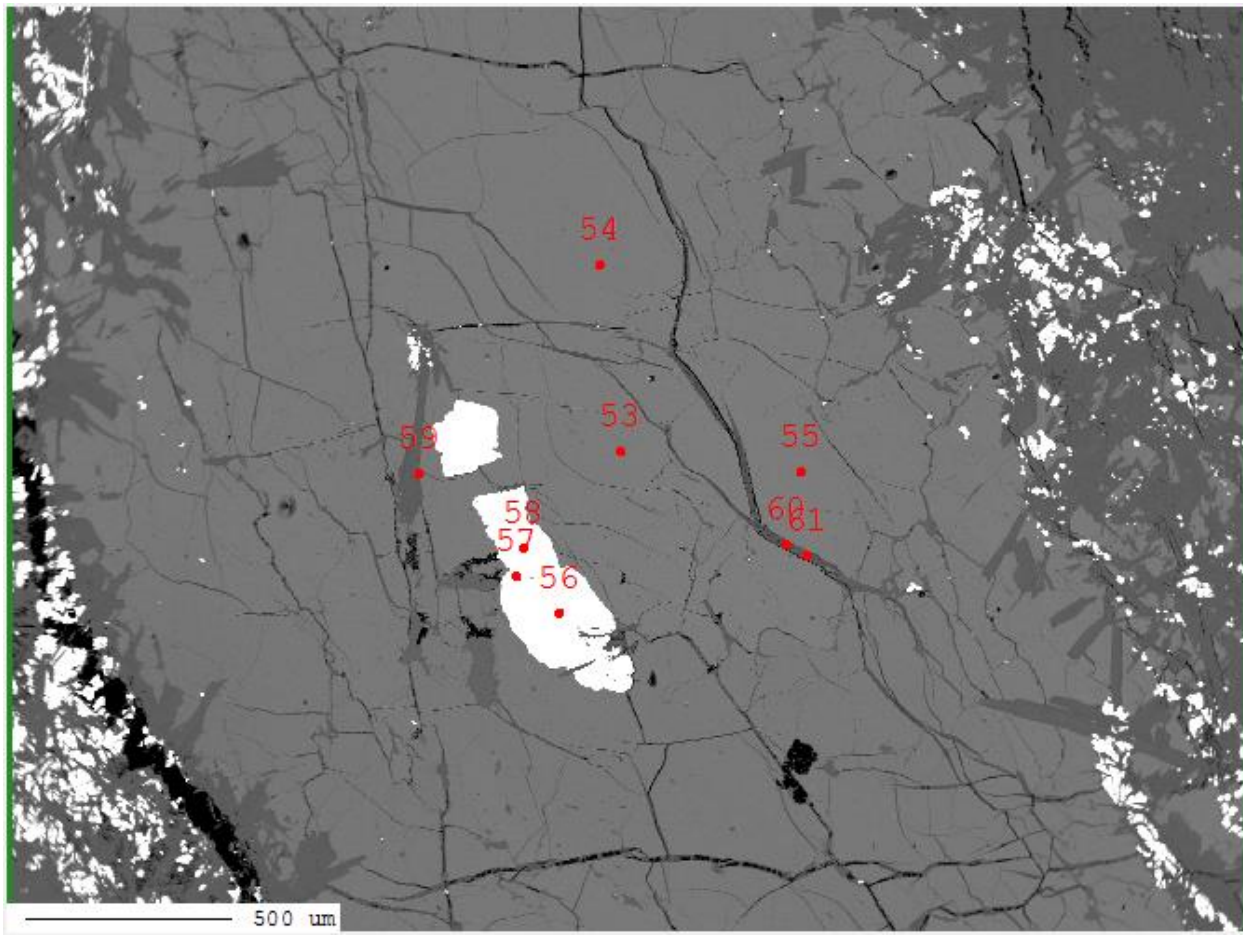

Sample 2ext1

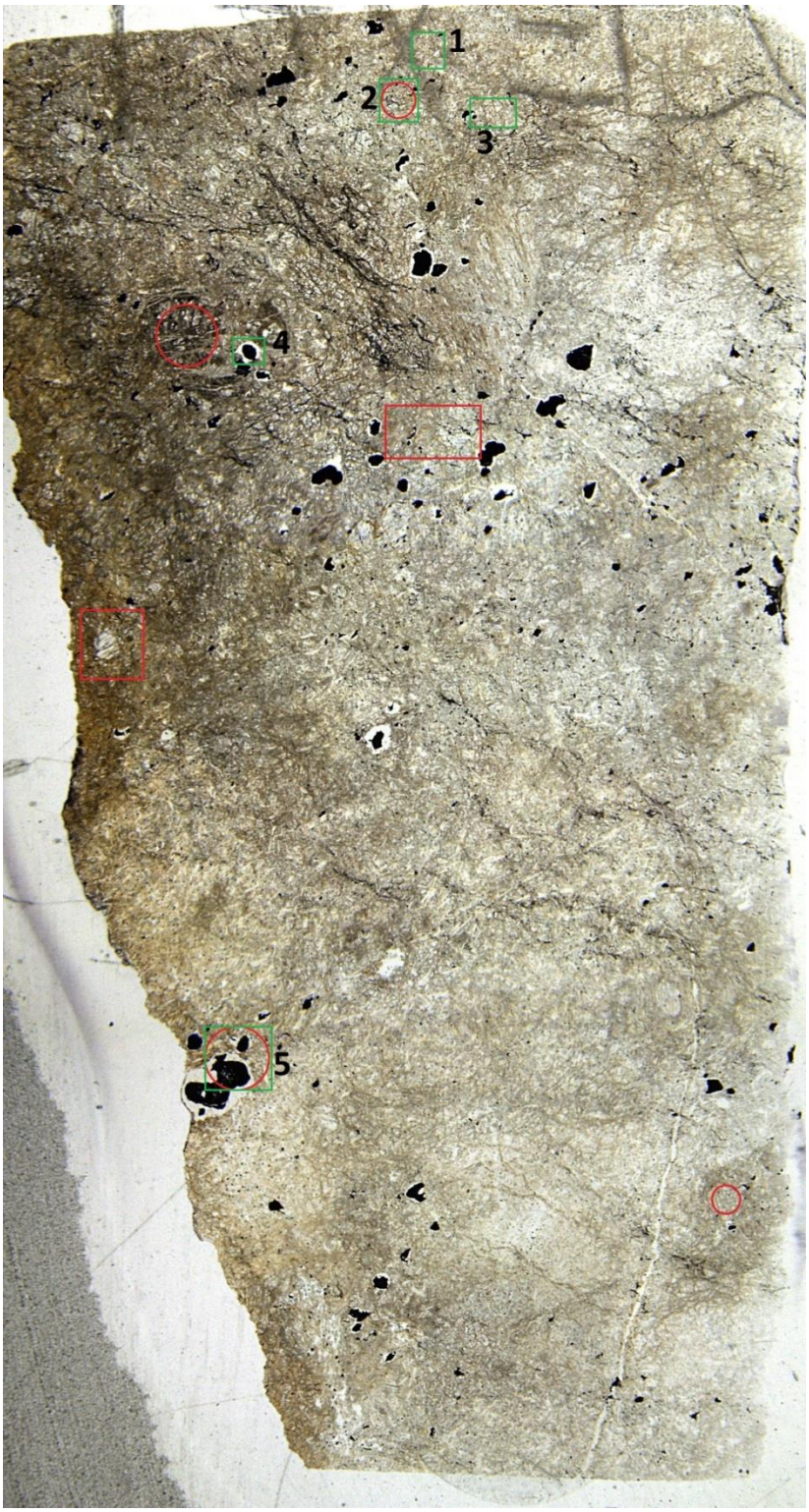

Sample 2ext1 has a different protolith essamblage in comparison to the protolith essamblage in sample 1.1, 1.2 and 1.4. Sample 2ext1 contains a large amount of CPX, up to 40% (location 1). The CPX is interpreted as protolith CPX because of the CPX lamealle it contains (see location 1). Olivine makes up the bulk of the sample, this is protolith olivine with very little alteration (see location 3). Large spinel grains are present, surrounded by a chlorite reaction rim (see location 4 & 5).

Sample 2ext1 Location 1

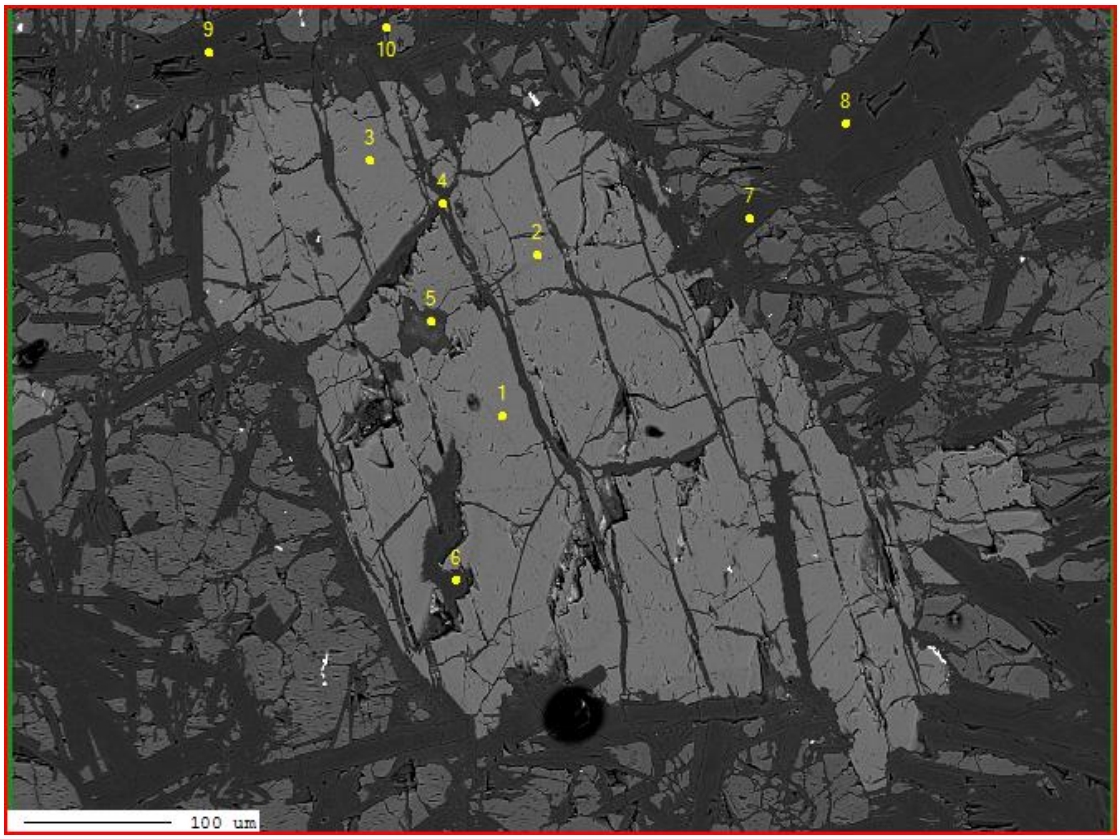

Sample 2ext1 Location 2

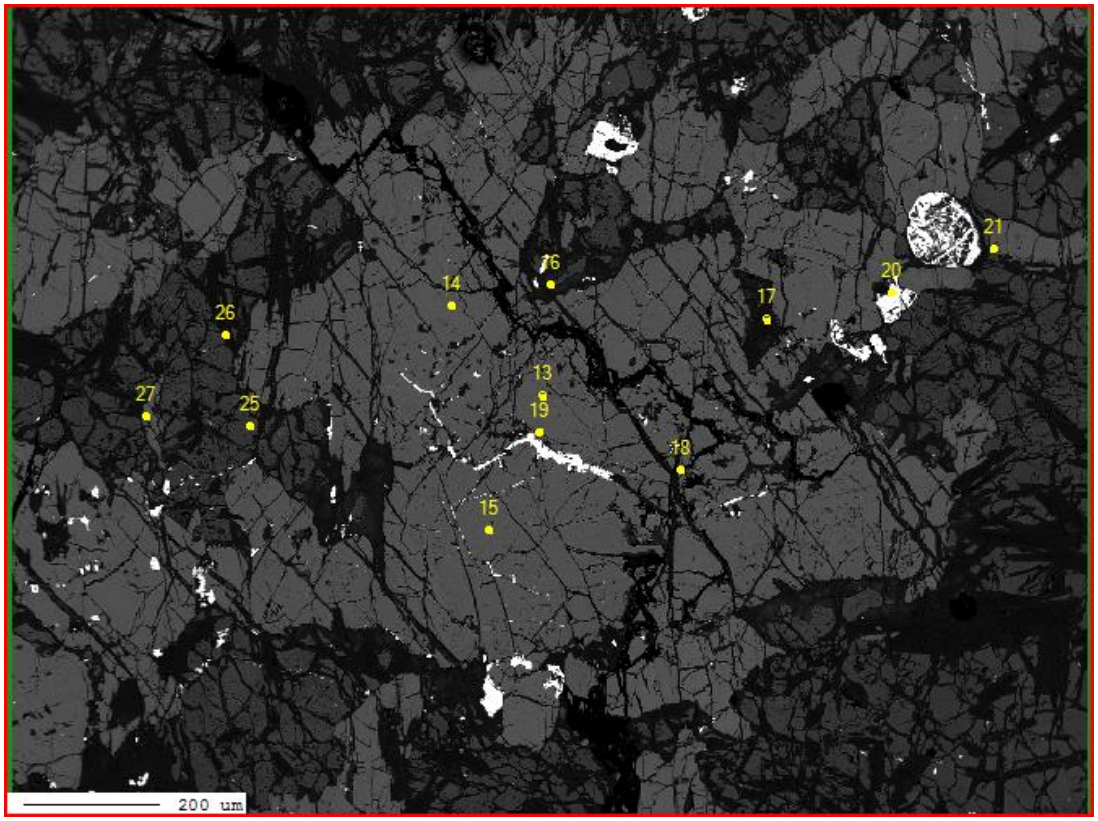

Sample 2ext1 Location 3

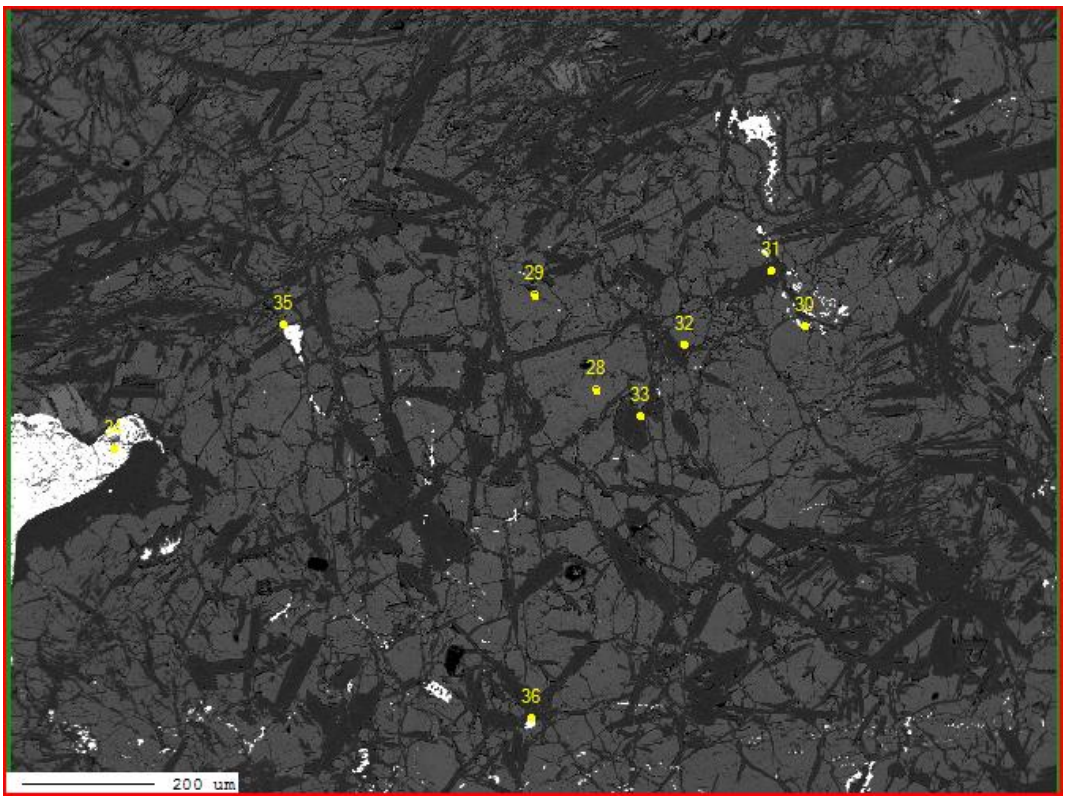

Sample 2ext1 Location 4

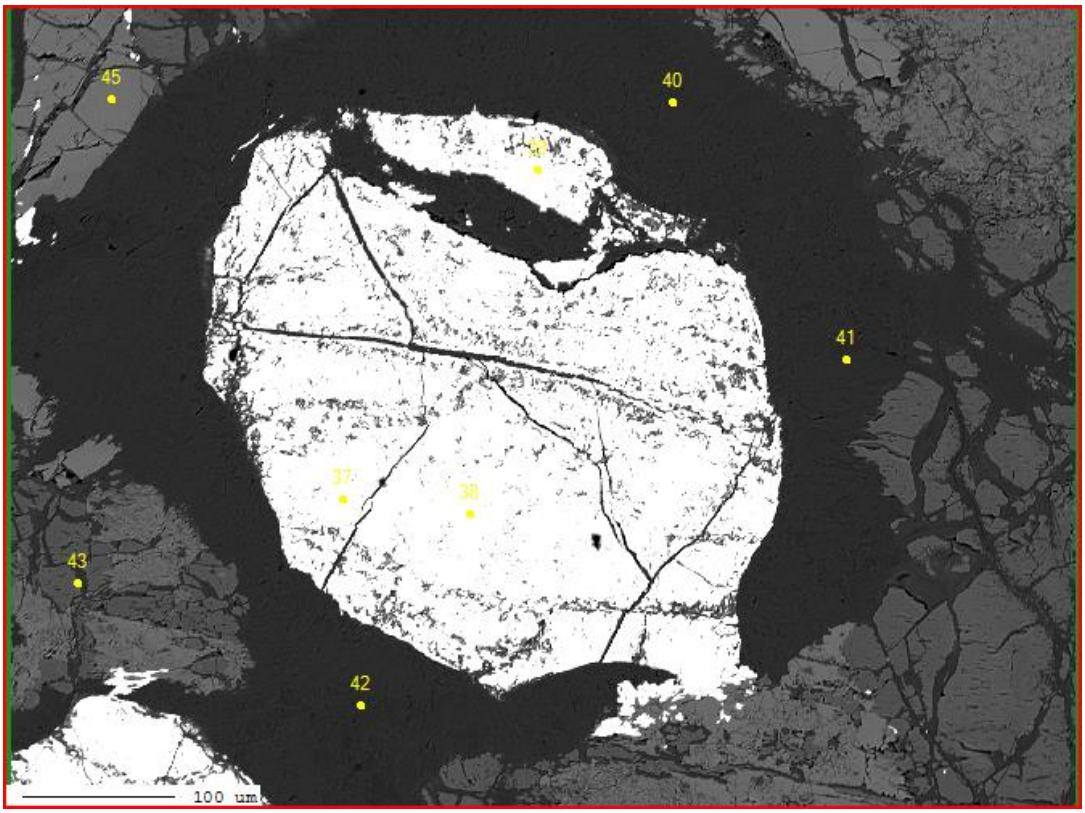

Sample 2ext1 Location 5

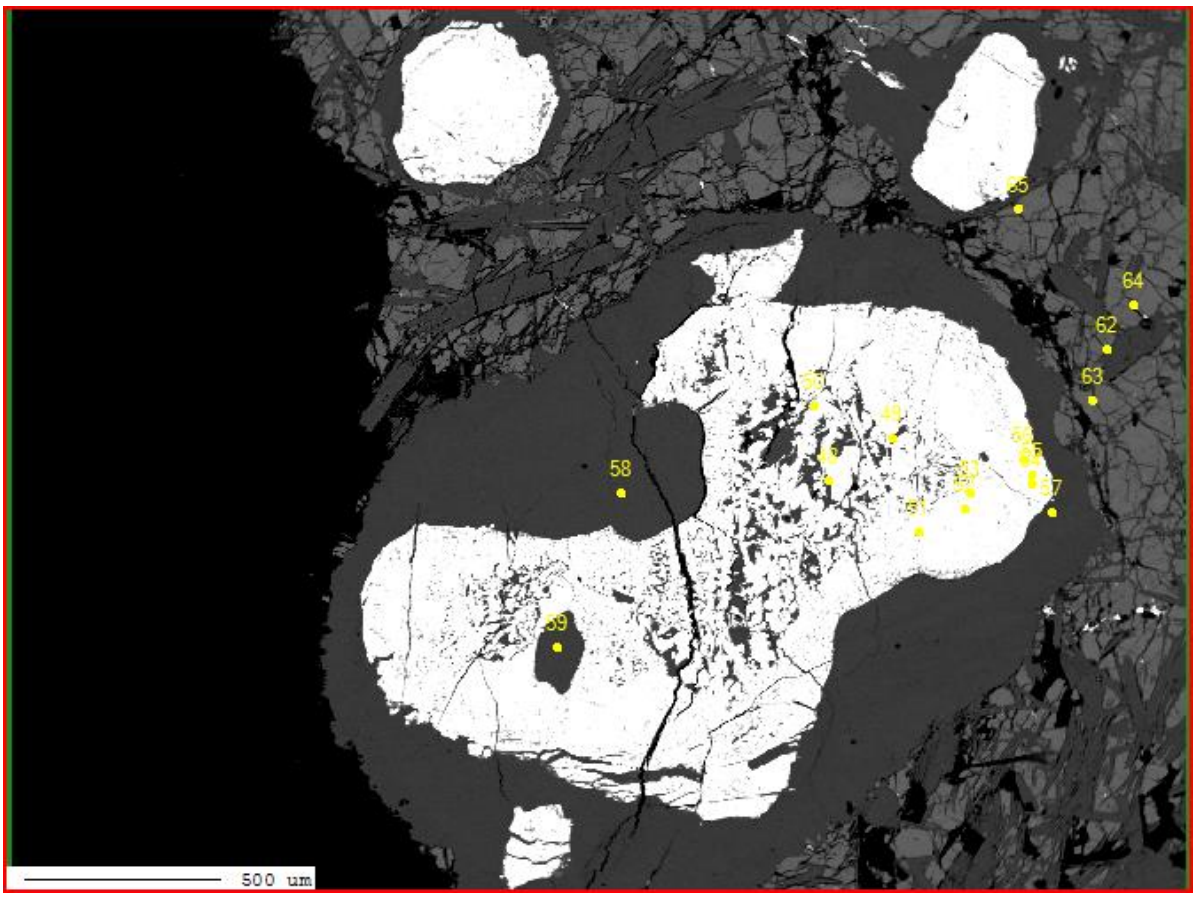

Sample 2ext2

Sample 2ext2 is heavily altered, showing mostly antigorite in clear patches and in bastites where OPX has been replaced by serpentine, brucite and tremolite.

Sample 3.2C

Sample 3.2C has been heavily altered, mostly consisting of antigorite. Large protolith spinels are still present surrounded by a chlorite reaction rim. Yellowish sulfides are present throughout the sample but were not further investigated.

Sample 3.3AB

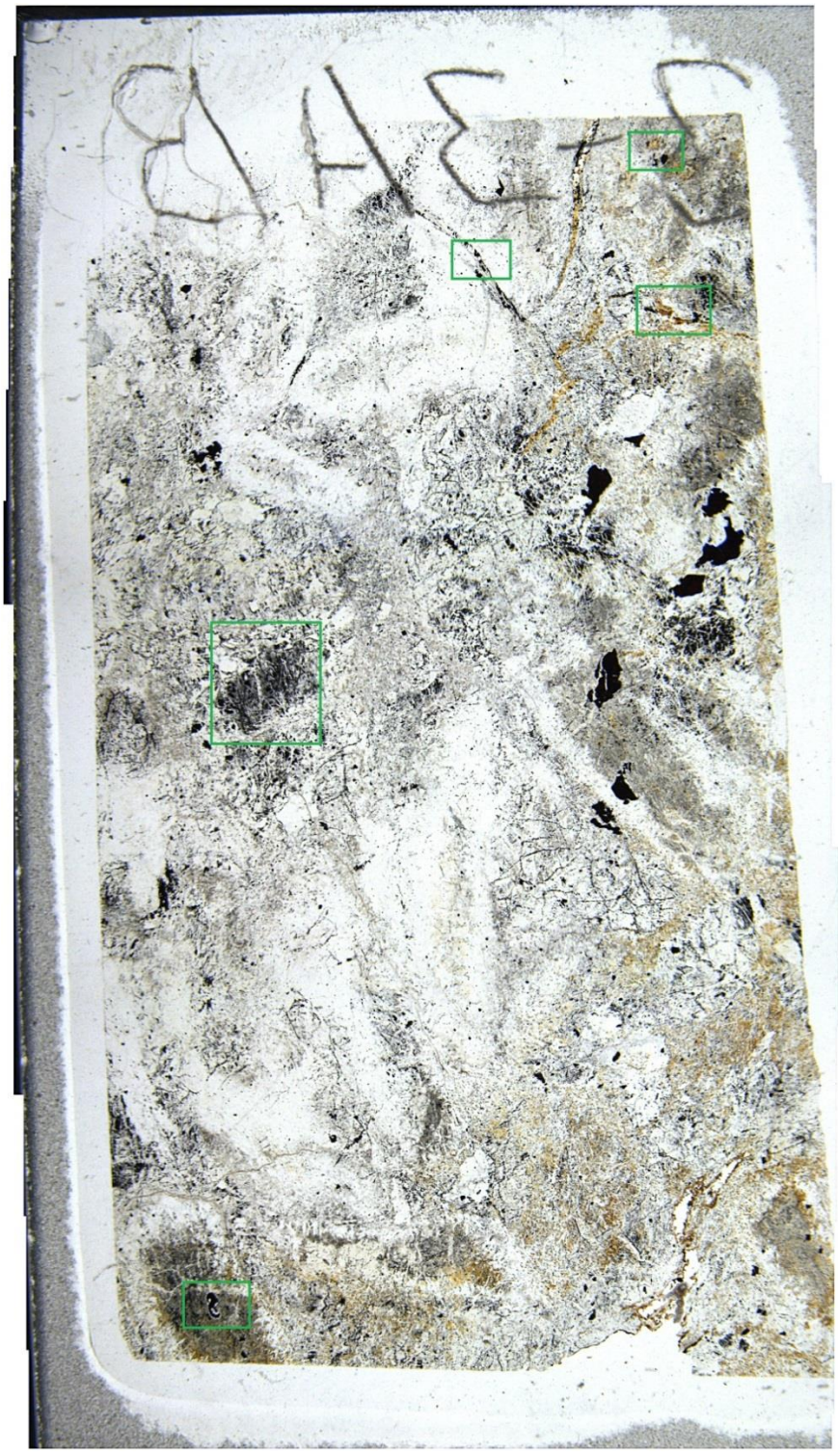

Sample 3.3AB has been heavily altered by antigorite serpentinisation. Metamorphic olivine (M3) is present overgrowing an antigorite matrix. A later antigorite phase overgrows the M3 olvine. Spinel is present as large grains with chlorite reaction rim and as fine grained magnetite throughout the matrix.

Sample 3.4.1

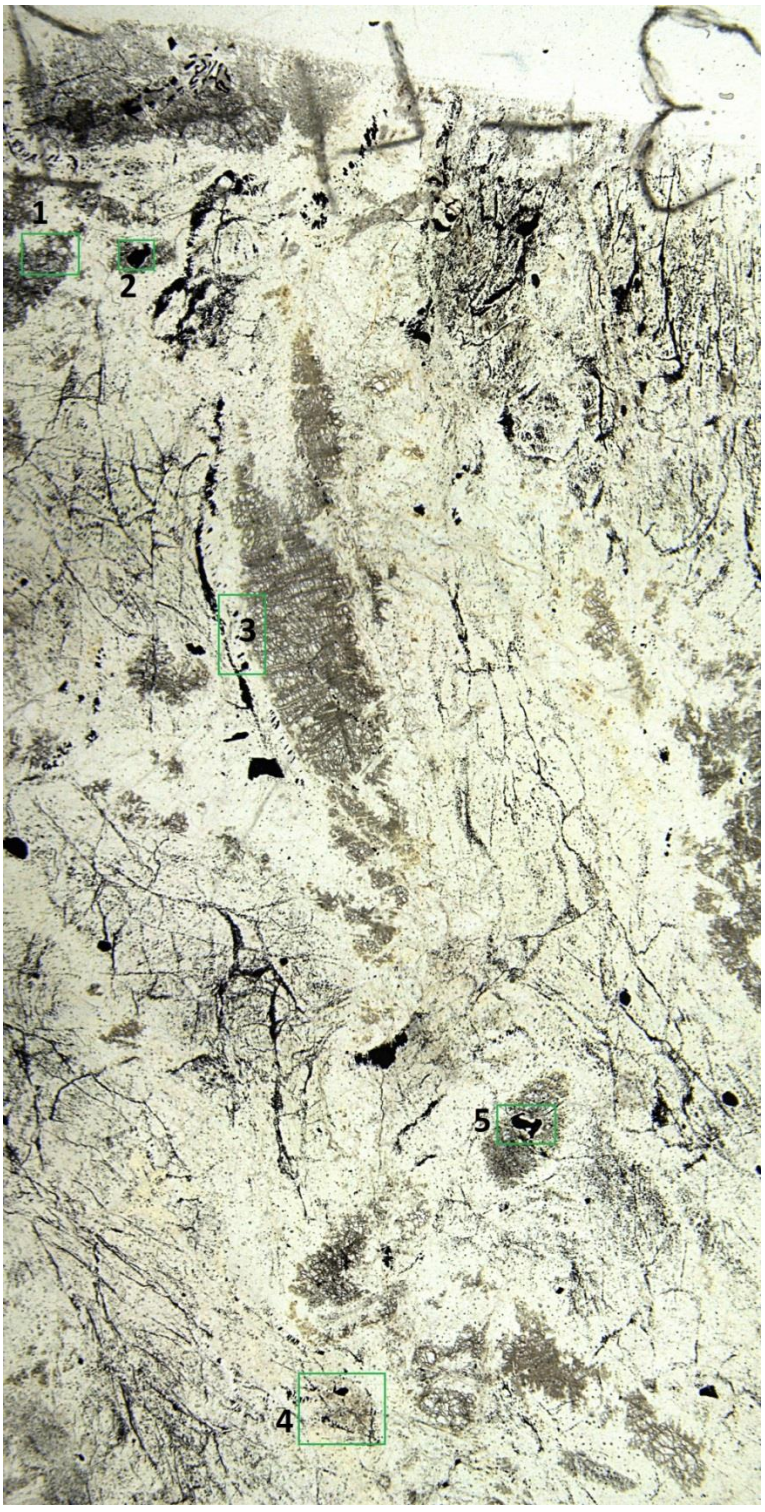

Sample 3.4.1 is made from an antigorite matrix overgrown by M3 olivine (location 1 & 2). Brucite has been chemically identified in the matrix (location 3). Large spinel grains often show a chlorite reaction rim (location 5). Finer grained magnetite grains are present in the matrix (location 1 & 4).

Sample 3.4.1 Location 1 M3 olivine.

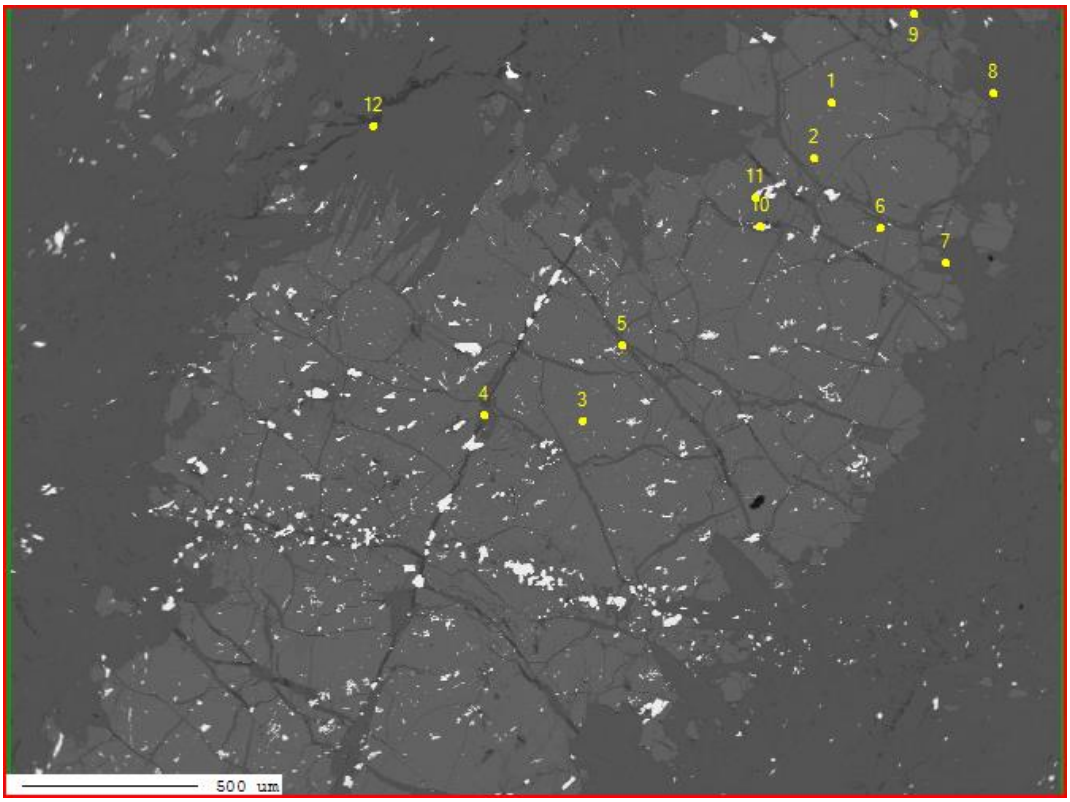

Sample 3.4.1 Location 2 protolith spinel with chemical zoning and chlorite reaction rim.

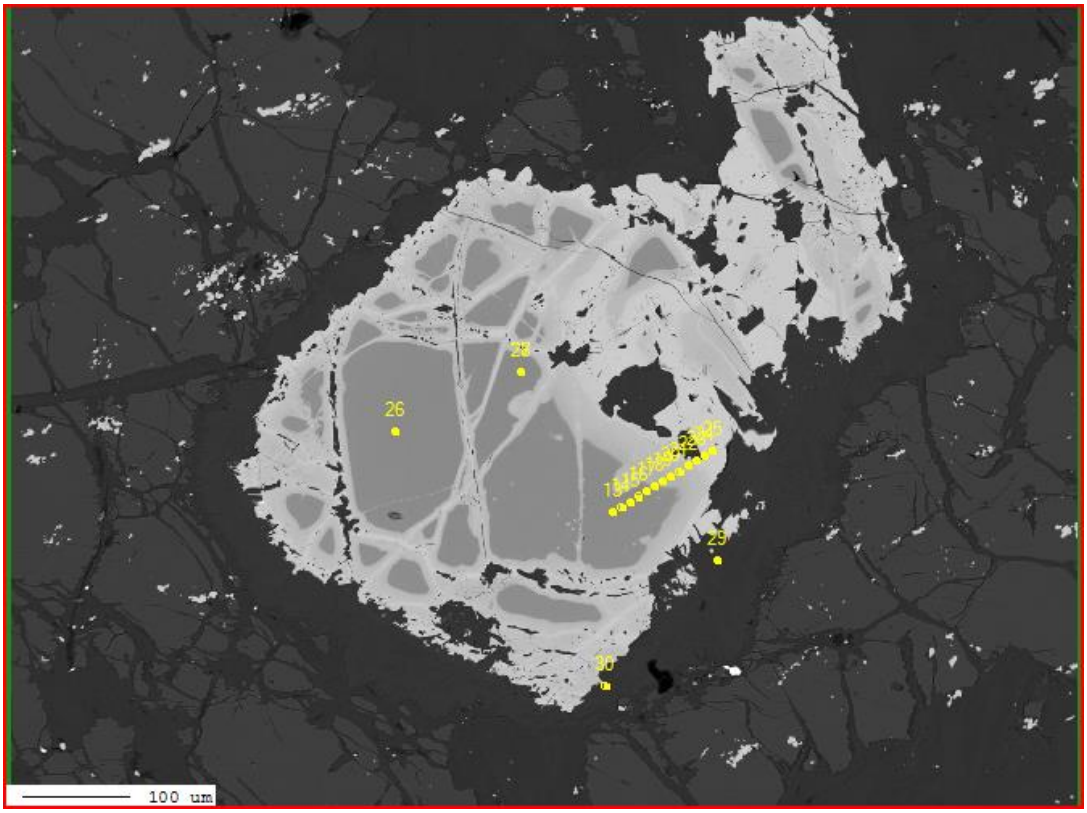

Sample 3.4.1 Location 3 M3 olivine.

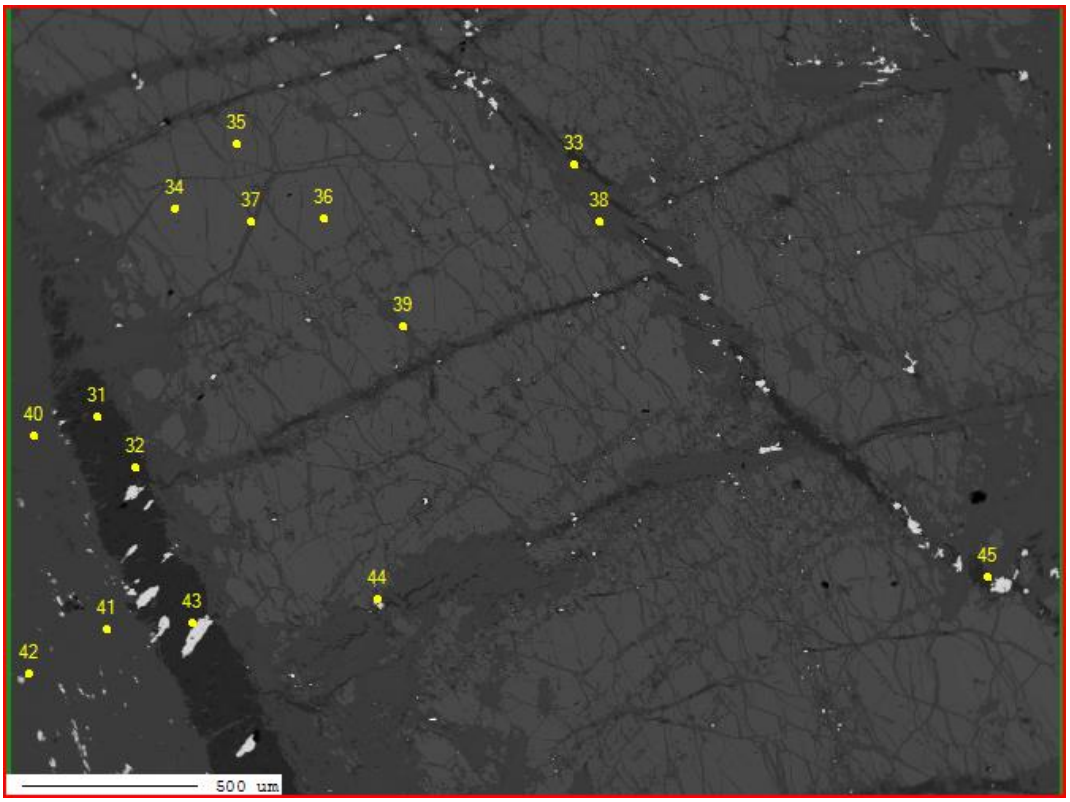

Sample 3.4.1 Location 4 M3 olivine and brucite (dark gray).

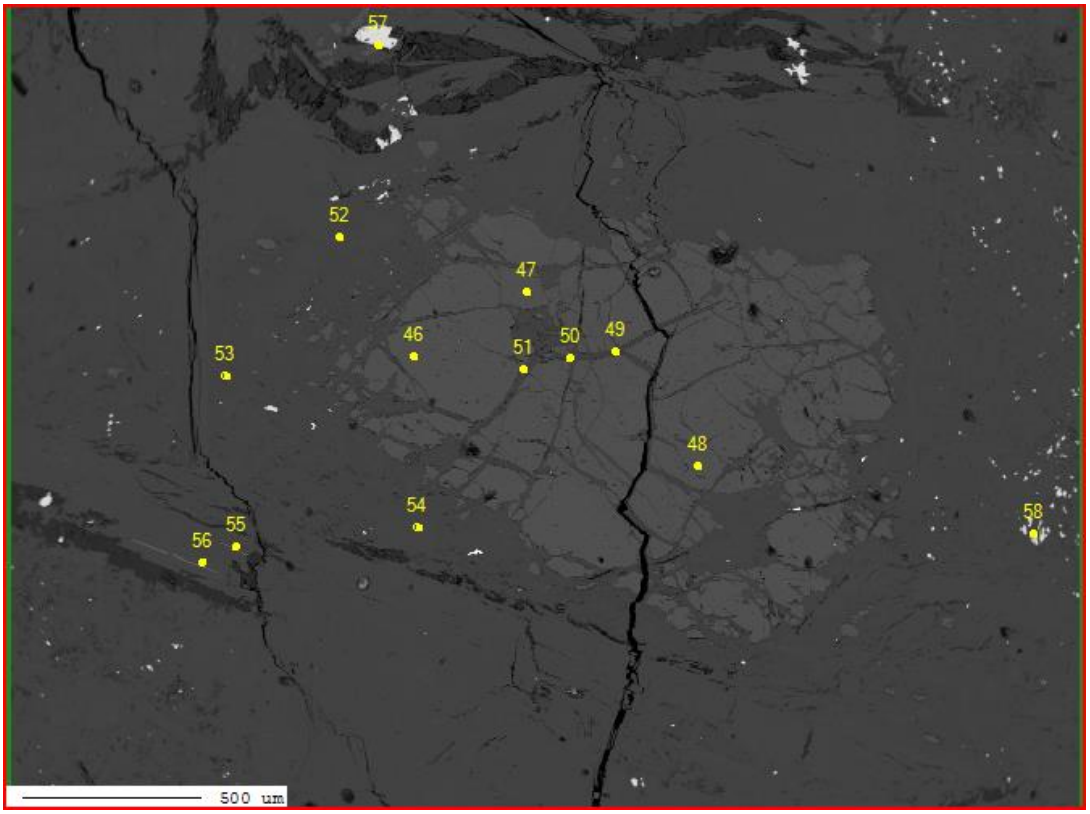

Sample 3.4.1 Location 5 protolith spinel with chemical zoning and a chlorite reaction rim.

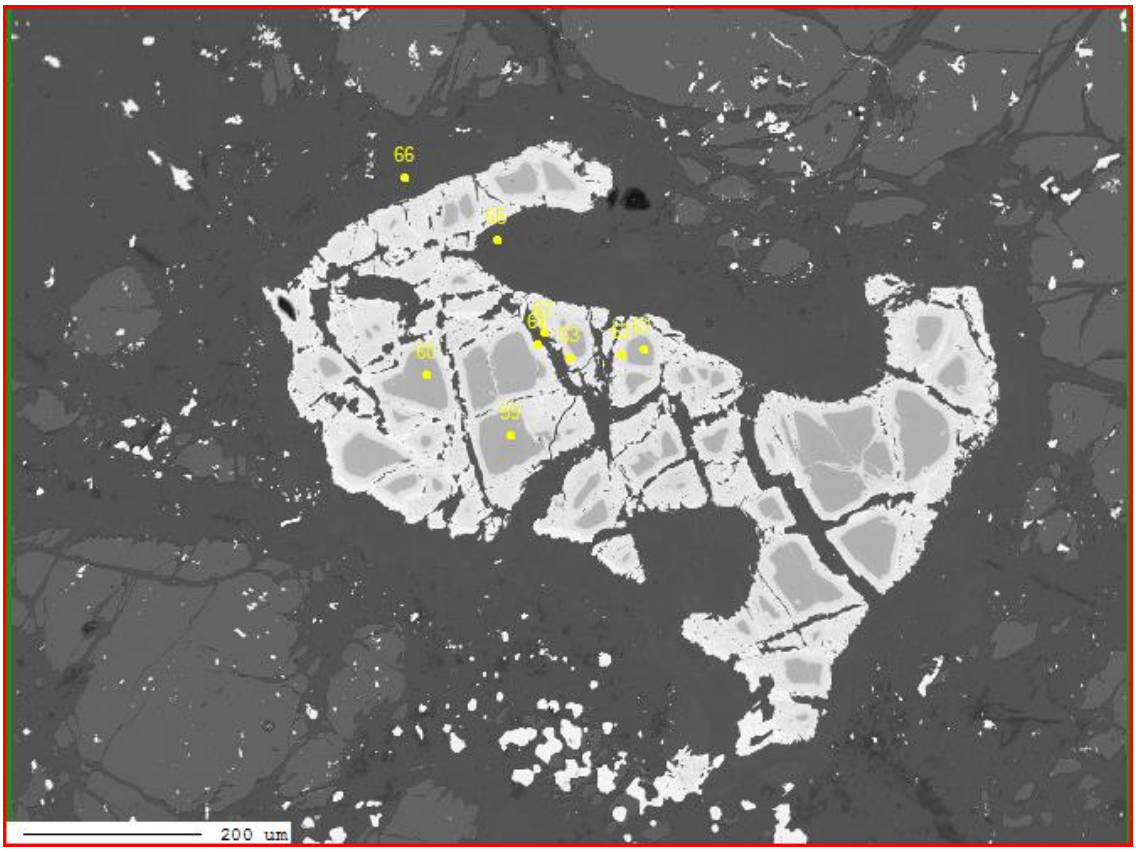

Sample 3.4.2

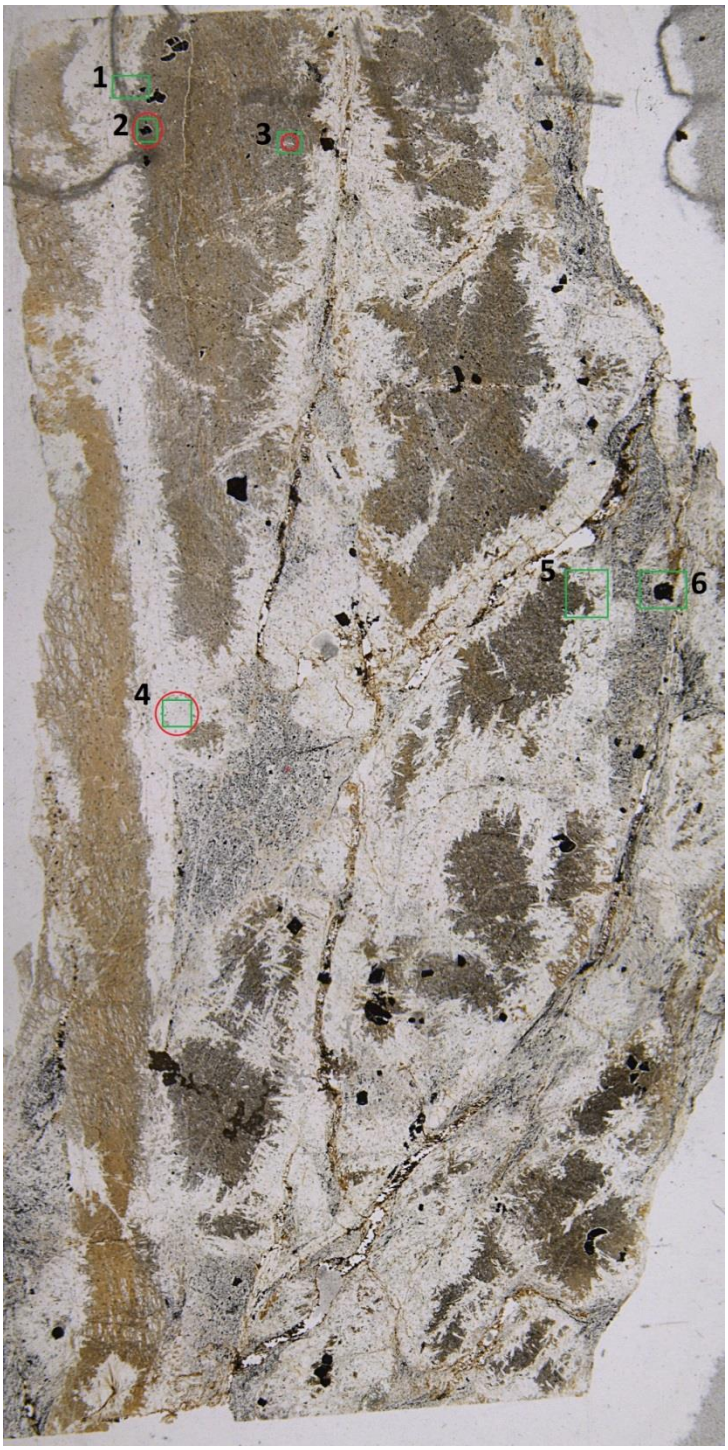

Sample 3.4.2 has undergone intense serpentinisation. M3 grows over the antigorite (M2) matrix, these olivine grains are large and seem to form vein like structures (location 1,2 & 3) (as in sample 2.1b1 & 2.1b2). Large spinel grains are present within the M3 olivine as inclusions including a chlorite reaction rim (location 1 & 2). A later serpentinisation phase resulted in the growth of antigorite (M4) over M3 olivine (location 4). There are no restants of the protolith essemblage.

Sample 3.4.2 Location 1 M3 olivine (M3) with large spinel inclusions.

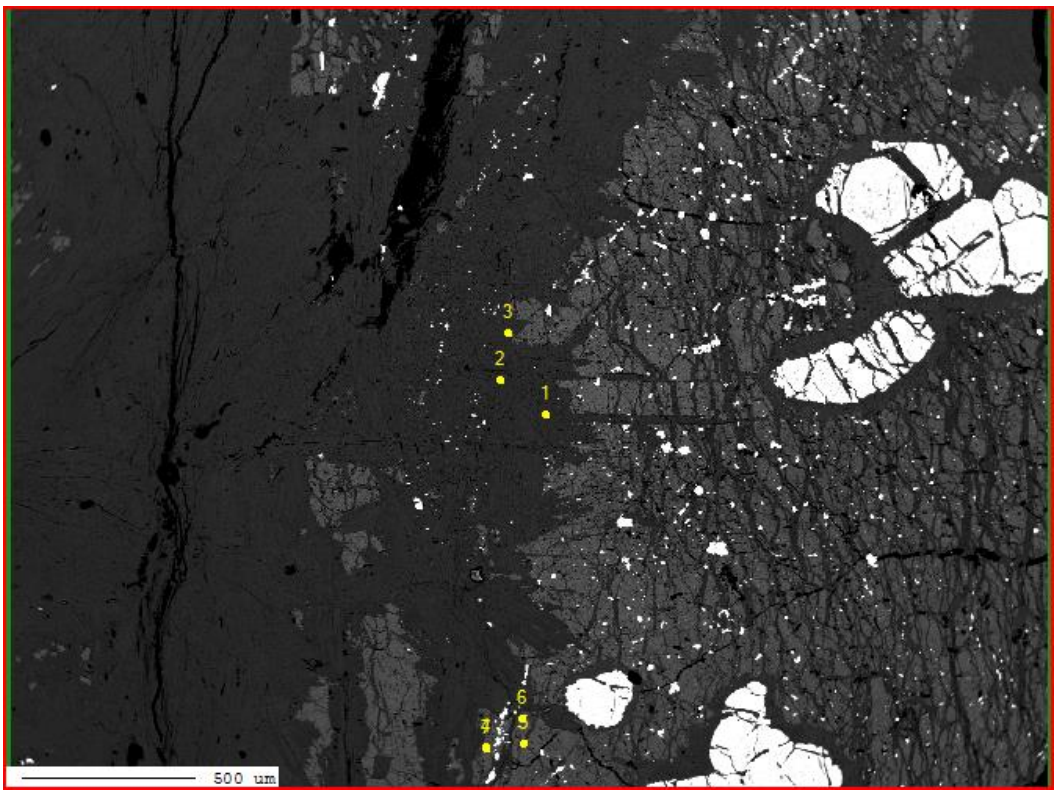

Sample 3.4.2 Location 2 olivine (M3) with large spinel inclusions.

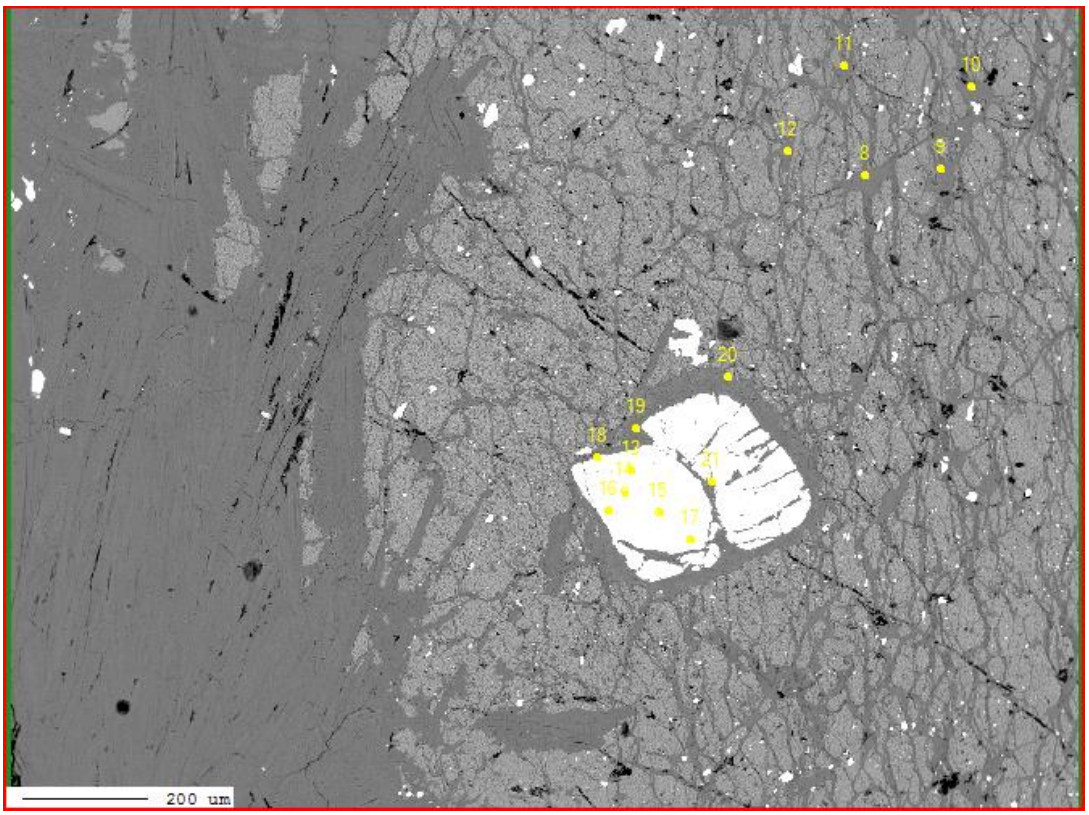

Sample 3.4.2 Location 3 M3 olivine with magnetite inclusions.

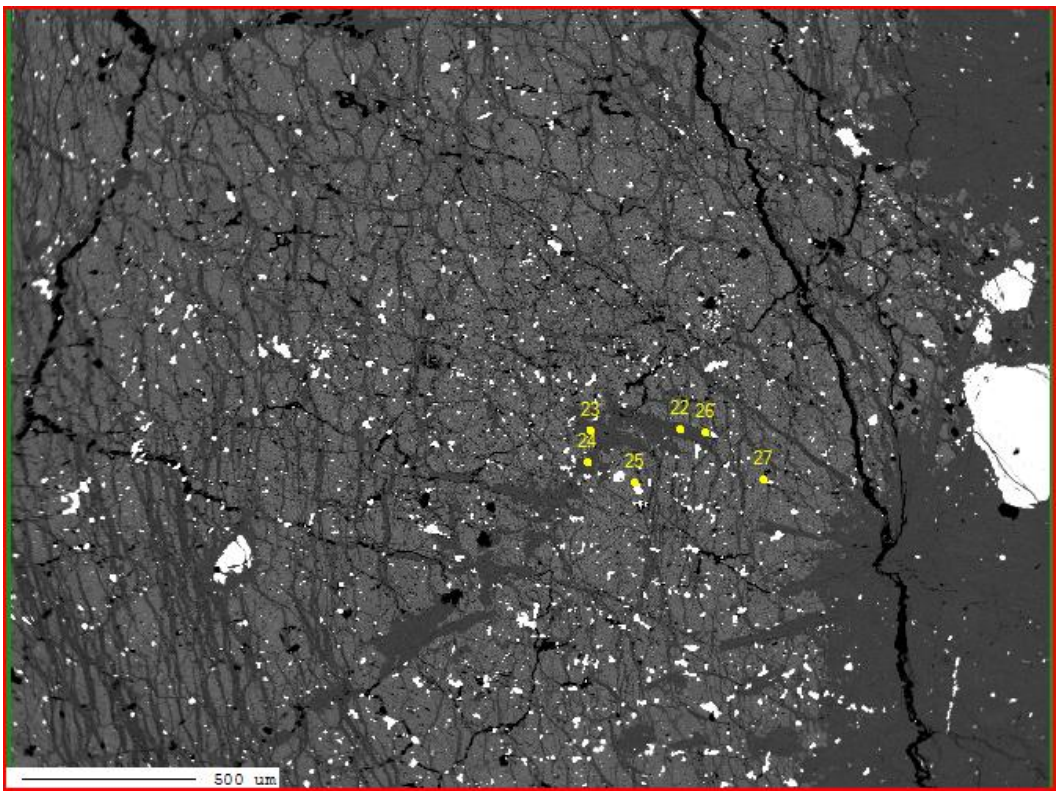

Sample 3.4.2 Location 4 M3 olivine in the M2 antigorite matrix overgrown by M4 antigorite.

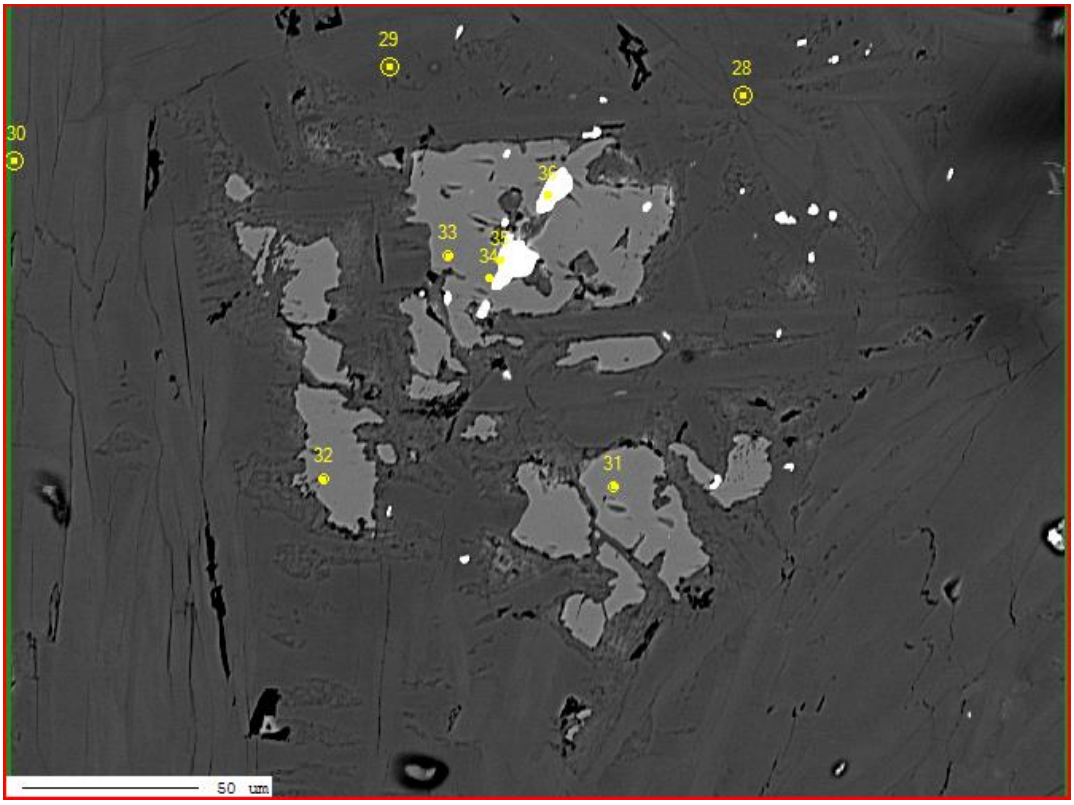

Sample 3.4.2 Location 5 M3 olivine with related magnetite.

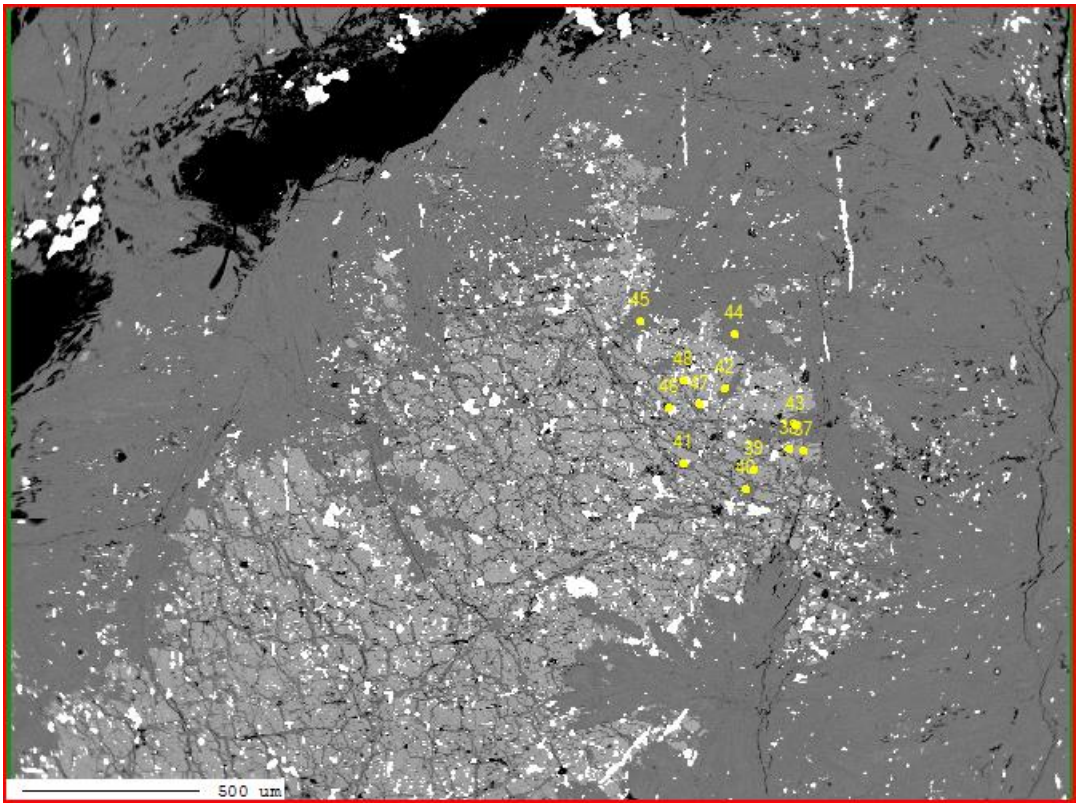

Sample 3.4.2 Location 6 Large spinel with chemical zoning and chlorite reaction rim.

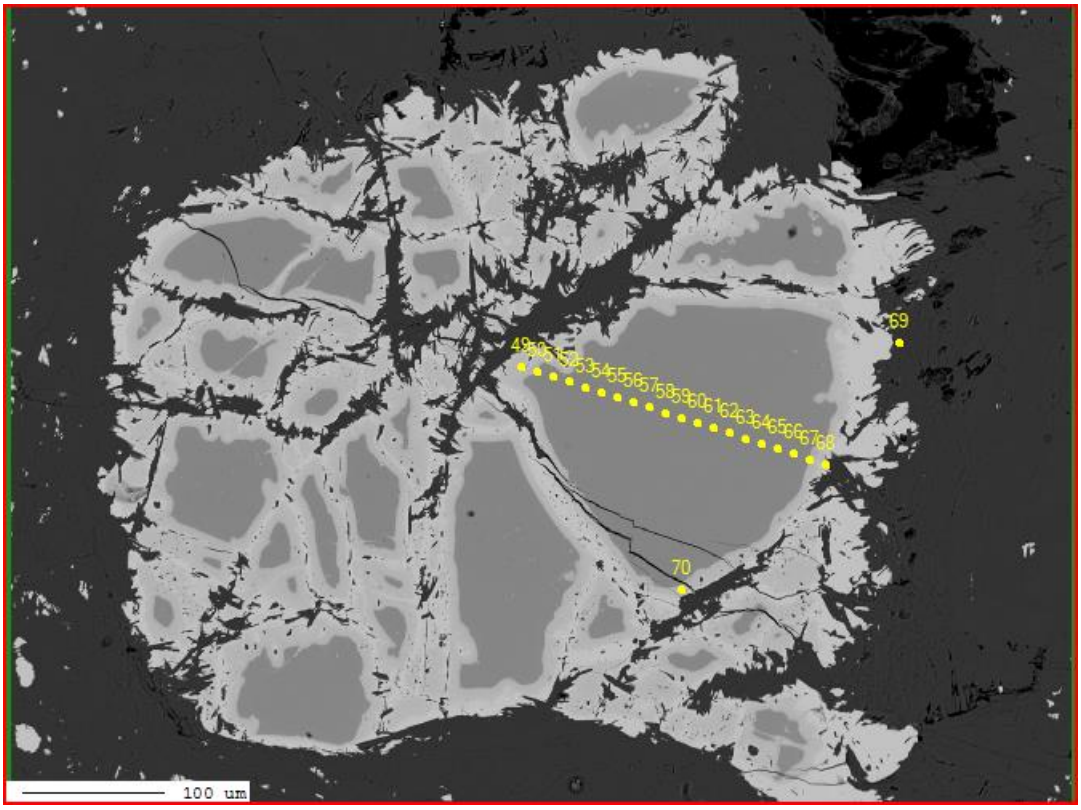

11.2 Raman spectroscopy

Sample 1.1 Location 1

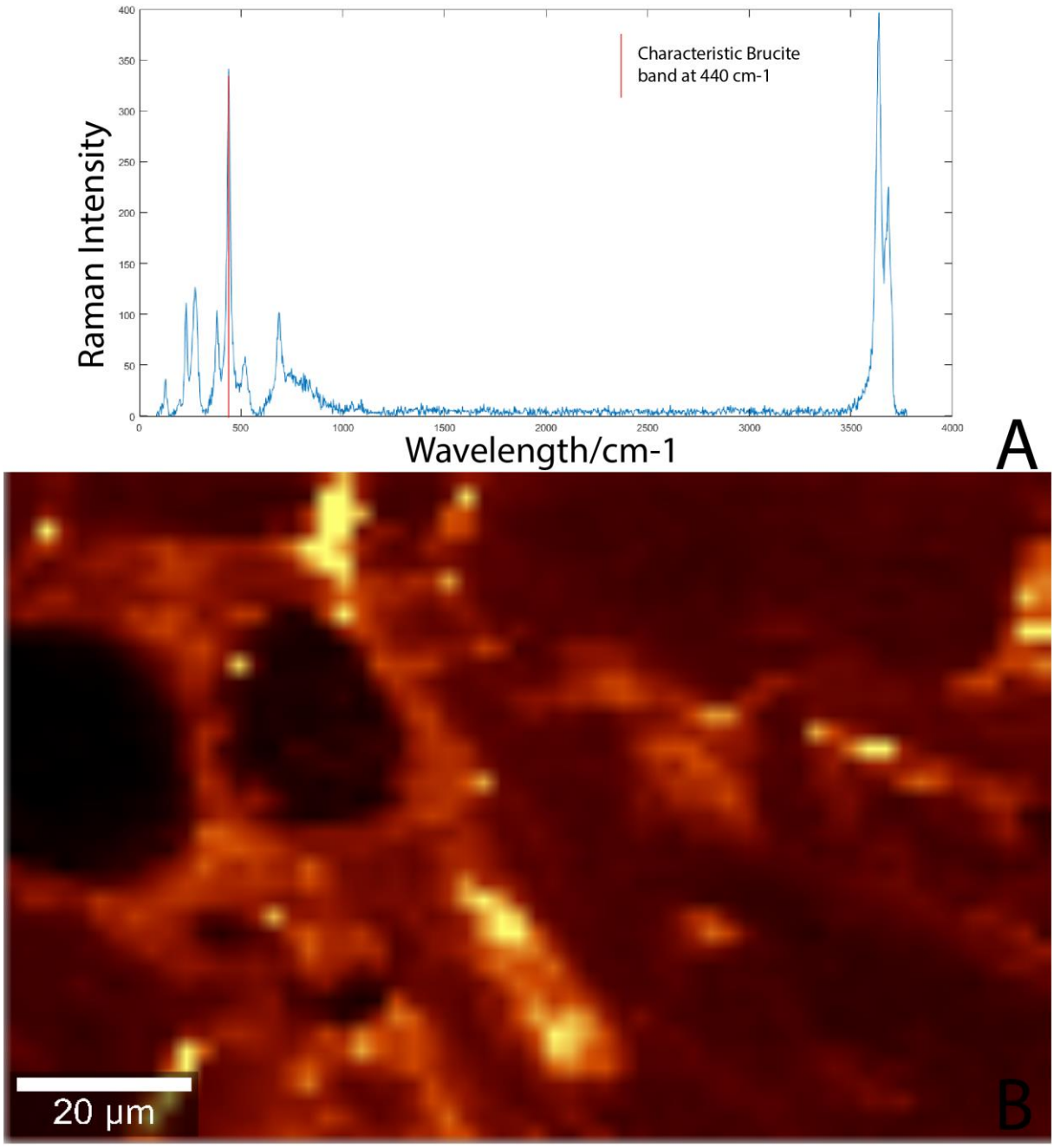

A) Raman Intensity of brucite in sample 1.1 location 1. Red line indicates the characteristic band for brucite. B) Raman intensity map of sample 1.1 location 1 at the 440 cm-1 band showing the distribution of brucite.

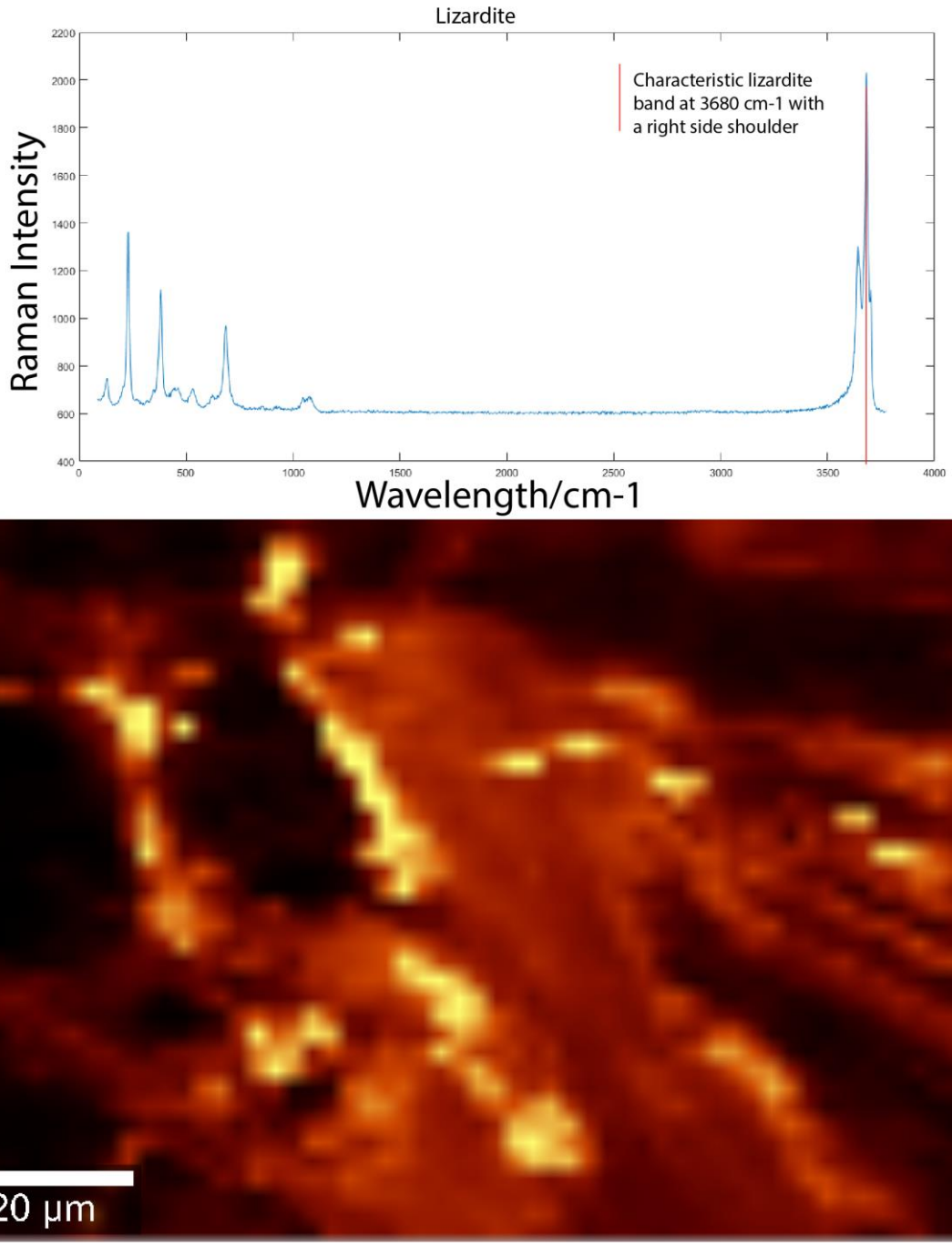

A) Raman Intensity of lizardite in sample 1.1 location 1. Red line indicates the characteristic wavelength band for lizardite at 3680, in addition with the lack of a large peak at 1040 cm-1. B) Raman intensity map of sample 1.1 location 1 at the 3680 cm-1 band showing the distribution of lizardite.

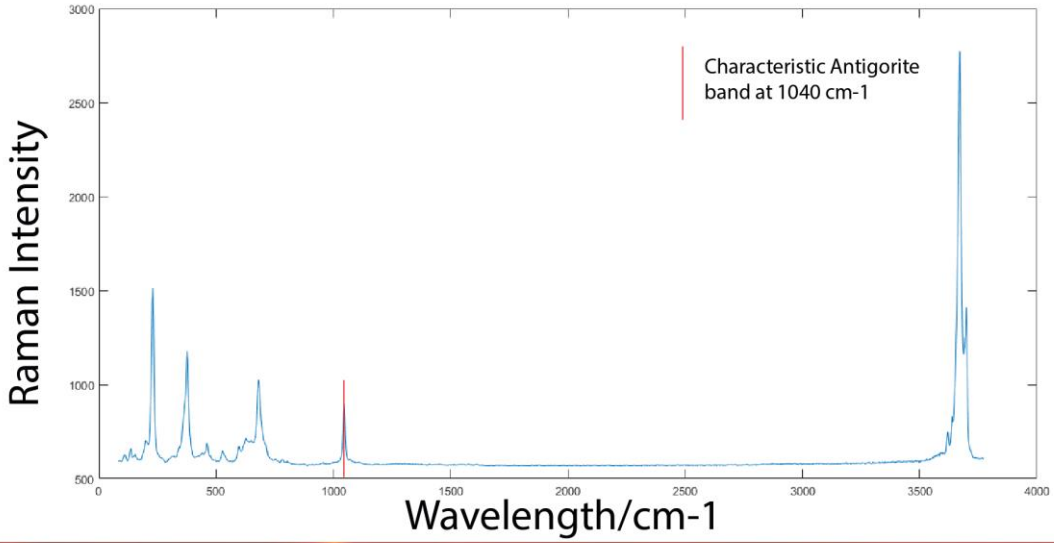

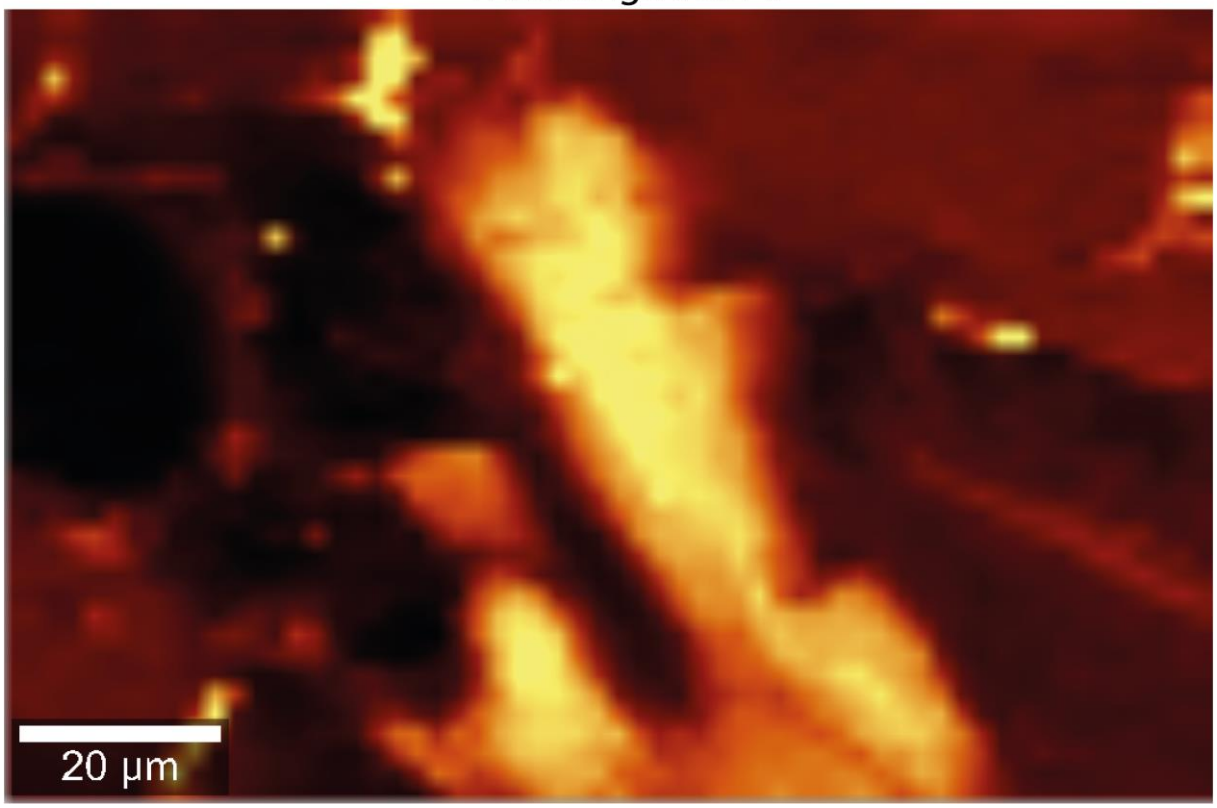

A) Raman Intensity of antigorite in sample 1.1 location 1. Red line indicates the characteristic wavelength band for antigorite, in addition with a small peak at 1040 cm-1. B) Raman intensity map of sample 1.1 location 1 at the 1040 cm-1 band showing the distribution of antigorite.

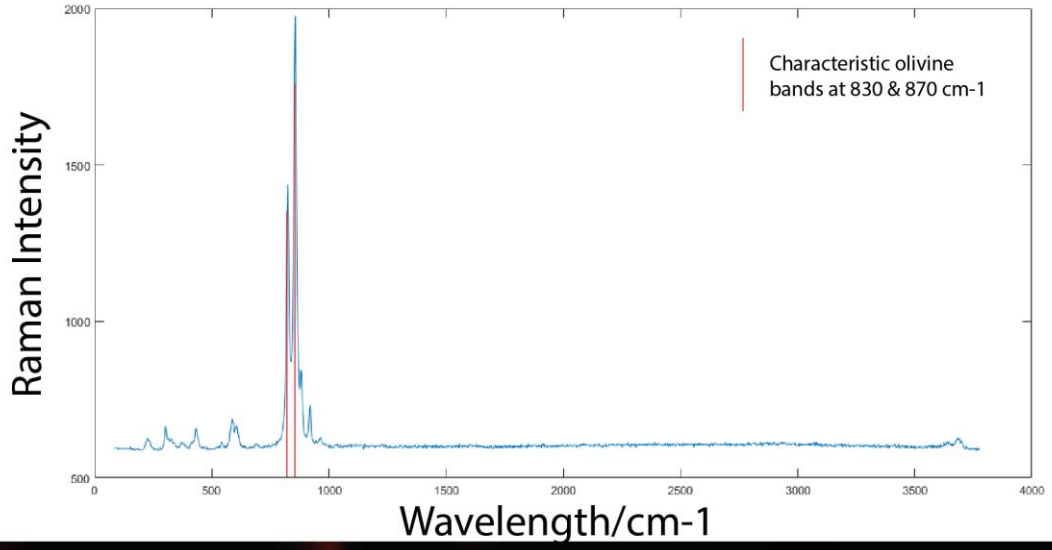

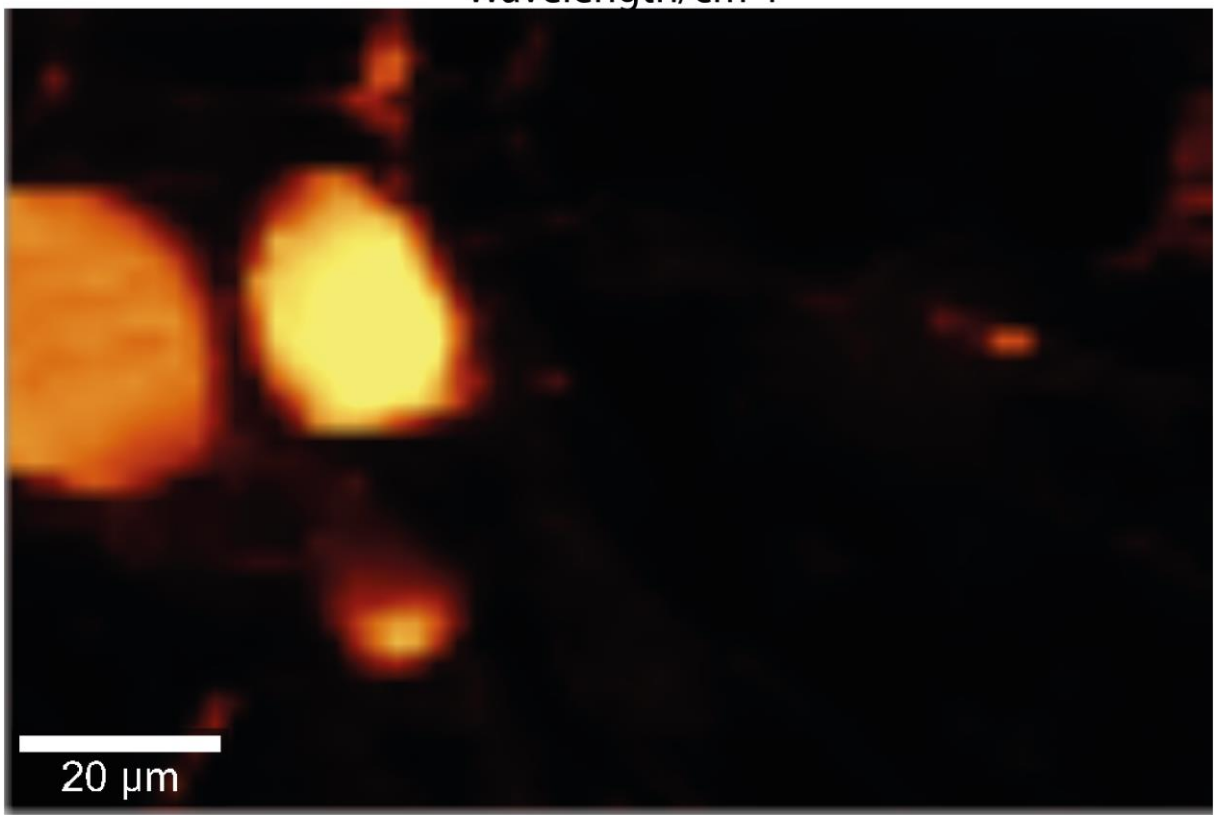

A) Raman Intensity of olivine in sample 1.1 location 1. Red lines indicate the characteristic wavelength bands for olivine. B) Raman intensity map of sample 1.1 location 1 at the 855 cm-1 band showing the distribution of olivine.

Sample 1.1 Location 2

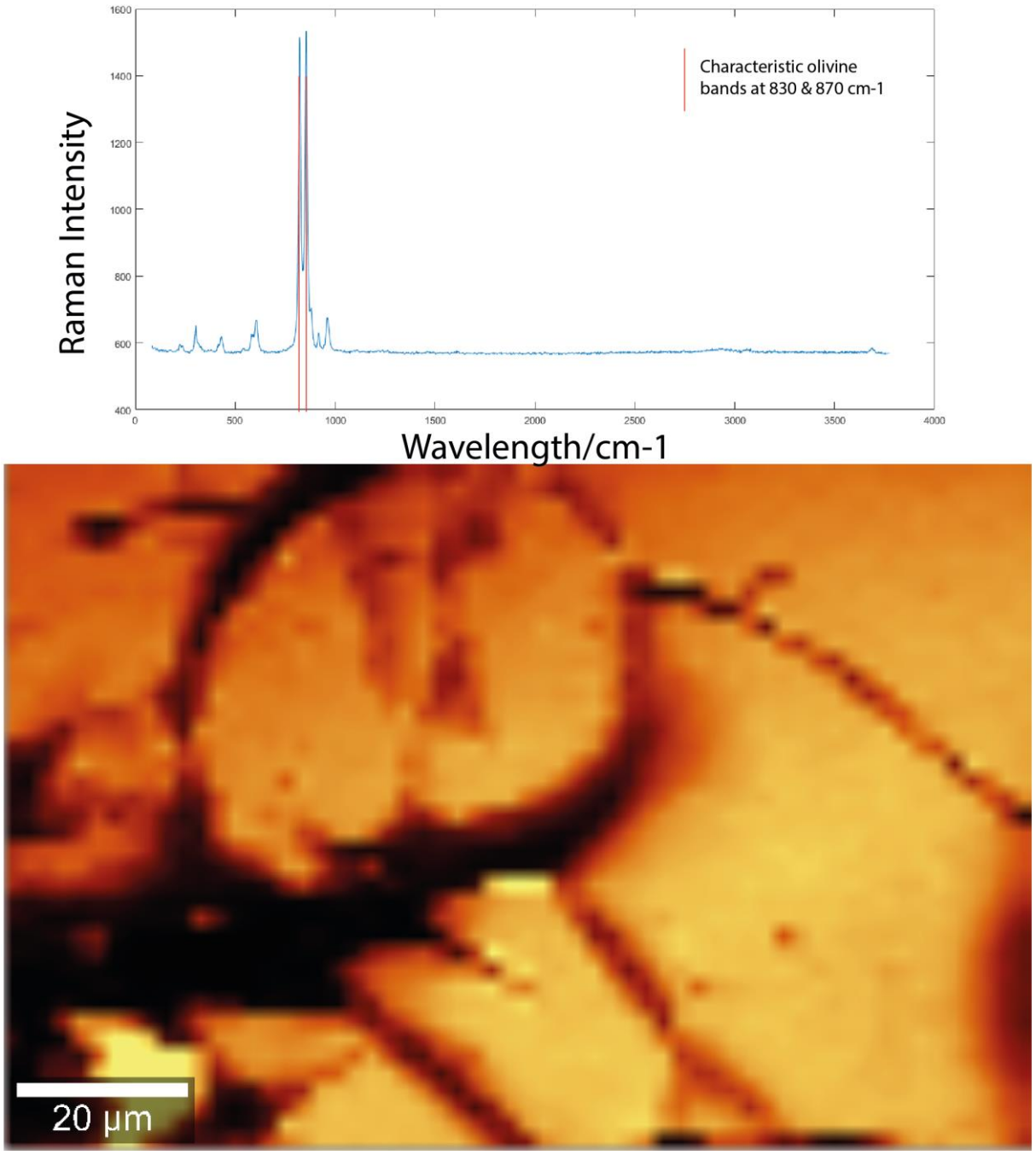

A) Raman Intensity of olivine in sample 1.1 location 2. Red lines indicate the characteristic wavelength bands for olivine. B) Raman intensity map of sample 1.1 location 2 at the 855 cm-1 band showing the distribution of olivine.

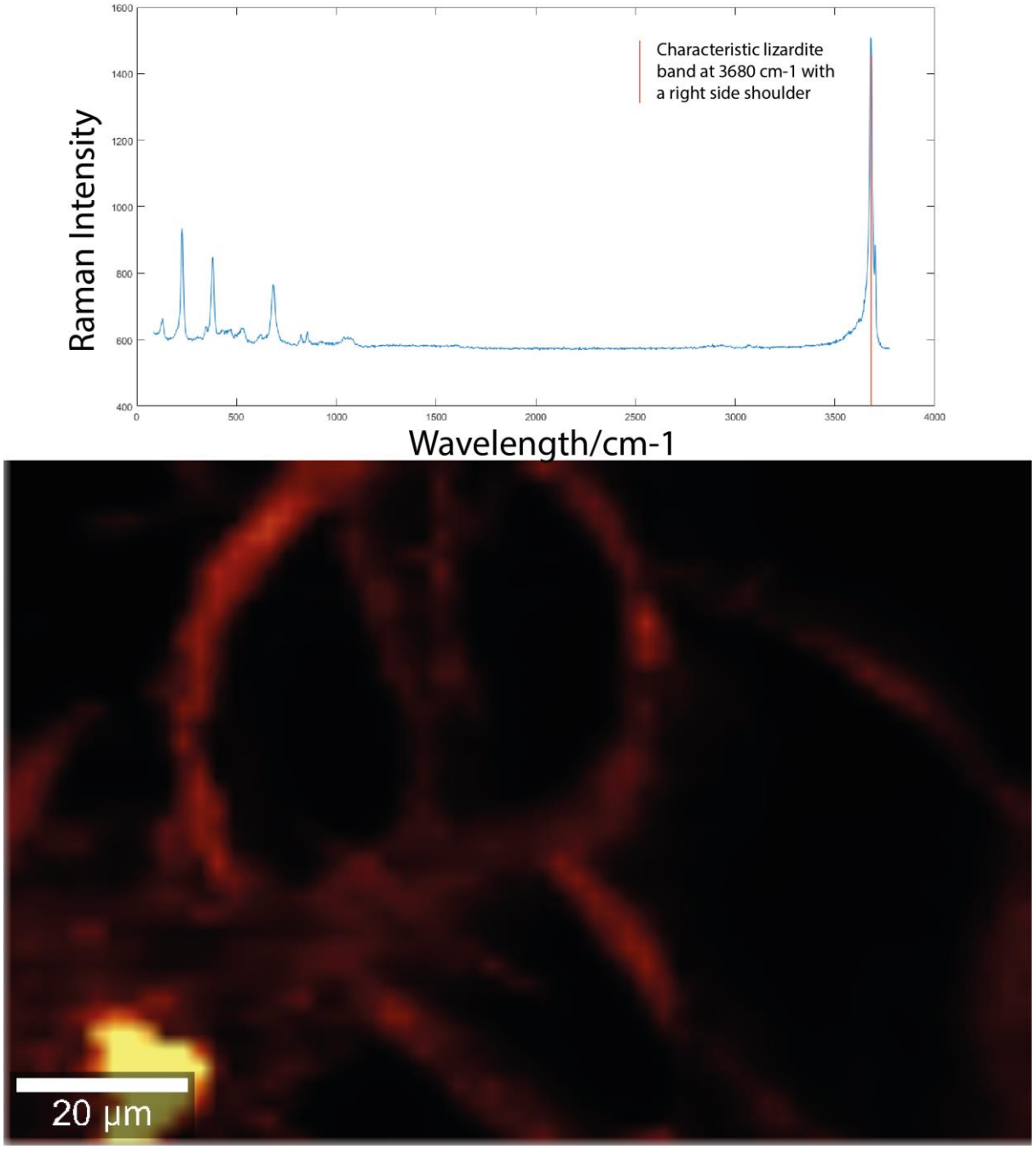

A) Raman Intensity of lizardite in sample 1.1 location 2. Red line indicates the characteristic wavelength band for lizardite at 3680, in addition with the lack of a large peak at 1040 cm-1. B) Raman intensity map of sample 1.1 location 2 at the 3680 cm-1 band showing the distribution of lizardite.

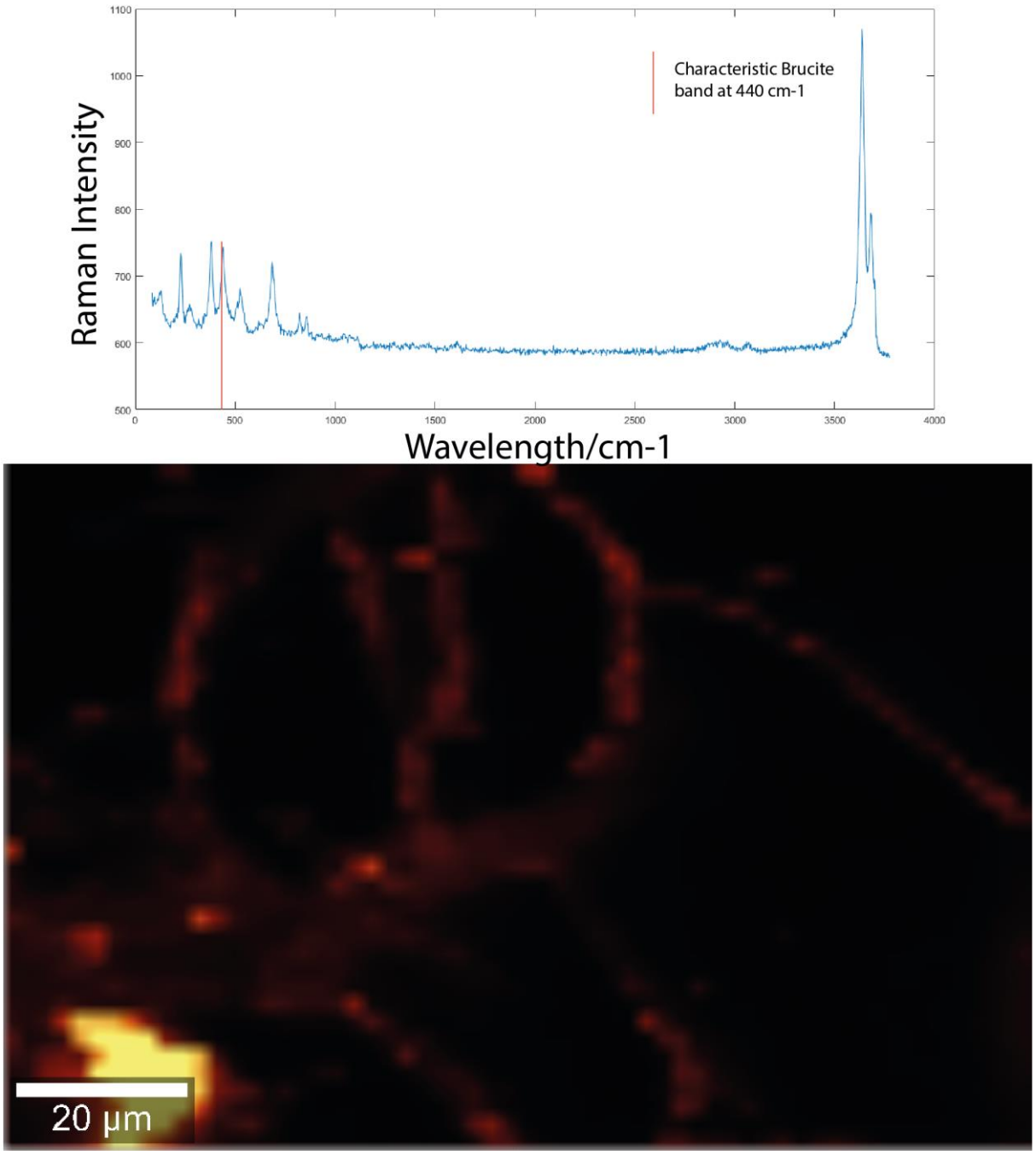

A) Raman Intensity of brucite in sample 1.1 location 2. Red line indicates the characteristic band for brucite. B) Raman intensity map of sample 1.1 location 2 at the 440 cm-1 band showing the distribution of brucite.

11.3 Olivine EMP data in mass%.

Comment	Seconday vs Primary	Mg#	Na2O	SiO2	TiO2	Cr2O3	K2O	CaO	MgO	Al2O3	FeO	MnO	NiO	Total
1.1-olivine-01-13	Primary	0,92	0,00	40,64	0,00	0,01	0,00	0,00	50,62	0,00	7,73	0,13	0,36	99,49
1.1-olivine-01-14	Primary	0,92	0,00	40,33	0,00	0,05	0,00	0,01	50,57	0,00	7,42	0,20	0,27	98,85
1.1-olivine-01-15	Primary	0,92	0,00	40,82	0,00	0,00	0,00	0,01	50,81	0,00	7,84	0,15	0,36	99,99
1.1-olivine-01-16	Primary	0,92	0,00	40,77	0,00	0,00	0,00	0,02	51,11	0,00	7,52	0,16	0,44	100,03
1.1-olivine-01-17	Primary	0,92	0,00	40,76	0,00	0,01	0,00	0,02	50,69	0,00	7,83	0,16	0,46	99,94
1.1-olivine-01-31	Primary	0,93	0,00	40,86	0,00	0,09	0,00	0,01	51,89	0,00	6,71	0,12	0,35	100,04
1.1-olivine-01-32	Primary	0,93	0,01	41,08	0,00	0,00	0,00	0,02	51,65	0,01	7,09	0,10	0,40	100,37
1.1-olivine-01-33	Primary	0,92	0,00	40,98	0,00	0,04	0,00	0,01	50,60	0,01	7,53	0,13	0,32	99,61
1.1-olivine-04-41	Primary	0,92	0,00	40,60	0,01	0,00	0,00	0,02	50,68	0,03	7,64	0,16	0,38	99,53
1.1-olivine-04-42	Primary	0,92	0,01	39,96	0,00	0,01	0,00	0,01	50,62	0,00	7,74	0,17	0,39	98,92
1.1-olivine-04-43	Primary	0,92	0,01	40,86	0,00	0,00	0,00	0,00	50,83	0,00	7,61	0,13	0,42	99,87
1.1-olivine-04-45	Primary	0,92	0,00	40,84	0,00	0,00	0,00	0,00	50,74	0,01	7,68	0,15	0,32	99,75
1.1-olivine-08-47	Primary	0,93	0,00	40,92	0,00	0,02	0,00	0,02	51,42	0,00	6,67	0,12	0,36	99,54
1.1-olivine-08-48	Primary	0,93	0,01	40,98	0,00	0,06	0,00	0,01	51,77	0,00	6,92	0,10	0,39	100,25
1.1-olivine-08-49	Primary	0,93	0,00	41,20	0,00	0,02	0,00	0,01	51,46	0,03	7,03	0,11	0,49	100,36
1.1-olivine-08-50	Primary	0,92	0,00	40,69	0,00	0,00	0,00	0,01	50,82	0,00	7,68	0,14	0,37	99,71
1.1-olivine-09-62	Primary	0,92	0,00	40,84	0,00	0,01	0,00	0,01	50,59	0,00	7,98	0,13	0,39	99,95
1.1-olivine-09-63	Primary	0,92	0,01	40,88	0,00	0,00	0,00	0,01	50,37	0,01	8,17	0,13	0,39	99,96

1.1-olivine-09-64	Primary	0,92	0,00	40,66	0,01	0,00	0,00	0,02	50,49	0,00	8,10	0,14	0,37	99,79
1.4-olivine-01-01	Primary	0,91	0,00	40,74	0,00	0,00	0,00	0,00	49,12	0,01	8,71	0,25	0,48	99,31
1.4-olivine-01-02	Primary	0,91	0,00	40,79	0,00	0,00	0,00	0,00	49,49	0,06	8,85	0,22	0,45	99,86
1.4-olivine-01-03	Primary	0,91	0,00	40,88	0,00	0,01	0,01	0,01	49,74	0,08	8,73	0,21	0,40	100,07
1.4-olivine-01-04	Primary	0,91	0,00	40,72	0,01	0,01	0,00	0,01	49,64	0,01	8,71	0,18	0,39	99,68
1.4-olivine-01-05	Secondary	0,96	0,01	43,87	0,00	0,12	0,00	0,02	38,64	1,52	2,80	0,04	0,20	87,24
1.4-olivine-01-06	Primary	0,91	0,02	40,99	0,02	0,00	0,00	0,01	49,93	0,04	8,50	0,21	0,38	100,09
1.4-olivine-01-07	Primary	0,91	0,00	40,33	0,01	0,00	0,00	0,02	49,66	0,15	8,50	0,21	0,38	99,25
1.4-olivine-01-08	Primary	0,91	0,00	40,82	0,02	0,00	0,01	0,00	49,97	0,06	8,83	0,22	0,40	100,33
1.4-olivine-02-31	Primary	0,91	0,01	40,69	0,00	0,03	0,00	0,02	50,03	0,01	8,53	0,16	0,36	99,83
1.4-olivine-02-32	Primary	0,92	0,00	40,66	0,00	0,00	0,00	0,00	50,20	0,00	8,00	0,13	0,38	99,38
1.4-olivine-02-33	Primary	0,91	0,00	41,03	0,02	0,00	0,00	0,01	50,39	0,02	8,53	0,17	0,42	100,60
2.1b2-olivine-01	Secondary	0,96	0,01	41,36	0,00	0,00	0,00	0,02	53,97	0,01	3,55	0,24	0,39	99,53
2.1b2-olivine-02	Secondary	0,96	0,01	41,87	0,01	0,00	0,00	0,01	54,14	0,00	3,51	0,23	0,30	100,08
2.1b2-olivine-03	Secondary	0,96	0,01	41,66	0,01	0,00	0,01	0,00	54,04	0,02	3,50	0,23	0,38	99,87
2.1b2-olivine-04	Secondary	0,96	0,00	41,79	0,00	0,01	0,00	0,02	53,88	0,00	3,67	0,22	0,31	99,90
2.1b2-olivine-17	Secondary	0,96	0,00	41,56	0,02	0,00	0,00	0,00	54,20	0,01	3,90	0,20	0,44	100,33
2.1b2-olivine-18	Secondary	0,96	0,00	41,56	0,00	0,02	0,00	0,00	54,15	0,00	3,67	0,23	0,38	100,01
2.1b2-olivine-19	Secondary	0,96	0,00	41,45	0,00	0,02	0,00	0,00	53,71	0,00	3,68	0,24	0,38	99,48
2.1b2-olivine-25	Secondary	0,96	0,00	41,48	0,00	0,00	0,00	0,01	53,81	0,02	4,11	0,24	0,29	99,95
2.1b2-olivine-27	Secondary	0,96	0,00	41,82	0,00	0,02	0,01	0,02	53,65	0,01	3,86	0,27	0,35	100,00

2.1b2-olivine-35	Secondary	0,97	0,00	41,70	0,00	0,00	0,00	0,01	54,46	0,00	3,51	0,25	0,38	100,31
2.1b2-olivine-36	Secondary	0,96	0,01	41,76	0,00	0,01	0,00	0,00	54,30	0,00	3,55	0,23	0,37	100,24
2.1b2-olivine-37	Secondary	0,96	0,00	41,95	0,00	0,01	0,00	0,00	54,34	0,00	3,71	0,23	0,35	100,60
2ext1-olivine-01-10	Primary	0,92	0,00	40,42	0,01	0,01	0,00	0,01	50,33	0,02	8,29	0,16	0,44	99,70
2ext1-olivine-01-11	Primary	0,92	0,00	40,68	0,00	0,00	0,00	0,01	50,51	0,00	8,29	0,13	0,32	99,94
2ext1-olivine-01-12	Primary	0,92	0,00	40,34	0,00	0,00	0,00	0,01	50,01	0,01	8,25	0,15	0,37	99,14
2ext1-olivine-02-25	Primary	0,91	0,00	40,88	0,00	0,00	0,00	0,02	50,26	0,02	8,55	0,17	0,39	100,29
2ext1-olivine-02-26	Primary	0,92	0,00	40,87	0,01	0,01	0,00	0,02	50,34	0,01	7,95	0,17	0,34	99,72
2ext1-olivine-02-27	Primary	0,92	0,00	40,66	0,00	0,01	0,00	0,05	50,42	0,16	7,63	0,16	0,36	99,46
2ext1-olivine-05-28	Primary	0,90	0,00	40,22	0,00	0,00	0,00	0,02	49,23	0,02	9,73	0,13	0,47	99,83
2ext1-olivine-05-29	Primary	0,91	0,00	40,19	0,00	0,00	0,00	0,02	49,65	0,14	9,01	0,14	0,40	99,55
2ext1-olivine-05-30	Primary	0,92	0,01	40,43	0,00	0,01	0,00	0,03	50,09	0,04	7,83	0,17	0,41	99,02
2ext1-olivine-06-43	Primary	0,92	0,01	40,75	0,01	0,03	0,00	0,06	50,49	0,02	7,80	0,16	0,39	99,72
2ext1-olivine-06-44	Primary	0,90	0,00	40,25	0,00	0,00	0,00	0,01	49,37	0,00	9,40	0,14	0,42	99,59
2ext1-olivine-08-63	Primary	0,91	0,00	40,64	0,00	0,01	0,00	0,01	50,10	0,00	9,04	0,15	0,46	100,40

2ext1-olivine-08-64	Primary	0,91	0,00	40,71	0,00	0,00	0,00	0,01	49,96	0,00	8,62	0,18	0,42	99,89
2ext1-olivine-08-65	Primary	0,92	0,00	40,62	0,00	0,01	0,00	0,02	50,36	0,01	8,30	0,16	0,42	99,90
3.4.2-olivine-01-04	Secondary	0,95	0,01	41,88	0,00	0,00	0,00	0,01	52,90	0,06	4,76	0,56	0,15	100,33
3.4.2-olivine-01-05	Secondary	0,95	0,01	41,21	0,00	0,00	0,00	0,01	52,72	0,02	4,69	0,88	0,16	99,71
3.4.2-olivine-01-06	Secondary	0,95	0,00	41,00	0,00	0,00	0,01	0,02	52,34	0,03	4,77	0,99	0,15	99,31
3.4.2-olivine-01-07	Secondary	0,95	0,00	41,01	0,00	0,00	0,00	0,03	52,91	0,05	4,54	0,53	0,18	99,27
3.4.2-olivine-07-31	Secondary	0,95	0,00	41,16	0,00	0,00	0,00	0,02	53,14	0,01	4,70	0,69	0,18	99,90
3.4.2-olivine-07-32	Secondary	0,95	0,00	41,25	0,00	0,00	0,00	0,01	53,24	0,00	4,50	0,38	0,15	99,54
3.4.2-olivine-07-33	Secondary	0,95	0,00	41,27	0,00	0,00	0,00	0,02	53,36	0,01	4,53	0,48	0,17	99,85
3.4.2-olivine-08-37	Secondary	0,96	0,00	41,57	0,00	0,00	0,01	0,00	53,72	0,01	4,09	0,30	0,14	99,84
3.4.2-olivine-08-38	Secondary	0,96	0,00	41,48	0,00	0,01	0,00	0,02	53,80	0,00	4,10	0,28	0,19	99,88
3.4.2-olivine-08-39	Secondary	0,96	0,00	41,67	0,01	0,00	0,00	0,01	54,32	0,00	3,78	0,28	0,20	100,28
3.4.1-olivine-01-01	Secondary	0,96	0,00	41,58	0,02	0,00	0,00	0,02	53,42	0,02	4,35	0,15	0,20	99,75
3.4.1-olivine-01-	Secondary	0,96	0,00	41,58	0,01	0,00	0,00	0,01	53,16	0,00	4,45	0,19	0,23	99,63

02														
3.4.1-olivine-01-03	Secondary	0,95	0,00	41,18	0,00	0,00	0,00	0,01	53,15	0,00	4,90	0,59	0,17	100,01
3.4.1-olivine-04-22	Secondary	0,96	0,00	41,35	0,00	0,01	0,00	0,00	53,58	0,00	4,22	0,09	0,21	99,47
3.4.1-olivine-04-23	Secondary	0,96	0,02	41,59	0,00	0,00	0,00	0,00	54,15	0,00	3,87	0,08	0,21	99,92
3.4.1-olivine-04-24	Secondary	0,96	0,00	41,41	0,01	0,02	0,00	0,01	54,07	0,00	4,07	0,10	0,20	99,89
3.4.1-olivine-06-34	Secondary	0,96	0,00	41,65	0,00	0,00	0,00	0,01	54,03	0,00	4,04	0,11	0,16	100,00
3.4.1-olivine-06-35	Secondary	0,96	0,00	41,20	0,00	0,01	0,00	0,00	53,72	0,00	4,15	0,12	0,18	99,39
3.4.1-olivine-06-36	Secondary	0,96	0,00	41,42	0,00	0,00	0,01	0,01	53,77	0,00	4,18	0,09	0,15	99,63

11.4 Spinel and magnetite EMP data in mass%.

Comment	Na2O	SiO2	TiO2	Cr2O3	K2O	CaO	MgO	Al2O3	FeO	MnO	NiO	Total
1.1-chromite-01-01	0,00	0,07	0,05	58,85	0,00	0,00	6,34	6,54	27,37	0,54	0,03	99,80
1.1-magnetite-01-02	0,00	41,24	0,00	0,01	0,00	0,01	50,22	0,01	7,86	0,13	0,38	99,86
1.1-magnetite-01-03	0,00	0,12	0,05	0,43	0,00	0,00	0,55	0,00	92,63	0,03	0,58	94,39
1.1-magnetite-01-04	0,01	0,48	0,02	0,05	0,00	0,02	1,01	0,69	89,00	0,00	0,55	91,83

1.1-magnetite-01-05	0,00	0,07	0,03	0,05	0,00	0,00	0,61	0,03	93,39	0,05	0,54	94,78
1.1-chromite-01-06	0,00	0,05	0,04	59,26	0,00	0,01	6,27	6,44	27,25	0,52	0,05	99,90
1.1-chromite-01-07	0,00	0,02	0,06	58,34	0,00	0,00	5,88	6,32	28,38	0,54	0,00	99,55
1.1-chromite-rim-01-08	0,00	0,42	0,03	3,84	0,00	0,02	1,12	0,60	85,89	0,06	0,54	92,52
1.1-chromite-rim-01-09	0,00	0,06	0,04	52,14	0,00	0,00	3,46	5,00	36,23	0,75	0,09	97,78
1.1-magnetite-01-10	0,03	1,17	0,00	8,67	0,00	0,01	0,97	0,36	87,09	0,13	0,61	99,04
1.1-magnetite-01-11	0,01	0,11	0,05	22,43	0,00	0,02	1,64	0,81	69,18	0,48	0,60	95,32
1.1-magnetite-01-12	0,00	0,07	0,04	4,75	0,00	0,00	0,68	0,04	87,96	0,07	0,75	94,35
1.1-magnetite-01-34	0,00	3,08	0,00	0,02	0,00	0,01	2,25	0,00	88,20	0,03	0,11	93,69
1.1-magnetite-01-35	0,00	0,05	0,01	0,24	0,00	0,00	0,47	0,03	92,50	0,01	0,44	93,77
1.1-magnetite-01-36	0,00	0,26	0,03	0,01	0,00	0,02	0,65	0,00	92,28	0,04	0,56	93,85
1.1-spinel-04-46 Line 001	0,00	0,05	0,05	56,74	0,00	0,00	5,33	6,23	30,12	0,62	0,00	99,14
1.1-spinel-04-46 Line 002	0,00	0,06	0,04	57,61	0,00	0,01	5,77	6,30	28,70	0,55	0,00	99,04
1.1-spinel-04-46 Line 003	0,00	0,05	0,05	58,39	0,00	0,00	6,07	6,44	28,00	0,50	0,03	99,54
1.1-spinel-04-46 Line 004	0,02	0,06	0,05	58,43	0,00	0,01	5,95	6,31	27,60	0,53	0,08	99,03
1.1-spinel-04-46 Line 005	0,00	0,03	0,05	59,73	0,00	0,01	6,25	6,35	27,36	0,56	0,00	100,34
1.1-spinel-04-46 Line 006	0,01	0,05	0,07	58,92	0,00	0,00	6,21	6,44	27,63	0,56	0,09	99,98

1.1-spinel-04-46 Line 007	0,00	0,05	0,05	58,93	0,00	0,00	6,13	6,36	27,78	0,57	0,00	99,87
1.1-spinel-04-46 Line 008	0,00	0,04	0,05	58,65	0,00	0,00	6,29	6,41	27,60	0,54	0,04	99,61
1.1-spinel-04-46 Line 009	0,00	0,03	0,06	58,99	0,00	0,00	6,17	6,49	27,70	0,57	0,01	100,01
1.1-spinel-04-46 Line 010	0,00	0,04	0,05	58,75	0,00	0,00	6,24	6,45	27,87	0,50	0,03	99,93
1.1-spinel-04-46 Line 011	0,00	0,05	0,07	58,43	0,00	0,00	6,02	6,53	28,47	0,58	0,00	100,15
1.1-spinel-04-46 Line 012	0,00	0,04	0,06	58,01	0,00	0,00	5,75	6,39	29,11	0,58	0,06	100,01
1.1-spinel-04-46 Line 013	0,00	0,04	0,06	56,96	0,00	0,00	5,39	6,27	30,51	0,64	0,06	99,92
1.1-spinel-04-46 Line 014	0,00	0,06	0,04	54,57	0,00	0,00	4,50	6,04	33,38	0,67	0,05	99,32
1.1-spinel-04-46 Line 015	0,00	35,81	0,00	0,89	0,00	0,02	40,42	0,06	5,83	0,08	0,37	83,48
1.1-magnetite-08-54	0,02	12,37	0,02	0,25	0,00	0,04	14,94	0,28	69,01	0,08	0,31	97,32
1.1-magnetite-08-55	0,02	13,43	0,00	3,56	0,00	0,01	27,72	0,65	50,43	0,10	0,60	96,52
1.1-magnetite-08-56	0,00	40,94	0,00	0,03	0,00	0,02	38,01	0,05	5,73	0,07	0,32	85,18
1.1-chromite-08-58	0,00	0,03	0,05	58,96	0,00	0,00	6,46	6,31	26,90	0,55	0,08	99,34
1.1-chromite-08-59	0,00	0,03	0,07	57,39	0,00	0,01	6,40	6,54	28,30	0,56	0,04	99,34
1.1-chromite-08-60	0,02	1,29	0,00	1,21	0,00	0,02	2,94	0,07	89,69	0,02	0,48	95,74
1.1-chromite-08-61	0,00	0,06	0,03	3,14	0,00	0,01	0,50	0,02	91,27	0,05	0,63	95,72
1.4-spinel-02-17	0,00	0,04	0,07	43,18	0,00	0,00	12,86	25,10	17,66	0,30	0,16	99,37

1.4-spinel-02-18	0,00	0,04	0,08	42,26	0,00	0,00	12,93	25,45	18,18	0,29	0,17	99,40
1.4-spinel-02-19	0,00	0,01	0,03	42,60	0,00	0,01	12,89	25,61	18,23	0,29	0,19	99,86
1.4-spinel-02-20	0,00	0,03	0,09	37,80	0,00	0,00	3,56	8,15	47,43	0,89	0,24	98,20
1.4-spinel-02-21	0,01	33,70	0,01	2,44	0,01	0,00	36,26	10,53	3,20	0,04	0,22	86,42
1.4-spinel-02-22	0,01	36,41	0,01	2,51	0,01	0,00	36,10	9,97	3,30	0,04	0,16	88,52
1.4-magnetite-02-23	0,01	40,92	0,02	0,00	0,00	0,01	49,91	0,00	8,91	0,17	0,37	100,33
1.4-magnetite-02-24	0,00	40,86	0,00	0,00	0,00	0,01	49,89	0,00	8,78	0,18	0,49	100,21
1.4-magnetite-02-25	0,00	0,32	0,03	0,28	0,00	0,00	0,78	0,01	91,89	0,02	0,45	93,78
1.4-magnetite-04-47	0,02	27,71	0,00	2,14	0,00	0,05	35,14	4,27	15,83	0,08	0,26	85,50
1.4-magnetite-04-48	0,00	40,45	0,02	0,25	0,00	0,02	49,70	0,54	8,30	0,22	0,42	99,94
1.4-magnetite-04-49	0,01	37,14	0,01	0,96	0,00	0,04	45,08	2,44	7,37	0,14	0,31	93,50
2.1b2-spinel-05	0,00	0,01	0,12	58,61	0,00	0,01	7,63	5,22	25,52	1,87	0,04	99,03
2.1b2-spinel-06	0,00	0,02	0,09	45,86	0,00	0,01	6,00	1,52	40,94	2,85	0,30	97,59
2.1b2-spinel-07	0,00	0,02	0,05	57,52	0,00	0,02	7,71	5,28	26,33	1,93	0,04	98,91
2.1b2-spinel-08	0,02	3,76	0,01	1,54	0,00	0,00	6,82	0,13	83,45	0,50	1,15	97,37
2.1b2-spinel-09	0,00	0,05	0,03	1,33	0,00	0,01	0,89	0,03	89,55	0,53	1,18	93,61
2.1b2-spinel-10	0,00	0,02	0,01	1,52	0,00	0,00	1,39	0,02	90,25	0,42	1,01	94,65

2.1b2-spinel-14 Line 001	0,00	0,03	0,17	53,99	0,00	0,00	6,74	3,30	31,57	2,30	0,07	98,17
2.1b2-spinel-14 Line 002	0,00	0,03	0,10	58,85	0,00	0,00	7,39	5,57	26,05	1,34	0,01	99,34
2.1b2-spinel-14 Line 003	0,00	0,02	0,09	59,47	0,00	0,01	7,01	5,77	26,84	1,02	0,03	100,26
2.1b2-spinel-14 Line 004	0,00	0,00	0,08	59,57	0,00	0,01	6,63	5,85	27,34	0,84	0,08	100,40
2.1b2-spinel-14 Line 005	0,00	0,01	0,11	59,64	0,00	0,00	6,44	5,94	27,61	0,68	0,00	100,43
2.1b2-spinel-14 Line 006	0,00	0,02	0,11	59,67	0,00	0,00	6,50	6,05	27,51	0,60	0,05	100,51
2.1b2-spinel-14 Line 007	0,01	0,01	0,12	60,04	0,00	0,00	6,41	6,13	27,16	0,58	0,05	100,50
2.1b2-spinel-14 Line 008	0,00	0,02	0,11	59,68	0,00	0,01	6,53	6,03	27,26	0,57	0,00	100,21
2.1b2-spinel-14 Line 009	0,00	0,03	0,10	60,15	0,00	0,00	6,54	6,07	27,24	0,55	0,00	100,68
2.1b2-spinel-14 Line 010	0,00	0,00	0,10	59,93	0,00	0,00	6,51	6,15	27,10	0,57	0,01	100,37
2.1b2-spinel-14 Line 011	0,03	0,02	0,12	59,99	0,00	0,40	4,97	4,96	26,76	0,58	0,05	97,87
2.1b2-spinel-14 Line 012	0,00	0,02	0,11	60,01	0,00	0,00	6,61	6,15	26,72	0,60	0,05	100,27
2.1b2-spinel-14 Line 013	0,00	0,02	0,12	60,26	0,00	0,00	6,61	6,14	26,65	0,66	0,09	100,54
2.1b2-spinel-14 Line 014	0,00	0,03	0,10	60,14	0,00	0,00	6,71	6,08	26,78	0,69	0,00	100,53
2.1b2-spinel-14 Line 015	0,00	0,02	0,12	60,20	0,00	0,00	6,80	6,00	26,93	0,68	0,07	100,82
2.1b2-spinel-14 Line 016	0,00	0,01	0,08	60,09	0,00	0,00	6,78	5,97	26,83	0,70	0,06	100,53
2.1b2-spinel-14 Line 017	0,02	0,00	0,09	60,31	0,00	0,00	6,83	5,91	26,83	0,81	0,04	100,85

2.1b2-spinel-14 Line 018	0,00	0,01	0,07	60,11	0,00	0,00	6,96	5,77	26,46	0,97	0,03	100,38
2.1b2-spinel-14 Line 019	0,00	0,02	0,11	60,15	0,00	0,01	7,43	5,50	25,91	1,22	0,01	100,36
2.1b2-spinel-14 Line 020	0,00	0,04	0,09	58,94	0,00	0,01	7,38	4,74	26,93	1,66	0,05	99,84
2.1b2-spinel-15	0,00	0,42	0,00	0,31	0,00	0,00	2,32	0,00	90,03	0,39	0,87	94,34
2.1b2-spinel-16	0,01	0,07	0,00	1,55	0,00	0,01	0,91	0,00	90,28	0,49	1,23	94,54
2.1b2-magnetite-23	0,03	0,12	0,01	0,16	0,00	0,00	1,06	0,01	91,07	0,42	1,18	94,05
2.1b2-magnetite-24	0,00	7,86	0,00	0,06	0,00	0,00	15,31	0,11	75,59	0,38	1,28	100,59
2.1b2-magnetite-32	0,00	0,24	0,00	0,02	0,00	0,00	0,97	0,04	90,84	0,38	1,08	93,58
2.1b2-magnetite-33	0,01	44,42	0,00	0,02	0,00	0,00	40,09	0,97	1,93	0,04	0,12	87,60
2.1b2-magnetite-34	0,00	45,01	0,00	0,05	0,01	0,01	41,00	0,72	1,28	0,02	0,07	88,18
2.1b2-magnetite-38	0,03	0,01	0,04	2,43	0,00	0,00	2,13	0,00	88,68	0,31	1,03	94,66
2.1b2-magnetite-39	0,00	0,03	0,02	1,63	0,00	0,01	1,53	0,01	89,48	0,47	1,09	94,28
2.1b2-magnetite-40	0,00	0,01	0,03	1,70	0,00	0,00	1,99	0,00	89,53	0,27	0,95	94,48
2ext1-magnetite-02-19	0,02	0,11	0,09	0,11	0,00	0,37	0,49	0,01	92,16	0,03	0,64	94,03
2ext1-magnetite-02-20	0,00	0,12	0,29	13,92	0,00	0,15	0,90	0,15	76,70	0,49	0,60	93,31
2ext1-magnetite-02-21	0,00	0,12	0,23	10,68	0,00	0,07	0,87	0,00	80,40	0,29	0,64	93,30
2ext1-spinel-05-34	0,00	0,04	0,34	13,73	0,00	0,00	1,05	0,02	77,10	0,46	0,75	93,49

2ext1-spinel-05-35	0,00	0,12	0,17	7,58	0,00	0,01	0,82	0,03	83,67	0,14	0,83	93,37
2ext1-spinel-05-36	0,00	0,12	0,08	0,34	0,00	0,01	0,52	0,00	91,91	0,04	0,60	93,62
2ext1-spinel-06-37	0,00	0,00	0,29	11,00	0,00	0,00	0,88	0,02	82,23	0,27	0,71	95,41
2ext1-spinel-06-38	0,00	0,01	0,57	19,33	0,00	0,00	1,44	0,06	72,49	0,61	0,66	95,18
2ext1-spinel-06-39	0,06	0,05	0,28	11,86	0,00	0,00	0,97	0,02	80,73	0,32	0,68	94,96
2ext1-spinel-08-48	0,02	0,03	0,46	25,21	0,00	0,00	1,83	0,16	66,99	0,57	0,61	95,88
2ext1-spinel-08-49	0,00	1,62	0,35	15,29	0,00	0,00	2,43	0,65	72,98	0,45	0,48	94,25
2ext1-spinel-08-50	0,00	0,02	0,52	24,30	0,00	0,00	1,77	0,09	68,05	0,57	0,54	95,85
2ext1-spinel-08-51	0,00	0,19	0,34	13,71	0,00	0,01	1,14	0,07	78,93	0,37	0,75	95,50
2ext1-spinel-08-52	0,02	0,08	0,34	13,50	0,00	0,00	1,01	0,01	79,50	0,36	0,84	95,65
2ext1-spinel-08-53	0,00	5,21	0,31	11,24	0,00	0,03	7,45	2,10	68,12	0,27	0,66	95,38
2ext1-spinel-08-54	0,00	0,04	0,15	5,39	0,00	0,00	0,73	0,00	87,27	0,06	0,80	94,44
2ext1-spinel-08-55	0,00	0,07	0,13	0,79	0,00	0,02	0,46	0,02	92,34	0,01	0,54	94,37
2ext1-spinel-08-56	0,01	0,14	0,08	0,40	0,00	0,00	0,56	0,08	92,62	0,05	0,53	94,47
3.4.2-spinel-03-13	0,00	0,10	0,21	40,51	0,00	0,00	10,85	19,55	25,56	0,74	0,15	97,68
3.4.2-spinel-03-14	0,00	0,01	0,23	40,84	0,00	0,00	11,42	20,52	25,59	0,57	0,13	99,30
3.4.2-spinel-03-15	0,00	0,05	0,21	41,30	0,00	0,01	11,56	20,89	24,75	0,40	0,13	99,29

3.4.2-spinel-03-16	0,01	0,08	0,20	34,18	0,00	0,01	2,75	0,35	50,96	6,61	0,22	95,36
3.4.2-spinel-03-17	0,00	0,24	0,15	37,18	0,00	0,04	6,58	7,51	42,20	2,25	0,18	96,32
3.4.2-spinel-03-18	0,00	0,35	0,18	26,13	0,00	0,03	2,50	0,95	59,73	4,51	0,32	94,70
3.4.2-magnetite-07-34	0,02	0,21	0,00	0,13	0,00	0,00	0,89	0,05	91,43	0,47	0,48	93,68
3.4.2-magnetite-07-35	0,01	0,80	0,00	0,19	0,00	0,03	1,79	1,62	90,22	0,48	0,39	95,52
3.4.2-magnetite-07-36	0,00	0,26	0,00	0,07	0,00	0,01	1,16	0,00	91,12	0,46	0,49	93,58
3.4.2-magnetite-08-46	0,01	0,17	0,04	0,04	0,00	0,01	0,95	0,00	92,53	0,41	0,37	94,53
3.4.2-magnetite-08-47	0,00	1,35	0,00	0,13	0,00	0,01	2,17	0,02	89,58	0,44	0,28	93,99
3.4.2-magnetite-08-48	0,01	0,54	0,00	0,09	0,00	0,00	1,60	0,12	90,13	0,42	0,45	93,35
3.4.2-magnetite-08-49 Line 001	0,00	0,04	0,25	35,20	0,00	0,00	3,36	0,21	52,40	4,74	0,22	96,43
3.4.2-magnetite-08-49 Line 002	0,00	0,02	0,22	36,01	0,00	0,00	3,99	1,38	51,71	3,50	0,22	97,04
3.4.2-magnetite-08-49 Line 003	0,00	0,02	0,24	42,53	0,00	0,00	12,46	23,21	20,07	0,88	0,05	99,46
3.4.2-magnetite-08-49 Line 004	0,00	0,02	0,29	42,64	0,00	0,01	12,49	23,24	20,26	0,74	0,17	99,85
3.4.2-magnetite-08-49 Line 005	0,00	0,06	0,23	42,78	0,00	0,00	12,57	23,55	20,11	0,49	0,09	99,87
3.4.2-magnetite-08-49 Line 006	0,00	0,00	0,24	42,56	0,00	0,00	12,63	23,30	20,56	0,40	0,11	99,80
3.4.2-magnetite-08-49 Line 007	0,00	0,03	0,25	42,53	0,00	0,00	12,59	23,18	20,31	0,33	0,13	99,35
3.4.2-magnetite-08-49 Line 008	0,00	0,05	0,26	42,88	0,00	0,00	12,53	23,23	20,44	0,33	0,14	99,86

3.4.2-magnetite-08-49 Line 009	0,00	0,03	0,25	42,66	0,00	0,00	12,52	23,28	20,65	0,35	0,14	99,87
3.4.2-magnetite-08-49 Line 010	0,00	0,02	0,28	42,64	0,00	0,00	12,32	23,14	20,35	0,36	0,14	99,25
3.4.2-magnetite-08-49 Line 011	0,00	0,02	0,21	42,78	0,00	0,00	12,65	23,22	20,41	0,32	0,19	99,80
3.4.2-magnetite-08-49 Line 012	0,03	0,03	0,27	42,71	0,00	0,00	12,48	23,07	20,50	0,31	0,06	99,45
3.4.2-magnetite-08-49 Line 013	0,00	0,03	0,26	42,77	0,00	0,01	12,50	23,10	20,39	0,34	0,12	99,52
3.4.2-magnetite-08-49 Line 014	0,00	0,03	0,25	42,55	0,00	0,00	12,51	23,08	20,74	0,33	0,14	99,63
3.4.2-magnetite-08-49 Line 015	0,02	0,03	0,23	42,73	0,00	0,00	12,50	23,04	20,85	0,33	0,16	99,90
3.4.2-magnetite-08-49 Line 016	0,00	0,03	0,26	42,44	0,00	0,00	12,57	23,05	20,77	0,33	0,12	99,58
3.4.2-magnetite-08-49 Line 017	0,01	0,03	0,26	42,62	0,00	0,00	12,47	22,97	21,00	0,36	0,10	99,83
3.4.2-magnetite-08-49 Line 018	0,00	0,05	0,24	42,54	0,00	0,00	12,39	22,86	21,07	0,43	0,05	99,63
3.4.2-magnetite-08-49 Line 019	0,00	0,01	0,23	42,14	0,00	0,00	12,26	22,86	20,88	0,77	0,09	99,23
3.4.2-magnetite-08-49 Line 020	0,00	0,04	0,29	34,87	0,00	0,00	3,08	0,47	52,11	5,38	0,25	96,48
3.4.2-spinel-08-50	0,00	0,05	0,00	0,35	0,00	0,00	0,83	0,01	93,14	0,45	0,19	95,01
3.4.2-spinel-08-51	0,00	0,04	0,26	35,79	0,00	0,00	4,27	1,48	51,61	3,25	0,27	96,97
3.4.1-spinel-01-13 Line 001	0,00	0,05	0,27	40,34	0,00	0,01	11,96	22,53	22,47	0,98	0,14	98,75
3.4.1-spinel-01-13 Line 002	0,00	0,07	0,28	40,15	0,00	0,00	11,86	22,62	22,86	1,04	0,12	98,99
3.4.1-spinel-01-13 Line 003	0,00	0,04	0,29	39,89	0,00	0,00	11,75	22,41	22,75	1,04	0,14	98,31

3.4.1-spinel-01-13 Line 004	0,00	0,04	0,27	39,26	0,00	0,00	10,83	20,37	25,97	1,51	0,18	98,43
3.4.1-spinel-01-13 Line 005	0,00	0,06	0,28	39,28	0,00	0,00	10,86	20,54	25,87	1,50	0,16	98,55
3.4.1-spinel-01-13 Line 006	0,00	0,04	0,20	37,83	0,00	0,00	9,50	15,34	34,36	2,05	0,20	99,53
3.4.1-spinel-01-13 Line 007	0,00	0,03	0,16	35,00	0,00	0,00	5,42	4,77	48,69	2,60	0,27	96,94
3.4.1-spinel-01-13 Line 008	0,00	0,01	0,17	32,93	0,00	0,00	3,94	1,55	53,34	3,33	0,27	95,53
3.4.1-spinel-01-13 Line 009	0,00	0,46	0,15	13,49	0,00	0,00	1,85	0,25	73,80	3,62	0,54	94,16
3.4.1-spinel-01-13 Line 010	0,00	0,26	0,03	1,55	0,00	0,00	1,23	0,15	91,21	0,37	0,48	95,29
3.4.1-spinel-01-13 Line 011	0,00	0,05	0,02	1,16	0,00	0,00	0,92	0,04	92,76	0,40	0,44	95,80
3.4.1-spinel-01-13 Line 012	0,00	0,07	0,03	1,49	0,00	0,00	0,86	0,06	92,37	0,43	0,49	95,80
3.4.1-spinel-01-13 Line 013	0,01	34,77	0,02	2,25	0,01	0,02	33,97	13,49	3,43	0,08	0,08	88,12
3.4.1-spinel-03-14	0,00	0,03	0,31	40,40	0,00	0,00	12,45	23,01	22,57	0,46	0,13	99,36
3.4.1-spinel-03-15	0,00	0,03	0,31	39,80	0,00	0,00	11,94	23,12	21,75	1,10	0,11	98,16
3.4.1-spinel-08-47	0,00	0,02	0,32	39,23	0,00	0,00	12,83	22,91	22,85	0,72	0,14	99,03
3.4.1-spinel-08-48	0,01	0,03	0,36	38,94	0,00	0,00	12,37	22,24	23,54	0,80	0,20	98,49
3.4.1-spinel-08-49	0,00	0,03	0,27	38,76	0,00	0,00	11,79	22,07	24,58	1,11	0,15	98,76
3.4.1-spinel-08-50	0,01	34,05	0,00	2,53	0,01	0,06	24,78	7,51	2,89	0,13	0,08	72,04
3.4.1-spinel-08-51	0,00	5,34	0,17	17,74	0,00	0,00	5,68	1,72	61,65	5,24	0,34	97,88

3.4.1-spinel-08-52		0,00	0,04	0,20	34,75	0,00	0,00	5,30	4,55	50,07	2,08	0,27	97,27

11.5 Serpentine data in Mass%

	Na2O	SiO2	TiO2	Cr2O3	K2O	CaO	MgO	Al2O3	FeO	MnO	NiO	Total
1.1-serpentine-01-18	0,00	43,88	0,00	0,03	0,00	0,01	39,83	0,24	2,12	0,01	0,22	86,33
1.1-serpentine-01-19	0,00	43,96	0,01	0,03	0,00	0,00	40,13	0,30	1,85	0,02	0,16	86,46
1.1-serpentine-01-20	0,00	44,12	0,00	0,00	0,01	0,01	39,97	0,24	2,01	0,03	0,20	86,58
1.1-serpentine-01-21	0,00	37,91	0,00	0,01	0,00	0,02	38,31	0,25	4,77	0,08	0,01	81,37
1.1-serpentine-01-22	0,00	39,31	0,01	0,00	0,00	0,03	38,93	0,05	4,27	0,05	0,10	82,75
1.1-serpentine-01-23	0,01	38,47	0,00	0,02	0,00	0,02	39,68	0,02	4,54	0,04	0,40	83,19
1.1-serpentine-01-24	0,00	41,58	0,00	0,03	0,00	0,02	50,75	0,01	7,38	0,12	0,42	100,32
1.1-serpentine-01-25	0,00	38,91	0,01	0,03	0,00	0,02	49,63	0,03	7,25	0,15	0,35	96,39
1.1-serpentine-01-26	0,00	39,01	0,00	0,01	0,00	0,02	40,69	0,08	6,35	0,09	0,23	86,48
1.1-serpentine-01-27	0,02	40,95	0,00	0,15	0,00	0,01	40,12	0,40	4,11	0,07	0,09	85,92
1.1-serpentine-01-28	0,01	36,91	0,00	0,01	0,01	0,02	39,31	0,02	4,41	0,10	0,21	81,00
1.1-serpentine-01-29	0,00	36,01	0,00	0,00	0,00	0,03	39,46	0,02	5,22	0,12	0,10	80,96
1.1-serpentine-01-30	0,00	37,03	0,00	0,01	0,00	0,03	40,94	0,07	4,16	0,05	0,31	82,61
1.1-serpentine-04-37	0,00	43,97	0,00	0,00	0,00	0,00	39,87	0,16	1,67	0,02	0,08	85,77

1.1-serpentine-04-38	0,00	44,03	0,00	0,00	0,00	0,01	39,78	0,32	1,98	0,00	0,08	86,21
1.1-serpentine-04-39	0,01	44,00	0,02	0,00	0,00	0,00	39,91	0,34	2,07	0,00	0,15	86,50
1.1-serpentine-04-40	0,01	43,85	0,01	0,02	0,00	0,00	39,94	0,31	1,86	0,01	0,04	86,05
1.1-serpentine-04-44	0,00	39,24	0,00	0,01	0,00	0,02	39,55	0,01	3,16	0,04	0,41	82,46
1.1-olivine-04-45	0,00	40,84	0,00	0,00	0,00	0,00	50,74	0,01	7,68	0,15	0,32	99,75
1.1-serpentine-08-51	0,02	36,71	0,00	0,00	0,00	0,01	40,97	0,01	4,78	0,07	0,27	82,85
1.1-serpentine-08-52	0,00	43,80	0,00	0,07	0,01	0,00	39,67	0,49	1,97	0,02	0,16	86,18
1.1-serpentine-08-53	0,01	34,31	0,00	0,01	0,03	0,03	40,68	0,02	5,72	0,09	0,39	81,30
1.4-serpentine-01-09	0,01	38,55	0,00	0,01	0,00	0,02	38,38	0,32	5,97	0,15	0,41	83,82
1.4-serpentine-01-10	0,00	39,26	0,02	0,03	0,00	0,01	37,67	0,25	5,64	0,09	0,40	83,36
1.4-serpentine-01-11	0,01	43,06	0,02	0,08	0,00	0,00	38,94	1,20	3,15	0,03	0,18	86,68
1.4-serpentine-01-12	0,02	42,64	0,00	0,06	0,00	0,00	39,76	1,73	2,21	0,03	0,11	86,56
1.4-serpentine-01-13	0,01	42,75	0,00	0,04	0,00	0,00	39,12	1,74	2,12	0,03	0,08	85,89
1.4-serpentine-01-14	0,01	37,84	0,01	0,02	0,00	0,02	37,81	1,58	5,22	0,11	0,34	82,96
1.4-serpentine-01-15	0,01	40,73	0,00	0,00	0,00	0,02	48,57	0,34	8,44	0,19	0,41	98,72
1.4-serpentine-01-16	0,02	41,01	0,01	0,14	0,01	0,03	38,55	1,99	4,34	0,13	0,21	86,43
1.4-serpentine-02-34	0,01	40,98	0,02	0,02	0,00	0,00	49,88	0,04	8,43	0,16	0,40	99,94

1.4-serpentine-02-35	0,01	30,74	0,01	0,09	0,00	0,07	40,53	0,61	8,53	0,30	0,35	81,23
1.4-serpentine-02-36	0,01	41,87	0,00	0,29	0,00	0,01	39,01	1,23	3,51	0,09	0,13	86,15
1.4-serpentine-02-37	0,01	38,23	0,00	0,03	0,00	0,03	45,78	0,11	7,76	0,18	0,37	92,49
1.4-serpentine-03-38	0,00	39,60	0,00	0,00	0,00	0,01	39,58	0,46	3,97	0,05	0,25	83,93
1.4-serpentine-03-39	0,01	42,82	0,00	0,01	0,00	0,01	39,43	0,70	2,54	0,02	0,10	85,65
1.4-serpentine-03-40	0,00	42,70	0,00	0,00	0,00	0,00	39,54	0,98	2,73	0,06	0,11	86,13
1.4-serpentine-03-41	0,00	43,56	0,00	0,02	0,00	0,01	39,45	0,98	3,49	0,10	0,09	87,70
1.4-serpentine-03-42	0,02	41,15	0,00	0,01	0,00	0,04	38,63	0,24	4,57	0,09	0,44	85,18
1.4-serpentine-03-43	0,00	33,80	0,00	0,00	0,00	0,04	41,37	0,05	6,02	0,16	0,54	81,98
2.1b2-serpentine-11	0,02	39,14	0,00	0,00	0,01	0,03	37,81	0,09	3,41	0,04	0,60	81,16
2.1b2-serpentine-12	0,00	40,24	0,00	0,01	0,00	0,01	38,81	0,06	3,04	0,03	0,64	82,85
2.1b2-serpentine-13	0,00	40,19	0,00	0,00	0,00	0,01	39,46	0,06	2,40	0,05	0,57	82,74
2.1b2-serpentine-20	0,00	43,72	0,01	0,03	0,00	0,00	39,97	0,80	1,55	0,04	0,12	86,24
2.1b2-serpentine-22	0,01	42,78	0,02	0,02	0,00	0,00	39,48	1,51	2,09	0,03	0,10	86,04
2.1b2-serpentine-26	0,00	44,26	0,00	0,02	0,00	0,00	39,96	0,57	1,42	0,05	0,17	86,46
2.1b2-serpentine-28	0,00	43,65	0,00	0,03	0,00	0,00	40,01	0,91	1,79	0,04	0,19	86,62
2.1b2-serpentine-29	0,04	43,46	0,00	0,02	0,14	0,00	39,82	0,80	1,51	0,04	0,15	85,98

2.1b2-serpentine-30	0,00	44,22	0,00	0,01	0,01	0,00	40,53	0,53	1,12	0,03	0,15	86,60
2.1b2-serpentine-31	0,01	44,58	0,00	0,01	0,01	0,00	40,49	0,24	1,00	0,04	0,16	86,54
2.1b2-serpentine-41	0,00	43,70	0,00	0,01	0,00	0,01	40,17	0,66	1,52	0,06	0,18	86,32
2.1b2-serpentine-42	0,01	39,20	0,00	0,01	0,01	0,03	35,17	0,15	4,49	0,17	0,81	80,05
2.1b2-serpentine-43	0,00	39,57	0,00	0,00	0,00	0,04	39,64	0,15	3,12	0,09	0,75	83,36
2ext1-serp-01-04	0,01	42,51	0,00	0,03	0,00	2,32	36,31	0,38	3,98	0,07	0,00	85,62
2ext1-serp-01-05	0,03	36,33	0,02	0,00	0,02	0,30	29,69	1,02	12,51	0,39	0,56	80,87
2ext1-serp-01-06	0,05	39,03	0,03	0,30	0,00	0,13	37,66	5,65	2,73	0,02	0,04	85,64
2ext1-serp-01-07	0,00	43,18	0,00	0,04	0,00	0,01	38,80	0,87	2,53	0,02	0,10	85,56
2ext1-serp-01-08	0,00	41,42	0,02	1,06	0,00	0,02	38,37	1,92	2,51	0,04	0,17	85,52
2ext1-serp-01-09	0,02	41,51	0,03	0,08	0,00	0,02	38,21	1,86	3,63	0,04	0,11	85,51
2ext1-serp-02-16	0,00	39,36	0,00	0,03	0,00	0,06	38,23	0,26	4,90	0,02	0,44	83,32
2ext1-serp-02-17	0,00	38,09	0,01	0,01	0,00	0,10	38,13	0,45	5,42	0,12	0,38	82,71
2ext1-serp-02-18	0,00	40,17	0,03	0,00	0,01	0,20	37,07	0,67	4,06	0,15	0,19	82,55
2ext1-serp-02-22	0,00	43,60	0,00	0,07	0,00	0,00	39,51	0,58	2,34	0,04	0,17	86,30
2ext1-serp-02-23	0,03	42,96	0,01	0,15	0,01	0,02	38,42	1,68	2,65	0,00	0,16	86,09
2ext1-serp-02-24	0,01	43,17	0,02	0,00	0,00	0,01	39,29	1,54	2,13	0,01	0,12	86,30

2ext1-olivine-02-25	0,00	40,88	0,00	0,00	0,00	0,02	50,26	0,02	8,55	0,17	0,39	100,29
2ext1-serp-05-31	0,04	40,82	0,00	0,93	0,00	0,00	38,52	2,52	2,73	0,02	0,15	85,73
2ext1-serp-05-32	0,02	41,25	0,04	0,89	0,01	0,01	37,56	2,31	3,38	0,07	0,14	85,69
2ext1-serp-05-33	0,01	41,93	0,00	0,52	0,00	0,01	38,35	1,62	3,12	0,03	0,16	85,74
2ext1-serpentine-08-60	0,02	43,78	0,00	0,03	0,00	0,01	39,08	0,46	2,25	0,01	0,22	85,87
2ext1-serpentine-08-61	0,01	43,80	0,01	0,01	0,00	0,00	39,12	0,49	2,29	0,02	0,17	85,92
2ext1-serpentine-08-62	0,00	43,90	0,00	0,04	0,00	0,01	39,61	0,17	2,20	0,01	0,17	86,11
3.4.2-serp-01-01	0,01	43,39	0,00	0,01	0,01	0,04	39,28	1,42	1,73	0,06	0,06	86,00
3.4.2-serp-01-02	0,03	43,41	0,00	0,00	0,01	0,03	38,99	0,88	1,51	0,18	0,08	85,12
3.4.2-serp-01-03	0,01	43,29	0,00	0,03	0,01	0,02	38,74	1,45	2,26	0,05	0,04	85,90
3.4.2-serp-01-08	0,01	42,28	0,00	0,00	0,00	0,04	39,72	0,19	2,65	0,09	0,07	85,05
3.4.2-serp-01-09	0,00	42,31	0,00	0,01	0,01	0,02	40,25	0,16	2,62	0,07	0,05	85,50
3.4.2-serp-01-10	0,01	42,03	0,01	0,00	0,00	0,02	39,86	0,25	2,67	0,06	0,02	84,93
3.4.2-serp-01-11	0,01	42,51	0,01	0,02	0,00	0,02	41,00	0,16	2,22	0,09	0,05	86,09
3.4.2-serp-01-12	0,03	41,51	0,00	0,00	0,04	0,04	40,54	0,06	2,04	0,19	0,12	84,57
3.4.2-serp-04-22	0,02	44,70	0,00	0,00	0,01	0,02	39,85	0,54	1,53	0,03	0,00	86,70

3.4.2-serp-04-23	0,01	43,98	0,01	0,05	0,01	0,02	39,64	0,61	1,49	0,21	0,06	86,08
3.4.2-serp-04-24	0,00	43,97	0,00	0,00	0,01	0,01	40,71	0,11	0,91	0,06	0,00	85,79
3.4.2-serp-07-28	0,00	43,35	0,00	0,01	0,00	0,00	39,32	0,55	1,62	0,03	0,18	85,06
3.4.2-serp-07-29	0,00	43,99	0,01	0,01	0,00	0,00	40,38	0,23	0,93	0,05	0,06	85,65
3.4.2-serp-07-30	0,00	43,34	0,00	0,04	0,01	0,01	39,67	0,92	1,68	0,03	0,06	85,75
3.4.2-olivine-07-31	0,00	41,16	0,00	0,00	0,00	0,02	53,14	0,01	4,70	0,69	0,18	99,90
3.4.2-serpentine-08-40	0,00	43,55	0,00	0,00	0,00	0,00	40,70	0,01	1,14	0,10	0,14	85,64
3.4.2-serpentine-08-41	0,00	11,94	0,02	0,01	0,00	0,01	6,46	0,08	73,42	0,37	0,34	92,65
3.4.2-serpentine-08-42	0,00	44,22	0,00	0,00	0,00	0,00	40,42	0,20	1,35	0,07	0,07	86,33
3.4.2-serpentine-08-43	0,00	43,08	0,00	0,01	0,00	0,01	39,36	1,09	2,19	0,04	0,02	85,79
3.4.2-serpentine-08-44	0,00	42,81	0,01	0,01	0,00	0,00	39,48	0,89	1,93	0,03	0,09	85,25
3.4.2-serpentine-08-45	0,00	42,29	0,00	0,06	0,00	0,01	39,11	1,72	2,66	0,05	0,04	85,94
3.4.1-serp-01-04	0,00	42,12	0,00	0,01	0,00	0,01	39,72	1,32	2,38	0,10	0,08	85,74
3.4.1-serp-01-05	0,02	41,89	0,02	0,00	0,01	0,01	42,25	0,11	1,34	0,07	0,00	85,71

3.4.1-serp-01-06	0,02	41,63	0,00	0,00	0,00	0,01	42,14	0,06	1,32	0,08	0,01	85,28
3.4.1-serp-01-07	0,01	43,45	0,01	0,00	0,00	0,00	40,06	0,75	1,60	0,04	0,02	85,94
3.4.1-serp-01-08	0,01	43,66	0,00	0,00	0,00	0,00	39,79	0,85	1,70	0,05	0,09	86,15
3.4.1-serp-01-09	0,00	43,87	0,00	0,00	0,00	0,00	40,66	0,32	0,95	0,02	0,03	85,85
3.4.1-serp-04-25	0,01	37,94	0,00	0,00	0,00	0,01	42,40	0,04	2,71	0,12	0,16	83,39
3.4.1-serp-04-26	0,00	44,38	0,01	0,00	0,00	0,00	40,64	0,17	1,20	0,04	0,09	86,53
3.4.1-serp-04-27	0,00	43,84	0,00	0,02	0,00	0,00	40,23	0,15	1,22	0,05	0,04	85,54
3.4.1-serp-04-28	0,01	43,62	0,00	0,10	0,00	0,00	40,22	0,80	1,35	0,04	0,08	86,21
3.4.1-serp-04-29	0,00	43,44	0,02	0,13	0,01	0,00	40,17	0,85	1,39	0,04	0,01	86,06
3.4.1-serp-04-30	0,01	43,80	0,01	0,08	0,00	0,00	40,40	0,46	1,23	0,06	0,01	86,07
3.4.1-serp-06-37	0,00	41,98	0,00	0,00	0,01	0,02	40,77	0,06	1,03	0,07	0,04	83,99
3.4.1-serp-06-38	0,02	41,41	0,02	0,00	0,01	0,02	41,12	0,07	1,44	0,19	0,07	84,37
3.4.1-serp-06-39	0,01	42,08	0,02	0,00	0,01	0,03	41,22	0,10	1,01	0,14	0,03	84,63
3.4.1-serp-06-40	0,01	43,30	0,00	0,02	0,02	0,00	39,66	0,61	1,52	0,03	0,07	85,24
3.4.1-serp-06-41	0,00	42,62	0,02	0,06	0,00	0,00	38,90	1,21	2,08	0,07	0,06	85,03
3.4.1-serp-06-42	0,01	42,98	0,00	0,22	0,01	0,01	39,67	0,89	1,63	0,02	0,05	85,49

11.6 Serpentine EMP data in mole% and seperation by type of serpentine.

	Na2O	SiO2	TiO2	Cr2O3	K2O	CaO	MgO	Al2O3	FeO	MnO	NiO	Total	Total(Mass %)	Mg/Si	~%water
flackey	0,00	41,64	0,00	0,01	0,00	0,01	56,35	0,13	1,68	0,01	0,17	100	86,33	0,74	14
flackey	0,00	41,60	0,00	0,01	0,00	0,00	56,61	0,17	1,46	0,02	0,12	100	86,46	0,73	14
flackey	0,00	41,73	0,00	0,00	0,00	0,01	56,36	0,13	1,59	0,02	0,15	100	86,58	0,74	13
between olivine	0,00	38,19	0,00	0,00	0,00	0,02	57,53	0,15	4,02	0,07	0,01	100	81,37	0,66	19
between olivine	0,00	38,88	0,01	0,00	0,00	0,03	57,40	0,03	3,53	0,04	0,08	100	82,75	0,68	17
between olivine	0,01	37,78	0,00	0,01	0,00	0,03	58,09	0,01	3,73	0,03	0,31	100	83,19	0,65	17
between olivine (needle like)	0,00	33,56	0,00	0,01	0,00	0,02	61,06	0,00	4,98	0,08	0,27	100	100,32	0,55	0
between olivine (needle like)	0,00	32,58	0,01	0,01	0,00	0,02	61,95	0,02	5,08	0,10	0,24	100	96,39	0,53	4
between olivine (needle like)	0,00	37,04	0,00	0,00	0,00	0,02	57,60	0,04	5,04	0,07	0,17	100	86,48	0,64	14
between olivine (needle like)	0,02	39,13	0,00	0,06	0,00	0,01	57,15	0,23	3,28	0,06	0,07	100	85,92	0,68	14
in shear zone	0,01	37,10	0,00	0,00	0,00	0,02	58,90	0,01	3,71	0,08	0,17	100	81,00	0,63	19
in shear zone	0,00	36,22	0,00	0,00	0,00	0,03	59,16	0,01	4,39	0,10	0,08	100	80,96	0,61	19
in shear zone	0,00	36,34	0,00	0,01	0,00	0,03	59,88	0,04	3,41	0,04	0,25	100	82,61	0,61	17
flackey	0,00	41,88	0,00	0,00	0,00	0,00	56,61	0,09	1,33	0,02	0,06	100	85,77	0,74	14
flackey	0,00	41,83	0,00	0,00	0,00	0,01	56,34	0,18	1,57	0,00	0,06	100	86,21	0,74	14
flackey	0,01	41,68	0,01	0,00	0,00	0,00	56,36	0,19	1,64	0,00	0,12	100	86,50	0,74	14

flackey	0,01	41,69	0,01	0,01	0,00	0,00	56,60	0,17	1,48	0,01	0,03	100	86,05	0,74	14
between olivine	0,00	38,76	0,00	0,00	0,00	0,02	58,23	0,01	2,61	0,04	0,33	100	82,46	0,67	18
in shear zone	0,02	35,95	0,00	0,00	0,00	0,01	59,82	0,01	3,92	0,06	0,21	100	82,85	0,60	17
in shear zone	0,00	41,70	0,00	0,03	0,01	0,00	56,29	0,28	1,57	0,01	0,12	100	86,18	0,74	14
in shear zone	0,01	34,24	0,00	0,00	0,02	0,04	60,51	0,01	4,77	0,08	0,31	100	81,30	0,57	19
between olivine	0,01	38,01	0,00	0,00	0,00	0,02	56,41	0,19	4,92	0,12	0,33	100	83,82	0,67	16
between olivine	0,00	38,98	0,01	0,01	0,00	0,01	55,76	0,14	4,68	0,07	0,32	100	83,36	0,70	17
between olivine	0,01	41,13	0,02	0,03	0,00	0,00	55,45	0,67	2,52	0,03	0,14	100	86,68	0,74	13
centre of vein	0,02	40,63	0,00	0,02	0,00	0,00	56,48	0,97	1,76	0,02	0,08	100	86,56	0,72	13
centre of vein	0,01	41,11	0,00	0,01	0,00	0,00	56,08	0,99	1,71	0,02	0,07	100	85,89	0,73	14
vein	0,01	37,87	0,01	0,01	0,00	0,02	56,41	0,93	4,37	0,09	0,27	100	82,96	0,67	17
vein	0,01	33,68	0,00	0,00	0,00	0,02	59,88	0,17	5,84	0,14	0,28	100	98,72	0,56	1
vein	0,01	39,56	0,01	0,05	0,01	0,03	55,43	1,13	3,50	0,11	0,17	100	86,43	0,71	14
between olivine	0,00	33,34	0,01	0,01	0,00	0,00	60,50	0,02	5,74	0,11	0,26	100	99,94	0,55	0
between olivine	0,01	30,95	0,00	0,03	0,00	0,07	60,84	0,36	7,18	0,25	0,28	100	81,23	0,51	19
between olivine	0,01	40,26	0,00	0,11	0,00	0,01	55,92	0,70	2,82	0,07	0,10	100	86,15	0,72	14
between olivine	0,01	33,68	0,00	0,01	0,00	0,02	60,12	0,06	5,72	0,13	0,26	100	92,49	0,56	8
flackey	0,00	38,65	0,00	0,00	0,00	0,01	57,59	0,26	3,24	0,04	0,20	100	83,93	0,67	16
flackey	0,00	41,07	0,00	0,00	0,00	0,02	56,38	0,39	2,04	0,02	0,08	100	85,65	0,73	14
flackey	0,00	40,80	0,00	0,00	0,00	0,00	56,32	0,55	2,18	0,05	0,09	100	86,13	0,72	14
flackey	0,00	41,08	0,00	0,01	0,00	0,01	55,46	0,54	2,75	0,08	0,07	100	87,70	0,74	12

flackey	0,02	39,88	0,00	0,00	0,00	0,04	55,81	0,14	3,70	0,07	0,34	100	85,18	0,71	15
flackey	0,00	33,42	0,00	0,00	0,00	0,04	60,97	0,03	4,98	0,13	0,43	100	81,98	0,55	18
between olivine	0,02	39,54	0,00	0,00	0,00	0,04	56,94	0,06	2,88	0,04	0,49	100	81,16	0,69	19
between olivine	0,00	39,75	0,00	0,00	0,00	0,01	57,15	0,03	2,51	0,03	0,51	100	82,85	0,70	17
between olivine	0,00	39,57	0,00	0,00	0,00	0,02	57,91	0,03	1,98	0,04	0,45	100	82,74	0,68	17
flackey	0,00	41,55	0,01	0,01	0,00	0,00	56,63	0,45	1,23	0,03	0,09	100	86,24	0,73	14
flackey	0,01	40,97	0,01	0,01	0,00	0,00	56,37	0,85	1,67	0,03	0,08	100	86,04	0,73	14
groundmass (flackey)	0,00	41,94	0,00	0,01	0,00	0,00	56,44	0,32	1,13	0,04	0,13	100	86,46	0,74	14
groundmass (flackey)	0,00	41,36	0,00	0,01	0,00	0,00	56,52	0,51	1,42	0,03	0,15	100	86,62	0,73	13
groundmass (flackey)	0,04	41,45	0,00	0,01	0,08	0,01	56,62	0,45	1,20	0,03	0,11	100	85,98	0,73	14
groundmass (flackey)	0,00	41,70	0,00	0,00	0,00	0,00	56,97	0,30	0,88	0,03	0,11	100	86,60	0,73	13
groundmass (flackey)	0,01	42,02	0,00	0,00	0,00	0,00	56,89	0,14	0,79	0,03	0,12	100	86,54	0,74	13
between olivine	0,00	41,44	0,00	0,01	0,00	0,01	56,78	0,37	1,21	0,05	0,14	100	86,32	0,73	14
between olivine	0,01	40,70	0,00	0,00	0,01	0,04	54,43	0,09	3,90	0,15	0,67	100	80,05	0,75	20
between olivine	0,00	38,76	0,00	0,00	0,00	0,05	57,89	0,09	2,56	0,07	0,59	100	83,36	0,67	17
between CPX	0,01	41,37	0,00	0,01	0,00	2,42	52,67	0,22	3,24	0,06	0,00	100	85,62	0,79	14
between CPX	0,03	39,14	0,01	0,00	0,01	0,35	47,69	0,65	11,27	0,36	0,49	100	80,87	0,82	19
between CPX	0,05	38,58	0,02	0,12	0,00	0,14	55,49	3,29	2,26	0,02	0,03	100	85,64	0,70	14
groundmass (flackey)	0,00	41,61	0,00	0,01	0,00	0,01	55,73	0,49	2,04	0,02	0,08	100	85,56	0,75	14
groundmass (flackey)	0,00	40,42	0,01	0,41	0,00	0,02	55,82	1,10	2,05	0,03	0,13	100	85,52	0,72	14
groundmass (flackey)	0,02	40,37	0,02	0,03	0,00	0,02	55,40	1,07	2,95	0,03	0,09	100	85,51	0,73	14

Between CPX	0,00	38,95	0,00	0,01	0,00	0,06	56,39	0,15	4,06	0,02	0,35	100	83,32	0,69	17
Between CPX	0,00	37,99	0,00	0,00	0,00	0,11	56,70	0,26	4,52	0,10	0,31	100	82,71	0,67	17
Between CPX	0,00	40,27	0,03	0,00	0,00	0,22	55,40	0,39	3,40	0,13	0,15	100	82,55	0,73	17
groundmass (flackey)	0,00	41,53	0,00	0,03	0,00	0,00	56,10	0,32	1,86	0,03	0,13	100	86,30	0,74	14
groundmass (flackey)	0,03	41,43	0,01	0,06	0,00	0,02	55,23	0,96	2,14	0,00	0,13	100	86,09	0,75	14
groundmass (flackey)	0,01	41,28	0,01	0,00	0,00	0,01	56,01	0,87	1,70	0,01	0,10	100	86,30	0,74	14
between olivine	0,04	39,80	0,00	0,36	0,00	0,00	55,99	1,45	2,23	0,02	0,12	100	85,73	0,71	14
between olivine	0,02	40,43	0,03	0,35	0,01	0,01	54,88	1,33	2,77	0,06	0,11	100	85,69	0,74	14
between olivine	0,01	40,69	0,00	0,20	0,00	0,01	55,48	0,92	2,53	0,03	0,12	100	85,74	0,73	14
between olivine/CPX	0,02	41,93	0,00	0,01	0,00	0,01	55,79	0,26	1,80	0,01	0,17	100	85,87	0,75	14
between olivine/CPX	0,01	41,92	0,00	0,01	0,00	0,00	55,81	0,28	1,83	0,01	0,13	100	85,92	0,75	14
between olivine/CPX	0,00	41,79	0,00	0,02	0,00	0,01	56,21	0,09	1,75	0,01	0,13	100	86,11	0,74	14
groundmass (flackey)	0,01	41,57	0,00	0,00	0,01	0,04	56,10	0,80	1,39	0,05	0,04	100	86,00	0,74	14
groundmass (flackey)	0,02	41,90	0,00	0,00	0,01	0,03	56,11	0,50	1,22	0,15	0,06	100	85,12	0,75	15
groundmass (flackey)	0,01	41,66	0,00	0,01	0,00	0,03	55,57	0,82	1,82	0,04	0,03	100	85,90	0,75	14
between olivine	0,01	40,65	0,00	0,00	0,00	0,04	56,93	0,11	2,13	0,07	0,05	100	85,05	0,71	15
between olivine	0,00	40,40	0,00	0,00	0,00	0,02	57,29	0,09	2,09	0,06	0,04	100	85,50	0,71	14
between olivine	0,00	40,44	0,01	0,00	0,00	0,02	57,17	0,14	2,15	0,05	0,02	100	84,93	0,71	15
between olivine	0,01	40,20	0,01	0,01	0,00	0,02	57,80	0,09	1,76	0,07	0,03	100	86,09	0,70	14
between olivine	0,03	39,90	0,00	0,00	0,02	0,04	58,08	0,04	1,64	0,15	0,09	100	84,57	0,69	15
overgrowing olivine	0,02	42,26	0,00	0,00	0,01	0,02	56,16	0,30	1,21	0,02	0,00	100	86,70	0,75	13

overgrowing olivine	0,01	41,90	0,01	0,02	0,01	0,02	56,30	0,34	1,19	0,17	0,04	100	86,08	0,74	14
overgrowing olivine	0,00	41,66	0,00	0,00	0,01	0,01	57,49	0,06	0,72	0,05	0,00	100	85,79	0,72	14
groundmass (flackey)	0,00	41,76	0,00	0,00	0,00	0,00	56,46	0,31	1,31	0,02	0,14	100	85,06	0,74	15
groundmass (flackey)	0,00	41,82	0,00	0,00	0,00	0,00	57,22	0,13	0,74	0,04	0,04	100	85,65	0,73	14
groundmass (flackey)	0,00	41,47	0,00	0,01	0,00	0,01	56,58	0,52	1,34	0,02	0,05	100	85,75	0,73	14
between olivine	0,00	41,33	0,00	0,00	0,00	0,00	57,57	0,01	0,91	0,08	0,11	100	85,64	0,72	14
between olivine	0,00	14,28	0,02	0,00	0,00	0,01	11,51	0,06	73,42	0,37	0,32	100	92,65	1,24	7
between olivine	0,00	41,78	0,00	0,00	0,00	0,00	56,93	0,11	1,07	0,06	0,05	100	86,33	0,73	14
groundmass (flackey)	0,00	41,31	0,00	0,00	0,00	0,01	56,26	0,61	1,76	0,03	0,01	100	85,79	0,73	14
groundmass (flackey)	0,00	41,20	0,01	0,00	0,00	0,00	56,64	0,50	1,55	0,02	0,07	100	85,25	0,73	15
groundmass (flackey)	0,00	40,69	0,00	0,02	0,00	0,01	56,09	0,97	2,14	0,04	0,03	100	85,94	0,73	14
between olivine	0,00	40,40	0,00	0,00	0,00	0,01	56,79	0,74	1,91	0,08	0,06	100	85,74	0,71	14
between olivine	0,02	39,46	0,01	0,00	0,01	0,01	59,33	0,06	1,06	0,06	0,00	100	85,71	0,67	14
between olivine	0,01	39,39	0,00	0,00	0,00	0,01	59,43	0,04	1,04	0,07	0,01	100	85,28	0,66	15
groundmass (flackey)	0,01	41,38	0,01	0,00	0,00	0,00	56,87	0,42	1,27	0,03	0,02	100	85,94	0,73	14
groundmass (flackey)	0,01	41,57	0,00	0,00	0,00	0,00	56,48	0,48	1,35	0,04	0,07	100	86,15	0,74	14
groundmass (flackey)	0,00	41,58	0,00	0,00	0,00	0,00	57,45	0,18	0,76	0,02	0,02	100	85,85	0,72	14
between olivine	0,01	36,59	0,00	0,00	0,00	0,01	60,96	0,02	2,19	0,10	0,12	100	83,39	0,60	17
between olivine	0,00	41,80	0,01	0,00	0,00	0,00	57,06	0,09	0,94	0,03	0,07	100	86,53	0,73	13
between olivine	0,00	41,75	0,00	0,01	0,00	0,00	57,12	0,08	0,97	0,04	0,03	100	85,54	0,73	14
groundmass (flackey)	0,01	41,42	0,00	0,04	0,00	0,00	56,93	0,45	1,07	0,03	0,06	100	86,21	0,73	14

groundmass (flackey)	0,00	41,33	0,01	0,05	0,00	0,00	56,98	0,48	1,11	0,03	0,01	100	86,06	0,73	14
groundmass (flackey)	0,01	41,54	0,01	0,03	0,00	0,00	57,12	0,26	0,98	0,05	0,01	100	86,07	0,73	14
between olivine	0,00	40,45	0,00	0,00	0,01	0,02	58,56	0,04	0,83	0,06	0,03	100	83,99	0,69	16
between olivine	0,01	39,73	0,02	0,00	0,00	0,02	58,81	0,04	1,16	0,15	0,05	100	84,37	0,68	16
between olivine	0,01	40,22	0,01	0,00	0,00	0,03	58,73	0,05	0,81	0,12	0,02	100	84,63	0,68	15
groundmass (flackey)	0,01	41,57	0,00	0,01	0,01	0,00	56,76	0,34	1,22	0,03	0,06	100	85,24	0,73	15
groundmass (flackey)	0,00	41,29	0,01	0,02	0,00	0,00	56,18	0,69	1,69	0,06	0,05	100	85,03	0,73	15
groundmass (flackey)	0,01	41,26	0,00	0,08	0,01	0,01	56,77	0,50	1,31	0,01	0,04	100	85,49	0,73	15

11.7 Chlorite EMP data in mass%.

	Na2O	SiO2	TiO2	Cr2O3	K2O	CaO	MgO	Al2O3	FeO	MnO	NiO	
1.4-chlorite-02-26	0,00	34,11	0,01	1,84	0,00	0,01	35,91	10,48	3,27	0,02	0,20	85,85
1.4-chlorite-02-27	0,03	36,93	0,00	2,06	0,01	0,01	37,00	6,96	2,45	0,02	0,07	85,55
1.4-chlorite-02-28	0,01	34,44	0,00	2,56	0,00	0,01	34,98	9,60	3,21	0,02	0,21	85,04
1.4-chlorite-02-29	0,02	34,10	0,00	2,99	0,00	0,01	35,49	10,56	3,06	0,02	0,16	86,41
1.4-chlorite-02-30	0,00	1,14	0,13	33,80	0,00	0,02	2,80	1,45	56,66	1,00	0,39	97,39
2ext1-chlorite-06-40	0,04	32,95	0,05	0,40	0,00	0,03	34,19	13,74	3,40	0,03	0,09	84,91
2ext1-chlorite-06-41	0,06	33,61	0,01	0,51	0,01	0,01	34,39	12,17	3,53	0,03	0,09	84,42
2ext1-chlorite-06-42	0,04	31,72	0,00	0,29	0,00	0,01	33,79	16,14	3,43	0,02	0,13	85,57
2ext1-chlorite-08-57	0,04	31,72	0,04	0,31	0,00	0,03	33,49	15,48	3,52	0,00	0,17	84,79
2ext1-chlorite-08-58	0,06	30,03	0,02	0,20	0,01	0,02	32,85	17,96	4,10	0,02	0,18	85,45
2ext1-chlorite-08-59	0,04	30,02	0,03	1,41	0,00	0,01	32,64	18,00	3,31	0,02	0,19	85,68
3.4.2-chlorite-03-19	0,00	34,34	0,01	0,16	0,00	0,02	35,07	13,22	2,47	0,03	0,10	85,42
3.4.2-chlorite-03-20	0,00	34,21	0,00	0,11	0,00	0,01	35,34	12,01	3,18	0,05	0,10	85,02
3.4.2-chlorite-03-21	0,01	32,80	0,00	1,82	0,00	0,02	35,64	11,34	3,63	0,30	0,03	85,60
3.4.1-chlorite-03-16	0,00	0,04	0,28	39,80	0,00	0,01	11,93	23,26	21,71	1,12	0,10	98,25
3.4.1-chlorite-03-17	0,01	33,76	0,00	0,49	0,00	0,00	35,27	12,60	3,20	0,06	0,08	85,48
3.4.1-chlorite-03-18	0,00	35,86	0,00	0,66	0,00	0,00	37,02	9,05	3,95	0,04	0,12	86,71
3.4.1-chlorite-08-53	0,00	32,87	0,00	1,00	0,00	0,01	35,18	12,83	3,18	0,07	0,04	85,18
3.4.1-chlorite-08-54	0,00	33,90	0,02	0,23	0,01	0,00	35,24	13,25	2,53	0,02	0,09	85,30

3.4.1-chlorite-08-55	0,01	32,04	0,01	2,39	0,00	0,02	35,83	13,26	2,84	0,08	0,06	86,54

11.8 CPX data in mass%

	Na2O	SiO2	TiO2	Cr2O3	K2O	CaO	MgO	Al2O3	FeO	MnO	NiO	Total
2ext1-cpx-01-01	0,33	53,11	0,14	0,48	0,00	23,72	17,18	2,61	1,89	0,06	0,01	99,54
2ext1-cpx-01-02	0,00	54,94	0,01	0,04	0,00	25,65	18,37	0,14	0,74	0,00	0,06	99,95
2ext1-cpx-01-03	0,19	53,39	0,11	0,35	0,00	23,95	17,26	2,24	1,88	0,08	0,04	99,49
2ext1-cpx-02-13	0,22	52,61	0,17	0,65	0,00	24,22	16,49	3,20	2,06	0,11	0,04	99,76
2ext1-cpx-02-14	0,25	52,13	0,15	0,71	0,00	23,58	16,16	3,88	2,28	0,09	0,06	99,29
2ext1-cpx-02-15	0,24	52,85	0,14	0,69	0,00	23,30	16,61	3,15	2,44	0,10	0,01	99,53
2ext1-cpx-06-45	0,18	53,22	0,17	0,38	0,00	24,07	17,09	2,45	2,02	0,08	0,07	99,73
2ext1-cpx-06-46	0,24	53,19	0,14	0,39	0,00	23,86	17,03	2,66	2,22	0,10	0,08	99,91
2ext1-cpx-06-47	0,11	53,57	0,00	0,21	0,01	22,75	19,60	0,62	1,24	0,04	0,06	98,21